Quantitative Microbial Risk Assessment for Drinking Water: Dose-Response Theory and Virus Filtration Dynamics

Kvantitativ mikrobiell risikoanalyse for drikkevann:
Dose-respons-teori og filtreringsdynamikk for virus

Philosophiae Doctor (PhD) Thesis

Vegard Nilsen

Department of Mathematical Sciences and Technology
Faculty of Environmental Science and Technology
Norwegian University of Life Sciences

Ås (2016)

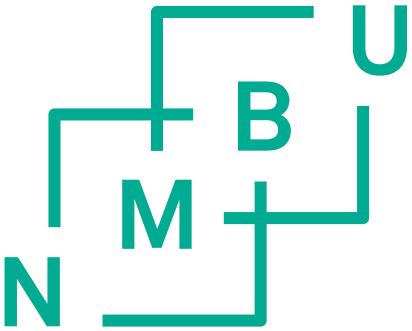

Thesis number 2016:58
ISSN 1894-6402
ISBN 978-82-575-1378-8

Supervisory team

Arve Heistad, Associate Professor (main supervisor)
Department of Mathematical Sciences and Technology
Norwegian University of Life Sciences

John Wyller, Professor (co-supervisor)
Department of Mathematical Sciences and Technology
Norwegian University of Life Sciences

Mette Myrmel, Associate Professor (co-supervisor)
Department of Food Safety and Infection Biology
Norwegian University of Life Sciences

Evaluation committee

Stein Wold Østerhus, Professor (1st opponent)
Department of Hydraulic and Environmental Engineering
Norwegian University of Science and Technology

Mads Peter Sørensen, Professor (2nd opponent)
Department of Applied Mathematics and Computer Science
Technical University of Denmark

Thomas Kringlebotn Thiis, Professor (committe administrator)
Department of Mathematical Sciences and Technology
Norwegian University of Life Sciences

Summary

Transmission of waterborne disease through drinking water remains a public health concern, even in developed countries. This is evidenced not only by the occurrence of small and large disease outbreaks in modern water supply systems, but also by studies that indicate a contribution of drinking water to endemic gastrointestinal infectious disease. In its guidelines for drinking-water quality, the World Health Organization promotes *quantitative microbial risk assessment* (QMRA) as a tool for assessing health risks from pathogenic microorganisms and developing water quality criteria based on quantified health risk targets.

In QMRA, exposure to pathogens is estimated by modeling the concentration of pathogens from source waters to the consumer's tap. Exposure is subsequently translated into health risks through dose-response relations, and compared to a health risk target. Conceptually, QMRA carries the potential to overcome existing challenges associated with low-sensitivity epidemiological methods and the somewhat obscure health risk relevance of faecal indicator organisms. However, its application is still limited by a lack of fundamental scientific understanding in certain areas as well as the lack of site-specific and pathogen-specific data. This thesis contributes to the advancement of QMRA through detailed investigations of (1) mathematical properties of the dose-response relations that are currently in use and (2) dynamic effects in deep-bed filtration on the removal of viruses (primarily) and bacteria from drinking water, and the associated implications for risk assessment. There is also (3) a study on metabolic lag effects in bacterial growth, which could be relevant in some QMRA-settings.

In **Paper I**, the mathematical structure of currently used dose-response models, known as "single-hit models", is reviewed. These models estimate the probability of infection as a function of the ingested dose and are based on a certain hypothesis about the infection process: Pathogens act *independently* of each other in overcoming host defenses, and infection results if *at least one* pathogen is successful in overcoming these defenses. The contribution of **Paper I** is a detailed dissection of the model structure, facilitated by introducing general variables that represent host properties and pathogen properties, respectively. This leads to a precise expression for the so-called "single-hit probability" in terms of these variables. Furthermore, it is demonstrated that the model-consistent expression for computing the risk from repeated exposures *deviates* (gives lower risk) from conventional expressions used in applications. This result affects e.g. annual risk estimates, which is usually the basis for health risk targets.

Paper II is a continuation of the analysis from **Paper I**. The baseline assumption on the probability distribution of microbial counts (i.e. the dose) in water samples is the Poisson distribution, and this forms the basis for the standard dose-response models. However, the literature is rich with speculation that microorganisms may frequently be clustered together, in which case the dose distribution is naturally represented by a *stuttering Poisson* distribution.

In **Paper II**, the single-hit dose-response model with general stuttering Poisson distributions is developed and analyzed. It is shown that the risk computed with this distribution is less than the risk computed with a Poisson distribution, assuming constant mean doses. An equivalent result is obtained for mixed Poisson distributions, another class of distributions that is used to model Poisson overdispersion. Finally, an upper bound on risk is developed from Jensen's inequality, taking the mean dose, λ_{d}, and the probability of zero dose, $p_X(0)$, as parameters. Numerical simulations indicate that the bound is quite close to exact computations, which suggests that parameters λ_{d} and $p_X(0)$ contain most of the information on the dose-distribution that is relevant in a single-hit model. The bound may serve as an approximate dose-response model, and an example with norovirus data is given.

Virus removal during filtration, in particular in relation to filter effluent turbidity, has been identified as a knowledge gap in QMRA. In **Paper III**, the removal of viruses (primarily) and bacteria during deep-bed filtration was studied using natural raw water in a pilot-scale experiment of dual-media contact-filtration, a common treatment process in Norway. A filter-run with unprecedented spatio-temporal sampling resolution for viruses was investigated. Results show that ripening and breakthrough fronts for both model viruses (bacteriophages), *E.coli* and turbidity migrated down the filter bed in wave-like manner. Removal efficiency for viruses and bacteria varied by a factor of about 50 and 200, respectively, during the period of operation when water is usually supplied to the consumer. Ripening was fast for bacteria, but removal peaked early. Ripening for viruses was slow and removal peaked right before turbidity breakthrough. Comparison of observed filter coefficients with predictions from ideal filtration theory suggests that the majority of microorganisms were floc-bound. Efforts to fit a dynamic filtration model to the data are ongoing.

The topic of **Paper IV** is the impact on risk estimates of such dynamic filtration effects that were observed in **Paper III**. It is shown that the *mean* removal efficiency of viruses and bacteria over the entire filter-cycle may be significantly lower than the more easily observed instantaneous removal efficiency. Furthermore, the maximum mean microorganism removal efficiency is reached only *after* microorganism breakthrough, and closer to turbidity breakthrough, which is reassuring from a risk management point of view. These results demonstrate the importance of sampling regimes that can capture dynamic filtration effects and correct mean removal efficiencies. Finally it is shown that these performance variations in themselves are unlikely to affect risk estimates as long as the correct mean removal efficiency is used. However, filtration dynamics *do* represent a vulnerability when coupled with short-term variations in either raw water pathogen concentrations and/or disinfection efficiency.

In **Paper V**, a model is proposed to account for metabolic lags in bacterial growth. Metabolic lags may occur when bacteria are adapting to a new environment, in particular changes in the available substrate types. Absent an explicit model of the metabolic pathways, such effects may be modeled by delay differential equations. The proposed model uses a distributed delay formulation in the form of a convolution integral which, when coupled with a certain integral kernel, produces a simple system of differential equations. The model was tested with published data on biodegradation of organic contaminants in a groundwater setting and was shown to simulate this system using fewer parameters than a previously published model. Although presented in a different context, it is hypothesized that the model may also be useful for risk assessment, for example in modeling growth of environmental pathogens or for incubation time distributions in population disease transmission.

Sammendrag

Spredning av vannbåren sykdom med drikkevann representerer en stadig folkehelseutfordring, også i høyt utviklede land. Dette viser seg ikke bare gjennom små og store sykdomsutbrudd i moderne vannforsyningssystemer, men også gjennom studier som anslår at drikkevann bidrar til forekomsten av endemisk sykdom fra mage-tarm-infeksjoner. I sine retningslinjer for drikkevannskvalitet fremhever Verdens helseorganisasjon *kvantitativ mikrobiell risikoanalyse* (QMRA) som et verktøy for å vurdere helserisiko fra patogene mikroorganismer og for å utvikle kriterier for vannkvalitet basert på tallfestede mål for helserisiko.

I QMRA estimeres forbrukerens eksponering for patogener ved å modellere konsentrasjonen av patogener i vannet fra råvann til tappepunkt. Eksponeringen blir deretter omsatt til helserisiko ved hjelp av dose-respons-funksjoner, og sammenlignet med et risikomål. QMRA har et teoretisk potensial til å omgå eksisterende begrensninger knyttet til lav sensitivitet i epidemiologiske metoder og den noe uklare sammenhengen mellom helserisiko og fekale indikatororganismer. Anvendelser begrenses imidlertid fortsatt av manglende vitenskapelig forståelse på enkelte områder, samt manglende sted-spesifikke og patogen-spesifikke data. Denne avhandlingen bidrar til videreutviklingen av QMRA gjennom detaljerte studier av (1) matematiske egenskaper ved dose-respons-funksjonene som benyttes pr. i dag og (2) dynamiske effekter ved dybdefiltrering på fjerningen av virus (primært) og bakterier i drikkevannsbehandling, og implikasjoner for risikovurderinger. Avhandlingen inneholder også (3) en studie av metabolske forsinkelseseffekter i bakterievekst, som vil kunne være relevant i enkelte QMRA-settinger.

I **Paper I** gjennomgås den matematiske strukturen til dose-respons-modellene som benyttes pr. i dag, kalt "ett-treffs-modeller". Disse modellene estimerer sannsynligheten for infeksjon som en funksjon av inntatt dose og er basert på en bestemt hypotese om infeksjonsprosessen: Patogener virker *uavhengig* av hverandre i å overvinne vertens forsvarsmekanismer og infeksjon oppstår hvis *minst en* av patogenene lykkes i å overvinne dette forsvaret. Bidraget fra **Paper I** er en detaljert disseksjon av modellstrukturen gjennom å innføre generelle variabler som representerer henholdsvis verts- og patogenegenskaper. Dette fører til en presis formulering av den såkalte "ett-treffs-sannsynligheten" uttrykt ved disse variablene. Videre blir det demonstrert at det modell-konsistente uttrykket for å beregne risikoen ved gjentatte eksponeringer *avviker* (gir lavere risiko) fra det uttrykket som konvensjonelt benyttes i anvendelser. Dette resultatet påvirker f.eks. estimater for årlig risiko, som er den vanlige enheten for helserisikomål.

Paper II er en fortsettelse av analysen fra **Paper I**. En grunnantakelse er at sannsynlighetsfordelingen for antall mikroorganismer (dvs. dosen) i en vannprøve følger Poisson-fordelingen, og dette er grunnlaget for de vanlige dose-respons-modellene. I litteraturen spekuleres det imidlertid i om mikroorganismer ofte kan være klumpet sammen, og i så fall vil dosefordelingen naturlig være representert ved en "snublende Poisson-fordeling" (en diskret sammensatt

Poisson-fordeling). I **Paper II** blir ett-treffs dose-respons-modeller med generelle snublende Poisson-fordelinger utviklet og analysert. Det vises at risikoen beregnet med denne fordelingen er mindre enn risikoen beregnet med Poisson-fordelingen, gitt at midlere dose holdes konstant. Et tilsvarende resultat fås for blandede Poisson-fordelinger, en annen klasse av fordelinger som kan modellere Poisson-overdispersjon. Til slutt utledes en øvre skranke for risiko fra Jensens ulikhet, som tar midlere dose, λ_{d}, og sannsynligheten for null-dose, $p_X(0)$, som parametere. Numeriske simuleringer antyder at skranken ligger ganske nær den eksakte risikoen, som innebærer at parameterne λ_{d} og $p_X(0)$ inneholder det meste av informasjonen om dosefordelingen som er relevant i en ett-treffs modell. Skranken kan tjene som en approksimativ dose-respons-modell, og et eksempel med data fra norovirus blir gitt.

Virusfjerning ved filtrering, og særlig sammenhengen med utløpsturbiditet, er identifisert som et kunnskapshull i QMRA. I **Paper III** studeres fjerningen av virus (primært) og bakterier ved dybdefiltrering med naturlig råvann i et pilotskala forsøk med to-media kontaktfiltrering, en vanlig behandlingsmetode i Norge. Én filtersyklus ble undersøkt med unikt høy prøvetakingsfrekvens både i tid og rom. Resultatene viser at modnings- og gjennombruddsfronter for begge modellvirus (bakteriofager), *E.coli* og turbiditet vandret nedover filtersengen som en bølge. Fjerningsgraden for virus og bakterier varierte med en faktor på hhv. 50 og 200 i den delen av syklusen hvor vannet vanligvis sendes til forbruker. Modningsperioden for bakterier var kort, men gjennombrudd oppstod tidlig. Modningsperioden for virus var lang, og gjennombrudd oppstod rett før turbiditetsgjennombruddet. En sammenligning av observerte filterkoeffisienter med prediksjoner fra ideell filtreringsteori, antyder at majoriteten av mikroorganismene var fnokk-bundet. Arbeid med å tilpasse en dynamisk modell til dataene pågår.

Temaet for **Paper IV** er innvirkningen på risikoestimater av slike dynamiske filtreringseffekter som ble observert i **Paper III**. Det blir vist at *midlere* fjerning av virus og bakterier over hele filtersyklusen kan være betydelig lavere enn den momentane fjerningen, som er enklere å observere. Videre blir det vist at den maksimale midlere fjerningen oppnås *etter* gjennombrudd av den aktuelle organismen, og nærmere turbiditetsgjennombruddet, som er betryggende fra et risikohåndteringsperspektiv. Disse resultatene viser viktigheten av å utarbeide prøvetakingsplaner som kan fange opp dynamiske effekter og korrekt midlere fjerning. Til slutt vises det at slike variasjoner i seg selv neppe kan påvirke risikoanslaget så lenge man benytter en korrekt midlere fjerningsgrad. Dynamiske filtreringseffekter representerer imidlertid en ekstra sårbarhet i forbindelse med raske variasjoner i råvannets innhold av patogener og/eller virkningen av desinfeksjonsprosesser.

I **Paper V** presenteres en modell som beskriver metabolske forsinkelseseffekter ved bakterievekst. Slike forsinkelseseffekter oppstår når bakterier tilpasser seg et nytt miljø, og særlig ved endringer i hvilke typer substrat som er tilgjengelig. I fravær av en eksplisitt modell for cellulære prosesser kan slike effekter modelleres ved hjelp av differensialligninger med forsinkelser. Den foreslåtte modellen benytter en formulering med distribuerte forsinkelser i form av et foldingsintegral som, med en bestemt integralkjerne, munner ut i et enkelt system av første ordens differensialligninger. Modellen ble testet med publiserte data for bionedbrytning av organiske forurensninger i grunnvannssammenheng og viste seg å kunne simulere dette systemet med færre parametere enn en tidligere publisert modell. Selv om modellen ble presentert i en annen kontekst, kan man anta at den også kan være nyttig for risikomodellering, for eksempel for å beskrive vekst av miljøpatogener eller fordelinger av inkubasjonstider i modeller for smittespredning.

The first principle is that you must not fool yourself — and you are the easiest person to fool.

Richard Feynman (1918-1988)
Nobel laureate in physics

Acknowledgements

The well-known Parkinson's law states that "work expands so as to fill the time available for its completion", from which Horstman's corollary supposedly follows: "Work contracts to fit in the time we give it". With the submission of this thesis, I contribute my share to an ever-growing body of evidence that the latter does not apply to PhD-candidates. In fact, Newton's three laws of graduation[1] seem to match the available data far better.

In seriousness, though, research isn't just any kind of work. If it were easy to plan and conduct, it probably wouldn't qualify as research. Glancing through the research proposal I submitted when I started this work, it is now easy to see that it was overly ambitious, lacking in specifics and only superficially related to the present end product. The lesson learned can hardly be overstated: Identifying good, researchable problems is the most difficult part of research, but also the most important. The rest is largely about perseverance[2] and remembering to enjoy even those days when progress seems remote.

There are many who deserve thanks at this stage. First and foremost I wish to express my gratitude to my main supervisor *Arve Heistad* and co-supervisor *John Wyller* for encouraging me to take on PhD-studies, and the department, IMT, for providing the financing through a stipend. I hope we made some progress in bringing the water group and the mathematics group closer, which was the stated intention from the beginning. *Arve*, thank you for your continued support, patience and confidence in my work, and for giving me the freedom to pursue my own ideas. Your courage to think big and your ability to always stay positive is admirable. Thank you also for directing significant funds towards equipment that was useful for my research. *John*, thank you too for your constant support and open door, always ready to help with my attempts in the world of mathematics. Your humility and willingness to work with non-mathematicians is a great asset to the department and in the spirit of our common alma mater: *Non scholae, sed vitae discimus.*

I also want to thank *Mette Myrmel*, my co-supervisor from NMBU Adamstuen, for your advice and support of the work that Ekaterina and I did together. Similar thanks go to *Tor Håkonsen*, colleague at Norconsult and Ekaterinas supervisor. And *Ekaterina*, I am lucky to have had the chance to work with you on the filtration project. Without your optimism, knowledge of microbiology, skills in the lab and your help in solving many small and big challenges along the way, the project would have stumbled long before the finishing line.

Sincere thanks also go to *Arne Svendsen* in the mechanical workshop at IMT. Without your skilled craftsmanship, the pilot-plant would have never seen the light of day. Similarly sincere thanks go *Tom Ringstad* in the electronics workshop; your skills and work was truly indispens-

[1] http://goo.gl/RCJT
[2] http://goo.gl/700o

able in getting the system to work as we needed it to. *Jon Fredrik Hanssen*, *Else Marie Aasen* and *Rannei Tjåland* at the microbiology lab at IKBM; thank you very much for helping us with preparations, letting us use the lab so freely and facilitating our work. *Anne Willumsen* and *Torbjørn Friborg*, thank you for pulling an all-nighter to get the virus analyses done as quickly as possible; your help was crucial. *Lars Molstad*, thank you for showing an interest in my work and using your programming and computational skills to help me out during these last stressful months.

I also wish to mention the Norwegian team for the VISK EU-project, in particular *Arve*, *Susan Petterson* and *Razak Seidu*, for introducing me to the ideas of QMRA, which eventually became the integrating theme of this thesis. I wish to thank my non-academic employer, *Norconsult*, for letting me keep a part-time position during my PhD-studies; I have enjoyed maintaining this link to the world outside academia. To the board at *Sameiet Herregårdsterrassen*, I apologize for jumping ship mid-term during demanding times for the board, and I am thankful for your understanding. Thanks also go to the extended *WESH-group* at IMT, present and former staff and students, for creating a friendly work environment; the group has grown immensely since I started and I believe the future looks bright.

Last, but not least I wish to thank my family; mom, dad, Asbjørn, Steinar, for your constant love, support and friendship. I cannot imagine sticking it out for the past couple of years without your help, financially and emotionally, and I am looking forward to having more time to spend with you.

Ås, June, 2016

Vegard Nilsen

Table of Contents

List of Figures

List of Tables

List of Acronyms

AGI	Acute gastrointestinal illness
DALY	Disability adjusted life years
DBP	Disinfection byproduct
DLVO	Derjaguin-Landau-Verwey-Overbeek
DNA	Deoxyribonucleic acid
DOC	Dissolved organic carbon
HACCP	Hazard Analysis and Critical Control Points
HCl	Hydrochloric acid
HPC	Heterotrophic plate counts
IAH	Independent action hypothesis
IEP	Isoelectric point
iid	Independent and identically distributed
mgf	Moment generating function
ML(E)	Maximum likelihood (estimate)
MPN	Most probable number
NOM	Natural organic matter
NRV	Nedre Romerike vannverk
PDE	Partial differential equation
pdf	Probability density function
PFU	Plaque forming unit
pmf	Probability mass function
pgf	Probability generating function
QMRA	Quantitative microbial risk assessment
RNA	Ribonucleic acid
RT-qPCR	Reverse-transcription quantitative polymerase chain reaction
SS	Suspended solids
SUVA	Specific UV absorption
TE	Tufenkji/Elimelech
TOC	Total organic carbon
USEPA	United States Environmental Protection Agency
UV	Ultra violet
WHO	World Health Organization
WSP	Water Safety Plan

List of Publications

This thesis is based upon the following appended papers, which will be referred to by their Roman numerals throughout the text. Papers I, II and V are reproduced with permission from the publishers.

Paper I

Nilsen, V. and J. Wyller (2016a). "QMRA for drinking water: 1. Revisiting the mathematical structure of single-hit dose-response models." *Risk Analysis* **36** (1), pp. 145–162.

Paper II

Nilsen, V. and J. Wyller (2016b). "QMRA for drinking water: 2. The effect of pathogen clustering in single-hit dose-response models." *Risk Analysis* **36** (1), pp. 163–181.

Paper III

Nilsen, V., E. Christensen, L. Molstad, M. Myrmel, and A. Heistad (2016). "Spatio-temporal dynamics of virus removal in dual-media contact-filtration for drinking water: Experimental results and inverse modeling." Manuscript in preparation.

Paper IV

Nilsen, V. (2016). "Some aspects of deep-bed filtration dynamics in QMRA for drinking water." Manuscript in preparation.

Paper V

Nilsen, V., J. A. Wyller, and A. Heistad (2012). "Efficient incorporation of microbial metabolic lag in subsurface transport modeling." *Water Resources Research* **48** (9), W09519.

1. Introduction and Research Motivation

This thesis treats two topics in waterborne infectious disease control with different developmental histories; *sand filtration* and *quantitative microbial risk assessment* (QMRA). Filtration in one form or another is an ancient technology for water treatment, and rapid sand filtration has been common practice for drinking water treatment since the early 20th century. Its importance for removing pathogens from water is well established. The application of quantitative risk assessment principles to drinking water is a more recent development that began in the early 1980s, and the field is still maturing. It represents an alternative approach to assessing hygienic water quality and informing management decisions, and is complementary to traditional epidemiological and faecal indicator methods.

Of the five papers on which this thesis is based, **Paper III** contributes new experimental data while the remaining four have a more theoretical character, using only published data, if any. Hence, the presentation does not lend itself very well to the conventional IMRAD[1] structure of scientific reporting. Instead of distinct methods and results chapters, the thesis contains three main chapters, Chapter 2 on dose-response models for QMRA, Chapter 3 on filtration and Chapter 4 on metabolic lags in bacterial growth. In these chapters, the relevant background is developed and the results of each paper is presented and discussed. The presentation should be fairly accessible even to an uninitiated reader.

This introductory chapter aims to provide some broad context for the thesis and indicate the overall role of the individual appended papers in the QMRA framework. Section 1.2 will review the occurrence of disease associated with drinking water in Norway and the Nordic countries, epidemiological data on the role of filtration, and current regulatory practices for drinking water. Section 1.3 introduces QMRA and its components, while Section 1.4 makes the objectives of the thesis concrete and briefly presents the methods that were employed. However, we begin with a motivating example from the early days of microbiology.

1.1 A historical prologue

In his biography of Robert Koch, Brock (1999) stated that "...water filtration has probably saved more lives than immunization and chemotherapy combined.". This statement is of course difficult to verify and should not be taken as fact, but it sets the stage: drinking water filtration has been and remains of prime public health importance (Cutler and Miller, 2005). Robert

[1] Introduction, Methods, Results and Discussion.

Koch is known for founding modern bacteriology and *Koch's principles* for identifying the etiologic agent of an infectious disease, but he also took an interest in sand filtration for drinking water treatment. His paper on the role of *slow*[2] sand filtration in preventing cholera (Koch, 1893, German original, 1894, English translation) serves as a nice historical background to both the filtration and microbial risk aspects considered in this thesis, and a brief summary follows.

From the mid-19th century, many European and (somewhat later) American cities established centralized public water supplies which often involved slow sand filtration as treatment (Kirkwood, 1869). For example, Norway's first filtration plant, which for several decades was also the only one, was commissioned in Larvik in 1869 (Johansen, 2004). During this period, the *germ theory* of disease gradually displaced the prevailing *miasmatic* theory, which held that disease was caused by foul air resulting from decomposing organic matter. John Snow famously demonstrated (Snow, 1855) that cholera could be transmitted with water when he identified the pump on Broad street as the focal point of the 1854 outbreak in London, a foundational event for the discipline of epidemiology. In 1884 Robert Koch identified the bacterium *Vibrio cholera* as the etiologic agent of the disease.[3] The work of Snow and Koch, then, is actually an illustrative example of the first step of a QMRA, *hazard identification*; identifying the disease causing microbial agent *and* relevant exposure routes.

Yet, by the 1890s, there was still opposition to the germ theory and Koch's paper on sand filtration was intended to both (1) prove his opponents wrong on the etiology of cholera (in surprisingly colorful language!) and (2) demonstrate the importance of sand filtration, including its skilful operation, in preventing the disease. The data he needed for (1) presented itself during the 1892-1893 cholera outbreak in Hamburg, Germany, which resulted in about 17000 cases and 8600 deaths and was the last major cholera outbreak in the developed world. A striking difference in cholera incidence in the adjacent cities of Hamburg and Altona (Koch estimated around 100 cases originating in Altona) called for an explanation. Both cities drew water from the river Elbe; Hamburg upstream of the city and Altona downstream of Hamburg's sewer outlets. The separation between affected and unaffected areas coincided with the border separating the two cities' water distribution networks. Cholera bacteria were found in the raw water of both cities, but not in Altona's finished water. Research at the Berlin water works had previously demonstrated the capacity of slow sand filters to remove cholera bacteria. Only Altona's water supply was filtered. In sum, Koch saw this as irrefutable evidence that the cholera bacteria had spread with the drinking water and that the Altona filters protected that city against infection.

Koch went on to present data for the filtration plant in Altona that indicated 2-3 $\log_{10}$-units removal of heterotrophic plate counts (HPC), which is not much different from what one could expect from a modern rapid sand filtration plant. As mentioned, he found cholera bacteria in the raw water and not in the filtered water, but noted that they probably would have been found if larger volumes could be sampled. Thus, he performed the rudiments of an *exposure assessment*, i.e. quantifying how many pathogens a given population is exposed to, and he understood that probabilistic concepts are involved in such assessment. Essentially, he only

[2]Slow sand filtration shares many characteristics with today's more common rapid sand filtration, but unlike rapid sand filtration, removal depends largely on the development of a surface mat of deposit/biofilm called a *schmutzdecke*.

[3]Only later was it widely recognized that Filippo Pacini actually isolated the bacterium already in 1854 (Pacini, 1854).

lacked a relationship between exposure and disease, a *dose-response* relation (the topics of **Paper I** and **Paper II**), before being able to make a rough *risk characterization*. Lacking these tools, he nevertheless expressed the following, which conveys a view on *acceptable risk*:

> All that we yet know of sand-filtration, therefore, compels us to admit that, even under the most favourable circumstances, it cannot afford absolute protection against infection, though, as I have already said, it does afford a protection with which, considering the practical conditions of life, one may rest content.

Koch went even further and discussed in detail the importance of proper *design* and *operation* of filters for bacterial removal, i.e. *risk management*, which is treated in **Paper IV**. He demonstrated his points by comparing the filters at Altona with those at Nietleben, Halle, a smaller water treatment plant supplying a mental asylum that experienced a cholera outbreak, and which showed a HPC-removal of less than 1 $\log_{10}$-units. His recommendations align almost perfectly with present views on good filtration practice, and included keeping the filtration rate as stable as possible, installing facilities for filtering to waste (and using them) after a filter has been cleaned, installing facilities for sampling from every filter in the gallery (not just from the mixed effluent), regular bacterial monitoring using rapid analysis methods, and shutting down a filter if effluent HPC exceeds 100/ml (a number which occurs in drinking water regulations even today).

Koch also called for technology-neutral government regulations regarding water quality and expressed the view that, if bacterial counts in the effluent were the target for regulatory requirements, no further regulations regarding the type or management of water treatment would be required. This, then, is a step on the path from technology-focused guidelines towards fully health-risk based guidelines (World Health Organization, 2011), for which QMRA is essential. Furthermore, Koch recommended a switch to using ground water as raw water supplies in order to take advantage of nature's own filtration system, and he discouraged point-of-use household filters for their unreliability.

Finally, his paper also included the following passage:

> Even with our best filtering arrangements then we cannot keep back all micro-organisms. This too must be attainable, but it would then be necessary to make the rate of filtration much slower even than it is, and perhaps to use thicker layers and other filtering material, all which would involve an enlargement of the works and an increase of expense that would exceed practicable limits. To all appearance we have attained the limit of capability with our present arrangements.

Much progress has been made since Koch's times in controlling pathogens in drinking water; rapid sand filtration largely took over for slow sand filtration and dedicated disinfection processes represent the main barrier in modern water treatment plants. However, it remains true that we cannot remove all microorganisms from drinking water everywhere and at all times. Koch's quote recognizes that microbial risks must be balanced with the cost of abatement, but only now, more than a 100 years later, are we beginning to apply risk assessment principles to address these issues in a systematic and quantitative way. This thesis attempts to make a contribution to that end.

1.2 Pathogens in drinking water: Epidemiology and regulations

1.2.1 Pathogens of concern

Waterborne pathogens (Leclerc et al., 2002) are pathogenic microorganisms that primarily use water as a vehicle of transport to reach and infect their hosts. Traditionally, the main concern for drinking water are waterborne pathogens that are transmitted by the fecal-oral route (*enteric* pathogens), i.e. they are shed in the feces of an infected host and transmitted through the aquatic environment and engineered facilities to reach a point of possible exposure. In addition, there is now increasing concern about *environmental* pathogens, such as *Legionella*, that may grow and multiply outside a host (Ashbolt, 2015).

The important groups of pathogenic microorganisms in drinking water are the following:

Bacteria are prokaryotic uni-cellular organisms of varying shape, typically a few micrometers in size. They multiply by binary fission and some may grow outside their hosts. Some have the ability to form endospores, a highly resistant dormant stage.

Viruses are nucleic acids (DNA or RNA) contained in a protein capsid, sometimes with a lipid envelope outside the capsid. They are small and have various shapes, typically 20-300 nm. They have no metabolism and cannot reproduce outside their host. Most have a lytic life cycle; they infect a host cell, reproduce within the cell and then lyse the cell to release the virus particles.

Protozoa are eukaryotic uni-cellular organisms several times larger than bacteria. They typically display two distinct life-cycle stages; an active, reproductive stage and an environmentally resistant dormant stage (cysts/oocysts). It's the cysts/oocysts that are excreted with feces and may subsequentally be ingested by new hosts. They multiply by binary or multiple fission.

Helminths are also known as parasitic worms and are multicellular organisms typically visible to the naked eye. They produce eggs (ova) that are environmentally resistant.

Table 1.1 on the facing page gives an overview of the pathogens in these groups that are known to be transmitted through drinking water, along with a qualitative evaluation of some important properties. In recent years, the main focus has been on protozoa and viruses (Gibson, 2014) as these tend to be environmentally persistent, are more resistant to chlorine disinfection and are quite infective. They are also frequently associated with waterborne outbreaks (Section 1.2.2). There are regional differences in importance, and helminths in drinking water is usually not an issue in developed countries. Some of these pathogens are host-specific, while others have the ability to infect both animals and humans (*zoonotic* pathogens).

Infection is identified with a pathogen succeeding in multiplying within a host, and may be symptomatic or asymptomatic. Common symptoms of infection by the pathogens in Table 1.1 include those associated with acute gastrointestinal illness (AGI) such as diarrhea, vomiting and abdominal pain, which are typically self-limiting in healthy adults. However, some pathogens can cause more serious illness and death if an infection is left untreated, in particular in children and immunocompromised individuals (Gerba et al., 1996a). Globally, it

Table 1.1: Pathogens known to be transmitted through drinking water; adapted from *Guidelines for Drinking-water Quality*, World Health Organization (2011), in which further specification of these qualitative characterizations may be found.

Pathogen	Health significance	Persistence in water supplies	Resistance to chlorine	Relative infectivity	Important animal source
Bacteria					
Burkholderia pseudomallei	High	May multiply	Low	Low	No
Campylobacter jejuni, C. coli	High	Moderate	Low	Moderate	Yes
Escherichia coli – Pathogenic	High	Moderate	Low	Low	Yes
E. coli – Enterohaemorrhagic	High	Moderate	Low	High	Yes
Francisella tularensis	High	Long	Moderate	High	Yes
Legionella spp.	High	May multiply	Low	Moderate	No
Leptospira	High	Long	Low	High	Yes
Mycobacteria (non-tuberculous)	Low	May multiply	High	Low	No
Salmonella Typhi	High	Moderate	Low	Low	No
Other salmonellae	High	May multiply	Low	Low	Yes
Shigella spp.	High	Short	Low	High	No
Vibrio cholerae	High	Short to long	Low	Low	No
Viruses					
Adenoviruses	Moderate	Long	Moderate	High	No
Astroviruses	Moderate	Long	Moderate	High	No
Enteroviruses	High	Long	Moderate	High	No
Hepatitis A virus	High	Long	Moderate	High	No
Hepatitis E virus	High	Long	Moderate	High	Potentially
Noroviruses	High	Long	Moderate	High	Potentially
Rotaviruses	High	Long	Moderate	High	No
Sapoviruses	High	Long	Moderate	High	Potentially
Protozoa					
Acanthamoeba spp.	High	May multiply	High	High	No
Cryptosporidium hominis/parvum	High	Long	High	High	Yes
Cyclospora cayetanensis	High	Long	High	High	No
Entamoeba histolytica	High	Moderate	High	High	No
Giardia intestinalis	High	Moderate	High	High	Yes
Naegleria fowleri	High	May multiply	Low	Moderate	No
Helminths					
Dracunculus medinensis	High	Moderate	Moderate	High	No
Schistosoma spp.	High	Short	Moderate	High	Yes

has been estimated that unsafe drinking water, sanitation and lacking handwashing practices contribute about 3.5 % of the total DALY (disability adjusted life years) burden of disease (GBD 2013 Risk Factors Collaborators, 2015), most of which occur in developing countries. However, even developed countries continue to face challenges with hygienic water quality, as discussed below, and climate change may intensify these challenges (Hunter, 2003; Semenza et al., 2012; Sterk et al., 2013).

1.2.2 Epidemic and endemic waterborne disease

In spite of advances in protecting drinking water from microbial contamination, waterborne disease still occurs in developed countries. The massive *Cryptosporidium* outbreak in Milwaukee, USA, in 1993 (Mac Kenzie et al., 1994), with approximately 400 000 cases and 100 deaths, is often taken as a case in point. However, the total disease burden is composed of cases associated with small and large outbreaks as well as the *endemic* disease burden, i.e. the "background" incidence of waterborne disease. The latter is extremely challenging to estimate (DeFelice et al., 2015; Murphy et al., 2014; Roy et al., 2006), but it is generally recognized that

the case numbers derived from detected outbreaks substantially underestimates the total case numbers (Ford, 1999). In the following, some evidence on the occurrence of disease associated with drinking water in Norway and the Nordic countries is reviewed.

Outbreaks in Norway and the Nordic countries

In Norway, several outbreaks of serious waterborne disease (typhoid fever, shigellosis, hepatitis A) occurred until the mid 20th century, after which drinking water quality improved (Nygård et al., 2003). Since the turn of the millennium, there have been two major drinking-water related outbreaks in Norway. In 2004, the city of Bergen experienced an outbreak of Giardiasis which resulted in 1253 laboratory-confirmed illness cases, more than 2500 receiving treatment and an estimated 5000-6000 cases overall (Eikebrokk et al., 2006; Nygård et al., 2006; Wensaas, 2011). Several patients reported long-term fatigue (Wensaas, 2011). The source of the outbreak was identified by Eikebrokk et al. (2006) as leaking sewers that contaminated surface raw waters.[4] Drinking water treatment at the time consisted only of straining and chlorine disinfection that was ineffective against *Giardia* cysts. After the outbreak, the treatment plant was upgraded with UV-disinfection and coagulation-filtration. In 2007, an outbreak of Campylobacteriosis occurred in the town of Røros (Jakopanec et al., 2008), with illness confirmed in about 1500 of the 3600 persons served by the municipal waterworks. The water was drawn from a well-protected, but untreated groundwater source and it was suspected, but not confirmed, that the distribution system was contaminated during a low-pressure event in the vicinity of a slaughterhouse.

In addition to these two major outbreaks, smaller outbreaks occur every year in Norwegian drinking water supplies, in particular in those systems which serve such a small number of persons as to not require public registration (Folkehelseinstituttet, 2014; Guzman-Herrador et al., 2015; Kvitsand and Fiksdal, 2010; Nygård et al., 2003; Stenström et al., 1994). Any infectious disease outbreak in Norway that is suspected to be associated with food or drinking water shall be reported to the Norwegian Institute of Public Health (*Norwegian Surveillance System for Communicable Diseases*). Kvitsand and Fiksdal (2010) compiled the available outbreak data for the period 1984-2007 and found that there had been registered 102 outbreaks with 17 243 disease cases, of which 50 outbreaks and 11 643 cases could be identified as stemming from surface water supplies. The proportion of outbreaks and cases associated with groundwater corresponded roughly to the number of groundwater works and people served by groundwater works, respectively. Norovirus, *Campylobacter* and *Giardia* (due to the Bergen outbreak) were the most common etiologic agents in those outbreaks where the agent was identified (60/120 outbreaks).

Guzman-Herrador et al. (2015) compiled outbreak data for all the Nordic countries (Denmark, Finland, Norway and Sweden) for the period 1998-2012 (for Sweden 1998-2011) in an update of previous work by Stenström et al. (1994). Denmark is distinguished with having fewer outbreaks compared to the other Nordic countries, due to the high proportion of municipal water works using ground water as their raw water source. The data for Finland, Norway and Sweden show that the countries are somewhat similar with respect to the number of outbreaks, number of cases, seasonality (more outbreaks in the summer season) and etiology.

[4] This conclusion appears to survive (Robertson et al., 2015) recent claims that dog faeces in the recreational area surrounding the water source was the cause of the outbreak (Landvik, 2015).

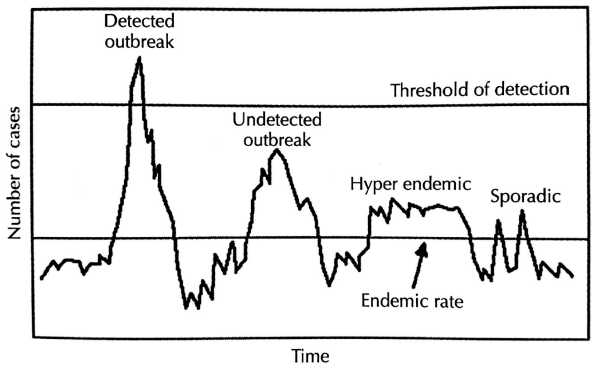

Figure 1.1: Conceptual relationship between epidemic and endemic waterborne disease. From Haas et al. (2014), adapted from Frost et al. (1996).

Norovirus and *Campylobacter* caused the largest number of outbreaks, while *Cryptosporidium* and *Giardia* caused few, but large outbreaks and affected many people.

Several large outbreaks have occurred in the Nordic region. In 2010 Östersund, Sweden, experienced the largest ever *Cryptosporidium* outbreak in Europe (Widerström et al., 2014) with about 27 000 cases. In 2008 Lilla Edet, Sweden, experienced a large norovirus outbreak, affecting approximately 2400 persons (Ekvall, 2010; Larsson et al., 2014). In 2007 Nokia, Finland, contamination of the distribution system led to an estimated 8453 illness cases from a range of pathogens (Laine et al., 2011). It is of interest to note that, in the study by Guzman-Herrador et al. (2015), in only a few cases could the outbreaks be classified as "strongly associated" with drinking water according to the classification scheme of Tillett et al. (1998), pointing to the difficulties of correctly quantifying the number of people affected by waterborne pathogens through drinking water, as well as identifying the precise causes of each outbreak.

Endemic waterborne disease

As already mentioned, it is believed that registered outbreaks are only the tip of the iceberg (Figure 1.1) of the total number of disease cases associated with drinking water in the developed world. Since AGI symptoms are frequently mild and self-limiting, people are not likely to seek medical attention and thus cases are under-reported. Furthermore, even if a case is registered with the health care system, it is often difficult to identify the etiologic agent, let alone identify drinking water as the source of exposure. Hence, more sensitive methods than disease surveillance are needed in order to estimate the total number of waterborne disease cases (Murphy et al., 2014). In the United States, the Environmental Protection Agency (USEPA) and Center for Disease Control have been required to develop a national estimate of the incidence of waterborne disease in community water supplies. The results of concerted efforts were published in a special issue of the *Journal of Water and Health* (Calderon et al., 2006) and by Reynolds et al. (2008).

Using data from household intervention trials such as the well-known studies by Payment et al. (1991) and Payment et al. (1997), Colford et al. (2006) estimated the US incidence of AGI to be between 4.26 - 11.69 million cases/year (surface water: 2.93 - 7.81 million cases/year). This was based on an assumption of 0.65 cases of AGI per person/year, of which 12 % was attributed to drinking water, along with further assumption on raw water quality and treatment regimes. Messner et al. (2006) assumed a distribution of AGI incidence among water

utilities and estimated the mean AGI incidence attributable to drinking water (surface and ground water) as 0.06 cases/person/year with 95 % credible interval of 0.02-0.12 (translating to a point estimate of 16.4 million cases each year). Reynolds et al. (2008) applied crude QMRA principles and estimated 18.4 cases of illness per year, including non-gastrointestinal illness. All these estimates are to be compared with the number of annually registered outbreak cases in the US, which has typically stayed below 10 000 cases/year throughout the 20th century (Craun et al., 2006). Major uncertainties notwithstanding, it seems safe to conclude that the endemic incidence is indeed much higher than the incidence associated with outbreaks.

No such studies to develop a national estimate have been undertaken in Norway. A naive application of the US estimates of the ratio of endemic to outbreak cases (roughly 100 - 1000), leads to an estimated 70 000 - 700 000 illness cases in Norway per year, using 700 registered illness cases/year from Guzman-Herrador et al. (2015). Possible differences in ground water vs. surface water use, source water quality, size of water systems, climate, treatment regimes and population-specific factors, leave such an estimate highly uncertain.

Kuusi et al. (2003) conducted a nation-wide retrospective survey (3000 participants, 61 % response rate) to investigate the incidence of AGI in Norway. They found an incidence rate of 1.2 cases/person/year, higher than the rate used for the US estimates, but the authors warn against possible biases of their study. No attempt was made to estimate the proportion of AGI attributable to drinking water, but a crude analysis of risk factors identified private water supplies as a risk factor and chlorinated water as protective in children younger than 15 years old.

The studies on outbreaks and endemic disease referred to above have only made crude estimates of the disease incidence attributable to source water quality/treatment on one hand and contamination of distribution systems on the other hand. Nygård et al. (2007)[5] found a 1.6 times increased risk of AGI in populations exposed to low-pressure episodes in the distribution system as compared to unexposed populations, and there was an association between the amount of water ingested and the incidence of AGI. Tinker et al. (2009) found a moderate positive correlation between residence time in a water distribution network and emergency department visits for AGI, suggestive of contamination of the distribution system with pathogens.

Although case numbers provide a starting point for the analysis of drinking water related disease and its societal impact, a more complete analysis must take into account measures of disease burden (Rice et al., 2006), such as the DALY, and the associated economic cost to society of this burden. However, the economic valuation of costs associated with disease is not straightforward (Haas et al., 2014, chap. 11). Costs include not only direct healthcare costs (Collier et al., 2012), but also the costs associated with loss of work days, loss of leisure time, and in some cases permanent disability or even death. The availability of cost estimates are more or less restricted to data from outbreaks. As an example, the 1993 *Cryptosporidium* outbreak in Milwaukee (400 000 cases) was estimated to cost $96.2 mill. (1993 dollars), of which two thirds was associated with loss of productivity (Corso et al., 2003) and one third with medical treatment. The 2008 norovirus outbreak in Lilla Edet, Sweden (2400 cases), was estimated to cost SEK 8.7 mill. (83 % due to lost productivity), but this included management costs in the municipality. *Cryptosporidium* causes more serious disease than norovirus, but accounting crudely for inflation and exchange rates, these estimates are actually similar on a per-case-basis.

[5]This study was also reported by Wahl (2005).

1.2.3 Evidence on the role of filtration

Besides disinfection processes (chlorine, ozone, UV-irradiation), filtration is considered the major pathogen-eliminating unit process in drinking water treatment. Rapid sand filtration is part of most larger water treatment plants world-wide, serving approximately 2 million people in 185 water utilities in Norway (Myrstad et al., 2015). It began taking over for slow sand filtration during the early 20th century. The first Norwegian rapid filtration plant was commissioned in Sarpsborg in 1913, using alum for coagulation and sedimentation before filtration (Johansen, 2004). In contrast, the capital, Oslo, didn't receive a filtered water supply until 1994 (Skullerud treatment plant) and 2008 (reconstructed Oset treatment plant), although its water was chlorinated since 1930 (Johansen, 2001).

We will return to pathogen removal capacities of deep-bed filtration in Chapter 3. Here we will review some studies that may provide some direct evidence of the role of filtration in preventing waterborne disease, as in the historical example from Hamburg given in section 1.1. Logsdon (1982) gave several examples from the early days of slow and rapid sand filtration, showing how reductions in typhoid fever cases coincided with the introduction of filtration in the water supply. Cutler and Miller (2005) used regression modeling in an attempt to isolate the contribution of filtration and chlorination to the reduced mortality in early 20th century United States. They estimated that the introduction of filtration reduced overall mortality by 16 %, infant mortality by 43 % and child mortality by 46 %. Lower effects were found for chlorination, which must be attributed mainly to the fact that introduction of filtration usually preceded chlorination in treatment plants.

In today's developed world, with generally better protection of drinking water supplies and lower incidence of disease, it is challenging to demonstrate links between filtration/filtration performance and endemic disease. However, some data exist. Finished drinking-water turbidity is highly influenced by the filtration process, and while no simple relationship between turbidity and pathogen content exists, increases in filter effluent turbidity is generally associated with increases in microorganism content (Huck et al., 2001). For example, the Milwaukee *Cryptosporidium* outbreak occurred during a period of unusually high effluent turbidity from one of the filtration plants in the city (Mac Kenzie et al., 1994).

Mann et al. (2007) reviewed time series studies that investigated associations between daily mean plant effluent turbidity and reported cases of AGI. They found five studies that met their quality-criteria for inclusion. Three of these studies found moderate associations between turbidity and incidence of AGI (Gilbert et al., 2006; Schwartz et al., 2000; Schwartz et al., 1997), while two didn't (Lim et al., 2012; Morris et al., 1998). After the Mann et al. (2007) review, Tinker et al. (2010) found no association. In an unfiltered water supply, Hsieh et al. (2015) recently found a weak association during spring season, especially for young children. It should be noted that correlating plant turbidity and AGI incidence in the population served by the plant is extremely challenging (Sinclair and Fairley, 2000), with issues such as accounting for lags due to incubation times and distribution system transport time. Taken together, the relationship between turbidity and AGI incidence is far from clear.

Another line of data on the effect of filtration on AGI disease stems from changes in community AGI incidence after upgrading treatment plants to include filtration, so-called community-intervention studies (Calderon and Craun, 2006). Upon introduction of filtration to the treatment train of a US city's water supply, Frost et al. (2000) found no reduction in *Cryptosporid-*

Table 1.2: Indicator organisms used in the Norwegian drinking water regulations (Drikkevannsforskriften, 2001).

Indicator organism	Regulatory requirement
Clostridium perfringens (incl. spores)	0/100 ml
E.coli	0/100 ml
Intestinal enterococci	0/100 ml
Heterotrophic plate count (HPC)	Should be below 100/ml
Coliform bacteria	0/100 ml

Note: The sampling frequency depends on the size of the water supply.

ium antibodies in the population served, suggesting that filtration didn't reduce *Cryptosporidium* infections, although the authors noted that seasonal variations in infection rates may have confounded the results. McConnell et al. (2001) investigated the change in rates of physicians' requests for stool sample analyses before and after introduction of filtration in 10 water supply systems in Australia. They found no consistent trends in the data, although only descriptive statistics were shown. Frost et al. (2009) investigated rates of AGI in a population before and after introduction of filtration and ozonation to a treatment plant that previously only used chlorination, and found no significant changes.

Finally, in a retrospective observational study in Vermont, USA, Birkhead and Vogt (1989) found a significantly greater incidence of *Giardiasis* in unfiltered water supplies as compared to filtered water supplies. A similar observation was made by Fraser and Cooke (1991) in Dunedin, New Zealand.

In sum, the studies cited above indicate that filtration has the potential to reduce the incidence of waterborne disease when raw water quality is poor and there is no disinfection (as the early 20th century data show), but it is generally more difficult to identify and estimate the effect of filtration in today's environment with better source water protection (due to better waste water management) and abundant disinfection processes in water treatment plants.

1.2.4 Regulations and guidelines

The above review of epidemiological data makes it clear that judgment on the hygienic safety of a water supply cannot be made on the basis of disease surveillance alone. However, routine monitoring of finished drinking water (as well as raw waters) for pathogens remains difficult and expensive, mainly because of the large array of different pathogens and low natural pathogen concentrations relative to analytical methods' quantification limits (Aw and Rose, 2012; Straub and Chandler, 2003). Regulations for microbial drinking water quality have therefore long been based on criteria for the concentrations of faecal indicator organisms in finished drinking water (Saxena et al., 2015). These are non-pathogenic microorganisms that are naturally present in faeces and also amenable to routine analysis. Among the desirable characteristics that an ideal indicator organism should possess, it should be specific to faeces and its survival in the environment should be at least as good as for enteric pathogens. Although no ideal indicator organism has been identified, *E.coli* is considered the best available (Edberg et al., 2000). The Norwegian drinking water quality regulations (Drikkevannsforskriften, 2001), which implement the EU drinking water directive (Council of the European Union, 1998), currently prescribe maximum levels for five categories of indicator organisms (Table 1.2).

There is no doubt that the indicator organism approach has been eminently useful in safeguarding drinking water from microbial contamination. However, it is also clear that it represents an indirect approach to assessing health risks since the correlation between indicator and pathogen concentrations may be poor or non-existent (Harwood et al., 2005), and likely influenced by such things as the local prevalence of AGI and variations in survival and inactivation between indicators and pathogens in both natural water environments and during treatment. The association with bacterial indicators may be particularly uncertain for pathogenic viruses, which tend to be more environmentally resistant than bacteria (Table 1.1 on page 5; Bosch, 1998; Bosch, 2007). Furthermore, pathogens have been found in finished drinking water that meets regulatory microbial indicator standards (e.g. Keswick et al., 1984) and outbreaks have also occurred in systems that meet standards (Hrudey et al., 2006; Mac Kenzie et al., 1994). Wu et al. (2011) analyzed indicator-pathogen correlations from 40 years of research and concluded that no single indicator performed consistently better than others, and that lack of correlations were often associated with small sample sizes. HPCs have not been found to be associated with any elevated health risk from drinking water (Allen et al., 2004; Edberg, 1996; Edberg and Allen, 2004).

Regardless of the extent of association between pathogens and indicators, it has long been recognized (Hrudey et al., 2006) that microbial water quality management must aim broader than simply monitoring the finished end product, i.e. treated drinking water, for the presence of indicator organisms. This is because (1) only a very small proportion of the treated water can feasibly be tested, (2) when indicators are detected in the treated water, compromised water will usually have reached consumers before a boil-water warning can be issued and (3) data from end-point monitoring provides very little guidance in identifying weak links in the water supply chain, i.e. areas where vigilance is required and the potential for risk reduction is the greatest.

One consequence of this recognition is the widespread adoption of the *multiple barrier* approach, which postulates that a water supply system should include several, independent "barriers" against pathogens, of which protection of source waters against contamination may constitute the first barrier. Furthermore, the World Health Organization's (WHO) *Guidelines for Drinking-water Quality* 2011 now advocates the development of comprehensive *water safety plans* (WSP; Davidson et al., 2005). In a water safety plan, the whole water supply system from source water to tap is considered, hazards and critical components are identified, and a monitoring and control program is developed to ensure the integrity of the system as a whole. HACCP (Hazard Analysis and Critical Control Points), a management approach originally developed for the food industry, has thus found its way into the drinking water industry (Damikouka et al., 2007; Havelaar, 1994).

As a regulatory requirement (Drikkevannsforskriften, 2001), any Norwegian surface water supply that serves more than 20 households or 50 persons must include at least two independent hygienic barriers, of which at least one barrier must be located in the water treatment plant. A hygienic barrier shall remove or inactivate pathogens, and dilute, remove or break down chemical and physical substances to such a level that these substances do not represent any health risk. What constitutes a hygienic barrier is defined operationally in the accompanying guidance document to the regulations (Mattilsynet, 2011). To some extent, the Norwegian drinking water regulations implement some of the principles of WSPs. However, the regulations are currently under review and the revised regulations will have an even stronger focus

on hazard identification and risk management, preventive safety measures and preparedness. Furthermore, maintenance of distribution systems will be emphasized. The revision is part of efforts to meet Norway's country specific targets under the United Nations' UNECE (1999).

In addition to official regulations and guidelines, the association of Norwegian water utilities has developed its own tool and guidelines to aid utilities in evaluating the hygienic safety of their water supplies. Formerly known as *Optimal disinfection practice* or *Good disinfection practice* (Ødegaard et al., 2006, 2009), it has been renamed in its latest iteration to *Microbial barrier analysis* and comes in Norwegian (Ødegaard et al., 2016b), English (Ødegaard et al., 2016a) and Swedish (Svenskt Vatten, 2015) versions. It is a simple tool and database to (1) determine the total required barrier, in terms of required $\log_{10}$ pathogen reductions, on the basis of raw water characteristics and size of the water supply, and (2) compute the removal/inactivation throughout the system to verify its hygienic safety and/or determine the final disinfection requirement. It actually incorporates many of the ideas of QMRA, described below, without relying on complicated probabilistic computations or measures of absolute health risk.

The WHO has sought to develop a harmonized framework for risk assessment and management to be used for all of its guidelines relating to water quality; drinking water, waste water reuse and recreational water. The development of this framework was described in an extensive background document (Fewtrell and Bartram, 2001). At the core of the framework is the idea that water-quality targets must reflect health targets and be grounded in sound scientific principles. The current drinking water guidelines (World Health Organization, 2011) implement this idea and promote QMRA as a tool to develop such health-based water quality targets for pathogens.

1.3 Quantitative microbial risk assessment

As a loose definition, *risk* is the potential for an adverse event to happen, i.e. an event that results in the loss of human health or well-being. It has two main dimensions, the *probability* that the event will occur and the *severity* of the event. For infectious diseases, the adverse event of interest is the occurrence of infection (symptomatic/asymptomatic), illness or some measure of disease burden, or even death, due to exposure to pathogenic microorganisms. Quantitative microbial risk assessment, then, is the application of sound scientific principles from diverse disciplines to characterize and *quantify* risks associated with exposure to pathogens, accounting for variability and uncertainty of inputs in the process. Risk *assessment* is typically considered the first component of *risk analysis*, which also includes *risk management* and *risk communication* (Haas et al., 2014).

1.3.1 Overview of QMRA

Historically, microbial risk has been approached by epidemiological methods as well as indicator monitoring. The advantages and limitations of these approaches have been discussed above. QMRA differs from these approaches in several respects; a simple comparison is attempted in Table 1.3 on the facing page. Rather than starting with observations on AGI incidence or faecal indicators in drinking water, QMRA is concerned with modeling the amount of pathogens

Table 1.3: Comparison of approaches to hygienic water quality.

	Indicator monitoring	**Epidemiology**	**QMRA**
Study object	Faecal indicator organisms	Illness (AGI) cases in DW consumers	Prob. of infection/AGI from DW
Approach	Monitor indicators	Monitor/map AGI in DW consumers	Model system from source to tap
Link to illness	Indirect	Direct	Semi-direct
Used in DW regulations	Yes, since early 1900s	No	Only Netherlands
Main benefit	Ease of data collection	Studies the real thing (illness)	Endemic risk, scenario risk
Main limitations	Obscure health significance	Low sensitivity, link to DW obscure	Data requirements, uncertainty

DW - drinking water

in drinking water from source to tap, and then quantifying the health-risk associated with pathogen exposure through dose-response relations. Thus, QMRA aims to provide a rational framework for evaluating epidemic *and* endemic microbial health risks associated with actual *and* hypothetical scenarios for water supply systems, a framework which is needed to inform cost-benefit analyses and ultimately decisions on water quality management (Medema and Ashbolt, 2006). Although QMRA is not without its own methodological problems and data scarcity (Petterson and Ashbolt, 2016), it is equipped to complement knowledge gained from traditional epidemiological and indicator methods.

Microbial risk assessment is a relatively new discipline, and was preceded by risk assessments of other hazards, mainly chemicals. There are important differences between chemical hazards and microbial hazards, including the ability of microbes to replicate/become inactivated, acute exposure and health effects of microbes as opposed to the (typically) accumulated effects of chemicals, and the possibility of secondary cases resulting from direct person-to-person transmission of microbial infections. There have been organized attempts to define frameworks for risk assessment that are tailored to microbial hazards (ILSI Risk Science Institute, 2000; ILSI Risk Science Institute Pathogen Risk Assessment Working Group, 1996; Soller, 2006; Teunis and Havelaar, 1999), but the frameworks laid out for chemical risk assessment (National Research Council, 1983) have largely been retained for microbial risk assessment as well (Haas et al., 2014). Therefore, the risk assessment process is typically divided into four main components, as shown in Figure 1.2 on the next page: Hazard identification, exposure assessment, dose-response assessment and finally risk characterization.

The exact content of each of these components will depend on the purpose of the risk assessment and the data and resources that are available to the risk assessor. Some possible questions that a QMRA may answer, or provide input for, are:

- What concentrations of pathogens can be accepted in drinking water without exceeding a given health risk target?
- Does a certain water supply comply with current guidelines for acceptable health risk?
- How will a proposed treatment upgrade affect the health risks associated with a water supply? Is the upgrade cost effective?

Figure 1.2 on the following page also shows that risk analysis is an iterative procedure: once a risk characterization has been performed, the impact of an actual or proposed management strategy on exposure can be assessed, and updated risk estimates can be computed.

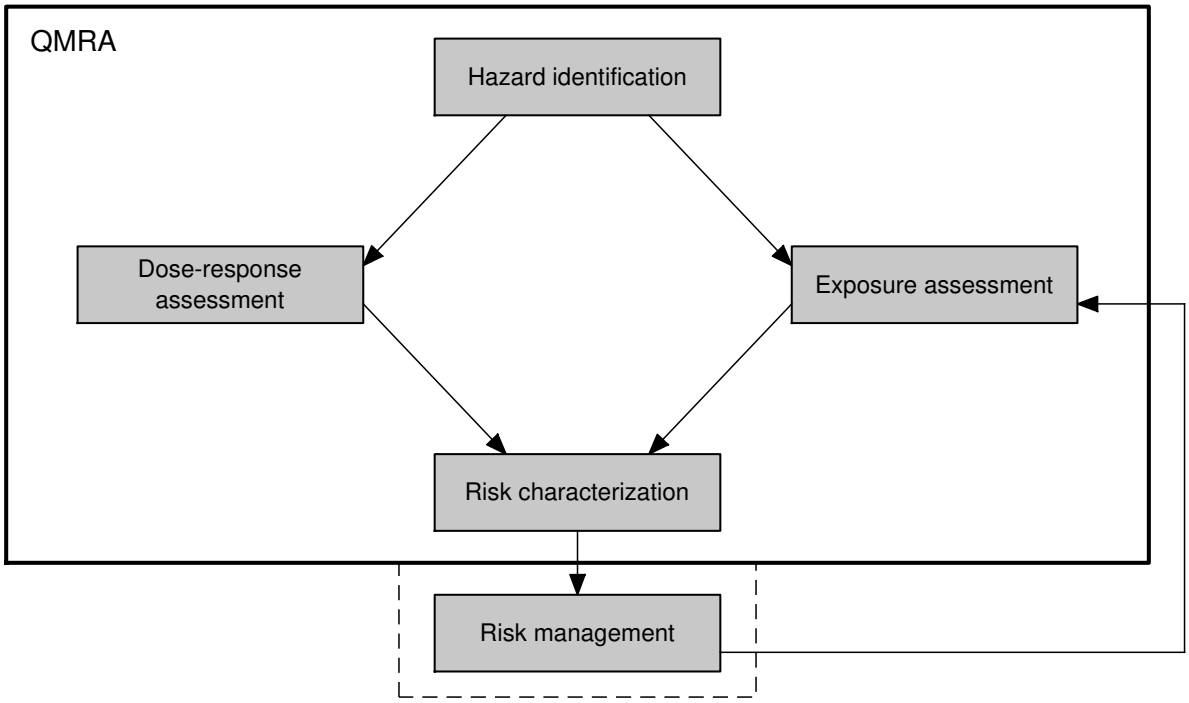

Figure 1.2: Overview of the components in the QMRA framework.

1.3.2 The components of QMRA

Hazard identification and problem formulation

The hazard identification step is largely qualitative and may be conceptually divided in two parts. One part is related to overall biomedical understanding; identifying infectious agents, establishing water as a transmission pathway and identifying health effects in humans. There is an ongoing concern about *emerging* waterborne pathogens (La Rosa et al., 2012; Nwachcuku and Gerba, 2004; Sharma et al., 2003), i.e. pathogens that were previously unknown or assumed not to be waterborne to any significant extent. This first part is a large scientific undertaking and not included in any given site-specific QMRA.

The second part is more site-related and involves selecting pathogens (so-called index pathogens) for risk assessment that are known to be important locally, or for which relevant local data on occurrence in water exists or may be feasibly collected. Often, one pathogen from each of the main groups (bacteria, viruses, parasites) is selected for analysis. This step should be accompanied by a clear problem formulation that may guide the data collection efforts and analysis in subsequent steps.

Exposure assessment

Exposure assessment is where the majority of the effort is expended in a typical risk assessment. While measures of exposure in epidemiology are often categorical, the goal of exposure assessment in QMRA is to quantify the actual number of pathogens (the *dose*) that are ingested through drinking water in the population of interest. There are two main components to consider: the *concentration* of pathogens in drinking water and the *volume* of (unboiled) tap water ingested (Westrell et al., 2006), including variations in these quantities in time or

between different sub-populations. Typically, the pathogen concentrations in finished drinking water are so low as to render monitoring infeasible for all but exceptional cases. The starting point for exposure assessment therefore has to be a point further upstream in the water supply system.

In principle, exposure assessment may draw on the entire body of scientific knowledge on (1) pathogen occurrence in faeces from infected individuals, in waste-water or in source waters (depending on the starting point of analysis), (2) transport, growth, inactivation and removal in waste-water treatment and transport systems (2) transport, growth and inactivation in the natural water environment, (3) removal and inactivation during drinking water treatment, (4) inactivation/growth or intrusion in distribution systems and (5) volume of unboiled water consumed. Expertise from a variety of disciplines is therefore a significant benefit in conducting a successful exposure assessment. The more site-specific data that is available, the better, but more often one has to rely on literature data for most of these steps. Statistical models rather than mechanistic process models are the more common approach to modeling, although there are exceptions (e.g. hydrodynamic modeling; Sokolova et al. (2012)). Often, pathogen-specific data is not available and one has to resort to data from surrogates (Petterson et al., 2016), in particular for modeling removal by treatment (Smeets et al., 2008).

Methods to detect and quantify microorganisms are relevant throughout exposure assessment (Aw and Rose, 2012). These methods come in many forms, but may be roughly subdivided into molecular methods (detection/quantification of nucleic acids), culturing methods (quantifying some observable effect of growth/multiplication of microbes) or direct observation and counting using light- or electron microscopy. Culturing methods confer more information on the viability/infectivity/virulence of the microorganisms, but are not available for all pathogens. Prior to employing these methods, there is often the need to perform a concentration step because the raw samples are too diluted for direct analysis (Ikner et al., 2012). Such concentration steps are prone to inefficiency, i.e. one looses a significant proportion of the microbes during the process, and this *recovery efficiency* may vary between samples. Issues regarding recovery efficiency of concentration procedures, as well as uncertainties in enumeration methods themselves, leave typical microbial concentration estimates uncertain. Quantifying this uncertainty is a central part of the exposure assessment (Emelko et al., 2008; Emelko et al., 2010; Petterson et al., 2015; Petterson et al., 2007; Schmidt and Emelko, 2011; Schmidt et al., 2013a).

Dose-response assessment

The objective of dose-response assessment is to translate doses estimated during the exposure assessment into measures of health risk (FAO/WHO, 2003; Haas, 1983; Teunis, 1997; Teunis et al., 1996). Most QMRA studies take infection (symptomatic or asymptomatic) as the health outcome of interest since data on infection is more readily available than for illness. Illness is then usually modeled as conditional on infection (Havelaar and Swart, 2014; Teunis et al., 1999a). As with many other forms of risk assessment, the doses required to elicit an observable response in a group of people is much higher than the doses that typically are needed for risk assessment. Extrapolation of dose-response curves to low doses is therefore required. In order to justify this extrapolation, QMRA for drinking-water has largely relied on a class of semi-mechanistic dose-response models called *single-hit* models, of which the

exponential model and beta-Poisson model are the prime examples. These models are based on a certain hypothesis about the infection process: Pathogens act *independently* of each other in overcoming host defenses and infection results if *at least one* pathogen is successful in overcoming these defenses. The mathematical properties of these models are the topic of **Paper I** and **Paper II**, and they are treated further in Chapter 2.

Data for dose-response relations are obtained in experimental feeding trials with human volunteers (or sometimes animals) (Teunis et al., 1996) or naturally, during outbreaks (Thebault et al., 2013; Zmirou-Navier et al., 2006). Most site-specific QMRAs will simply retrieve an established dose-response relation from the literature. A large collection of data and fitted models is available at the *QMRA Wiki* of the Center for Advancing Microbial Risk Assessment, Michigan State University. It is important that pathogen concentrations in an exposure assessment are determined using methods that are fairly consistent (and if not, differences should be accounted for) with the methods that were used to quantify doses for dose-response assessment, since estimated dose-response parameters necessarily are specific to the enumeration methods that are used.

Risk characterization

Risk characterization integrates the exposure assessment with the dose-response relation to produce the final risk estimates. In the simplest case, the inputs are point estimates and a point estimate of risk is obtained. It is generally recognized that point estimates are of limited value and that interval estimates or distributions of risk reflecting the uncertainty and/or variability in the input data is much more useful (Haas et al., 2014). Such distributions are typically obtained using Monte-Carlo methods. Disentangling uncertainty from variability is an ongoing challenge in QMRA, and some risk assessments employ so-called *second-order* risk characterization that includes another level of uncertainty, such as uncertainty associated with dose-response parameters (Donald et al., 2011; Pouillot et al., 2004). In some cases, it may also be relevant to incorporate infectious disease transmission models to include secondary cases in the risk estimate (Eisenberg et al., 1996).

1.3.3 Acceptable risk

In order for a risk estimate to be useful, an idea of *acceptable* risk is needed (Haas, 1996a; Hunter and Fewtrell, 2001). The issue of determining a health risk target that is deemed acceptable is complicated, involves ethical as well as economical considerations, and may depend on local circumstances. The USEPA has been using 10^{-4} infections/person/year as an acceptable level of risk from consumption of drinking water (Macler and Regli, 1993),[6] and this has largely been adopted by microbial risk professionals world-wide.

According to Haas (1996a), the USEPA target arose from (1) the observation that the annual reported waterborne disease incidence in the US was roughly 1/10 000, (2) such an incidence was deemed acceptable at the time and (3) using infections rather than illness for the risk target introduced additional conservatism. Endemic disease occurrence was not considered and Haas (1996a) suggests that the risk target may be too stringent. Signor and Ashbolt

[6] It seems to be rarely discussed, but this target is usually applied on a per-pathogen basis, which implies that the acceptable total risk from *all* pathogens is higher.

(2009) recommended a daily risk target instead of an annual as a way to incentivize managers to focus on short-term risks that may often dominate overall risk.

The WHO has defined its risk target in terms of DALYs (Havelaar and Melse, 2003) and recommended a maximum acceptable risk from waterborne disease of 10^{-6} DALYs/person/year (World Health Organization, 2011). The DALY measure sums the contribution from years of life lost due to premature death and the years of life lost due to disability (accounting for the duration and degree of disability for the disease in question). Using DALYs is intended to better capture the burden of disease, allow comparison with non-microbial risks and hence prioritization of public health investments.

1.3.4 Applications and limitations for drinking water

Early applications of QMRA for drinking-water appeared in the US as the USEPA developed standards for drinking-water quality based on health-risk targets (Gerba and Haas, 1988; Haas et al., 1993; Macler and Regli, 1993; Regli et al., 1991; Rose et al., 1991; Rose and Gerba, 1991; Sobsey et al., 1993) and focused on *Giardia* and rotaviruses (Gerba et al., 1996b). Several studies have since been performed for many pathogens, including *Cryptosporidum* (Cummins et al., 2010; Masago et al., 2002; Pintar et al., 2012; Teunis et al., 1997), bacterial opportunistic pathogens (Rusin et al., 1997), Coxsackie virus (Mena et al., 2003; Vivier et al., 2002), adenovirus (Heerden et al., 2005) and norovirus (Masago et al., 2006; Petterson et al., 2013).

Many studies have also been conducted with specific management challenges in mind, such as balancing the risks from enteric pathogens and disinfection byproducts (Ashbolt, 2004; Havelaar et al., 2000), the effect on risk from failures in a drinking water system (Hamouda et al., 2016; Westrell et al., 2003), the effect on risk from closing the drinking water intake during high-contamination events (Åström et al., 2007), the risk from recycling filter backwash water to the plant inlet (Loret et al., 2013), the feasibility, or lack thereof, of monitoring finished water for pathogens to ensure compliance with health risk goals (Signor and Ashbolt, 2006), and the usefulness of online monitoring data for informing a QMRA (Nilsson et al., 2007). Traditionally given less attention in QMRA, distribution systems are increasingly being included in the analysis (Besner et al., 2011; Lieverloo et al., 2007; Teunis et al., 2010; Yang et al., 2011).

Although QMRA guidelines have been published by major agencies (USDA/FSIS and USEPA, 2012; USEPA, 2014; World Health Organization, 2003), it remains a tool that for the most part is used by researchers and not utilities themselves. Conducting a full QMRA for a given water supply is a task that requires a substantial amount of input data, either carefully chosen from the voluminous literature or collected locally with significant effort, as well as the skill and experience to compute risk estimates and interpret the results in light of uncertainties. However, there have been some efforts to make QMRA more available for utilities and managers, demonstrate how it can be useful in practice (Medema and Smeets, 2009; Smeets et al., 2010) and how it can be integrated into the work with water safety plans (Microrisk, 2006).

The Netherlands has been at the forefront of QMRA implementation, with utilities required by regulations to perform a QMRA for selected pathogens on a regular basis (Bichai and Smeets, 2013; Smeets et al., 2009). To assist utilities in this, a software tool was developed (Schijven et al., 2011). Health Canada promotes the use of QMRA in its guidelines and

has developed a simple spreadsheet application intended for utilities (Tfaily et al., 2015). In Sweden, the Swedish Water & Wastewater Association developed a simple software tool for utilities (Lundberg Abrahamsson et al., 2009). In Norway, QMRA hasn't seen much use outside research institutions, although there have been reflections on how it can fit into the Norwegian drinking water management landscape (Fiksdal et al., 2008; Seidu, 2013; Seidu et al., 2007). An EU-financed Scandinavian research project (VISK, 2013) recently focused on the risk of waterborne disease from viruses and obtained data on norovirus and adenovirus occurrence in the river Glomma (Grøndahl-Rosado et al., 2014a; Grøndahl-Rosado et al., 2014b; Petterson et al., 2016) and performed a QMRA case study for the Nedre Romerike Vannverk water supply system (Petterson et al., 2013).

Petterson and Ashbolt (2016) recently reviewed studies that applied QMRA for drinking water, and identified the most important knowledge gaps that limit its use for water safety planning. They characterized the current state of knowledge with respect to fundamental research questions with a subjective grading of 1-4 (1 - high uncertainty, 4 - low uncertainty). The areas that received a grade of 1 were (a) knowledge of the proportion of pathogens excreted by hosts (animal/human) that are viable and human infectious, (b) knowledge on expected log-removal by treatment barriers, for which uncertainties stem from generalizations from surrogate data or site-specific data, (c) knowledge on dose-response relationships, for which uncertainties stem from having few datapoints and the unknown representativity of hosts/strains used in experiments, and (d) knowledge on the conditions for growth of environmental pathogens. Regarding dose-response, one might add the knowledge gap associated with the low-dose extrapolations thath are ubiquitous in QMRA applications, and for which no direct empirical validation is available.

In addition to the above, two of the areas that received the grade 2 were (a) knowledge on causes as well as the frequency and duration of poor treatment performance, and (b) knowledge on the relationship between filter effluent turbidity and filter removal efficiency of pathogens. Regarding the latter, Petterson and Ashbolt noted that this relationship was "[n]ot well characterized for viruses, and [turbidity] may be a completely inappropriate indicator of virus removal performance, depending on process". In a guide to the operation of coagulation-filtration plants in Norway, Eikebrokk (2012) also concluded that more data was needed on virus removal during contact filtration and direct filtration, which is the filtration configuration typically used in Norway.

As briefly laid out below, this thesis aims to contribute to narrowing the knowledge gaps with respect to (1) the structure and mathematical properties of dose-response models, (2) dynamic effects in filtration removal efficiency of viruses and (3) metabolic lags in bacterial growth, possibly relevant for environmental pathogens. A more complete introduction to each of these topics is given in the respective chapters.

1.4 Aims and objectives of the thesis

As emphasized in the introductory sections, most inputs to a QMRA are subject to variation, usually represented by random variables. However, it is not always made explicit exactly what variation these random variables are intended to represent. Rather, probability distributions are often fitted to available data sets with little consideration of the characteristics

of the processes that generated the variation. The variation represented by a random variable is therefore typically the lumped effect of variation in several sub-processes (such as e.g. treatment efficiency of unit processes in a treatment train), each of which may have its own characteristic time and spatial scale. This is not a criticism of such an approach; typically data is simply not available to decompose variation into its constitutive components.

Still, the field of QMRA should strive to do better. The *overall aim* of this work, and a unifying principle among the appended papers, is therefore to sharpen the analysis and data availability with respect to *variation* in some of the QMRA inputs; a better understanding of the sources and scales of variation in the inputs to QMRA will lead to more precise risk estimates and pave the way for more targeted risk management interventions.

As identified in the previous section, the main focus will be on dose-response assessment and virus removal during filtration. The specific objectives of this work may be stated for each of the appended papers:

- **Paper I**: Develop a stringent formulation of the single-hit dose-response model in which variation in pathogen properties, host properties and doses is clearly distinguished from one another.
- **Paper II**: Investigate, in some generality, the effect in single-hit models of having dose-distributions that are overdispersed relative to the default Poisson distribution (i.e. dose variation in excess of Poisson-variation, e.g. as a result of pathogen clustering).
- **Paper III**: Undertake a high-resolution pilot-scale experimental investigation to characterize variation in virus removal efficiency throughout the filter cycle in a coagulation contact-filtration process.
- **Paper IV**: Investigate how the dynamics uncovered in **Paper III** affects risk estimates and whether opportunities exist for optimizing filter operation to minimize risk.
- **Paper V**: Develop a conceptually appealing and numerically tractable model for incorporating microbial lag effects in bacterial growth, which may also be relevant for the growth of environmental pathogens.

The role of the individual papers within the larger QMRA framework is depicted in Figure 1.3 on the next page.

1.4.1 Data and methodological tools

Table 1.4 on the following page gives a brief overview over data and modeling tools that were employed in each paper. These are described more fully in the respective chapters. Only **Paper III** contributes new experimental data; the remaining papers either do not use experimental data (**Paper I**), or use data that were published before (**Paper II**; **Paper V**) or data from **Paper III** (**Paper IV**). Modeling approaches were selected eclectically; in **Paper I**, **Paper II** and **Paper IV** elementary techniques from mathematical statistics were used, **Paper III** uses models from filtration theory while **Paper V** uses delay differential equations coupled with partial differential equation (PDE) models for contaminant transport.

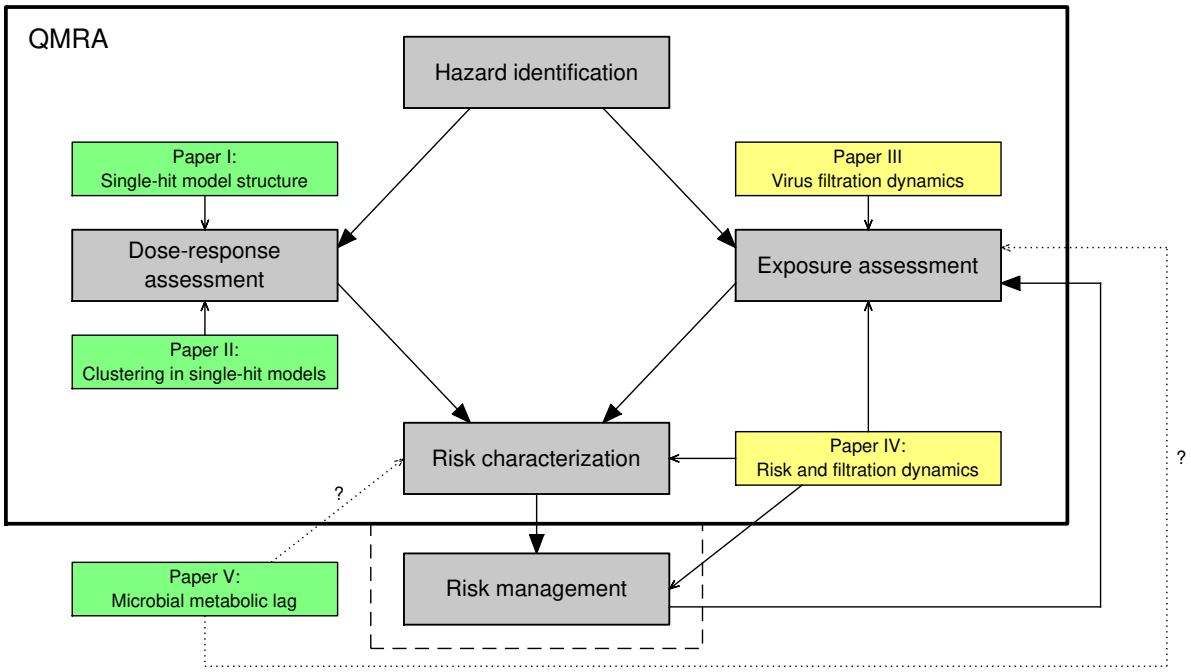

Figure 1.3: The relationship between the appended papers and the individual components of QMRA. Papers in green boxes have been published while papers in yellow boxes are still in a manuscript stage.

Table 1.4: Overview of tools and methods employed in the thesis.

Paper	**Data**	**Models and theory**
I: Single-hit model structure	-	Mathematical statistics Generating functions Jensen's inequality
II: Clustering in single-hit models	Published norovirus dose-response data	Generating functions Jensen's inequality Maximum likelihood est.
III: Virus filtration dynamics	Pilot-scale filtration experiments Plaque assay, RT-qPCR, MPN assay	Colloid filtration theory Coupled PDEs
IV: Risk and filtration dynamics	Data from Paper III	Mathematical statistics Ideas from paper I/II
V: Microbial metabolic lag	Published biodegradation data	Coupled PDEs with delay Linear chain trick Method of lines (num.sol.)

MPN - Most probable number; PDE - partial differential equation
RT-qPCR - Reverse-transcription quantitative polymerase chain reaction

1.4.2 Synopsis of the appended papers

The following is a brief summary of each paper.

Paper I: Single-hit model structure

Dose-response modeling is the link between exposure levels and health consequences and therefore essential to microbial risk assessment. Generally supported by available data, the probability of infection has long been modeled by single-hit models, as briefly defined in Section 1.3.2. **Paper I** is a detailed investigation of the structure and assumptions of these probabilistic models, including the role played by distinct random variables that represent pathogen properties, host properties and dose, respectively. A precise expression for the so-called *single-hit probability* R in terms of these variables is developed, and it is confirmed that only host variation enters into the variation in R. One consequence of this interpretation is that the expression that hitherto has been used in QMRA to compute the risk from multiple exposure events should be replaced by a model-consistent expression, for which the deviation from the conventional expression may be non-negligible in practice. This latter point is important, since it affects annual and lifetime risk estimates that are the basis for regulations and guidelines.

Paper II: Clustering in single-hit models

Although difficult to verify experimentally, there have been speculations in the literature that pathogens may sometimes occur naturally as clusters rather than dispersed pathogens, or that clustering may be promoted during conventional water treatment. Furthermore, clustering was observed in the laboratory for noroviruses during feeding trials for dose-response assessment. Clustering will induce overdispersion in the dose distribution, i.e. greater variance than can be accommodated by the default Poisson dose distribution. **Paper II** therefore investigates, in some generality, the effect of clustering in single-hit dose-response models. It is argued that a so-called stuttering Poisson distribution (also known as a Poisson-stopped sum) is a natural model for the dose-distribution in the presence of clustering. It is shown that, assuming constant mean doses, the risk computed with a stuttering Poisson distribution is less than that computed with a Poisson distribution. A similar result is obtained for mixed Poisson-distributions, which is the other common generalization of dose distributions in QMRA. Finally, a bound on risk is derived from Jensen's inequality that is valid regardless of the nature of the dose-distribution. This bound takes the probability of zero dose as a parameter in addition to the mean dose and appears to be very close to exact computations when there is severe overdispersion. It may also serve as an approximate single-hit dose-response model; this was exemplified by fitting the model to published norovirus dose-response data.

Paper III: Virus filtration dynamics

Rapid sand filtration is usually the most dynamic process in the treatment train with performance varying systematically throughout the filtration cycle. Typically, performance with respect to effluent turbidity improves initially (the ripening phase), then is relatively stable for an extended time period before declining towards the end of the cycle (the breakthrough phase). Most data on microbial removal performance, and viruses in particular, has been

collected during the stable operating phase. The motivation for **Paper III** was therefore to carry out a pilot-scale filtration experiment for viruses with a sampling regime that permits detailed characterization of removal performance during the whole filtration cycle and at different depths of the filter. A purpose-built automatic sampler made the latter possible. The data so obtained may be appropriate for fitting a dynamic filtration model. The results show that, in contrast to turbidity, there was hardly any period of stable operation for viruses (*Salm.* typh. 28B and MS2) and bacteria (*E.coli*) - performance improved continuously throughout the cycle until breakthrough for each organism was reached. This happened mid-cycle for bacteria and slightly before turbidity breakthrough for viruses. Mean log-removal rates during the period when water is usually sent to the consumer were significantly lower than peak removal rates. The study demonstrates the importance of carefully designing sampling regimes in order to correctly estimate microorganism removal efficiencies.

Paper IV: Risk and filtration dynamics

Having established the potential for highly dynamic microbial removal performance in **Paper III**, **Paper IV** is an investigation of how such dynamic effects may impact risk estimates and what opportunities exist for optimizing filter operation. It is shown how the *mean* removal efficiencies of viruses and bacteria develop as the filter-cycle progresses and that the peak in this mean removal rate actually occurs *after* microorganism breakthrough, by mathematical necessity. However, continuing filtration until turbidity reaches the regulatory guideline of 0.2 NTU may be highly detrimental to the mean removal. Finally, it is shown that pathogen concentration variations induced by filtration, assuming otherwise stable plant performance and raw water concentrations, are unlikely to affect the risk estimate as long as the correct mean concentration is used in the dose-response model. However, filtration dynamics *do* represent an additional vulnerability when coupled with other short-term variations in either raw water pathogen concentrations and/or disinfection efficiency.

Paper V: Microbial metabolic lag

The basis for **Paper V** is that bacterial communities may display a lag phase in which growth rates do not follow typical growth kinetics as e.g. Monod kinetics. This phase may be explained by the introduction of a new kind of substrate, which requires adaptation on the part of the bacteria before they can utilize it. **Paper V** is an attempt to model this lag phase by a temporal convolution over the history of substrate concentrations. This is not a new idea, but the integral kernel used in **Paper V** makes it possible to rewrite the integro-differential system of equations as a system of ordinary differential equations through the *linear chain trick*. This facilitates the use of standard integration packages for numerical solution of the resulting equations. The new lag formulation was used with a subsurface transport model for organic compounds that are subject to biodegradation. It was found that the new model could fit the data as well as a previously suggested models, but with fewer parameters. While not presented in a QMRA context, the lag formulation may possibly be useful for modeling the growth of environmental pathogens or incubation times in population disease transmission models, which is also a lag phenomenon for which temporal convolutions have been used.

2. Dose-response for QMRA: Papers I and II

It has been said (Teunis and Havelaar, 2000) that QMRA as a discipline began when Haas (1983) fitted dose-response models to data from experiments in which human volunteers were administered known amounts of pathogens, so-called feeding trials, and extrapolated the models to environmentally relevant exposure levels.

It is not obvious how to construct such dose-response models, though. For infection and illness to occur, pathogens must defeat the host immune system, which comprises a sequence of complex defense mechanisms, some general (*innate* immune system) and some targeted (*adaptive* immune system) towards the specific infectious agent. The detailed workings of the immune system is not explored further here, since it is not required for developing conventional dose-response models. A general overview for gastrointestinal pathogens is given by Duncan and Edberg (1995) and in relation to dose-response theory by Teunis (1997) and Buchanan et al. (2000).

Most dose-response studies focus on infection as the endpoint of interest since infection is a necessary step in the sequence of steps leading to clinical illness; further sequelae is then modeled with probabilities that are conditioned on the presence of infection (e.g. Haas et al. (1993)). Infection is typically defined as the invasion and multiplication of pathogens within the host. In practice, infection is determined by the detection of pathogens in stool samples, elevated levels of antibodies in the host's blood stream or symptoms of illness.

The presence of infection has traditionally been taken as a simple Bernoulli random variable; i.e. either infection is established, with associated probability p_{I}, or it is not. With this approach, no consideration is given to the extent of infection, such as the number of pathogens detected in the stool, or to the time between exposure and detected infection (the host is monitored for pathogen shedding for some time after the exposure). It is not immediately clear that the Bernoulli assumption is appropriate; possibly one should work with graded and timed infections instead. Some references to such work are given in section 2.5.

With the Bernoulli assumption on infection, we may state some general requirements for the dose-response model. Microbes are discrete entities and if we denote the number of ingested pathogens by x, the dose-response model becomes a function $f_{\mathrm{c}}\colon \mathbb{N}_0 \to [0,1]$ that relates the probability of infection to the dose x, $p_{\mathrm{I}} = f_{\mathrm{c}}(x)$. Subscript c denotes "conditional" from terminology introduced by Haas (2002), as opposed to *marginal* dose-response models introduced below.

We may reasonably require $f_{\mathrm{c}}(0) = 0$ (no infection if no pathogens are ingested), $f_{\mathrm{c}}(x_2) \geq$

$f_c(x_1)$ for all $x_2 > x_1$ (larger doses produces at least the same probability of infection as smaller doses) and $\lim_{x\to\infty} f_c(x) = 1$ (as the dose becomes infinitely large, all hosts are infected if there is no complete immunity). As such, the basic characteristics of f_c are coincident with those of the cumulative probability distribution of a discrete random variable with support on the set of positive integers. Usually, there is no possibility of knowing the dose x precisely and we must treat it as a random variable X with support on $\mathbb{N}_0$ and with probability mass function (pmf) p_X. In this case, a *marginal* dose-response model is obtained by marginalizing the discrete dose-response model over X, i.e.

$$p_I = f_m(\lambda_d) = \sum_{x=0}^{\infty} f_c(x) p_X(x) \tag{2.1}$$

Here, $f_m \colon \mathbb{R}_{\geq 0} \to [0, 1]$ is written as a function of the mean of the dose distribution, λ_d.

When searching for a useful model formulation for f_m, two approaches may be discerned (Haas et al., 2014):

1. Select any model that best fits the data, i.e. pure curve fitting (but taking care to avoid overfitting).
2. Select a model from a subset of mechanistically based and biologically plausible models, even if better-fitting models exist.

An advantage of the second approach is that mechanistic models make a clear distinction between the exposure part of the model and the host-microbe interaction part (i.e. a precise identification of f_c is made), while these aspects may be entangled in the first approach where only f_m is explicitly defined. If both parts are reasonable representations of reality, mechanistic models will permit generalizations to other exposure scenarios (other dose levels, other probability distributions for the number ingested) than the one that applied during data collection and parameter fitting. The main disadvantage is that there will typically be models that fit the data better.

In general, the second approach has been deemed preferable for QMRA. The main reason is the need for extrapolating to dose levels beyond regions of data availability. In drinking water applications, we are often concerned with low mean doses, but a very high number of exposed individuals; the net effect may be a significant health impact. Since the effect of such dose levels cannot feasibly be observed in experimental studies with a limited number of subjects, higher dose levels are used and extrapolation to low dose levels is performed. Models that fit the available data equally well may differ markedly upon extrapolation (Haas, 1983). This motivates the use of (semi-) mechanistically based, biologically plausible dose-response models.

The term *infectious dose* is sometimes used in a manner that suggests the existence of a threshold dose, and that ingestion of lower doses than the infectious dose produces no infection. Such concepts are not supported empirically, and there is evidence that ingesting a single infectious pathogen may lead to infection (Section 2.4). The concept of infectious dose should therefore more appropriately be interpreted as the ID_{50}, the dose that produces infection in 50 % of hosts, which may be thought of as a parameter of the pertinent dose-response model. The idea that a single ingested organism may be sufficient to cause infection, and the general agreement with data of models that are derived from this hypothesis, has led to the widespread use of so-called *single-hit* models for microbial dose-response in QMRA. These models are the subject of **Paper I** and **Paper II**, and are introduced below as these papers are presented.

2.1 The structure of single-hit models: Paper I

The fundamental assumption of single-hit models is that pathogens, when interacting with a host, act *independently* of each other in overcoming the host defenses and that infection results if *at least one* pathogen succeeds. In practice this means that a clinically identifiable infection results not from the cumulative effect of several pathogens multiplying, but from the overwhelming multiplication of one of the pathogens contained in the inoculum. Note that this does not imply that several pathogens cannot contribute to an identifiable infection; only that among those pathogens contributing, there will always be one that in itself would have sufficed to make the infection identifiable. While Greenwood and Yule (1917) employed similar ideas in developing statistical methods for the dilution assay[1], Halvorson (1935) and Druett (1952) are credited for introducing the concept in the context of microbial infection in animal-pathogen systems. Kunkel (1934) is being cited for an experimental demonstration in a plant-pathogen system. Similar concepts were also introduced in the context of cancer dose-response (Crowther, 1924; Iversen and Arley, 1950).

Paper I is essentially a detailed review of the structure and properties of single-hit models. In order to introduce them, let r be the probability that a single pathogen establishes infection. Then the probability that at least one pathogen succeeds is the complement to the probability that no pathogens succeed:

$$p_{\mathrm{I}} = f_{\mathrm{c}}(x) = 1 - (1 - r)^x \tag{2.2}$$

If r is variable for some reason, we treat it as a random variable R with probability density function (pdf) f_R and get

$$p_{\mathrm{I}} = f_{\mathrm{c}}(x) = 1 - \int_0^1 (1 - r)^x f_R(r)\,\mathrm{d}r \tag{2.3}$$

This is the general expression for a single-hit model if the dose x is known precisely, and has been termed a *conditional* (Haas, 2002) dose-response model in the literature. If X also varies according to a pmf $p_X(x)$, we get

$$p_{\mathrm{I}} = f_{\mathrm{m}}(\lambda_{\mathrm{d}}) = 1 - \int_0^1 \sum_{x=0}^{\infty} (1 - r)^x p_X(x) f_R(r)\,\mathrm{d}r \tag{2.4}$$

where we assume that we may choose the order of summation and integration freely. The summation in the integrand is, by definition, the probability generating function (pgf) of X, G_X, evaluated at $1 - r$:

$$p_{\mathrm{I}} = f_{\mathrm{m}}(\lambda_{\mathrm{d}}) = 1 - \int_0^1 G_X(1 - r) f_R(r)\,\mathrm{d}r \tag{2.5}$$

This is a general formulation of the single-hit models. A basic review of the properties of pgfs may be found in the appendices of **Paper I** and **Paper II**. Making use of the pgf-formulation was instrumental in arriving at many of the results in these papers. Moran (1954a) and Moran (1954b) asserted that variability in R, as opposed to a constant r equal to $\mathrm{E}(R)$, will make the dose-response curve flatter, a property that is expressed formally in Proposition 1 in **Paper I**.

[1] The dilution assay is performed to quantify the number of organisms in some sample and is essentially dose-response backwards. One observes the response (e.g. bacterial growth in a test tube) and infers the dose.

2.1.1 Separating host and pathogen properties

A key motivation for developing **Paper I** was to identify, in general, the role played by pathogen and host properties in determining the distribution of R. The early single-hit literature appears to have been consistent in interpreting variability in R as representing *host* variability and that pathogen variability is averaged out (Armitage, 1959; Armitage and Spicer, 1956; Moran, 1954b; Peto, 1953). Fazekas de St Groth and Moran (1955), in particular, came to this conclusion after studying a detailed model of host-pathogen interaction.[2] The more recent QMRA literature tends to diverge somewhat on this issue and it has sometimes been implied that variation between pathogen individuals also enters into the variability in R (e.g. Teunis et al., 2008).

In order to study this problem in **Paper I**, random variables were introduced to represent both pathogen and host properties and we precisely defined a probabilistic experiment, whose outcome is described by the dose-response model (**Paper I**, p. 147):

1. Randomly select one host from the population of hosts, i.e. obtain a sample of $\mathbf{S}$, a random vector describing host properties.
2. Take a random sample from the water source; this will contain a random number X of pathogens from the population of pathogens. That is, obtain X samples of $\mathbf{T}$, a random vector that describes pathogen properties.
3. Let the host ingest the water sample.

By applying single-hit assumptions and a sequence of statistical independence assumptions among these variables, one can arrive at a single-hit model formulation in terms of these variables, which will show (**Paper I**, eq. (12)) that the random variable R may be written as

$$R = R(\mathbf{S}) = \mathrm{E}_{\mathbf{T}|\mathbf{S}}[g(\mathbf{S}, \mathbf{T})] \tag{2.6}$$

Here, the interaction function g maps these variables onto $[0, 1]$ and represents the probability that any randomly chosen pathogen individual in a randomly chosen host succeeds in establishing infection. $\mathrm{E}_{\mathbf{T}|\mathbf{S}}$ denotes conditional expectation; hence the pathogen properties $\mathbf{T}$ are integrated out and R represents host variability. No statistical independence assumption between $\mathbf{S}$ and $\mathbf{T}$ is needed. For eq. (2.6) to be directly useful in practice, further specification of g, $\mathbf{S}$ and $\mathbf{T}$ is required; an example was given by Fazekas de St Groth (1955) and in **Paper I**. Ideally, this expression may help facilitate incorporation of measurable properties of pathogens and hosts into parametrized dose-response models (Teunis et al., 2002a,b), in particular as such properties become more experimentally available.

Having established eq. (2.6), the remainder of **Paper I** is concerned with firmly establishing some consequences of the fact that variability in R only stems from host variability, and conveniently formulating the single-hit model in terms of generating functions. Some of the results are briefly reviewed here. In order to use the general single-hit expression in (2.5) in applications, parametrization of X and R is needed. First, it was shown in **Paper I** that a model-consistent representation of complete host immunity in part of the host population is a

[2] The paper by Fazekas de St Groth and Moran (1955) appears not to be cited in the QMRA literature and was not known to us when **Paper I** was developed. Only after our paper was accepted did we become aware of it. Some of our results may be said to be a rediscovery of their results, using a slightly more general approach and modern probability nomenclature.

simple scaling of equation (2.5):

$$p_{\mathrm{I}} = f_{\mathrm{m}}(\lambda_{\mathrm{d}}) = (1-\phi)\left(1 - \int_0^1 G_X(1-r) f_{R,s}(r)\,\mathrm{d}r\right) \tag{2.7}$$

where ϕ is the proportion of immune hosts and $f_{R,s}$ is the distribution of R in the susceptible portion of the host population. We have $f_R(r) = \phi\delta(r) + (1-\phi) f_{R,s}(r)$ where δ is Dirac's delta function. Often, the data used for fitting dose-response models was obtained using subjects that was pre-selected for susceptibility so that the fitted model may not be representative for the whole host population if it is not adjusted for immunity (which rarely seems to be done).

In the following it is assumed that $\phi = 0$. The baseline assumption on X is that it is Poisson distributed (see Section 2.2), which gives

$$p_{\mathrm{I}} = 1 - \int_0^1 e^{-\lambda_{\mathrm{d}} r} f_R(r)\,\mathrm{d}r = 1 - M_R(-\lambda_{\mathrm{d}}) \tag{2.8}$$

where M_R is the moment-generating function (mgf) of R (Moran, 1954b; **Paper I**). Any model on the form (2.8) exhibits low-dose linearity (**Paper I**, p. 154). Two choices for R has dominated in QMRA. Either R is taken to be a constant, i.e. a single point mass distribution, which gives the exponential model

$$p_{\mathrm{I}} = 1 - e^{-\lambda_{\mathrm{d}} r} \tag{2.9}$$

Alternatively, R is taken to have a beta distribution, which has probability density function

$$f_R(r) = \frac{r^{\alpha-1}(1-r)^{\beta-1}}{B(\alpha,\beta)} \tag{2.10}$$

where $\alpha, \beta > 0$ are shape parameters and $B(\alpha, \beta$ is the beta function. Using (2.10) in (2.8), we get Euler's integral representation of Kummer's confluent hypergeometric function ${}_1F_1$ (Abramowitz and Stegun, 1964):

$$p_{\mathrm{I}} = 1 - {}_1F_1(\alpha, \alpha+\beta, -\lambda_{\mathrm{d}}) \tag{2.11}$$

Evaluating ${}_1F_1$ numerically is challenging and something of a research field in itself (Pearson, 2009; Pearson et al., 2015). Moran (1954b) suggested replacing the beta-distribution with a gamma-distribution with a small mean (since the gamma distribution has support on $[0, \infty)$), thereby arriving at the same parametric form that Furumoto and Mickey (1967a,b) derived, using series-expansions, as an approximation to (2.11), known as the approximate beta-Poisson model:

$$p_{\mathrm{I}} = 1 - \left(1 + \frac{\lambda_{\mathrm{d}}}{\beta}\right)^{-\alpha} \tag{2.12}$$

The joint criteria $\beta \gg 1$ and $\beta/\alpha \gg 1$ (as well as keeping λ_{d} small) have been used to delineate a region where the approximation is sufficiently good. These criteria ensure that a Gamma-distributed R has negligible probability mass at values $r > 1$ (Schmidt et al., 2013b). Teunis and Havelaar (2000) showed that parameter estimates using the two variants of the beta-Poisson model tended to be very close, but confidence intervals for the approximate version could exceed the probability of exposure, which is unnatural. Equation (2.12) is unique in the sense that no other distribution f_R than the Gamma-distribution turns equation (2.8) into equation (2.12) (**Paper I**, Proposition 2), which means that (2.12) is not strictly a single-hit model (since the support of the Gamma distribution is the entire positive real line).

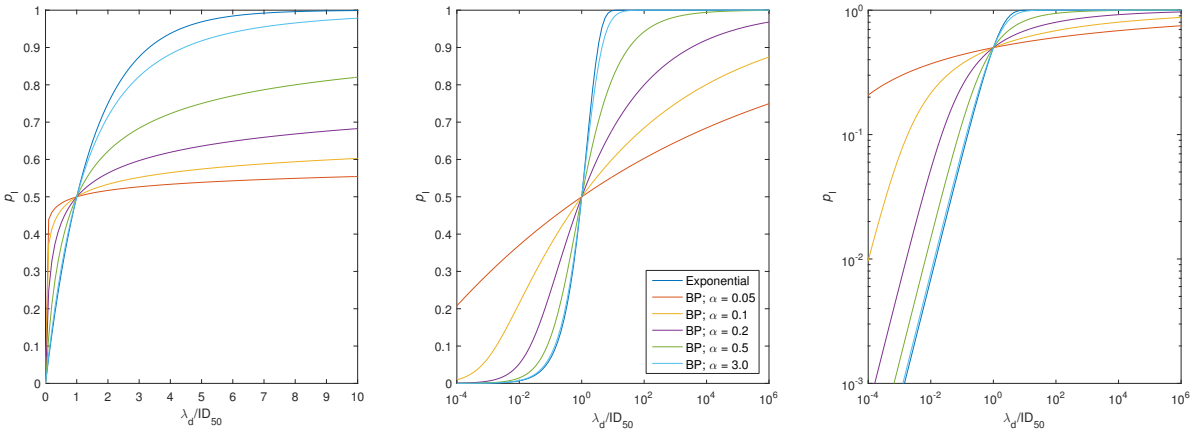

Figure 2.1: Influence of parameter values on the shape of the exponential model and beta-Poisson models in a linear plot, semilog plot and log-log plot. Note that these curves do not share the same value of $\mathrm{E}(R)$.

The exponential and approximate beta-Poisson models may conveniently be written in terms of the ID_{50} by solving $f_{\mathrm{m}}(\mathrm{ID}_{50}) = 0.5$ and eliminating r and β, respectively:

$$p_{\mathrm{I}} = 1 - e^{-\lambda_{\mathrm{d}} \ln 2/\mathrm{ID}_{50}} = 1 - 2^{-\lambda_{\mathrm{d}}/\mathrm{ID}_{50}} \tag{2.13}$$

$$p_{\mathrm{I}} = 1 - \left[1 + \frac{\lambda_{\mathrm{d}}}{\mathrm{ID}_{50}}\left(2^{1/\alpha} - 1\right)\right]^{-\alpha} \tag{2.14}$$

It is easily shown that the slope of (2.14) with respect to λ_{d} is lower than the slope of (2.13), both evaluated at ID_{50}. Some example plots to illustrate the shape of these two models are given in Figure 2.1. Most available human dose-response data can be fitted to one of these two equations and pass a goodness-of-fit test (*QMRA Wiki*; Teunis et al., 1996). Experimental data to support (or not) single-hit models is reviewed in Section 2.4.

2.1.2 Risk from repeated exposures

The most important consequence of the interpretation that R represents host variability, is related to the computation of risk from repeated exposure events. Conventionally, the risk from n repeated exposures (assuming no acquired immunity), each drawn from independent and identically distributed (iid) dose distributions with mean λ_{d}, is computed as

$$p_{\mathrm{I,n}} = 1 - [1 - f_{\mathrm{m}}(\lambda_{\mathrm{d}})]^n \tag{2.15}$$

It was shown in **Paper I**, p. 156-157, that this expression represents the probability of infection if n random hosts each are exposed *once*. Instead, we want the risk when a single random host is exposed n times. The model-consistent expression for this is actually given by

$$p_{\mathrm{I,n}} = f_{\mathrm{m}}(n\lambda_{\mathrm{d}}) \tag{2.16}$$

More generally, the risk from repeated exposures is obtained by interpreting G_X in equation (2.5) on page 25 as the pgf of the *accumulated* dose instead of the single-exposure dose. It was also established in **Paper I** that (2.16) gives smaller risk estimates than (2.15) when R is not a point mass distribution (**Paper I**, Proposition 3).

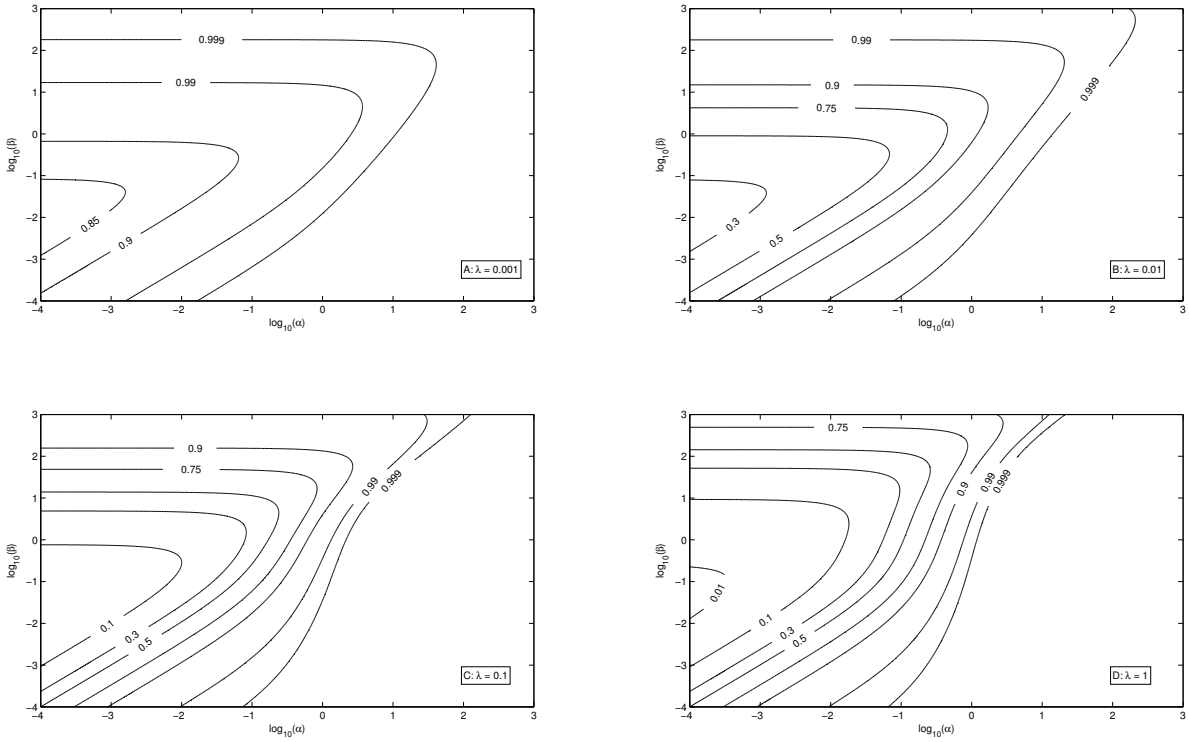

Figure 2.2: Ratio of (2.16) to (2.15) for annual risk estimates ($n = 365$). λ_d is the per-exposure dose and the exact beta-Poisson, equation (2.11), is the dose-response model used. From **Paper I**.

The difference between these two expressions is not merely of academic interest - they play a direct role in the calculation of annual or lifetime risk, for which regulatory or guideline limits have been set (Macler and Regli, 1993; Smeets et al., 2009; World Health Organization, 2011). Figure 2.2 and Figure 2.3 on the following page demonstrate this difference, showing the ratio of risk calculated with (2.16) to that calculated with (2.15), using the exact beta-Poisson as the dose-response model. It is clear that the conventional expression (2.15) is considerably more conservative for some parameter values.

Further exploration is needed to investigate for which pathogens and under what exposure scenarios the difference between these expressions become important in practice. Based on a superficial review of pathogen parameter estimates available at *QMRA Wiki*, most estimates seem to be located in the middle of the plots in Figures 2.2 and 2.3, which means that the difference between eq. (2.16) to eq. (2.15) would be moderate. However, the figures were made by assuming iid Poisson dose distributions for all exposures, and the effect of other dose distributions, including overdispersion, should be investigated. For practical risk characterizations, care should be taken in correctly representing the risk from repeated exposures in Monte Carlo methods.

Finally, in **Paper I**, p. 157-158, it was also established that previous recommendations (Haas, 1996b) on the appropriate way to average microbial concentrations from multiple samples for risk assessment survives even if equation (2.16) is used as a starting point instead of equation (2.15).

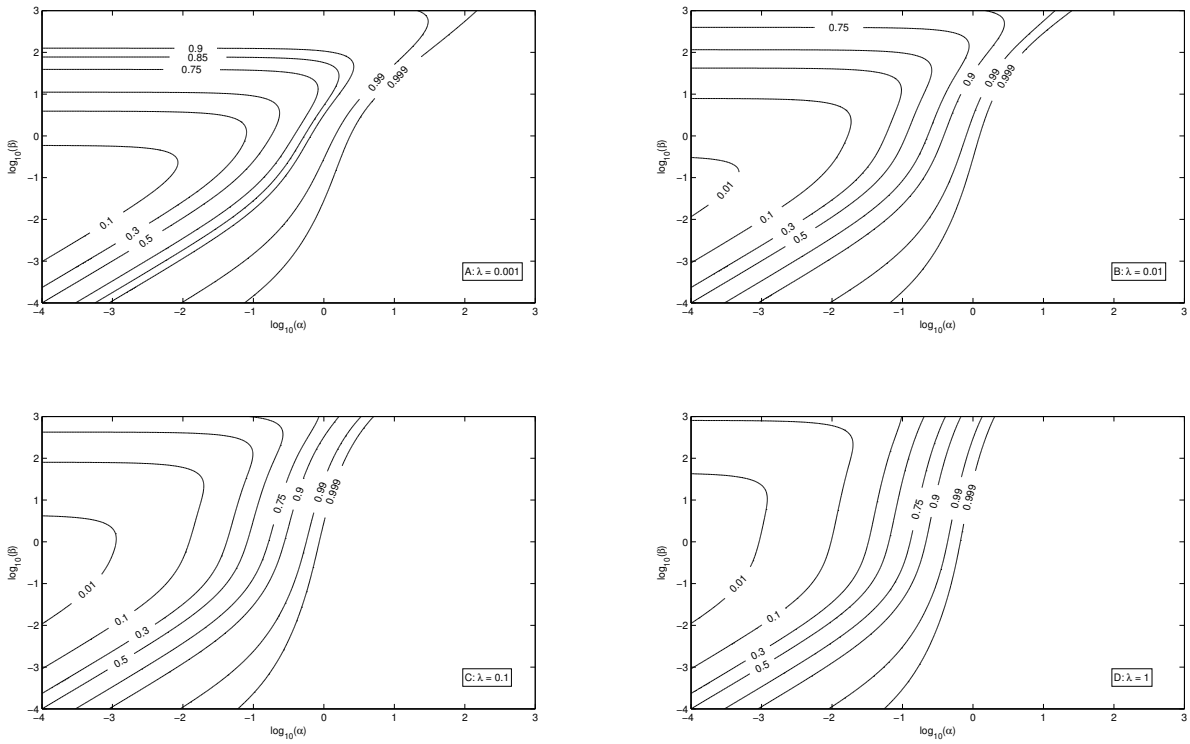

Figure 2.3: Ratio of (2.16) to (2.15) for lifetime risk estimates ($n = 365 \cdot 80 = 29200$). λ_d is the per-exposure dose and the exact beta-Poisson, equation (2.11), is the dose-response model used.

2.2 Single-hit models with overdispersed dose-distributions: Paper II

Until data suggests otherwise, the microbial count X (with support $\mathbb{N}_0$) in a water sample is usually assumed to conform to the Poisson distribution with probability mass function

$$p_X(x) = \frac{{\lambda_\mathrm{d}}^x e^{-\lambda_\mathrm{d}}}{x!} \tag{2.17}$$

and the single parameter $\lambda_\mathrm{d} > 0$. The Poisson distribution is applicable when sampling from a water source in which microbes are fully and randomly dispersed in the water source, i.e. not clustered or systematically concentrated in space or time. For the Poisson distribution, $\mathrm{E}(X) = \mathrm{Var}(X) = \lambda_\mathrm{d}$ and λ_d may be interpreted as the product of microbe concentration in the water source (number of organisms pr. unit volume), c, and the sample volume, v.

2.2.1 Overdispersed microbial count distributions

While the assumption of Poisson-distributed doses is usually adopted in controlled laboratory dose-response studies, it is often observed that environmental microbial counts are overdispersed compared to the Poisson, i.e. the variance is larger than what can be accommodated by the one-parameter Poisson distribution (Haas and Heller, 1988; Schmidt and Emelko, 2011). This may be caused by true deviations from the Poisson distribution or imperfections in enumeration methods, in particular variable recovery efficiencies (Schmidt et al., 2014). If overdispersion is caused solely by temporal variations in microbial concentrations, the Pois-

son distribution may still be appropriate if we restrict the analysis to a fixed point in time; overdispersion may then be modeled as random variation in λ_d, a so-called *mixed Poisson* distribution. The pmf of a mixed Poisson distribution is given by

$$p_X(x) = \int_0^\infty \frac{{\lambda_d}^x e^{-\lambda_d}}{x!} f_{\Lambda_d}(\lambda_d)\, \mathrm{d}\lambda_d \tag{2.18}$$

where f_{Λ_d} is known as the mixing distribution (Gamma or log-normal distributions are common).

However, if spatial variation, i.e. clumping/clustering, is responsible for the overdispersion, the Poisson distribution is not appropriate even if we fix a point in time. Clustering of microorganisms and pathogens is often discussed in many microbiological studies (Gale et al., 1997, 2002; Grant, 1994; Langlet et al., 2007; Silva et al., 2011; Teunis et al., 2005), but it is unclear how common the phenomenon is in drinking water, even though coagulation-flocculation processes are designed to promote particle aggregation. It is also possible that pathogens that are shed with faeces may be introduced into the water environment in an already clustered form, or that multiple pathogens adsorb to a common particle and thereby become clustered. If clustering is present, it can be argued (Haas et al., 2014; **Paper II**; Teunis et al., 2008) that the count distribution is naturally modeled by a Poisson-stopped sum of discrete random variable, whose distribution is called a *stuttering Poisson* distribution:

$$X = \sum_{n=1}^{N_c} A_n \tag{2.19}$$

Here $A_n, n = 1, 2, \ldots$, is a set of iid random variables representing the distribution of cluster sizes, and the number of terms to be summed (i.e. the number of clusters) is a Poisson distributed variable N_c (if $N_c = 0$, we have the empty sum). Under certain conditions the distribution of X in (2.19) is equivalent to a mixed-Poisson distribution, so there is some overlap between the two categories of distributions (Haas et al., 2014). A recursive formula exists for the pmf of X in (2.19) that works with any parametrization of A_n (Kemp, 1967). The corresponding pgf has a simple, explicit expression and is what we need for the single-hit model formulation in (2.5). The details are given in **Paper II**.

Apart from the effect on the dose-distribution, clustering of pathogens draws into question the appropriateness of the independent action hypothesis of single-hit models, since any pathogens that are clustered are likely to encounter host barriers at the same location and same time. Nevertheless, the available dose-response data for norovirus (summarized in **Paper II**) has prompted the application of single-hit models that discard the Poisson assumption (Messner et al., 2014; Schmidt, 2014; Teunis et al., 2008) since some of the inoculum in norovirus feeding trials has been observed in electron microscopy to consist of aggregated viruses. Teunis et al. (2008) considered a negative-binomial dose-distribution, which is both a mixed-Poisson and stuttering Poisson distribution. When the pgf of the negative binomial is used in eq. (2.5) on page 25, along with a beta-distributed R, an integral formulation for Gauss' hypergeometric function ${}_2F_1$ is obtained as the dose-response model:

$$p_I = 1 - {}_2F_1(\lambda_d/b, \alpha; \alpha + \beta, -b) \tag{2.20}$$

Here, b is a dispersion parameter. The numerical evaluation of this function is similarly

challenging as for ${}_1F_1$ (Pearson, 2009; Pearson et al., 2015). Messner et al. (2014) studied a simplified model that assumed hosts were either fully immune or fully susceptible; this obliviated the need to consider the full dose-distribution and only required specification of the mean dose and the mean number of viruses per cluster. Schmidt (2014) showed that the maximum likelihood estimates of the dose-response parameters in these models are poorly identifiable given the currently available data. He also introduced a parameter to represent complete immunity in part of the host population and showed that this can dramatically alter the parameter estimates.

2.2.2 Effect on single-hit risk

The speculation in the literature that clustering of pathogens may occur in water, and the studies on norovirus dose-response, motivated the development of **Paper II**. The goal was to investigate, in some generality, the effect on risk estimates of clustering/overdispersion when incorporated into the dose-distribution of single-hit models. It is emphasized that the independent-action-hypothesis was retained even in the case of pathogen clustering.

The details are left to **Paper II**. The main result is that, in general, compared to using a Poisson distribution with an equivalent mean dose, the single-hit risk estimate is reduced with both stuttering Poisson distributions (**Paper II**, Proposition 1) and mixed Poisson distributions (**Paper II**, Proposition 2). Thus, if the mean dose for an exposure scenario is known with (sufficient) certainty, using the Poisson distribution is conservative in a single-hit framework. This may be convenient since closed form expressions are available in this case, and one can rest assured that further data collection efforts to characterize the dose distribution in greater detail will only contribute to increased precision in the risk estimate, and not conservativeness.

Furthermore, it was shown in **Paper II** that moderate overdispersion in the form of a Hermite distribution (no clusters with more than two pathogens in it; Kemp and Kemp, 1965) is unlikely to significantly affect the risk estimate as long as $\mathrm{E}(R) \ll 1$. In dilute suspension, only moderate clustering seems plausible (Grant, 1994) unless pathogens are introduced into the water in a clustered form. However, extensive overdispersion, which may occur as a result of temporal variations in pathogen concentrations (Englehardt et al., 2012) *will* lead to a marked decrease in the single-hit risk. For this case, the bound presented below may be useful.

2.2.3 An improved upper bound on risk

The risk computed with a Poisson distribution represents an upper bound on risk, as established by Propositions 1 and 2 of **Paper II**. However, at the expense of introducing another parameter (in addition to the mean dose) $p_X(0)$, a better bound can be obtained for highly overdisperse dose-distributions. The following risk bound was derived using Jensen's inequality (**Paper II**, Proposition 3):

$$p_{\mathrm{I}} \leq (1 - p_X(0)) \cdot f_{\mathrm{c}}\left(\frac{\lambda_{\mathrm{d}}}{1 - p_X(0)}\right) \tag{2.21}$$

This bound is valid for any dose-distribution and any *concave* conditional dose-response function f_{c} that can be defined on the whole real line. In **Paper II**, we used f_{c} as defined in eq. (2.3) on page 25 and treated x as a continuous variable. The bound may be sharpened

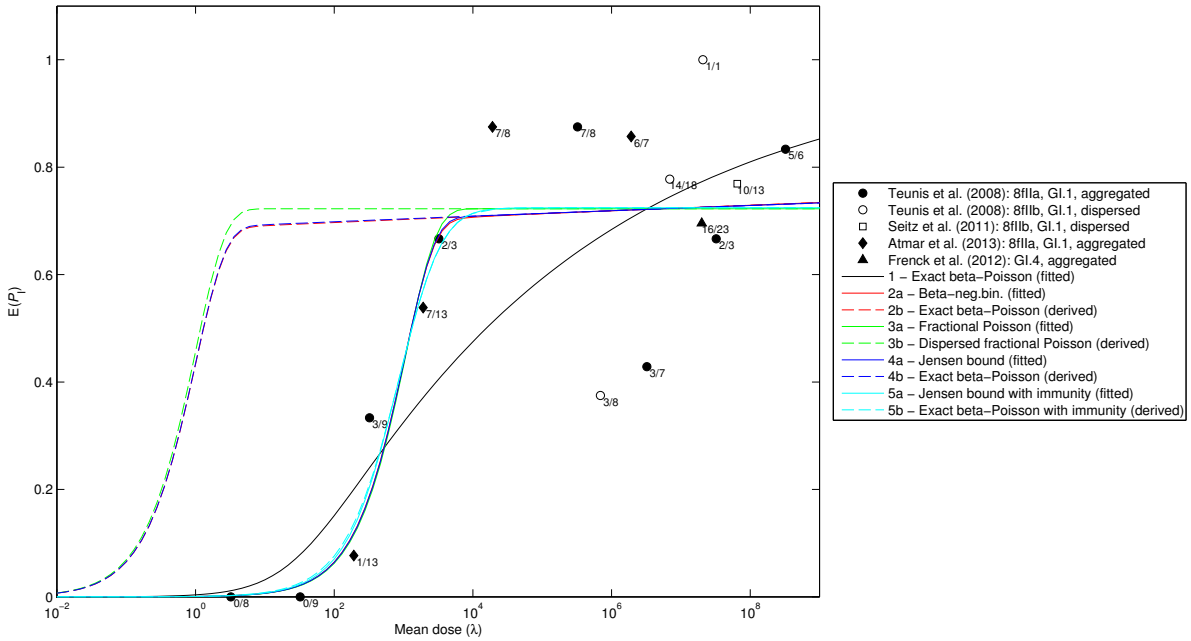

Figure 2.4: Norovirus dose-response data and fitted models. "Derived" models are identical to fitted models, but a dispersion parameter is fixed to a value corresponding to fully dispersed pathogens. The full details are given in **Paper II**, from which this figure is taken.

somewhat by taking f_c in (2.3) as the (continuous) piecewise linear function constructed by connecting the function values at integer x with line segments.

Numerical simulations in **Paper II** showed that the bound in (2.21) tends to be considerably closer to the exact risk estimate, compared to a simple Poisson-model, when there is extensive overdispersion in the dose-distribution. For example, it closely approximated the risk computed with the discrete Weibull distribution (Englehardt et al., 2009; Englehardt and Li, 2011; Englehardt et al., 2012), suggested as a distribution that can model extreme overdispersion in long-term microbial counts in drinking water resulting from e.g. treatment plant upsets. This suggests that the two parameters λ_d and $p_X(0)$ contain the bulk of the information on the dose distribution that is relevant for a single-hit dose-response model. However, for moderately overdisperse dose-distributions the simple Poisson bound may be more precise.

The closeness of the bound to exact risk computations suggests that it may serve as an approximate single-hit dose-response model. This was illustrated by fitting the bound, with beta-distributed R, to the currently available norovirus dose-response data, using maximum likelihood estimation (see next section). Figure 2.4 shows the results. It was found that estimated beta parameters were very similar to those obtained by fitting the beta-negative binomial model in equation (2.20). Similarly to Schmidt (2014), we found that including an immunity parameter in the model has a dramatic effect on the estimated beta parameters, with a reduction in the mean single-hit probability $\mathrm{E}(R)$ of three orders of magnitude. Given that the doses in the feeding trials were determined by qPCR, it seems somewhat unlikely that $\mathrm{E}(R)$ could be close to 0.7 as estimated by the beta-neg.bin. model, since more commonly only a fraction of PCR-units are actually infectious. More experimental data on norovirus dose-response would therefore be valuable, and progress in developing a culturing method for norovirus may lead to better assessment of infectivity in future studies (Jones et al., 2014).

2.3 Model fitting

Data for dose-response assessment stems either from feeding trials or from outbreak data. Regardless of the source, the data will be of the same type. Groups of subjects, indexed by i, will be fed varying levels of mean doses $\lambda_{\mathrm{d},i}$. The total number of subjects is n_i and the number of positive responses (infection, illness) is p_i. A general reference for modeling this type of data, so-called quantal response, is Morgan (1992). Maximum likelihood (ML) methods are typically used to to estimate parameters. The likelihood function is given by the product of binomial likelihood functions, where each factor corresponds to a certain dose level:

$$L(\omega) = \prod_i \binom{n_i}{p_i} [f_{\mathrm{m},i}(\lambda_{\mathrm{d},i}, \omega)]^{p_i} [1 - f_{\mathrm{m},i}(\lambda_{\mathrm{d},i}, \omega)]^{n_i - p_i} \tag{2.22}$$

Here, ω is a parameter vector and we allowed the functional form of $f_{\mathrm{m},i}$ to depend on i. The MLE is given by the value of ω that maximizes L; the binomial coefficient may be dropped in the optimization since it doesn't affect the MLE. It is often convenient to work with the logarithm $\ln(L)$ instead of L. The *deviance* of the model is given by

$$Y = -2 \ln \frac{L(\omega)}{L_{\mathrm{s}}} \tag{2.23}$$

where L_{s} is the likelihood function for the *saturated* model, i.e. a model with one parameter for each data point so that the data is fitted exactly:

$$L_{\mathrm{s}} = \prod_i \binom{n_i}{p_i} \left(\frac{p_i}{n_i}\right)^{p_i} \left(1 - \frac{p_i}{n_i}\right)^{n_i - p_i} \tag{2.24}$$

Maximizing likelihood corresponds to minimizing deviance; numerical optimization is required. There may be several local maxima which warrants care in the numerical search. The curvature of the likelihood surface in the neighbourhood of the MLE is related the confidence interval for the parameter estimates.

Once the MLE has been found, goodness-of-fit may be checked by a likelihood-ratio test (Haas et al., 2014). The null hypothesis of acceptable fit is rejected if the minimized deviance, $Y_{\min}$, exceeds the critical value of the χ^2-distribution with $k - m$ degrees of freedom at the chosen confidence level, k being the number of dose levels in the data and m the number of fitting parameters in the chosen dose-response model. Uncertainty analysis may be performed by likelihood-ratio methods, bootstrapping methods or Markov chain Monte Carlo methods.

2.4 Empirical support for single-hit models

The single-hit concept has historically been contrasted with ideas of a "threshold" or "minimal" dose for infection to be established (Meynell and Stocker, 1957), i.e. a postulate that requires a minimum number of pathogens to be ingested *or* a minimum number to succeed in multiplying before the host suffers an identifiable infection.[3] Threshold hypotheses are also known as

[3] Meynell and Stocker (1957) seem to imply an *ingestion* threshold while the QMRA references (Haas, 1983; Haas et al., 2014) employ models that specify a threshold for the *number of multiplying pathogens*. The latter was used in the supporting material of **Paper II**.

hypotheses of cooperation or synergism. The threshold models have the property that their slope at a dose equal to ID_{50} is steeper than a single-hit model with the same ID_{50} (Haas et al., 2014). Data to support such steeper microbial dose-response relations are almost non-existent[4] (Haas et al., 2014), and practically all available human dose-response can be fitted to the exponential model or the (approximate) beta-Poisson model and pass a goodness-of-fit test (*QMRA Wiki*).

There are other lines of evidence besides generally acceptable single-hit model fits to data. Meynell (1957a) and Rubin (1987) reviewed these and concluded that the independent-action-hypothesis (IAH) is generally supported.[5] First, several authors (e.g. Meynell (1957b) and Meynell and Stocker (1957)) have inoculated test animals (typically mice) with a well-defined mix of bacteria differing only in some marker property and not in their virulence or rate of in-vivo multiplication. Under the IAH it is expected that at high doses, i.e. well above the ID_{50}, the proportion of each marker type recovered post-infection from blood or stools should be similar to the composition of marker types in the inoculum. Furthermore, at doses below the ID_{50}, one expects that one of the marker types in the inoculum will dominate among those recovered post-infection, while under a cooperative infection mechanism one would expect a mix of strains even at doses less than ID_{50}. The single-hit expectations are generally consistent with the observed data for both bacteria and viruses.

A modern test of the IAH along these ideas was presented by Zwart et al. (2009) in virus-larvae systems, using RT-qPCR methods to quantify different genotypes (i.e. markers). They found that the IAH could not be rejected in two out of six host-virus systems studied, but they acknowledged that an oversimplified model, which did not consider host variability and variability in ingested dose, may have contributed to the rejection of the IAH in the other four cases. A subsequent study confirmed that the observations could be reconciled with the IAH if host variability was properly accounted for (Werf et al., 2011). Zwart et al. (2011) tested the IAH in a plant-virus system using similar methods and found that the IAH could not be rejected.

A second line of evidence cited by Meynell (1957a) and Rubin (1987), is the observation that the time course of inoculation of a given total inoculum (i.e total dose) seems to be non-essential to the development of infection. Under a cooperation hypothesis, one would expect the probability of infection to be higher when all of the inoculum is administered instantaneously. Meynell (1957a) also cited observations that the incubation time seems to be dose-independent once the inoculum falls below the ID_{50}, which is consistent with the IAH.

Finally, Rubin (1987) notes that there are observations of the ID_{50} being very low (2-3 organisms) and, of estimated doses in detected drinking water outbreaks being well below the ID_{50}, both of which which go against an hypothesis of cooperation. There have been several (fairly successful) attempts to validate dose-response models that were developed based on data from feeding trials against data from outbreaks, e.g. for E.coli O157:H7 (Haas et al., 2000) and Giardia (Zmirou-Navier et al., 2006). Haas et al. (2014) assert that a Cryptosporidium dose-response model has been validated against the 1993 Milwaukee outbreak (Mac Kenzie et al., 1994).

[4] Though frequently observed in chemical dose-response.

[5] The literature does not distinguish very well between the "one-may-be-enough" hypothesis $f_c(1) \neq 0$ and the real IAH hypothesis $f_c(x) = 1 - (1 - r)^x$ (where the latter implies the first, but not vice versa), and it is really not clear which part of the IAH is being tested, but more often it seems that it is the first of these assertions that is being discussed.

However, recently the IAH has been called into doubt by the increasingly numerous observations of fundamental cooperative behavior among microorganisms (Raymond et al., 2012), in particular for pathogens that cause disease by toxin production. In fact, Cornforth et al. (2015) entitled their paper "Bacterial cooperation causes systematic errors in pathogen risk assessment due to the failure of the independent action hypothesis." They presented an insect-bacteria system in which the bacteria produce a toxin that enhances their ability to cause *septicemia*, i.e. invasion of the blood stream. The interaction of toxins and bacteria produced mortality rates that were inconsistent with IAH assumptions. Furthermore, the authors showed that fitting an IAH model to only high-dose data significantly overestimated the low dose mortality rates in this system.

In summary, the available data is generally consistent with single-hit models, but the lack of data to test the low-dose behavior of models as well as fundamental biological observations of cooperative behavior among some pathogens, signal that future advances in dose-response modeling may involve some modification of the single-hit concept.

2.5 Alternative and extended modeling approaches

Here, some alternative and extended dose-response modeling approaches are briefly mentioned. There have been occasional attempts to use models from chemical dose-response for microbial agents (Kodell et al., 2002; Moon et al., 2004). Examples are the log-logistic, log-probit and Weibull models. These may generally be written

$$p_{\mathrm{I}} = f_{\mathrm{m}}(\lambda_{\mathrm{d}}) = \int_0^{\lambda_{\mathrm{d}}} f_Y(y)\,\mathrm{d}y \tag{2.25}$$

where $f_Y(y)$ is the so-called tolerance distribution in the population of interest (Haas et al., 2014). Unless ${f_{\mathrm{m}}}''(\lambda_{\mathrm{d}}) = f'_Y(\lambda_{\mathrm{d}}) < 0$ for all λ_{d}, these models are convex in part of their domain and therefore resembling threshold-models, which are not well-supported empirically.

Most commonly, morbidity and mortality ratios (the probability of illness and death, respectively, given that infection is already established) have been treated as independent of dose. Teunis et al. (1999a) and Havelaar and Swart (2014) developed models that relaxed this assumption.

Most dose-response studies (experimental and theoretical) disregard the time it takes from inoculation to a response is observed, i.e. the *incubation time*. Some early papers studied this problem as a birth-death process of pathogens (Armitage et al., 1965; Williams, 1965). Haas et al. (2014) assert that the Williams formulation implicitly specifies an exponential dose-response model. More recently, Huang and Haas (2009) incorporated the incubation time in single-hit models by simply making the parameter r (exponential model) or ID_{50} (beta-Poisson model) an explicit function of time. Mayer et al. (2011) and Pujol et al. (2009) developed extended birth-death models that explicitly incorporate immune system responses, and may account for dose-timing effects.

3. Deep-bed Filtration of Viruses: Papers III and IV

Deep-bed filtration (also known as granular filtration, sand filtration, rapid filtration, depth filtration or packed-bed filtration) refers to the retention of suspended and/or colloidal particles by a granular (or fibrous) porous medium as the suspension passes through it, and is a process of interest in many areas of science and engineering (Tien and Ramaro, 2007). For water quality control, the prime examples are sub-surface particle transport (Bradford et al., 2014; Ryan and Elimelech, 1996; Sen and Khilar, 2006) and water and waste water treatment (Hijnen and Medema, 2010; Jegatheesan and Vigneswaran, 2005). There are numerous other applications, including e.g. air-filters and certain types of oil production methods where the goal is typically to *limit* filtration (Alvarez, 2005; Zamani and Maini, 2009).

From the outset we should clearly distinguish granular filtration from membrane filtration, which is also used for particle removal, including viruses (Fiksdal and Leiknes, 2006). In membrane filtration, suspended particles are removed mainly because they are larger than the pores of the filter, i.e. we have removal by straining/sieving. Particle removal during granular filtration, on the other hand, is effected through a range of mechanisms of both physical/mechanical and chemical character, and there is a potential to remove particles that are much smaller than typical pore sizes of the medium. Hereafter, "filtration" is taken to mean deep-bed filtration.

The purpose of this chapter is to put **Paper III** and **Paper IV** in context and present and discuss their main findings. Section 3.1 introduces filtration for drinking water treatment with an emphasis on the Nordic context and summarizes the literature on virus removal in drinking water filters. Section 3.2 reviews removal mechanisms and both fundamental models as well as macroscopic models that aim to capture the dynamic aspects of filtration. Section 3.3 presents the methods and results from the pilot-plant study (**Paper III**) and Section 3.4 presents the results from **Paper IV** on the effect of dynamic filtration effects on risk estimates.

3.1 Filtration for drinking water treatment

Rapid sand filtration became a mainstay of drinking water treatment during the early 20th century. Its main original purpose was to remove particles from the water, including pathogens, but it may also be made effective in removing natural organic matter (NOM) following coagulation. NOM refers to the complex array of organic compounds that is present in natural waters, often dominated by high molecular weight molecules such as humic acids that straddle

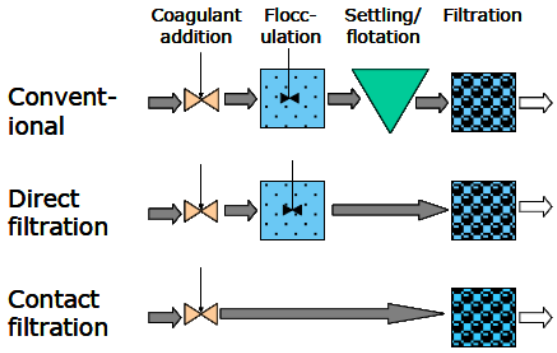

Figure 3.1: Position of filtration in the treatment train. From Ødegaard et al. (2010).

the border between dissolved and suspended matter, but behaves much like colloids during coagulation (Matilainen et al., 2010). Traditionally, NOM was mainly an aesthetic nuisance in that it imparts color to the water, but during the 1970s studies showed that reactions between chlorine and NOM resulted in disinfection by-products (DBP; mainly trihalomethanes) that were carcinogenic (Boorman, 1999). This led to shift a in the drinking water industry, wherein removal of DBP precursors became important. Coagulation-separation processes that target NOM removal in addition to particle removal are often called *enhanced coagulation* (Edzwald and Tobiason, 1999) and typically involves higher coagulant doses and stricter pH-control than is common for particle removal alone. The NOM-content has been observed to be increasing in Norway for several decades (Eikebrokk et al., 2004a).

3.1.1 Design, operation and regulations

In order for filtration to be effective, it is usually necessary to employ *coagulation* as a pre-treatment, i.e. add a chemical (the coagulant) to the water in order to destabilize the particles/NOM and thereby promote particle growth and particle-filter grain attraction. Thus, in designing a filtration process, the filter unit should not be viewed in isolation from its pre-treatment and vice versa (Bache and Gregory, 2010; O'Melia, 1985). The most commonly used coagulants are salts of iron and aluminum, which go through a series of hydrolyzing reactions when added to the water. Often, pre-hydrolyzed versions of these salts are used, partly because they consume less alkalinity (Ødegaard et al., 1990). The mechanisms by which the coagulant destabilizes the NOM/particles are complex (Amirtharajah and Mills, 1982), but are usually categorized as (1) adsorption of positively charged metal species on negatively charged particles ("adsorption-charge neutralization"), (2) enmeshment of particles/NOM in large amorphous metal precipitates ("sweep coagulation"), (3) compression of the diffuse part of the electric double layer and (4) bridging of negatively charged particles by positively charged polymeric metal species. Among these, the third mechanism is typically less important in water treatment, but it may be difficult to identify the relative contribution of each.

Coagulation-filtration comes in several configurations, as shown in Figure 3.1. The conventional setup is used for waters that are high in suspended solids. It includes a flocculation step to promote particle aggregation into larger *flocs* and then a sedimentation step (or in some cases, flotation) before filtration. For waters that are lower in suspended solids, the sedimentation step may be dropped (direct filtration) or both flocculation and sedimentation

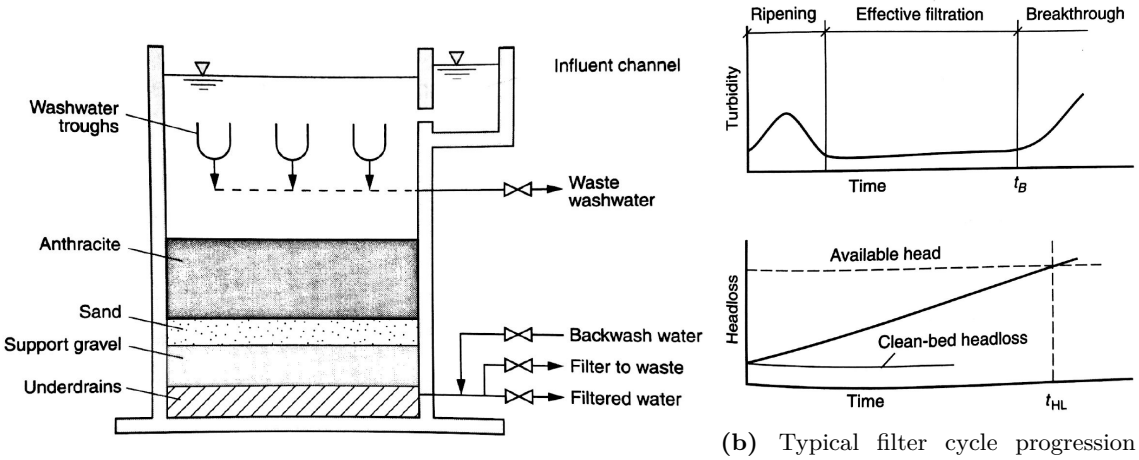

(a) Typical filter design.

(b) Typical filter cycle progression (ripening period not to scale).

Figure 3.2: Typical filter design and filter cycle progression. From Crittenden et al. (2005).

may be dropped (contact filtration). In the latter case, flocculation may instead occur to some extent in the pores of the filter. Direct and contact-filtration are the more common configurations used in Norway, where raw waters are usually low in turbidity and medium to high in NOM-content (Ødegaard et al., 2010; Ødegaard et al., 1999). The efficiency of the filtration process depends on the suspension to be filtered (particle size, density and surface charge properties), the filter media (grain size and surface charge properties) and operational conditions (coagulation, filtration rate, filter depth etc.). Rapid mixing of the coagulant with water is usually important (Amirtharajah and Mills, 1982; Vrale and Jorden, 1971), but possibly less so for the contact filtration configuration (Eikebrokk, 2012). Filter design is generally based on practical experience and/or pilot testing, although it has been suggested that more rational design methods may now be possible (Lawler and Nason, 2006).

Figure 3.2a shows a typical filter design. The more common situation is to have the filters operating in downflow mode with two or sometimes three[1] different filter media. The top layer has coarser grains with lower mass density and the bottom layer has finer grains with higher mass density. The size gradient is there to promote utilization of the entire filter bed and the density gradient ensures that the layering stays the same after backwashing. The filter bed rests on a foundation of gravel that protects the underdrains, and there are systems to control the flow of water, backwash water and backwash air (if used). A filter will usually have to be backwashed with an interval of 12-36 hours. A water treatment plant usually contains at least two filters, connected in hydraulic parallel, so that water production can continue when one filter is being backwashed. Unless there is advanced flow-control systems, this will usually lead to an increased hydraulic load for the filters that are not being backwashed, which may have an adverse effect on the filtrate quality (Kim and Lawler, 2012), including pathogens such as *Cryptosporidium* (Emelko, 2001).

Effluent turbidity is universally used to monitor the filtration process. Figure 3.2b shows the progression of a typical filter cycle in terms of turbidity and headloss. The dynamic behavior occurs because captured particles effectively alter the physico-chemical character of the grain surfaces as well as the pore geometry, which in turn affects the rate of particle capture and the

[1] A common configuration in Norway, the "Molde-process" has a third layer of crushed limestone to control pH, alkalinity and calcium content.

resistance to flow through the medium. Initially, it takes some time for the effluent turbidity to stabilize; this period is called the ripening period and water is filtered to waste until effluent turbidity improves. The early peak in turbidity stems from remnant backwash water in and above the media (Amirtharajah, 1985). Then turbidity declines as the filter begins to capture particles, which further enhances the particle-removal capacity (O'Melia and Ali, 1979). After ripening, there is a prolonged period during which turbidity remains quite stable - this is the operational period when water is directed to the consumer. Eventually, the filter capacity is exceeded and turbidity starts to rise - the breakthrough period. Sometimes, a so-called filter-aid (usually a cationic polymer) is also added before the filter in order to increase floc-strength and delay break-through. After breakthrough, the filter is backwashed using high flowrates (often aided by pressurized air) to clean the filter media and restart the process. Also, as particles captured by the filter, the resistance to flow increases and manifests itself as increased headloss. Unless, there is extensive (undesirable) surface filtration, the rate of headloss increase is approximately linear as in the lower panel of Figure 3.2b.

Figure 3.2b shows only the effluent turbidity and not what is going on inside the filter bed. In fact, at any given time, much of the particle removal occurs in a relatively small portion of the bed, as observed by Adin and Rebhun (1974) during contact-filtration. This *active layer* moves down the bed as the cycle progresses, i.e. there are ripening and breakthrough fronts that propagate down the depth of the filter in wave-like manner and breakthrough occurs when the wave reaches the filter outlet. Hence, the dynamic behavior of the filter is a spatiotemporal phenomenon. Furthermore, turbidity performance may not reflect the behavior of variably sized particles. Several studies have found ripening to occur faster for larger particles than smaller particles (Clark et al., 1992; Kim and Lawler, 2008; Moran et al., 1993a) and breakthrough to occur earlier for larger particles than smaller particles (Moran et al., 1993a). Thus, ripening, stable performance (if at all) and breakthrough occur simultaneously for different particles sizes, an observation that is central to the removal of pathogens by filtration processes.

It is well-known that filtration processes are capable of achieving significant pathogen removal rates (Hijnen and Medema, 2010). As mentioned in Section 1.2.4, the Norwegian drinking water regulations (Drikkevannsforskriften, 2001) require the presence of at least two hygienic barriers in a water supply system. The associated guidance document (Mattilsynet, 2011) to the regulations further specify that a treatment process should be able to remove 99.9 % (3 $\log_{10}$) of bacteria/viruses and 99 % (2 $\log_{10}$) of parasites for it to be considered a hygienic barrier against pathogens. This document also specifies criteria in terms of process indicator parameters that, if met, are taken to ensure that the process meets the hygienic barrier requirement. The criteria that apply to coagulation-filtration processes are shown in Table 3.1.

However, according to the recent revision of the *Microbial barrier analysis* tool (Ødegaard et al., 2016a,b, see Section 1.2.4), direct filtration and contact filtration systems are only credited with a removal-capacity for viruses of 1.5 $\log_{10}$ if turbidity is less than 0.2 NTU and 2 $\log_{10}$ if enhanced coagulation is used with effluent turbidity < 0.1 NTU and color removal is better than 70 %. The corresponding removal credits for both bacteria and parasites are 2.25 and 2.5, respectively. The Norwegian water industry has also issued guidelines (Eikebrokk, 2012, 2014) on the operation of coagulation-filtration processes, focused on ensuring a hygienically safe operation. It was observed that, often, the upper limit on residual aluminum determines the

Table 3.1: Criteria for a coagulation-filtration process to be recognized as a hygienic barrier according to the guidance document (Mattilsynet, 2011) to the Norwegian drinking water regulations (Drikkevannsforskriften, 2001).

Parameter	Upper limit	Comment
Aluminium [mg Al/l]	0.15	If Al is used for coagulation
Iron [mg Fe/l]	0.15	If Fe is used for coagulation
Color [mg Pt/l]	10	Should be less than 5 if Al/Fe is used for coagulation
TOC [mg C/l]	3	If volume < 10000 m3/day, COD may be measured instead
Turbidity [FNU]	0.2	Applies to each filter individually
Particle counts [1/ml]	500	Particle size 2-400 μm; applies to each filter individually

coagulant dose, i.e a *higher* coagulant dose is needed to achieve < 0.15 mg/l Al in the effluent than is required to meet the other criteria in Table 3.1. It was recommended by Eikebrokk (2012) that the virus removal capacity of the high NOM and low turbidity contact-filtration process used in Norway be investigated, since the available data on virus removal under these conditions is limited, as seen in the next section.

3.1.2 Observations on virus removal

Many studies on virus removal during rapid filtration have been reported in the literature. The earliest appear to be Carlson et al. (1942), Kempf et al. (1942) and Neefe et al. (1947). Carlson et al. (1942) studied the removal of poliovirus by inoculating mice with pre- and postfiltration water. They observed a reduction in paralysis in the mice after filtration, and in particular when the filter surfaces had been covered with alum floc. Kempf et al. (1942) similarly studied the removal of poliovirus, but used monkeys instead of mice. Only one or two monkeys were used per experiment, but poliomyelitis occurred in two monkeys after sedimentation and filtration, and was taken as an indication that the process could not remove all viruses. Neefe et al. (1947) observed a 40 % reduction (as compared to a control) in Hepatitis incidence, and an increase in incubation time, in volunteers ingesting water that had been coagulated and passed through a diatomite filter, although the sample size was too small to judge statistical significance.

These early studies did not allow an estimation of the fraction of virus removed, but later studies often have. Reviews have been provided by Berg (1973), Leong (1983), Payment and Armon (1989) and more recently by Hijnen and Medema (2010). The experimental conditions have varied greatly, with bench-scale to full-scale studies and different filter configurations, raw water qualities and viruses used. For the summary in Tables 3.2 and 3.3, the literature was searched for those studies that (1) studied drinking water in particular (not waste water) (2) employed coagulation in at least some of the reported runs (in general, poor removal is observed without coagulation) and (3) quantified removal across the filtration unit instead of the combined effect of multiple unit processes. All studies were performed with surrogate viruses added to the filter influent water, except for the full-scale studies that employed high-volume sampling to quantify viruses that were naturally present in the water.

The most obvious observation that can be made from these tables is the highly variable removal efficiencies that are reported. This may be related to differences between viruses (e.g. Abbaszadegan et al., 2008, runs 49-52), between different raw water qualities and experimental conditions (e.g. Hendricks et al., 2006, runs 39 vs. 40) and probably also variations in analytical

Table 3.2: Overview of results from previous studies on virus removal by rapid filtration: Experimental conditions.

Reference	Index	Scale | media[a] | type	F.rate [m/h]	Raw water	RW turb. [NTU]	RW org.mat.	RW pH	Coagulant[b] (dose)
Paper III	1	Pilot | F-S | contact	5.9	River	0.7-0.8	TOC=3.03 mg/l	7.3	PACl (1.5 mg Al/l)
Gilcreas and Kelly (1955)	2	Bench | S | conventional	4.8	Spring water	n/a	n/a	n/a	Alum (?)
Robeck et al. (1962)[c]	3	Pilot | A-S | contact	4.9	River	8	n/a	7.7-8.1	Alum (10 ppm)
"	4	Pilot | A-S | conventional	4.9	River	8	n/a	"	Alum (50 ppm)
"	5	Pilot | A-S | contact	4.9	River	27	n/a	"	Alum (n/a?)
"	6	Pilot | A-S | conventional	4.9	River	27	n/a	"	Alum (n/a?)
"	7	Pilot | A-S | contact	14.7	Tap	0.2	n/a	"	Alum (10 ppm)
"	8	Pilot | A-S | contact	14.7	Tap	0.2	n/a	"	Alum (5 ppm)
"	9	Pilot | A-S | contact	14.7	Synthetic	40	n/a	"	Alum (10 ppm)
"	10	Pilot | A-S | contact	4.9	Synthetic	12	n/a	"	Alum (10 ppm)
"	11	Pilot | A-S | contact	14.7	Synthetic	10	n/a	"	Alum (10 ppm)
Foliguet and Doncoeur (1975)	12	In French, no translation available to the author.						
Guy et al. (1977)	13	Pilot | A-S | conventional	n/a	River	n/a	n/a	n/a	Ferric sulphate (40 ppm)
"	14	Pilot | A-S | conventional	n/a	River	n/a	n/a	n/a	Ferric sulphate (40 ppm)
"	15	Pilot | A-S | conventional	n/a	River	n/a	n/a	n/a	Ferric sulphate (40 ppm)
Stetler et al. (1984)	16	Full (1 pl.) | n/a | conventional	n/a	River/poor	25.4 (mean)	n/a	n/a	Alum (n/a)
Keswick et al. (1984)	17	Full (1 pl.) | n/a | conventional	n/a	River/poor	26	n/a	7.4	Alum (n/a) + cat.pol.
Keswick et al. (1985)	18	Full (1 pl.) | n/a | conventional	n/a	Lake/poor	7.7	n/a	n/a	Alum (n/a) + cat.pol.
Payment et al. (1985)	19	Full (5 pl.) | n/a | conventional	n/a	Variable/poor	Var./high	Var./high	Var	n/a
Agbalika et al. (1985)[c]	20	Full (1 pl.) | n/a | conventional	3.6-5.1	River	12-36	COD=2.7-4.6 mg/l	8-8.1	Water alum. chloride (15-20 ppm)
Joret et al. (1986)	21	Full | n/a | conventional	5	River	n/a	n/a	n/a	n/a
Rose et al. (1986)	22	Full (3 pl.) | n/a | conventional	n/a	River/poor	3.4	n/a	n/a	Alum (31 mg/l) + cat. pol.
Rao et al. (1988)	23	Bench | CSG | conventional	4.7	Lake	42	n/a	n/a	Alum?
"	24	Bench | CSG | conventional	4.7	Lake	34	n/a	n/a	Alum?
"	25	Bench | S | conventional	4.7	Lake	34	n/a	n/a	Alum?
"	26	Bench | S | conventional	4.7	Lake	25	n/a	n/a	Alum?
"	27	Bench | CSG | conventional	4.7	Lake	12/14/26	n/a	n/a	Alum (15 mg/l) + cat.pol.
Payment and Franco (1993)	28	Full (3 pl.) | n/a | conventional	n/a	Variable/poor	n/a	n/a	n/a	Various
"	29	Full (3 pl.) | n/a | conventional	n/a	Variable/poor	n/a	n/a	n/a	Various
"	30	Full (3 pl.) | n/a | conventional	n/a	Variable/poor	n/a	n/a	n/a	Various
"	31	Full (3 pl.) | n/a | conventional	n/a	Variable/poor	n/a	n/a	n/a	Various
Nasser et al. (1995)	32	Pilot | S | contact	n/a	Kaolin+humic acid	∼10	TOC=3.7 mg/l	n/a	Alum (30 ppm)
"	33	Pilot | S | contact	n/a	Kaolin+humic acid	∼10	"	n/a	Alum (30 ppm) + pol.
Gitis et al. (2002)	34	Bench | S | contact	10	Synthetic	12.8	n/a	7.5?	Alum (10 mg/l)
Gerba et al. (2003)	35	Pilot | GAC-S | conventional	24	n/a	n/a	n/a	n/a	Alum (20-23 mg/l) + cat.pol.
Harrington et al. (2003)[d]	36	Pilot | 2M / 3M | conventional	5-20	Lake	∼8.6	UV_{254}=0.074 cm^{-1}	∼7.6	Alum (50-80 ppm)
Hendricks et al. (2006)	37	Pilot | A | contact	12.2	Lake	1.2-3.5	TOC=3 mg/l	n/a	Alum (26 mg/l)
"	38	Pilot | A-S | contact	12.2	Lake	1.2-3.5	"	n/a	Alum (26 mg/l)
"	39	Pilot | A | conventional	12.2	Lake	1.2-3.5	"	n/a	Alum (26 mg/l)
"	40	Pilot | A | contact	12.2	Lake	1.2-3.5	"	n/a	Alum (13 mg/l)
"	41	Pilot | A | contact	12.2	Lake	1.2-3.5	"	n/a	No coagulant
"	42	Pilot | A-S | contact	12.2	Lake	1.2-3.5	"	n/a	No coagulant
Abbaszadegan et al. (2007)	43	Pilot | GAC-S | conventional	12	Mix:surface+ground	13.2-17.7	DOC=4.86 mg/l	8.25	$FeCl_3$ (40 mg/l) + cat.pol.
"	44	Pilot | GAC-S | conventional	24	Mix:surface+ground	14-19	"	8.25	$FeCl_3$ (40 mg/l) + cat.pol.
Templeton et al. (2007)[e]	45	Bench | A-S | direct	1.9-6.8	Tap+kaolin clay	n/a	n/a	7.2	Alum (25mg/l)
"	46	Bench | A-S | direct	1.9-6.8	Tap+humic acids	n/a	n/a	"	Alum (50mg/l)
"	47	Bench | A-S | direct	1.9-6.8	Tap+kaolin clay	n/a	n/a	"	Alum (25mg/l)
"	48	Bench | A-S | direct	1.9-6.8	Tap+humic acids	n/a	n/a	"	Alum (50mg/l)
Abbaszadegan et al. (2008)	49	Pilot | GAC-S | conventional	12	Mix:surface+ground	<0.2	n/a	8	Ferric chloride (20 mg/l) + cat.pol.
"	50	Pilot | GAC-S | conventional	12	Mix:surface+ground	<0.2	n/a	"	Ferric chloride (40 mg/l) + cat.pol.
"	51	Pilot | GAC-S | conventional	24	Mix:surface+ground	<0.2	n/a	"	Ferric chloride (20 mg/l) + cat.pol.
"	52	Pilot | GAC-S | conventional	24	Mix:surface+ground	<0.2	n/a	"	Ferric chloride (40 mg/l) + cat.pol.
Shirasaki et al. (2010)	53	Bench | S | conventional	5	River	0.63	DOC=0.76mg/l	6.8	PACl (0.54 mg Al/l)
"	54	Bench | S | conventional	5	River	0.63	"	6.8	PACl (1.08 mg Al/l)
"	55	Bench | S | conventional	5	River	0.63	"	6.8	PACl (1.62 mg Al/l)
"	56	Bench | S | conventional	5	River	0.63	"	6.8	Alum (1.08 mg Al/l)
"	57	Bench | S | conventional	5	River	0.63	"	6.8	$FeCl_3$ (2.24 mg Fe/l)
"	58	Bench | S | conventional	5	River	0.63	"	5.8	$FeCl_3$ (2.24 mg Fe/l)
Boudaud et al. (2012)	59	Pilot | S | conventional	2.3	River	5.4-18.3	TOC=2.5-3.1 mg/l	7.6-8.2	PAX-XL7 (2.25 mg Al/l)
Asami et al. (2016)	60	Full (1 pl.) | A-S | conventional	12-20	River	51-185	n/a	6.8-7.2	Alum (45-60 mg/l)

[a] Filter media keys: A - anthracite; CSG - coal, sand and garnet mix; F - Filtralite; GAC - granular activated carbon; S - sand.
[b] PACl - poly-aluminium chloride; PAX-XL7 - aluminium polyhydroxychlorosulfate; cat. - cationic; pol. - polymer.
[c] Robeck et al. (1962) reported turbidity in Jackson turbidity units (JTU).
[d] Harrington et al. (2003) investigated a wide range of filter media and experimental conditions.
[e] Templeton et al. (2007) used declining rate filtration.

Table 3.3: Overview of results from previous studies on virus removal by rapid filtration: Virus removal data.

Reference	Index	Virus[a]	Typical $\log_{10}$ removal	Note particularly
Paper III	1	S.t. 28B | MS2	2-3 | 2-3	Prolonged ripening, virus breakthrough shortly before turbidity breakthrough
Gilcreas and Kelly (1955)	2	Coxsackie A | Theiler | T4	1 | 1 | 1.7	Samples taken during initial ripening?
Robeck et al. (1962)	3	Polio I	1.7	Prolonged ripening
"	4	Polio I	>2	-
"	5	Polio I	1-1.3	Prolonged ripening
"	6	Polio I	>2	-
"	7	Polio I	ca. 2	Virus breakthrough, but no turbidity breakthrough
"	8	Polio I	ca. 1.2	-
"	9	Polio I	>2	Short run
"	10	Polio I	ca. 2	Long run, no virus breakthrough
"	11	Polio I	ca. 2	Virus and turbidity breakthrough coincided
Foliguet and Doncoeur (1975)	12	In French, no translation available to the author.		
Guy et al. (1977)	13	Natural phages	ca. 0.2	
"	14	T4	0-0.9	Time since last backwash important
"	15	Polio I,II,III	0.1-0.2	Time since last backwash important
Stetler et al. (1984)	16	Culturable enteric viruses	0.6	Large volume sampling
Keswick et al. (1984)	17	Coliphages | Enteroviruses | Rotavirus	1 | 0.3 | 0.7	Rainy season, large volume sampling
Keswick et al. (1985)	18	Rotavirus	Negative removal	Dry season (Mexico), large volume sampling
Payment et al. (1985)	19	Enteroviruses	1.2	Large volume sampling
Agbalika et al. (1985)	20	Enteroviruses	0.35	Large volume sampling
Joret et al. (1986)	21	Enteroviruses	0.6 - 2	Only abstract available
Rose et al. (1986)	22	Coliphages | Enteroviruses | Rotavirus	1.2 | >1 | -0.6	Large volume sampling
Rao et al. (1988)	23	Polio I	0.43	Samples taken during initial ripening?
"	24	Rotavirus	0.45-0.64	Samples taken during initial ripening?
"	25	Rotavirus	0.1-0.15	Samples taken during initial ripening?
"	26	Hepatitis A	0.5	Samples taken during initial ripening?
"	27	Polio I | Rotavirus | Hepatitis A	1.06 | 2.55 | 0.36	Samples taken during initial ripening?
Payment and Franco (1993)	28	Culturable human enteric viruses	>1.8 | 3.8 | -0.5	Large volume sampling
"	29	Somatic phages (E.coli host)	1.1 | 2.6 | -0.2	Large volume sampling
"	30	F-specific phages	n/a | 1.8 | -0.6	Large volume sampling
"	31	Somatic phages (Salmonella host)	n/a | 0.8 | -1.5	Large volume sampling
Nasser et al. (1995)	32	MS2 | Polio I | Hepatitis A	1.15 | 0.7 | n/a	
"	33	MS2 | Polio I | Hepatitis A	2 | 1.05 | >1.15	Worse with humic acids / early Polio I breakthrough
Gitis et al. (2002)	34	MS2	0.4 | 0.7	With 20 cm | 40 cm beds, respectively
Gerba et al. (2003)	35	MS2 | PRD1 | Fr | Feline calicivirus	0.68 | 1.07 | 1.24 | 0.56	
Harrington et al. (2003)	36	MS2	2-3.5	Combined removal of sedimentation+filtration.
Hendricks et al. (2006)	37	MS2 | Polio | ϕ-X174 | Echovirus-12	2.9 | 2.2 | 5.1 | 2.4	
"	38	MS2 | ϕ-X174	2.9 | 5.1	
"	39	MS2 | ϕ-X174	2.8 | 5.3	
"	40	MS2 | ϕ-X174	0.9 | 1.4	
"	41	MS2 | ϕ-X174	0 | 0.05	
"	42	MS2 | ϕ-X174	0.02 | 0.1	
Abbaszadegan et al. (2007)	43	MS2 | PRD1 | ϕ-X174 | Fr	0.66 | 2.94 | 0.66 | 0.57	
"	44	MS2 | PRD1 | ϕ-X174 | Fr	2.58 | 3.11 | 0.94 | 3.53	
Templeton et al. (2007)	45	T4	2.1 | 2.8 | 2.0	Ripening | stable period | breakthrough, respectively
"	46	T4	2.5 | 3.3 | 2.5	Ripening | stable period | breakthrough, respectively
"	47	MS2	2.8 | 3.3 | 2.8	Ripening | stable period | breakthrough, respectively
"	48	MS2	2.8 | 3.4 | 1.6	Ripening | stable period | breakthrough, respectively
Abbaszadegan et al. (2008)	49	MS2 | PRD1 | ϕ-X174 | Fr	2.9 | 0.7 | 0.3 | 2.0	
"	50	MS2 | PRD1 | ϕ-X174 | Fr	2.2 | 1.4 | 0.5 | 1.9	
"	51	MS2 | PRD1 | ϕ-X174 | Fr	3.0 | 1.1 | 0.3 | 3.4	
"	52	MS2 | PRD1 | ϕ-X174 | Fr	3.0 | 2.0 | 0.6 | 3.0	
Shirasaki et al. (2010)	53	Noro-VLP | MS2 | Qβ	$\sim$0	10 cm column
"	54	Noro-VLP | MS2 | Qβ	1.7 | 0.5 | 0.5	10 cm column
"	55	Noro-VLP | MS2 | Qβ	1.8 | 0.7 | 0.6	10 cm column
"	56	Noro-VLP | MS2 | Qβ	1.3 | 0.1 | 0.3	10 cm column
"	57	Noro-VLP | MS2 | Qβ	$\sim$0	10 cm column
"	58	Noro-VLP | MS2 | Qβ	1.5 | 1.5 | 2.0	10 cm column
Boudaud et al. (2012)	59	MS2 | Qβ | GA	4.24 | 2.74 | 1.03	Combined removal of sedimentation+filtration. RT-qPCR used.
Asami et al. (2016)	60	PMMoV | JC PyV	1.3 (0.8) | 0.5 (0.6)	RT-qPCR used.

[a] Noro-VLP - Norovirus virus-like-particles; PMMoV - Pepper mild mottle virus; JC PyV - JC polyomavirus.

methods. This makes it rather challenging to make general statements on the virus removal capacity of deep-bed filters. The authors that studied the effect of varying filter media types and depths found only moderate variations in removal (Harrington et al., 2003; Hendricks et al., 2006). Indeed, Hijnen and Medema (2010) reported no systematic correlations between removal and process conditions (including wastewater studies). Furthermore, they concluded that coliphages appeared to be good surrogates for enteric viruses in the filtration process.

One clear trend, though, is that the studies that were carried out under full-scale conditions tend to report lower removal efficiencies than pilot or bench-scale studies. Although full-scale studies are a priori desirable and are favored by some authors (Hijnen and Medema, 2010; Payment and Armon, 1989), they rely on methods that involve high-volume sampling and subsequent concentration in order to detect and enumerate viruses. Such methods suffer from low and variable recovery efficiencies (Petterson et al., 2015), which leave the removal estimates uncertain. An indication of this is the frequent reporting of negative removal in full-scale studies. On the other hand, bench and pilot-scale studies may suffer from scale-associated effects that are not present in full-scale, and they use influent concentrations of lab-cultured viruses that are much higher than what occurs naturally. Hence, extrapolating such results to full-scale conditions is not straightforward.

Although a number of studies were performed under direct or contact filtration conditions, few studies reported a turbidity and organic matter content (if they reported at all) that are clearly representative of Norwegian filtration practice. Hendricks et al. (2006) are probably those who come closest in experiments 37 and 38 (experiment 40 was to study the effect of underdosing). They also studied conventional filtration in run 39 (compare with 37) and found similar removal for MS2 as compared to contact filtration, but better removal during conventional filtration for ϕX174. Robeck et al. (1962) compared contact filtration and conventional filtration under similar conditions (runs 3 vs. 4 and 5 vs. 6), and observed lower removal and prolonged ripening during contact filtration.

Most of the reported studies did not attempt to capture the full dynamics of the filter cycle, but relied on samples taken during the stable period. However, Robeck et al. (1962) sampled more frequently and were able to observe prolonged ripening of viruses compared to turbidity in several instances. Templeton et al. (2007) took samples during each of the filter stages and observed significantly lower removal during ripening and breakthrough. Harrington et al. (2003) observed increasing effluent virus concentrations during turbidity breakthrough. However, none of these studies used sufficiently frequent sampling to compute true average removal efficiencies for the entire filter cycle and it appears that only Templeton et al. (2007) sampled from within the filter bed (one sampling event during stable operation from the interface between the anthracite and sand layers, showing approximately equal log-removal in the two layers). These were shortcomings that motivated the work behind **Paper III**, and may also explain some of the variation in reported removal rates.

The next section will briefly review fundamental filtration theory and models. It is worth noting, though, that viruses to be removed in drinking water filters are likely to be associated with flocs (Gerba, 1984; Tanneru et al., 2013; Templeton et al., 2007; Templeton et al., 2008), which are highly complex particles (Bache and Gregory, 2010; Gregory and Dupon, 2001), whose properties depend on local conditions. Thus, the virus-filter grain interaction may actually be dominated by the floc-filter grain interaction, and theoretical expectations based on virus-grain interactions may be of limited value in understanding virus removal in

coagulation-filtration processes.

3.2 Filtration mechanisms and models

Models to describe or predict the behavior of filters have been widely researched. Reviews by at various times in the history of the field include Ives (1964), Ives and Cleasby (1972), Tien and Payatakes (1979), McDowell-Boyer et al. (1986), Amirtharajah (1988) and Jegatheesan and Vigneswaran (2005). Schijven and Hassanizadeh (2000) reviewed virus transport in the subsurface.

In rapid-filtration applications, transport is usually assumed to be one-dimensional and advection-dominated (high Peclet numbers; Logan (2001)). A particle conservation equation for the porous filter, modeled as a continuum, may then be written as

$$\frac{\partial}{\partial t}(\epsilon c + \sigma) + q\frac{\partial c}{\partial z} = 0 \tag{3.1}$$

Here, t is time, z is the space coordinate, q is the filtration rate (Darcy velocity), c represents the aqueous phase mass concentration of particles (mass of particles pr. unit volume of aqueous suspension), ϵ is the porosity of the medium (volume of voids per unit volume of porous medium) and σ is the mass of particles deposited on the filter grains (mass of particles per unit volume of porous medium). Note that q does not change with depth. Furthermore, the filtration rate is usually kept constant (except in declining rate filtration) by hydraulic control so that q is a given constant. Hence, the unknowns are c and σ (and possibly ϵ). In addition to initial and boundary conditions, a constitutive equation for the relation between c and σ is needed. Filtration modeling started with Iwasaki (1937) suggesting the following first-order (in space) relation, which remains the starting point for most analyses:

$$\frac{\partial c}{\partial z} = -\lambda c \tag{3.2}$$

Ideally, a complete model for the filtration process should be capable of (1) predicting the initial removal efficiency before significant particle capture takes place, (2) describe the effect of already captured particles on the particle capture rate and (3) describe the effect of already captured particles on the resistance to flow through the medium. However, two main lines of research may be identified:

1. *Fundamental, microscopic* models take λ as a constant, which is assumed to be valid in the early stages of filtration before deposited particles alter the conditions for filtration; hence the name *clean-bed theory*. The goal is to predict λ from first-principles descriptions of particle transport and attachment at the pore-scale in idealized geometries, using measurable properties of the particles, filter medium and water.

2. *Phenomenological, macroscopic* models take λ as a function of σ and aim to describe the behavior of the entire filter cycle. Parametrizations of the filtration function $\lambda(\sigma)$ are given in the literature, but case-specific parameters must be determined using data from experiments. A related problem is to determine the resistance to flow throughout the cycle, which similarly involves parameter-estimation of a headloss function (Tien and Ramaro, 2007). When q is given externally, these two problems become decoupled.

In the following, a brief overview of filtration mechanisms is given.

3.2.1 Transport, attachment, straining and detachment

At the pore-scale, the mechanisms responsible for particle removal may be categorized in two (Elimelech et al., 1995):

1. Transport of a particle from the bulk pore water to the surface of a filter grain (termed *collector* in filtration theory).
2. Interaction between the filter grain and the particle, resulting in attachment (or not).

The interaction forces between a filter grain and particles are generally very short-ranged, on the order of a few dozen nanometers, while the typical dimension of a pore may be 1000 - 10000 times larger. Hence, the transport step and attachment step are considered to be largely independent and are also treated as such in most fundamental mathematical models.

Transport

Figure 3.3 gives a schematic overview of transport mechanisms assumed to be operating during the transport step. If particles simply followed the fluid streamlines perfectly, they would never encounter the collector except when a streamline is very close to the collector (*interception* - a). Hence, there are other mechanisms that are responsible for transporting particles across streamlines. *Brownian motion* (b), the random movement of particles due to collisions with thermally vibrating water molecules, is an important mechanism for colloidal-sized particles ($<$ 1-3 μm) such as viruses. For particles that are not neutrally buoyant, *inertial deviation* (c) from streamlines and *sedimentation* (d) are important. *Hydrodynamic forces* (e) refer to such effects as non-uniform frictional drag across the particle (especially for non-spherical particles) that cause rotations and deviations from streamlines, as well as hydrodynamic resistance that arises as a particle comes close to the collector.

Attachment

The two main forces considered for the attachment step in fundamental filtration models are electrostatic interactions and van der Waals forces, which formed the basis for the original DLVO-theory (see below). Electrostatic interactions may be attractive or repulsive while van der Waals forces are always attractive.

Most particles dispersed in aqueous electrolytes carry a net positive or negative surface charge, which sets up a potential difference between the surface and the bulk solution. The surface charge is balanced by an accumulation of oppositely charged ions (*counter-ions*) in the volume surrounding the particle. The surface-charge and the layer of accumulated counter-ions together constitute the *electrical double-layer*. Except for the very near-surface region, the layer of counter-ions is only loosely adsorbed to the particle and referred to as the *diffuse layer* and the ionic composition of the diffuse layer approaches that of the bulk solution as the distance from the particle increases. The extent of the double-layer is heavily dependent on the ionic strength, with higher ionic strength resulting in compression of the diffuse layer, but usually between 1 and 100 nm in aqueous solutions (Elimelech et al., 1995). For most

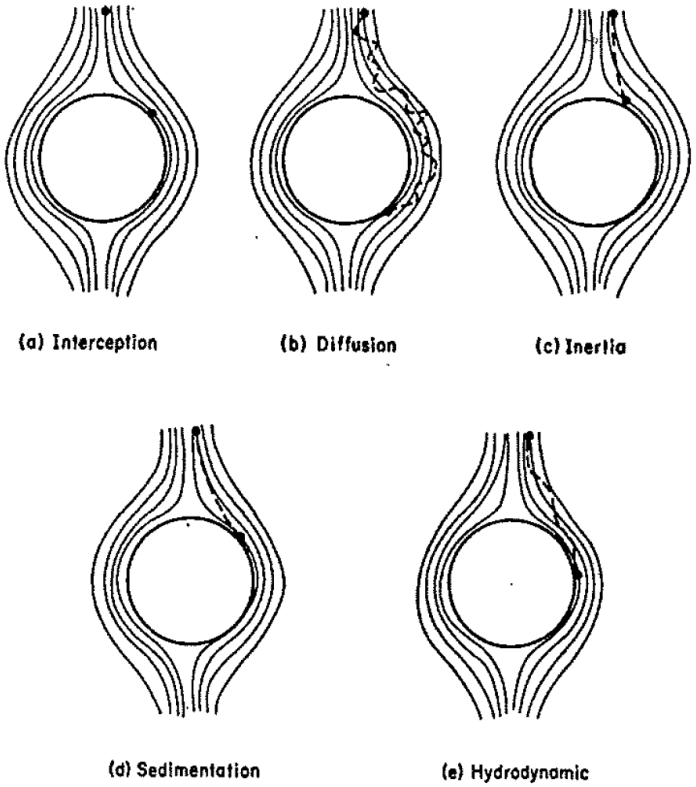

Figure 3.3: Pore-scale transport mechanisms. From Ives (1970).

practical and modeling purposes, the surface potential is equated with the experimentally available electro-kinetic potential (or zeta-potential), which is the potential at the shear-plane separating mobile ions and immobile ions. When two particles/surfaces approach each other, their diffuse layers start to overlap which leads to repulsion or attraction, depending on the surface charges. Models exist to compute the interaction energy, most relying on simplified geometries, ions as point charges, and assumptions on thermodynamic equilibrium (Elimelech et al., 1995).

One important way in which particles acquire surface charge is by ionization of surface functional groups. The pH which results in a net surface charge of zero is called the isoelectric point (IEP), and for most mineral surfaces and biocolloids (including viruses, Michen and Graule (2010)), the IEP is found at pH-values (significantly) less than neutral and therefore most surfaces become negatively charged in natural waters.

Van der Waals forces are intermolecular forces that arise from the interaction of permanent and/or induced dipoles, and are always attractive due to a correlation of the fluctuating electromagnetic fields associated with the induced dipoles. Hamaker's method (Hamaker, 1937) is usually used for computing van der Waals forces between macroscopic bodies, and relies on an assumption that the pairwise interaction between every molecule may be simply *added* to compute the total net force. The non-geometric aspect of this problem is characterized by the Hamaker constant, A, which depend on material properties, largely the polarizibility, of the materials involved, i.e. particles and suspending medium, e.g. water (Elimelech et al., 1995).

DLVO-theory was developed independently by Derjaguin and Landau (1941) and Verwey and Overbeek (1948), from whom the theory derives it name. The fundamental idea of DLVO-

theory is to interpret colloidal stability in terms of the sum of interaction energies from electrostatic forces and van der Waals forces (interaction energy as a function of separation distance between two particles), see Figure 3.4.

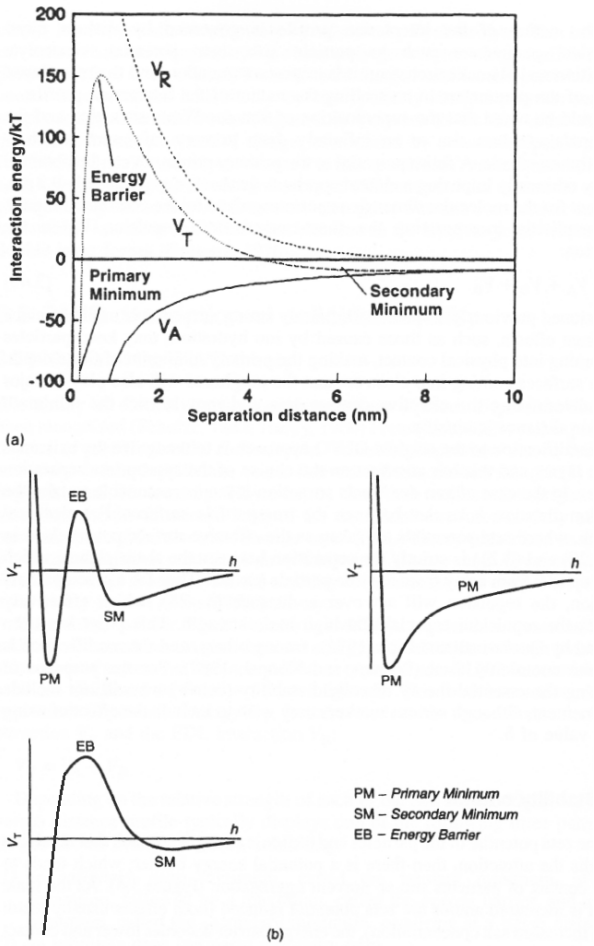

Figure 3.4: Examples of DLVO energy profiles. In a), V_R is the electrical double layer interaction energy and V_A is the van der Waals interaction energy for two equal spherical particles of 1 μm diameter. V_T is the sum of these two energies. The profile was calculated based on a 1-1 electrolyte, a zeta potential of 30 mV, electrolyte concentration of 50 mM and Hamaker constant of $8.3 \cdot 10^{-21}$. In b), three qualitatively different energy profiles are shown. From Elimelech et al. (1995).

We see from the figure that we can have quite different energy profiles, depending on the properties of the particles involved. There will always be an energy well at close separation distance to the surface (*primary minimum*) that results from the increasing van der Waals force as the particle approaches the surface. When electrostatic interactions are repulsive, there will be a peak (*energy barrier*) in the energy profile that, if higher than the thermal energy of particles, poses a hindrance for attachment in the primary minimum. If there is an energy barrier, there may also be a small energy well at large separation distances (*secondary minimum*). If there is no energy barrier, every particle that comes close enough will in theory be deposited in a primary energy minimum, and deposition is said to be transport-limited.

While DLVO-theory is widely applied in particle deposition problems (Adamczyk and Weroński, 1999; Hermansson, 1999), often non-DLVO forces are invoked to explain observations (Grasso et al., 2002). These include steric forces, bridging, Born repulsion and hydration forces (Elim-

elech et al., 1995), hydrophobic forces (Donaldson et al., 2015) and depletion forces (Weroński et al., 2003).

Straining and detachment

The importance of interstitial straining and detachment of previously captured particles has been somewhat controversial in the filtration literature. A conventional rule of thumb (Herzig et al., 1970) is that straining is relatively insignificant if particle diameters are less than 5 % of the porous medium grain diameter. In porous medium micromodels straining was observed to be important for particle to *pore throat* ratios larger than 40 % (Auset and Keller, 2006). Note that there is no simple relationship between grain size distribution and pore throat size distribution. It has been argued that researchers have been too quick to invoke straining as a mechanism when conventional filtration theory fails to explain experimental observations (Johnson et al., 2011).

Regarding detachment, the early filtration literature contained the opposing views of Ives and Mints (the "Mints-Ives controversy"), where Ives (e.g. Ives, 1969) held that detachment did not occur while Mints (e.g. Mints, 1966) considered it important. A growing body of theoretical (Bai and Tien, 1997; Bergendahl and Grasso, 2003) and experimental evidence (Kim and Lawler, 2006; Kim and Tobiason, 2004; Moran et al., 1993b) suggests that particle detachment do play a role, in particular during the latter stages of a filter cycle (Moran et al., 1993b) and during hydraulic shock loads (Kim and Lawler, 2006). However, there seems to be no general consensus on the relative importance of attachment and detachment. Furthermore, models for the detachment process are not as well-developed as for the attachment step and consequently detachment tend to be overlooked in applications.

3.2.2 Fundamental models

First-principles models to predict λ employ mathematical descriptions of the transport and attachment mechanisms in the previous section. To this end, an idealized porous medium model is needed so that the pore-scale fluid flow field can be computed (Payatakes et al., 1974). Stokes flow is usually assumed, neglecting inertial terms in Navier-Stoke's equation. Early studies (Yao et al., 1971) relied on the isolated sphere model, but the most commonly used model has been the Happel-sphere-in-cell model (Happel, 1958), which is considered to represent the influence of nearby grains more realistically (Nelson and Ginn, 2005, 2011; Rajagopalan and Tien, 1976; Tufenkji and Elimelech, 2004).

Regardless of which porous medium conceptual model is chosen, the goal is to compute the *single collector efficiency*, which is defined as

$$\eta = \frac{\text{Rate at which particles attach to the collector}}{\text{Rate at which particles approach the collector}} = \frac{I_{\text{attachment}}}{I_{\text{approach}}} \tag{3.3}$$

where the rate of approach is usually computed simply from the particle flux towards the projected area of a single collector. The difficult part is to compute the rate of particle attachment to the single collector.

In fact, it has proven very difficult to obtain agreement with experimental data when there is an electrostatic energy barrier to deposition (Johnson et al., 2007; Tufenkji, 2007). In the

presence of energy barriers, the relative deposition of differently charged particles (including viruses; e.g. Dowd et al. (1998)) may be qualitatively consistent with theoretical expectations, but the observed deposition rates tend to be orders of magnitudes higher than predicted by theory. Deposition in the secondary energy minimum and heterogeneity of grain surfaces (e.g. Tufenkji and Elimelech, 2005), as well as straining (e.g. Bradford et al., 2006) have been invoked to explain this phenomenon. There are also shortcomings in the classical DLVO-theory (Adamczyk and Weroński, 1999) and, at least in the case of microbial particles, it has been suggested that more refined models are needed to characterize their electrohydrodynamic properties (Dika et al., 2011; Duval and Gaboriaud, 2010; Langlet et al., 2008). Developments in pore-scale experimental techniques may also help in making progress in understanding filtration mechanisms at a fundamental level (Keller and Auset, 2007).

Because of these challenges, models have instead focused on computing η in the *absence* of energy barriers, which is assumed to be equal to normalized collision rate and called the single-collector contact efficiency η_0:

$$\eta_0 = \frac{\text{Rate at which particles collide with the collector}}{\text{Rate at which particles approach the collector}} = \frac{I_{\text{collision}}}{I_{\text{approach}}} \tag{3.4}$$

With this approach, η is computed as

$$\eta = \eta_0 \frac{I_{\text{attachment}}}{I_{\text{collision}}} = \eta_0 \alpha \tag{3.5}$$

where α is known as the sticking efficiency and is determined by fitting the model to experimental data. The relationship between η and λ is most often obtained by considering the number density of collectors in the porous medium (Elimelech et al., 1995) and results in:

$$\lambda = \frac{3(1-\epsilon)\alpha\eta}{2d_c} \tag{3.6}$$

where d_c is the grain diameter of the medium. Logan et al. (1995) and Nelson and Ginn (2011) discussed the issue of which reference velocity (pore-water velocity or approach velocity) to use for fundamental pore-scale modeling and the appropriateness of equation (3.6).

Several studies have focused on obtaining practically useful expressions for η_0 (Long and Hilpert, 2009; Long et al., 2010; Ma et al., 2009; Nelson and Ginn, 2011; Rajagopalan and Tien, 1976; Tufenkji and Elimelech, 2004; Yao et al., 1971). They differ in the porous medium model chosen, which mechanisms are included and the choice between *Eulerian* approaches (solving a convection-diffusion equation; Tufenkji and Elimelech, 2004; Yao et al., 1971) and *Lagrangian* approaches (solving a particle trajectory equation; Long and Hilpert, 2009; Long et al., 2010; Ma et al., 2009; Rajagopalan and Tien, 1976). Except for Yao et al. (1971), they all share the feature that closed-form expressions for η_0 are developed by regressing exact numerical computations for η_0, obtained by exploring a large part of the parameter space, against dimensionless variables that are assumed to characterize the problem; hence the name "correlation" equations.

The most widely used equation is the one developed by Tufenkji and Elimelech (2004) (TE), which was shown to fit experimental data somewhat better than previous models. Building

Table 3.4: List of dimensionless parameters used in equations (3.8)-(3.10). Adapted from Tufenkji and Elimelech (2004).

Parameter	Definition	Name	Physical interpretation
A_s	$\frac{2(1-p^5)}{2-3p+3p^5-2p^6}$	Happel parameter	Inherited from the Happel model; $p=(1-\epsilon)^{1/3}$
N_R	$\frac{d_p}{d_c}$	Aspect ratio	Ratio of particle diameter to collector diameter
N_{Pe}	$\frac{qd_c}{D}$	Peclet number	Ratio of convective transport to diffusive transport
N_{vdW}	$\frac{A}{k_bT}$	van der Waals number	Ratio of van der Waals interaction energy to thermal energy
N_A	$\frac{A}{3\pi\mu {d_p}^2 q}$	Attraction number	Represents the combined influence of van der Waals forces and fluid velocity on deposition rate due to interception
N_G	$\frac{{d_p}^2(\rho_p-\rho_w)g}{18\mu q}$	Gravity number	Ratio of Stokes settling velocity to fluid approach velocity

ϵ - porosity; d_p - particle diameter; d_c - collector diameter; q - approach velocity
D - particle diffusion coefficient from Stokes-Einstein equation; A - Hamaker constant
k_b - Boltzmann's constant; T - absolute temperature; μ - dynamic viscosity
ρ_p - particle density; ρ_w - water density; g - acceleration of gravity

on the earlier studies, they used the additivity assumption

$$\eta_0 = \eta_D + \eta_I + \eta_G \tag{3.7}$$

where η_D, η_I and η_G are the single-collector contact efficiencies obtained when only diffusion, interception and sedimentation is included in the numerical model, respectively. They found the following after regression analysis:

$$\eta_D = 2.4 A_S^{1/3} N_R^{-0.081} N_{Pe}^{-0.715} N_{vdW}^{0.052} \tag{3.8}$$

$$\eta_I = 0.55 A_S N_R^{1.675} N_A^{0.125} \tag{3.9}$$

$$\eta_G = 0.22 N_R^{-0.24} N_G^{1.11} N_{vdW}^{0.053} \tag{3.10}$$

Definitions of all the dimensionless terms may be found in Table 3.4. Similarly to the other correlation equations, η_0 has a U-shape when plotted against particle size (see Figure 3.10 on page 61) with a minimum close to 1 μm. For smaller particle sizes, η_0 is dominated by η_D (Brownian particles) and for larger particles by η_I and η_G.

3.2.3 Macroscopic models for filtration dynamics

The fundamental models presented in the previous section do not attempt to describe the effect of already captured particles on the filter efficiency. There are pore-scale first-principles attempts at this too (Tien and Ramaro, 2007), but conventionally a macroscopic approach has been adopted which includes a *filtration function* whose parameters must be determined from experimental data. The problem is briefly presented here as a skeletal background for

the model sketch presented in the Appendix of **Paper III**.

The starting point are the fundamental equations introduced earlier:

$$\frac{\partial}{\partial t}(\epsilon c + \sigma) + q\frac{\partial c}{\partial z} = 0 \tag{3.1}$$

$$\frac{\partial c}{\partial z} = -\lambda c \tag{3.2}$$

By either comparing the size of terms or introducing a "corrected" time coordinate, the particle conservation equation has usually been simplified by, in effect, dropping the first term on the left hand side (Dábrowski, 1988; Horner et al., 1986):

$$\frac{\partial \sigma}{\partial t} + q\frac{\partial c}{\partial z} = 0 \tag{3.11}$$

The inaccuracy inherent in this simplification is generally considered negligible (Dábrowski, 1988), except possibly for the very early stages of a filter run. With equation (3.1) replaced by equation (3.11), the Iwasaki expression can be replaced with a first-order (now in time) filtration rate expression:

$$\frac{\partial \sigma}{\partial t} = \lambda q c \tag{3.12}$$

As the filter cycle progresses, the filter coefficient λ is assumed to change with the amount of deposited particles so one defines

$$\lambda = \lambda(\sigma) = \lambda_0 F(\sigma) \tag{3.13}$$

where λ_0 is the initial filter coefficient and $F(\sigma)$ is a correction factor known as the *filtration function*. In order for the filtration equations to describe an entire filter run, with ripening, stable operation and breakthrough, F needs to be first increasing, than decreasing with σ. Several parametrized expressions for F that have this property have been presented in the literature (Jegatheesan and Vigneswaran, 2005; Tien and Ramaro, 2007). The one that is considered the most flexible was suggested by Ives (1969):

$$F(\sigma) = \left(1 + \frac{b\sigma}{\epsilon_0}\right)^{n_1} \left(1 - \frac{\sigma}{\epsilon_0}\right)^{n_2} \left(1 - \frac{\sigma}{\sigma_{\text{ult}}}\right)^{n_3} \tag{3.14}$$

where b, n_1, n_2, n_3 and σ_{ult} are fitting parameters, and ϵ_0 is the clean-bed porosity. The parameter σ_{ult} represents the maximum value that σ can attain and is considerably smaller than ϵ_0.

Generalizations of the problem above may be required. If detachment is considered non-negligible, equation (3.12) must be modified to include a detachment term (e.g. Adin and Rebhun, 1987), or in general one needs an expression on the form

$$\frac{\partial \sigma}{\partial t} = F_{\text{gen}}(c, \sigma, q) \tag{3.15}$$

where the property $F_{\text{gen}}(0, \sigma, q) < 0$ for at least some $\sigma > 0$ expresses the possibility of detachment. If the filtration rate q is not given, it becomes a variable to be determined together with c and σ, which requires another constitutive expression (and a boundary condition) for the relationship between headloss and σ (Tien and Ramaro, 2007). Finally, if there are multiple

particle types, one may need separate mass balance and filtration rate expressions for each particle type.

Initial and boundary conditions for the set of equations (3.11) and (3.15) are usually taken as:

$$c(z,0) = \sigma(z,0) = 0 \qquad z \geq 0 \tag{3.16}$$

$$c(0,t) = c_{\text{in}}(t) \qquad t > 0 \tag{3.17}$$

Herzig et al. (1970) showed that when the filtration rate is on the form (3.12), this coupled system of partial differential equations can be rewritten as a set of ordinary differential equations that can be solved sequentially.

The inverse problem of determining the parameters of F_{gen} from experimental data involves optimization of some objective function, typically minimizing a sum of squared errors (Bai and Tien, 2000), using for example the Levenberg-Marquardt method or possibly Markov chain Monte Carlo methods. The problem has been studied from a more mathematical viewpoint (in an oil production setting) by Alvarez et al. (2013), Alvarez (2005), and Alvarez et al. (2006, 2007).

3.3 Pilot-scale filtration experiment: Paper III

The observation that previous studies on virus removal during coagulation-filtration in drinking water treatment had practically only sampled from the filter effluent, using only relatively coarse sampling frequencies, was the main motivation for undertaking the experimental study. In addition, it was desirable to obtain more data for virus removal for the contact-filtration process. The main purpose of the study was therefore to characterize in detail the spatio-temporal pattern of virus retention in a filtration system that was reasonably representative of Norwegian filtration practice, and investigate how virus removal relates to particle removal (as measured by turbidity) throughout the depth of the filter and the entire filter cycle. Hopefully, the collected data can be used to fit a dynamic filtration model, but this is still work in progress. The impact of different experimental conditions was not a focus of this study, since the work load associated with such high-resolution sampling is substantial. There were plans to run replicate filtration cycles, which unfortunately had to be discarded due to considerations of time, cost and raw water availability.

3.3.1 Experimental setup and methods

A summary of the experimental approach is provided here; the full details may be found in **Paper III**.

Pilot plant and operational conditions

A pilot-scale filtration plant was designed and constructed specifically for the purposes of this experiment. A schematic overview of the plant is given in Figure 3.5 on the following page and a photograph in Figure 3.6 on page 55. The filter column was a 10 cm diameter PVC pipe and the filter media were chosen to conform with the filter design at Nedre Romerike Vannverk

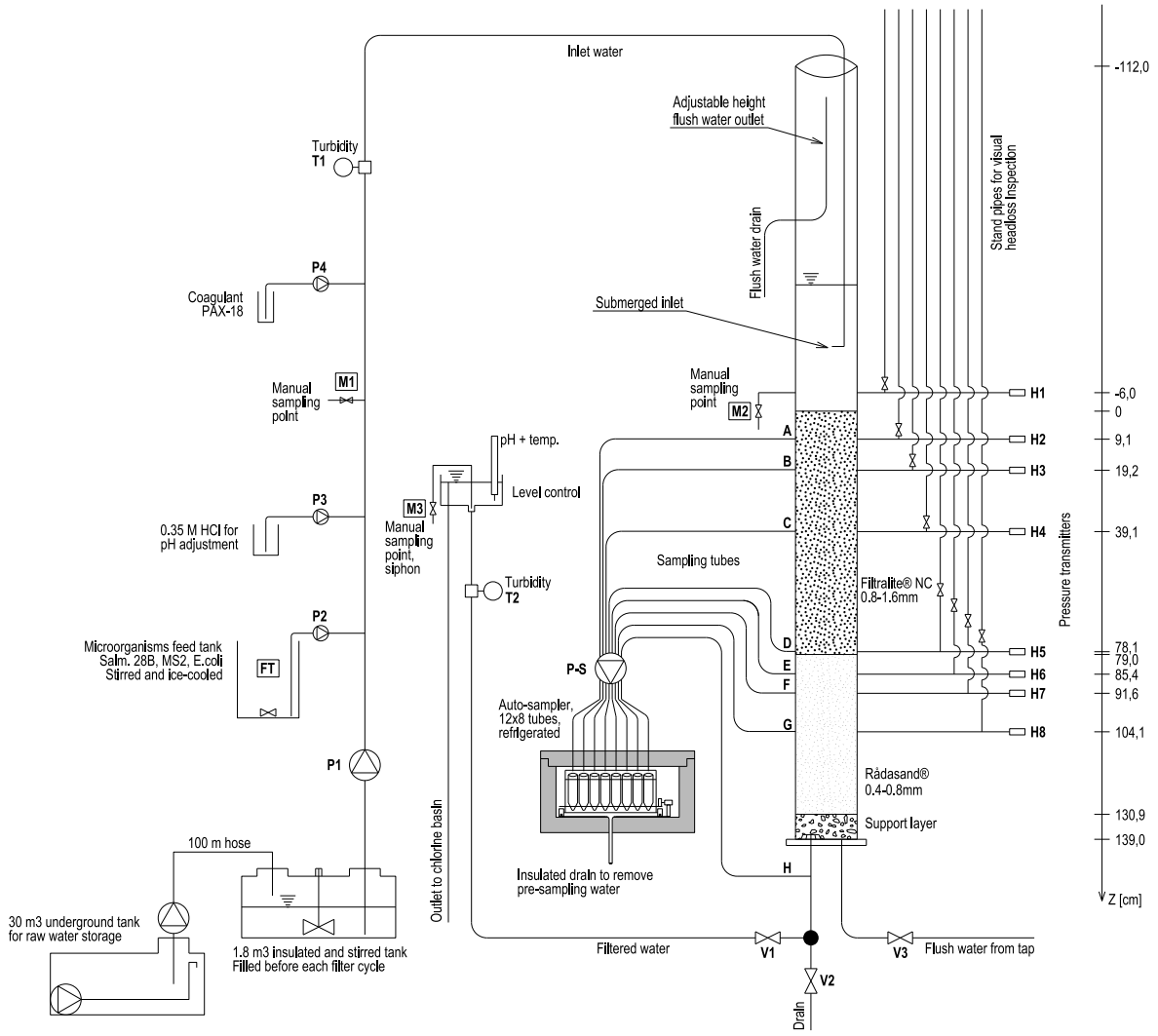

Figure 3.5: Schematic overview of the pilot-plant. From **Paper III**.

(NRV), Strømmen.[2] Physical characteristics of the two media are given in Table 3.5a on page 56. The top layer, Filtralite NC 0.8-1.6 mm (normal density, crushed), is an expanded clay material with a high internal grain porosity. The performance of Filtralite has generally been on par with the more conventional anthracite media, but with slower headloss increase (Eikebrokk and Saltnes, 2001, 2002; Saltnes et al., 2002a,b). The bottom layer, Rådasand 0.4-0.8 mm, is a typical quartz sand. The ratio of column diameter to effective grain size was greater than 50, the recommended minimum ratio to minimize wall effects (Lang et al., 1993; Mehta and Hawley, 1969). A shallow support layer of graded gravel covered the outlet arrangement.

The pilot-plant was equipped with an extensive system for control, monitoring, sampling and dosing of chemicals/microorganisms, as shown in Figure 3.5. The filtration rate was kept constant at 5.9 m/h by a feed pump while hydraulic head at the filter outlet was kept constant by an overflow. Thus, the filter was run in constant flow, rising head mode. The coagulant used was PAX-18 (Kemira AS), a 42 % basicity poly-aluminium chloride that is being used at NRV and is a commonly used coagulant in Norway. No filter aid was used.

[2]This plant uses a conventional configuration with sedimentation before filtration. The total filter depth may be somewhat greater than usual.

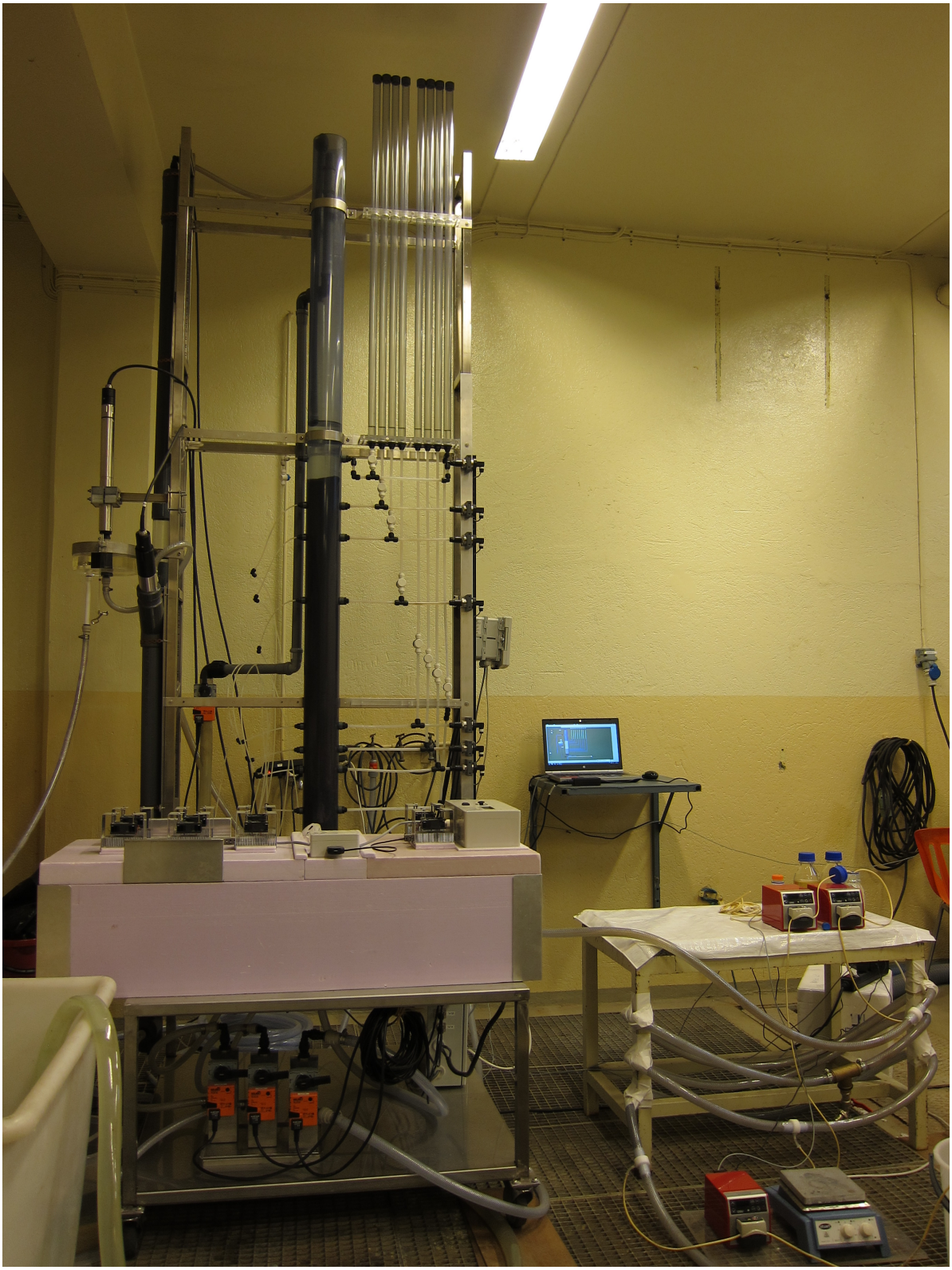

Figure 3.6: Photograph of the pilot-plant.

Table 3.5: Filter material data, raw water characteristics and operational conditions. From **Paper III**.

(a) Filter material physical data, based on the respective manufacturer's information.

Parameter	Filtralite	Rådasand
Layer depth (m)	0.79	0.5
Grain size, nom. range (mm)	0.8-1.6	0.4-0.8
Effective grain size, d_{10} (mm)	0.95	0.4
Column diameter/d_{10} (-)	105	250
Uniformity coefficient, d_{60}/d_{10} (-)	< 1.5	< 1.8
Primary porosity (-)	0.58	0.45
Bulk porosity (-)	0.80	0.45
Grain density (kg/m^3)	1260	2600
Bulk density (kg/m^3)	530	1440

(b) Raw water characteristics and operational conditions.

Parameter	Value
Raw water turbidity (NTU)	0.7-0.8
Raw water color (mg Pt/l)	26
Raw water TOC (mg/l)	3.03±0.61
Raw water UV absorption (1/m)	13.1
Raw water SUVA[a] (l/(m·mg))	> 4.3
Raw water pH (-)	7.3
Raw water alkalinity (mM)	0.28
Raw water temp. (°C)	15-16
Filtration rate (m/h)	5.9
Flow rate (l/min)	0.77
PAX-18 dose (mg Al/l)	1.5
HCl dose (mM)	0.12
Initial total headloss (cm)	26

[a]Specific UV absorption (UV abs./DOC)
TOC/DOC: Total/dissolved organic carbon

Hydrochloric acid (HCl) was used for pH adjustment. Pressure transmitters and ports for automatic sampling were installed with non-uniform spacing along the column in order to focus data-collection on the regions where the largest changes were expected to occur. Sampling ports protruded approximately 5 mm into the filter media to avoid wall effects, and were connected through equal-length tubes to an automatic sampler that was designed to take samples (12 times 8 samples) from all ports simultaneously at programmed intervals and store them in a refrigerated box. Prior to each sampling event, three tube volumes would be drained by the sampler to discard "old" water. The flow rate of the sampler was adjusted so as to not disturb the flow in the column excessively. Manual samples could be taken from ports M1 (before coagulant), M2 (after coagulant) and M3 (from the effluent).

Raw water was collected from the river Glomma at NRV and stored at campus in an underground tank. After some initial sedimentation, turbidity remained stable. Raw water characteristics and operational conditions are given in Table 3.5b. The relatively high value of >4.3 for the specific UV absorption (SUVA) indicates that the organic material is rich in aromatic compounds and well suited to treatment by coagulation (Matilainen et al., 2010). The optimal dosing regime was determined by testing in the pilot plant itself since jar-tests are not fully informative for the optimal dosing in a contact-filtration system. The lowest dose that resulted in compliance with the criteria (aluminium, color, turbidity) in Table 3.1 was 1.5 mg Al/l and a coagulation pH of 5.8 seemed optimal. This dose is in agreement with empirical models for the optimal dose developed by Eikebrokk et al. (2004b). A test run then showed that turbidity breakthrough occurred after approximately 15 hours.

Prior to a filter-run, a batch of raw water was pumped from the underground tank to a smaller steel tank in the lab. The column would be backwashed with tap water at a rate of 50-60 m/h for approximately 15 minutes. Some intermixing of the filter materials were observed after settling even when the backwash rate was gradually reduced. The column was then run with raw water for approximately 15 minutes to displace the tap water in the column as this was consider to give a more realistic initial condition for the experiment. Dosing of HCl, coagulant and microorganisms were then initiated simultaneously and dosing continued throughout the filter cycle.

Microorganisms

Two model viruses were included in this study. F-specific coliphage MS2 is an icosahedral single-stranded RNA virus with a diameter of 27 nm (Strauss and Sinsheimer, 1963), while *Salmonella* Typhimurium phage 28B (Lilleengen, 1948) is double-stranded DNA virus with a 50 nm head attached to a ∼10 nm baseplate, and infects *Salmonella* Typhimurium type 5 (Svenson et al., 1979). The former was included since it is commonly used as a pathogenic virus surrogate (Table 3.3) and the latter was included since our research group has used it extensively (Heistad et al., 2009a; Heistad et al., 2009b) for wastewater studies and the virus is easy to work with. We believe this study, along with Willumsen (2015), is the first to use it for deep-bed filtration experiments, but it has been used previously in a drinking water biofiltration study in Sweden (Persson et al., 2005).

MS2 was enumerated (relative concentrations) primarily by reverse transcription quantitative polymerase chain reaction (RT-qPCR) as described in **Paper III**. Preliminary investigations found no inhibitory effects of the coagulant in the RT-qPCR assay. Some samples were also enumerated by double-layer plaque assay against *E.coli* Famp for comparison with RT-qPCR results. Previous studies, and preliminary investigations for this study, have shown an inactivation effect in plaque assays of poly-aluminium chloride coagulants on F-specific phages like MS2 (Kreißel et al., 2014; Matsui et al., 2003; Matsushita et al., 2011). In order to reduce the impact of this effect, a modification of the method proposed by Matsushita et al. (2004) was used.

Phage 28B was enumerated by double-layer plaque assay. Preliminary studies, reported in the master's thesis of Willumsen (2015), revealed a slow inactivation and/or aggregation effect of PAX-18 on 28B, resulting in a reduction of concentrations of up to 2 $\log_{10}$ units during one week of storage. In order to reduce the impact of this effect, all 28B samples were plated within 4 hours after sampling. Not all dilutions could be plated in replicates (due to hundreds of plates < 24 hours), but at least two plates were incubated for every sample (two dilutions and/or parallels of the same dilution). Concentration estimates for a sample were computed as

$$\hat{c} = \frac{x}{v_{\mathrm{p}} \sum_{i=1}^{k} d_i} \tag{3.18}$$

where x is the total plaque count for all plates, d_i is the dilution factor for plate i (counting duplicates twice) and v_{p} is the volume of sample per plate. This corresponds to a maximum-likelihood estimate, assuming Poisson-distributed counts.

For comparison with the viruses, the bacterium *E.coli* was also included in the study and enumerated using the Colilert-18 method (IDEXX Laboratories) with Quanti-Tray/2000 trays (one tray per sample). Stock microorganism suspensions were mixed with distilled water in the ice-cooled and stirred feed tank. No adverse effects on the filtration process could be observed from adding the microorganism suspension, when comparing with the trial filter runs that were performed without microorganisms. Approximately 150 water samples were taken during the filter cycle; all samples were analysed for 28B and a subset were analysed for MS2 and *E.coli*. An overview of the sampling regime is given in the supporting material to **Paper III**.

Table 3.6: Water quality results and influent microorganism concentrations. From **Paper III**.

Parameter	Value
Influent turbidity (-)	2.05
Influent SS (mg/l)	8.2
Influent coagulation pH (-)	5.8
Effluent pH (-)	5.9-6.0
Effluent color (mg Pt/l)	3
Effluent residual Al-content (mg Al/l)	0.031^a/$<0.010^b$
Influent mean (M1 and M2) 28B conc. (PFU/ml)	$2.57 \cdot 10^5$
Influent mean (M1) MS2 conc. (PFU/ml)	$1.96 \cdot 10^6$
Influent mean (M1 and M2) *E.coli* conc. (MPN/100ml)	$9.31 \cdot 10^5$

[a]During dose optimization, total Al; [b]During experiment, dissolved Al
SS - suspended solids; PFU - plaque forming units; MPN - most probable number

3.3.2 Results and discussion

Measured water quality parameters and mean influent microorganism concentrations c_{in} are shown in Table 3.6. Influent microorganism concentrations were quite stable and these mean concentrations were used in computing removal efficiencies. It took 2-3 hours for the effluent pH to decline from about pH 7 to pH 5.9, which is likely a result of a pH-increasing effect of the Filtralite medium, which ceased when the grains were covered with deposit.

Figures 3.7a - 3.7c on the facing page shows the logarithm of the probability of passage, $\log_{10}(\pi) = \log_{10}(c/c_{\text{in}})$, for all sampling points for 28B, MS2 and *E.coli* respectively. Here c is the microorganism concentration in a sampling point. The conventional log-removal is simply $-\log_{10}(\pi)$. Figure 3.7d shows the manual turbidity measurements on a log-scale. Time zero in these figures corresponds to the arrival of coagulated water at the filter surface. Effluent turbidity became completely stable only after approx. 3 hours and turbidity breakthrough started at 14.2 hours.

From Figure 3.7a we can clearly see ripening and breakthrough fronts for 28B moving in a wave-like manner through the filter. The first auto-sample at 1 h 20 min was apparently taken too late to capture the breakthrough (i.e. concentration minimum) in ports A-C. After breakthrough in a port, the concentrations increase and eventually reach a stable value. There is some removal in the upper part of the column even at the end of the cycle. The effluent samples (M3) show that ripening for 28B continued for most of the cycle until breakthrough occurred after approx. 13 hours, about 1 h before turbidity breakthrough.

The MS2 data in Figure 3.7b has a coarser temporal resolution, but is qualitatively similar to the 28B data, with the exception that there is a mid-cycle peak in effluent concentrations (M3). It may be speculated that this is related to a breakthrough in the upper parts of the sand layer (where some intermixing with Filtralite was observed) before sufficient ripening had occurred for MS2 in the bottom part of the sand layer. However, the samples that were analysed by plaque assay do not show any sign of following the same trend. Thus the peak may also be related to poor mid-cycle removal of some non-infectious MS2 or some unknown measurement artifact. Apart from this observation, the plaque assay samples are largely in agreement with the RT-qPCR samples, but showing slightly higher removal. This could be due to some residual inhibition from PAX-18 which couldn't be reversed by the methods described

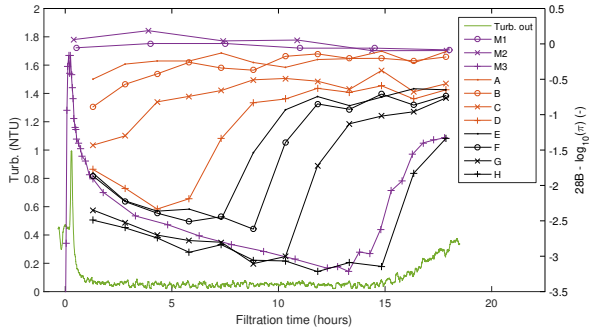

(a) Phage 28B concentrations normalized to influent concentrations.

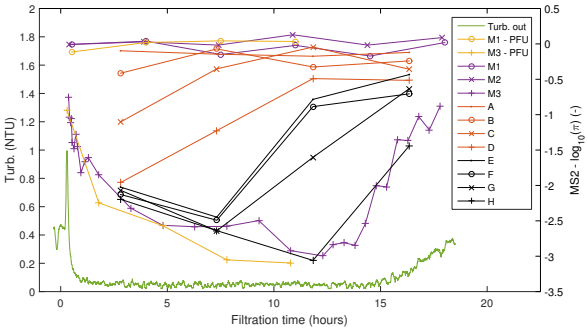

(b) Phage MS2 concentrations normalized to influent concentrations. All datapoints obtained with RT-qPCR except those labeled as PFU.

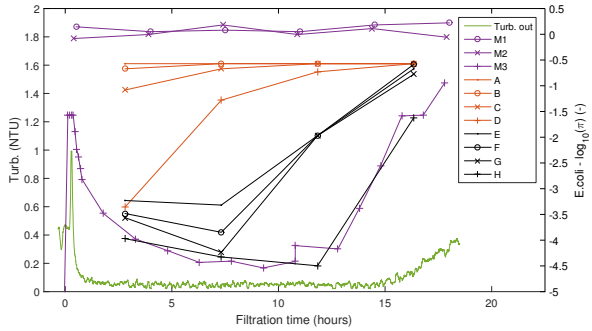

(c) *E.coli* concentrations normalized to influent concentrations. Note that several samples were above enumeration limits (see supporting material of **Paper III**).

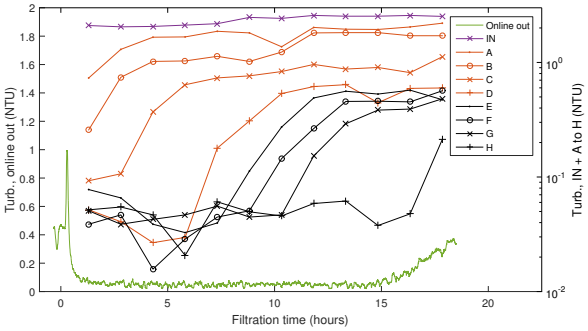

(d) Turbidity.

Figure 3.7: Spatio-temporal passage of microorganisms and turbidity. From **Paper III**.

in **Paper III**.

The autosampler *E.coli* data for ports A-G in Figure 3.7c should be interpreted with caution since several samples were above the enumeration limit (see supporting material of **Paper III**). The *E.coli* results are nevertheless qualitatively similar to the virus results. The effluent samples (M3), however, show that ripening was faster for *E.coli* and breakthrough occurred earlier, as compared to viruses. The breakthrough was also not as sharp as for viruses, as seen by the lesser curvature at the concentration minimum.

Finally, the turbidity data show a similar pattern as for 28B, but noise in the low-turbidity region makes it difficult to discern ripening in the ports below port E. The rising limbs of the turbidity breakthrough curves are slightly steeper than the 28B curves for the Filtralite layer and less steep than the 28B curves for the sand layer. It is currently not clear how to interpret this observation. It might simply be an artifact related to the greater precision of the virus analyses for low concentrations, where turbidity measurements hit the noise floor.

For all microorganisms, no systematic differences between samples from M1 (before coagulant addition) and M2 (after coagulant addition) could be observed (Figures 3.7a - 3.7c). For 28B and *E.coli*, which were enumerated by culturing methods, this indicates that the coagulant did not have any significant inactivating effect during the time span in question and also that there was no excessive aggregation. For MS2, which was enumerated by RT-qPCR, aggregation cannot be assessed, but the similarity between M1 and M2 samples confirmed the results of

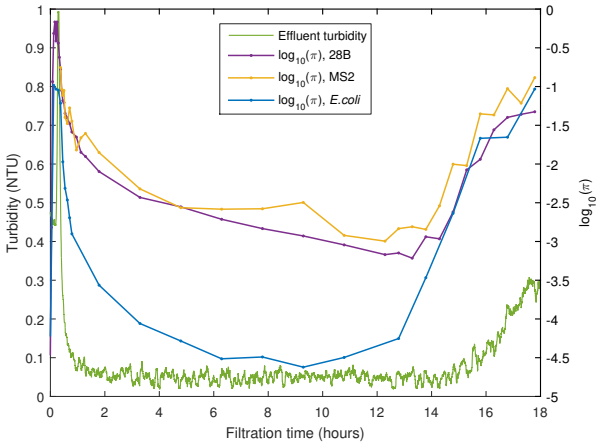

Figure 3.8: Overall passage compared. Note that we discarded one suspicious data point for *E.coli* at approx 11. hours (compare Fig. 3.7c), where we had two data points. From **Paper III**.

preliminary investigations that did not show inhibitory effects of the coagulant.

Figure 3.8 compares the passage of all three microorganisms in a single plot. This makes it clear that the two viruses behave quite similarly while *E.coli* is both removed to a greater extent and shows different dynamics in that ripening was faster and breakthrough occurred earlier. These observations are consistent with earlier observations on the ripening and breakthrough behavior of differently sized particles (Clark et al., 1992; Kim and Lawler, 2008; Moran et al., 1993a). However, towards the end of the cycle the removal efficiencies appear to converge, which suggests that removal mechanisms that are more independent of particle properties dominate at this stage.

No dynamic model has yet been fitted to the data, but work is ongoing. A sketch of how a coupled model for virus (28B) and particle removal (as measured by turbidity) in both filter media may be constructed is given in the Appendix to **Paper III**. If successful, this may give a more precise description of the dynamics of the system and the and the relationship between overall particle removal and virus removal. However, we may gain some insight by working directly with the data. Figure 3.9 on the facing page shows mean filter coefficients between two sample ports computed directly from the data based on the solution to equation (3.2), assuming a constant λ:

$$\lambda_{i,i+1} = \frac{1}{z_{i+1} - z_i} \ln\left(\frac{c_i}{c_{i+1}}\right) \tag{3.19}$$

Here i and $i+1$ indexes two consecutive sample ports. Again we see the wave moving down the filter bed, with all three microorganisms and turbidity behaving similarly, qualitatively speaking. Note the lower temporal resolution of the MS2/*E.coli* data, which masks some of their dynamics. Note also that the distance between sample ports varied so that one may expect that some peaks are "averaged down" as one moves the rightmost panels in Figure 3.9. For the bottom layer (sand), the peak in λ occurs approximately when the hydraulic gradient is at its steepest. The hydraulic gradient between ports G and H started to rise before turbidity breakthrough, and thus served as an "'early warning"' of imminent breakthrough.

The peak in λ-values in Figure 3.9 may be interpreted as corresponding to fully favorable conditions to particle deposition, i.e. $\alpha = 1$. Obviously, these are not clean-bed conditions, but we will assume that we can apply ideal filtration theory at the time when the peak

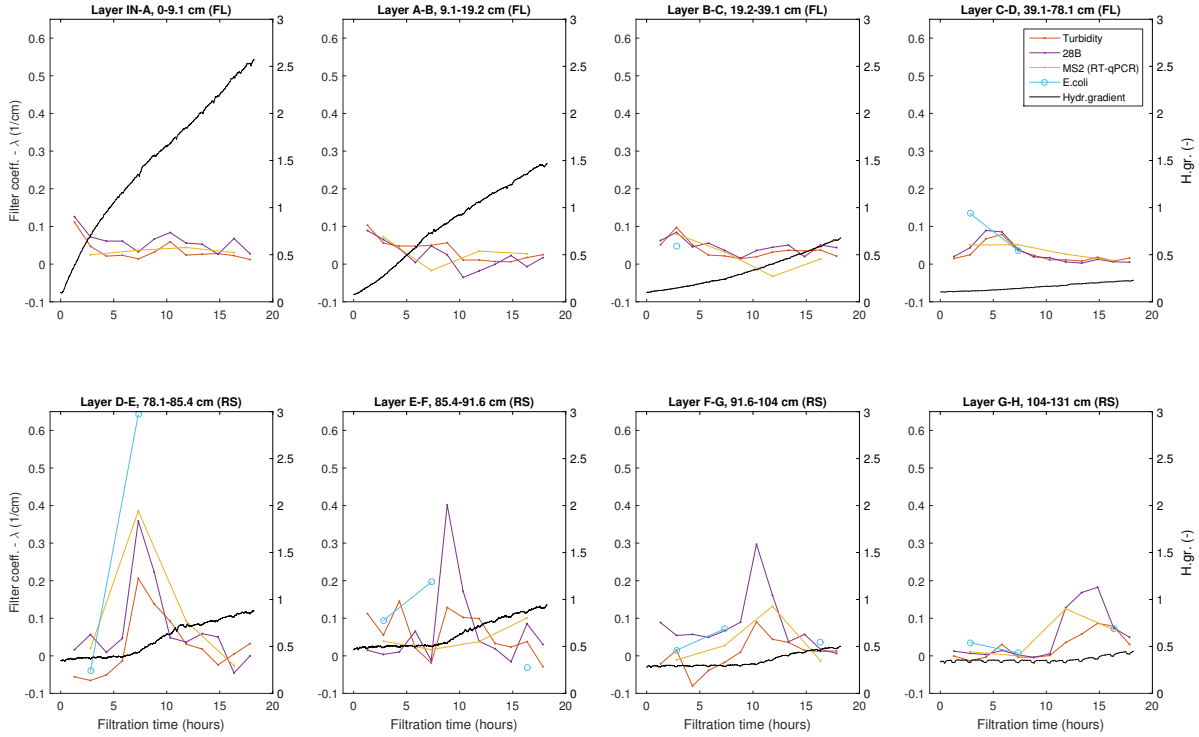

Figure 3.9: Estimated filter coefficients from a solution to equation (3.2), and hydraulic gradients. Filter coefficients for *E.coli* could not be computed for several layers/times because samples were above the enumeration limit. FL- Filtralite; RS - Rådasand. From **Paper III**.

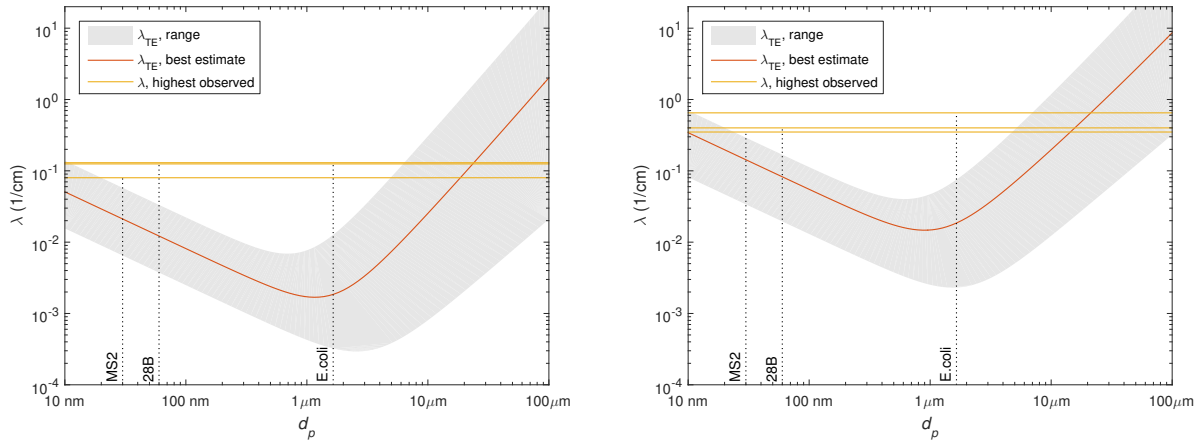

(a) Comparison for Filtralite. The grey area is the possible range of λ-values using the following parameters, with the parameters used for the best estimate in the middle: Porosity 0.48 - 0.58 - 0.63; Grain size 0.7 - 0.95 - 1.6 mm; Hamaker constant 1e-21 - 1e-20 - 1e-19 J; Density 1000 - 1250 - 2600 kg/m^3.

(b) Comparison for Rådasand. The grey area is the possible range of λ-values using the following parameters, with the parameters used for the best estimate in the middle: Porosity 0.35 - 0.45 - 0.50; Grain size 0.35 - 0.40 - 0.8 mm; Hamaker constant 1e-21 - 1e-20 - 1e-19 J; Density 1000 - 1250 - 2600 kg/m^3.

Figure 3.10: Comparison of peak values of λ from Figure 3.9 with those predicted by the TE correlation equation. All computations were carried out for water at 15°C. From **Paper III**.

occurred, under the conditions that prevailed in the bed at *that* time. This has been done for Figure 3.10, where we compared the peak λ-values to those predicted by the TE correlation equation (eqs. (3.7) - (3.10)), assuming a very wide range of the input parameters. It is seen that the observed λ-values are not consistent with those predicted based on the size of each microorganism, but are more consistent with particle sizes in the neighborhood of 20 μm. It is unlikely that straining plays any role for singly dispersed viruses. Hence, the most reasonable interpretation is that most viruses (as well as *E.coli*) were adsorbed to flocs and removed with flocs. This is not surprising, given that viruses (as well as *E.coli*) are known to be removed even during coagulation-sedimentation processes (e.g. Abbaszadegan et al., 2008), which rely completely on virus-floc associations.

The observed differences in removal between each microorganism (*E.coli* $\gg$ 28B $>$ MS2) is more difficult to explain. There could be differences between them in the proportion of microorganisms that are adsorbed to flocs. As discussed in **Paper III**, 28B may be slightly more negatively charged than MS2 at the pH in the experiment and therefore adsorb a little better to positively charged aluminium-flocs, and thereby show a little better removal. However, the difference between the two viruses is slight and may also be related to the different enumeration techniques used. The better removal observed for *E.coli* is currently unexplained. It is larger than the viruses (approx. 1 μm $\times$ 3 μm), rod-shaped, and its surface charge appears to lie between those of the viruses (Lytle et al., 2002). If it were not floc-bound, one would expect poorer removal than for the viruses (Figure 3.10), but the opposite is observed.

As noted before, the experiments in Tables 3.2 and 3.3 on pages 42-43 that come closest to our experimental conditions are the ones by Hendricks et al. (2006), labeled 37 and 38. Compared to our experiment, their filtration rate was about twice as high and their alum dose in terms of aluminum (approx. 2.4 mg Al/l) was higher. Their reported removal efficiency for the MS2 virus, 2.9 $\log_{10}$ units, is still quite similar to our results. However, some other researcher have reported significantly lower removals for MS2 (Table 3.3) under other experimental conditions.

Even though our results were obtained in a single filter run, and generalizations of our computed removal efficiencies should be performed with care, the dynamic microorganism removal observed, even during the period of stable effluent turbidity, signals that care should be taken when characterizing microbial removal efficiencies during filtration. Either samples should be taken frequently, such as in this study, or at flow-proportional continuous sampling should be employed so that one can obtain a correct mean removal efficiency, as discusses in the next section.

The usefulness of surrogates, such as phages, for studying removal and inactivation of pathogenic viruses is a continuous concern (Mesquita and Emelko, 2012; Sinclair et al., 2012). Hijnen and Medema (2010) suggested that coliphages are appropriate surrogates for pathogenic viruses in deep-bed filtration. Since *Salmonella* typhimurium phage 28B is easy to work with, it would be a useful addition to the set of candidate surrogate phages if it can be confirmed that it behaves similarly to MS2 and/or other coliphages under a wider range of conditions.

A final concern regarding the applicability of these results, and those from most other pilot-scale studies, is the high influent concentrations used for the microorganisms; much higher than what occurs naturally. If it can be assumed that microorganisms behave independently of each other during both coagulation and filtration, then removal rates are not expected to depend on influent concentrations. However, Assavasilavasukul et al. (2008) observed better

removal of *Cryptosporidium* during conventional treatment with higher *Cryptosporidium* influent concentrations, and Prasanthi et al. (1997) observed better removal with higher influent particle concentrations in laboratory columns without coagulation. It is not clear, though, if these results would apply to viruses in our experiment. The virus volume is negligible compared to the total floc volume, virus aggregation was not observed, and according to standard theory for hetero-flocculation the virus-floc aggregation rate is expected to scale linearly with virus concentrations (Crittenden et al., 2005). Further research is needed to clarify these issues. The role of virus detachment in extrapolating results from pilot-scale to full-scale is also not clear (Kim and Tobiason, 2004). If virus detachment is not negligible compared to virus attachment, the observed removal efficiencies may be a function of the amount of viruses available for detachment and thereby a function of influent concentrations. This should also be further explored in future studies.

3.4 Filtration dynamics and health risks: Paper IV

3.4.1 Conceptual model

The purpose of **Paper IV** is to explore the role of such dynamic effects uncovered in **Paper III** on optimal filter operation and health risk estimates in QMRA. That is, for a filter operating as observed in **Paper III**, when should the filter-to-waste period be terminated and when should backwash be initiated in order to minimize pathogen passage? And is the variation in filter performance throughout the cycle relevant to health risk estimates or is it sufficient to work with the mean performance? The studies mentioned in Section 1.2.3 that claim correlations between short-term variations in turbidity and incidence of AGI signal that the dynamic effects cannot be ruled out a priori.

Several assumptions need to be made in order to facilitate analysis. First, the data from the pilot-experiment must be assumed to be representative of the performance of a full-scale filter. Second, it is assumed that the raw water pathogen concentration and the performance of other treatment processes are both stable on the time-scale of a single filter cycle. This means that filtration is the only source of short-term temporal variation in pathogen concentrations leaving the treatment plant. Third, simplifying assumptions on the operation of filters in parallel is made (Figure 3.11 on the next page), in that filters perform identically except for time-shifts in their filtration cycles, and flow through every filter is kept constant when another filter is being backwashed. Fourth, a distinction is made between *dispersive* and *non-dispersive* distributions systems, where the former is assumed to smooth out all temporal variations while the latter conserve them. Finally, it is assumed that water consumers may be considered to be flow-proportional samplers, i.e. each volume of water produced has the same chance of being ingested by a consumer. It is acknowledged that there are several strong assumptions here, which will be discussed below. Still, **Paper IV** demonstrates what kind of computations can be made when high-resolution data on removal efficiency is available.

We will relegate most of the technical details to **Paper IV**. The main thing to establish is that under these conditions the dose distribution experienced by a consumer in a *non-dispersive* distribution system is naturally assumed to be mixed Poisson (aggregation assumed negligible)

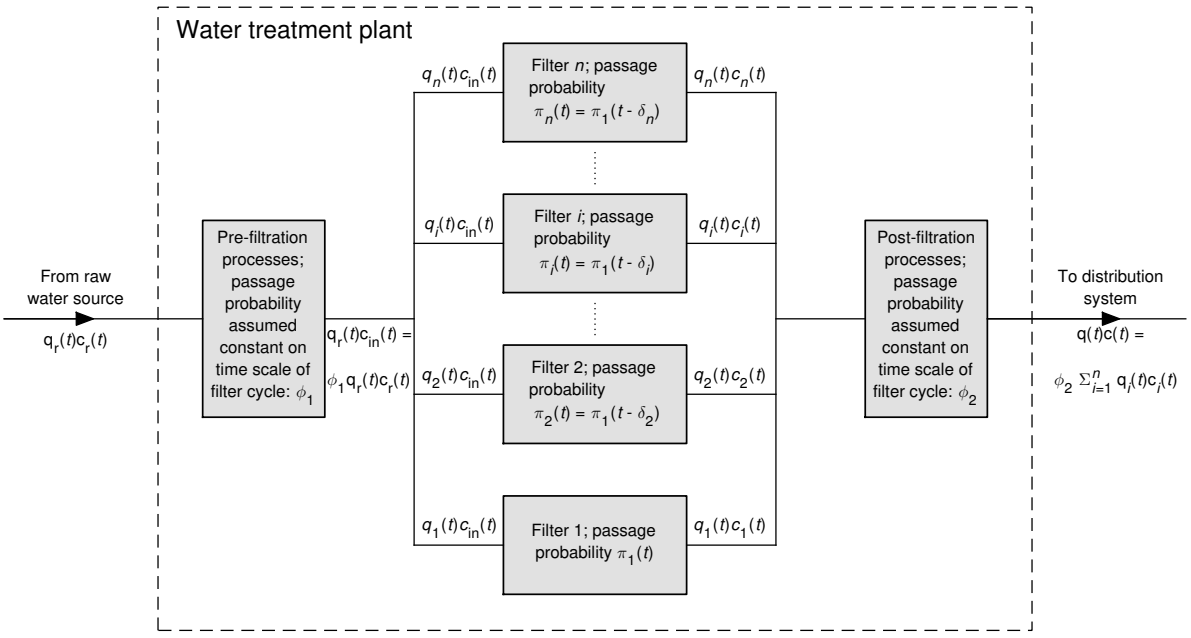

Figure 3.11: Conceptual layout of a water treatment plant with n filters operating in parallel. The labels represent mass fluxes of pathogens at the locations shown. From **Paper IV**.

and given by

$$p_X(x) = \int_0^\infty \frac{e^{-\lambda_d} {\lambda_s}^x}{x!} f_{\Lambda_d}(\lambda_d)\, d\lambda_d \tag{3.20}$$

where $\Lambda_d = k\Pi$ is a random variable that represents the temporal variation in the Poisson parameter λ_d, k represents the combination of raw water pathogen concentrations, ingestion volume and removal by non-filtration processes (all assumed constant) and Π is a random variable that represents the temporal variation in passage probability across a set of parallel filters due to filtration dynamics. Under identical conditions in a *dispersive* distribution system, the dose is simply Poisson-distributed with mean dose equal to $E(\Lambda_d) = kE(\Pi)$. We know from **Paper II**, Proposition 2, that the computed risk will be smaller in the non-dispersive distribution system, the question is whether it can be said to be of any practical relevance.

3.4.2 Results and discussion

The *mean* pathogen passage probability during filtration is important both in a dispersive and a non-dispersive distribution system. For a dispersive distribution system, in our simplified model, it is the *only* quantity associated with filtration that matters. Figure 3.12 on the facing page shows how the mean passage probability (blue curves) develops as the filter cycle progresses. These curves were obtained by direct trapezoidal integration of experimental datapoints. Each curve represents a different starting point for the filter cycle, at turbidity 0.1 NTU, 0.2 NTU or at stable turbidity (after 3 hours), respectively. The latter is hardly an option in practice since a large amount of water then must be filtered to waste.

It is easily demonstrated mathematically (**Paper IV**) that, for any "u-shaped" curve for the instantaneous passage probability (red curves in Figure 3.12), the minimum *mean* passage probability (blue curves in Figure 3.12) occurs when the instantaneous and mean passage probabilities are equal, which occurs *after* breakthrough of the microorganism in question,

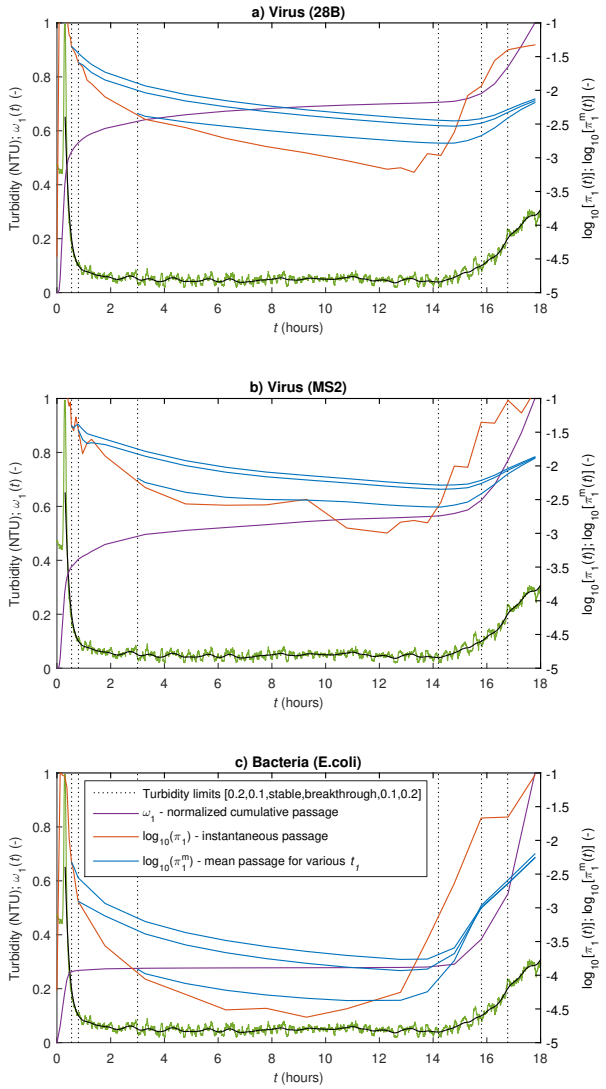

Figure 3.12: Turbidity, normalized cumulative passage and instantaneous and mean probability of passage. From **Paper IV**.

i.e. after the minimum of the instantaneous passage. This results depends only on the qualitative shape of the passage curve, and is therefore expected to be robust. For example, for *E.coli*, breakthrough occurred around 9 hours after filtration started, while the minimum mean passage occurred after about 13 hours when filtration is started at 0.1 or 0.2 NTU. For the viruses, this time difference between the respective minima is smaller. Furthermore, the difference between the minimum instantaneous passage and the minimum mean passage is up to 1 $\log_{10}$ unit for all microorganisms. The minimum mean passage occurred before turbidity breakthrough for bacteria, concurrently with turbidity for MS2 and slightly after turbidity breakthrough for 28B.

The idea that the optimal time to stop filtration for a given pathogen occurs after breakthrough for that pathogen may appear counterintuitive. In the beginning of the filter cycle, poor performance incurs a "debt" that must be repaid during periods of better performance later in the cycle. Repayment should continue until the current performance is worse than the mean performance up to the current time. Continuing filtration until turbidity reaches 0.2 NTU, which would still comply with the criteria in Table 3.1, is detrimental to overall performance,

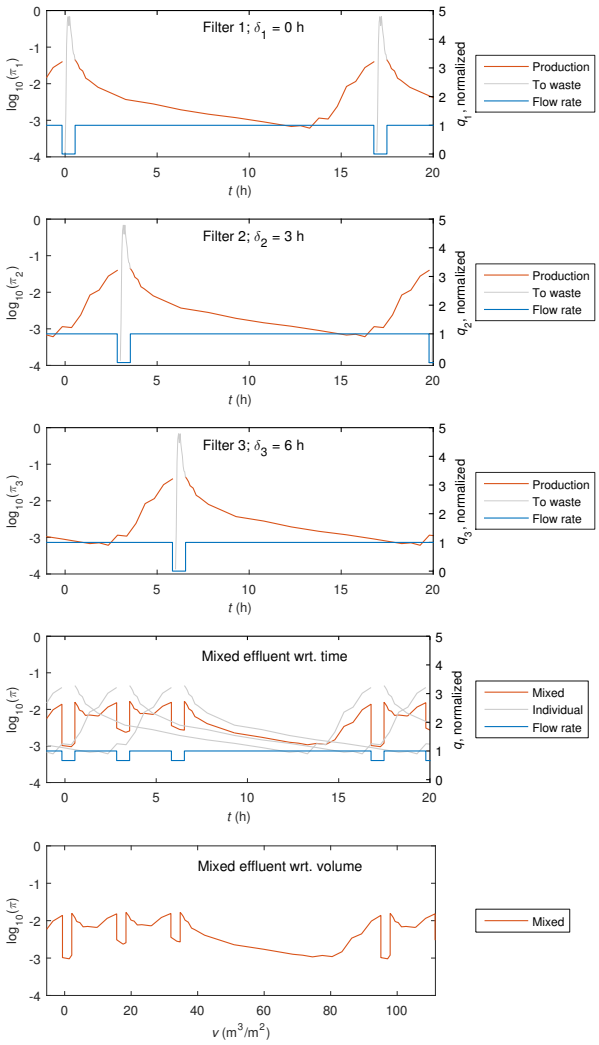

Figure 3.13: Reference filter performance (upper panel), time-shifted filters (2nd and 3rd panels), net passage probability $\pi(t)$ as a function of time (4th panel) and net passage probability $\pi(t(v))$ as a function of produced volume (lower panel). From **Paper IV**.

in particular for bacteria.

The extensive variation in microorganism removal efficiency observed during a single filter cycle in our experiment may explain some of the variation in reported removal efficiencies in previous studies (Table 3.3 on page 43). In order to facilitate comparison of results from different studies, it is suggested that (1) high temporal resolution sampling regimes be used in future studies and (2) results be reported as both instantaneous and mean removal efficiencies as a function of filtered water volume per unit filter area (multiply axis-values in Figure 3.12 by 5.9 m/h). Using filtered volume will normalize for differences in filtration rate.

In order to test whether filtration dynamics affects risk estimates, the net performance of a set of parallel filters were constructed by assuming that each filter performs identically to the filter in our experiment. Each filter cycle was displaced in time from a reference filter cycle by an integer multiple of a time shift δ, so that the net performance curve of all filters depends on this δ. Figure 3.13 shows an example. We assumed that the flow through each filter stayed constant when one of the other filters were being backwashed. In reality there may be hydraulic steps that worsen filter performance (Kim and Lawler, 2012), in which case the dips in π in the

lower panel of Figure 3.13 would not be so pronounced. This would complicate modeling since the mean performance of the parallel filters would likely depend on δ, unlike in our simplified model. Performance curves as in the lower panel of Figure 3.13 were used to construct dose distributions of pathogens and used in conjunction with the exponential dose-response model to compute risks. The exponential model was convenient since its parameter r is incorporated into the parameter k as presented following equation (3.20).

Results show (figures presented in **Paper IV**) that filtration dynamics, as displayed by the 28B data and *E.coli* data, is unlikely to affect risk estimates at pathogen concentrations normally encountered in drinking water, since risk estimates accounting for the dynamics are very close to risk estimates that are based on equivalent mean constant pathogen concentrations. This is of course related to the linearity of exponential models in the low-dose region and is expected to generalize to other single-hit models that are flatter than the exponential model (**Paper I**, Proposition 1). The only situation where filtration dynamics appears to play a potential role is in extremely high-risk situations where the attack rate is above 10 %. In this case, accounting for filtration dynamics gives a lower risk estimate. Furthermore, reducing δ reduces the risk and more so when there are only a few filters. Thus, in theory, in a non-dispersive distribution system, timing backwashes so that they occur consecutively may have some dampening effect on attack rates in extreme outbreaks. However, this cannot be recommended as an operational strategy until more research is conducted on the effect of backwashing/hydraulic steps on the net removal efficiency of a set of filters in parallel.

Our model assumed that raw water concentrations and the performance of other treatment processes stayed constant on the time-scale of a filter cycle. This is not necessarily so in reality. If there are other short-term variations present, the finished water pathogen concentration may be written:

$$C = C_{\mathrm{r}} \Pi_{\mathrm{f}} \prod_i \Pi_{\mathrm{o},i} \tag{3.21}$$

where C_{r} is the raw water concentration, Π_{f} the passage probability of filtration and $\Pi_{\mathrm{o},i}$ the passage probability of other treatment processes indexed by i. If all quantities are mutually statistically independent, the mean of C is simply the product of the mean of each quantity in (3.21) and the mean passage probabilities in Figure 3.12 are still perfectly relevant. However, the variance of C will be greater than in our model, and the dynamic effects discussed in the preceding paragraph may be even more pronounced.

The independence assumption is not obviously valid though, as microbial raw water quality may very well be correlated with other raw water quality parameters that affect treatment performance. Furthermore, there may be interactions between the treatment performance of sequential treatment units. For example, Templeton et al. (2007) found a reduced virus inactivation of downstream UV-processes when treating water from the breakthrough stage of the upstream rapid filter, a result which could imply that the optimal time to terminate a filter cycle occurs earlier than the time of minimum mean passage in Figure 3.12. Another complication is related to the time-scales of variation of the processes that generate the random variables in (3.21), which may be vastly different among the variables. This means that it may take a very long time, longer than the time period of interest, to obtain a realization of C. In fact, it may be difficult to meaningfully assign a probability distribution to variables that are dominated by rare events, in which case C and its mean is ill-defined. Thus, proper considerations of time-scales of variation should be a focus of QMRA.

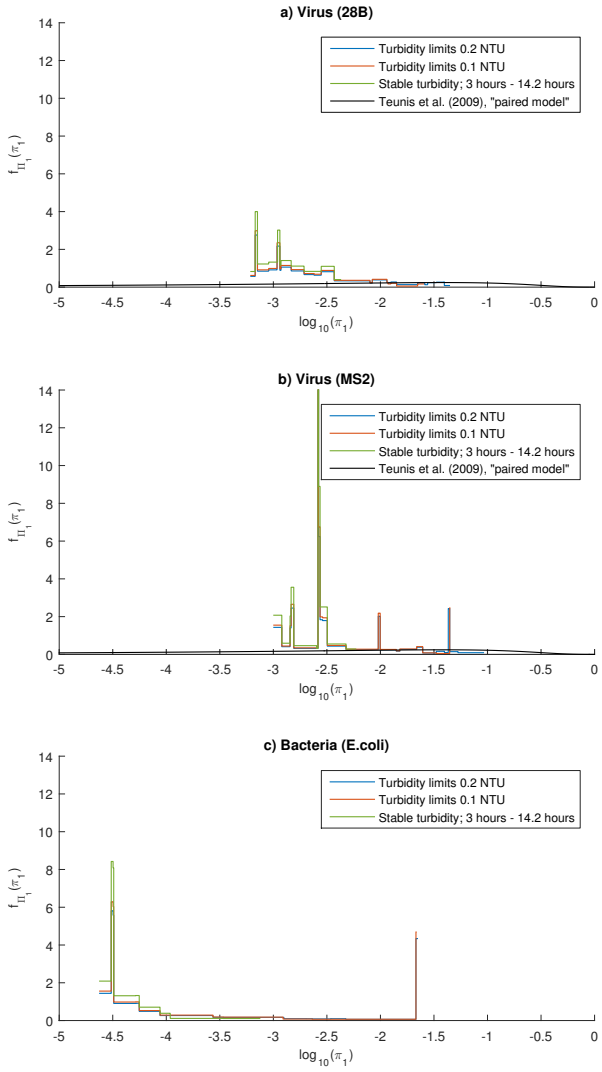

Figure 3.14: Probability density functions derived from $\pi_1(t)$ in the example data of Figure 3.8, using the methods outlined in the appendix of **Paper IV**. From **Paper IV**.

The variability in removal that was observed in our experiment may be used as an input to Monte Carlo models for risk characterization. In Figure 3.14 the probability distributions generated by sampling from Π uniformly in time for the duration the filter cycle are shown. The distribution was computed directly from the experimental data as explained in the Appendix of **Paper IV**. Smoother versions may be developed. Also shown in Figure 3.14 is a distribution of Π developed by Teunis et al. (2009) based on methods developed by Teunis et al. (1999b). They used data for F-specific phage removal from two plants in the Netherlands to develop this distribution. The mean of the distribution is close to -1.5, and it is obvious that the variability is very much greater than observed in our filter cycle. However, the distribution was developed based on a total of 17 samples and uncertainty intervals were very wide.

4. Metabolic Lag in Bacterial Growth: Paper V

4.1 Background and model development

Figure 4.1 shows a typical growth curve for a bacterial culture after inoculation in a closed system (except possibly for gases), i.e. a system where there is limited space, no replenishment of nutrients and no elimination of wastes. An initial lag phase, which is our interest here, is followed by a phase of exponential growth until environmental limitations enforce a plateau and eventually a net die-off. The lag phase may occur in response to changes in substrate availability, e.g. because of the need to synthesize compounds that are needed for substrate utilization or because of the need to perform cell repair before substrate utilization can begin (Huang, 2015).

There have been attempts to model bacterial growth using systems biology approaches with descriptions of internal cell metabolism and gene regulation (Koutinas et al., 2011; Steinmeyer and Shuler, 1989), which in principle could include explicit descriptions of the mechanisms that cause the appearance of a lag phase (Hassan et al., 2014). However, simpler models that disregard internal cell processes are used in most applications.

Natural bacterial communities are usually not confined to closed systems, and growth may instead be limited by the availability of a few substrate types (possibly only one) called *limiting substrates*, with concentration denoted by s. We may then assume that the growth rate of a

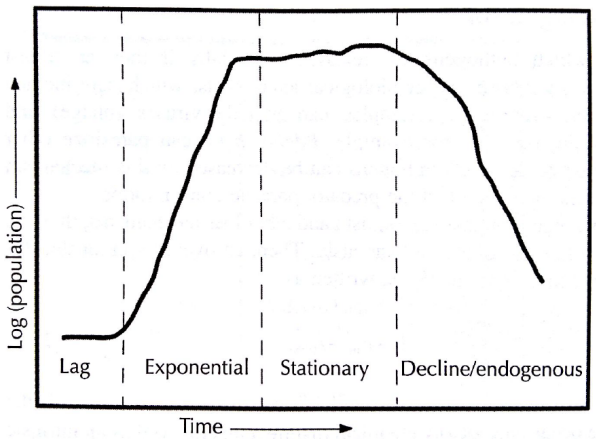

Figure 4.1: Typical growth curve for bacteria. From Haas et al. (2014).

bacterial community in the absence of lag effects may be written as

$$\frac{\mathrm{d}M_\mathrm{b}}{\mathrm{d}t} = \Psi_\mathrm{max}(M_\mathrm{b}, s) \tag{4.1}$$

where M_b is the bacterial mass and Ψ_max is the growth rate function. The Monod equation (Monod, 1949) is often adopted:

$$\frac{\mathrm{d}M_\mathrm{b}}{\mathrm{d}t} = \mu M_\mathrm{b} \frac{s}{K_s + s} \tag{4.2}$$

Here, μ is the maximum specific growth rate and K_s is the so-called half-saturation constant. Equation (4.2) should be coupled with equations that describe depletion of substrate as it is being utilized by the bacteria, as well as external influences on substrate availability (transport, interacting microbial communities etc.).

The above growth expressions must be modified if a lag phase is to be described. Several approaches have been suggested, which range in complexity from postulating simple substrate thresholds for growth to begin (Park et al., 2001) to models that employ delay differential equations (Bocharov and Rihan, 2000; Cushing, 1977; Driver, 1977). With the latter, the rate of change of the system variables can be made dependent on the history of these variable and not just the current state of the system. In **Paper V**, we explore the latter approach, as described in the following.

Wood et al. (1995) cited Powell (1967) as the source of the following modification to account for metabolic lags:

$$\frac{\mathrm{d}M_\mathrm{b}}{\mathrm{d}t} = \Psi_\mathrm{max}(M_\mathrm{b}, s)\lambda_\mathrm{m}(t) \tag{4.3}$$

Here, $\lambda_\mathrm{m} = \Psi/\Psi_\mathrm{max}$ is a scalar between 0 and 1 and is called the metabolic potential, and Ψ is the *actual* growth rate. λ_m is a functional, assumed to depend on the past history of substrate concentrations, $s(\tau)|_{\tau<t}$. Based on the previous studies by Powell (1967) and Caperon (1969), Wood et al. (1995) suggested the following convolution integral:

$$\lambda_\mathrm{m}(t) = \int_{-\infty}^{t} H[s(\tau)]K(t-\tau)\,\mathrm{d}\tau \tag{4.4}$$

Here H is some function that maps s onto the unit interval and K is a weight function that should have the properties of a normalized probability density function on the positive real line. Thus (4.4) represents a weighted average of the history of H. It has been suggested (Edwards, 1970) that the onset of growth is sensitive to the limiting substrate s crossing a certain critical substrate concentration s_c. It is therefore natural to look for sigmoidal-shaped candidates for H and in **Paper V** we suggest the Hill function:

$$H(s) = \frac{s^p}{{s_\mathrm{c}}^p + s^p} \tag{4.5}$$

where p is a steepness parameter. As $p \to \infty$, H approaches the Heaviside function, which was used by Wood et al. (1995).

Wood et al. (1995) postulated a piecewise linear form for $\lambda_\mathrm{m}(t)$ in response to s crossing s_c and deduced the functional form of K needed to produce the desired behavior. This approach required several parameters and special care was needed to handle fluctuations of s around

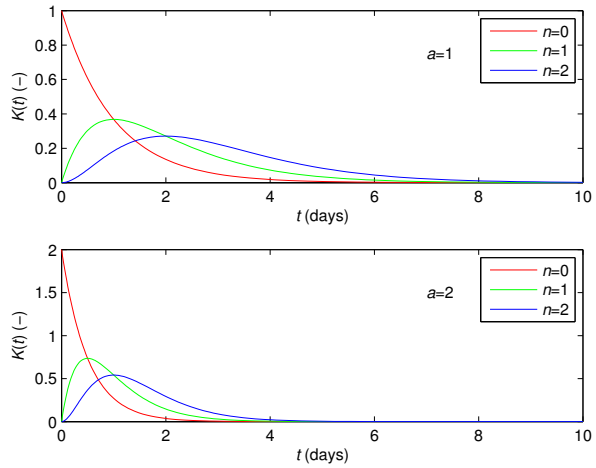

Figure 4.2: Examples of the kernel used in the distributed delay formulation. From **Paper V**.

s_c. In **Paper V** we instead propose a function K that will turn out to simplify the problem, namely the probability density for a Gamma distribution (Figure 4.2) with integer shape parameter n and positive rate parameter a:

$$K_a^n(t) = \frac{a^{n+1}t^n e^{-at}}{n!} \tag{4.6}$$

In the appendix of **Paper V**, it is shown how this weight function transforms the convolution integral (4.4) into a system of $n+1$ differential equations in auxiliary variables $z_1, \ldots, z_{n+1}$, using what is known as the *linear chain trick* (MacDonald, 1978):

$$\begin{aligned} \lambda_m &= z_{n+1}(t) \\ z_1'(t) &= a\{H[s(t)] - z_1(t)\} \\ z_2'(t) &= a[z_1(t) - z_2(t)] \\ &\vdots \\ z_{n+1}'(t) &= a[z_n(t) - z_{n+1}(t)] \end{aligned} \tag{4.7}$$

This reformulation of the convolution integral may be useful both from the point of view of implementing the lag formulation numerically, but it may also facilitate analysis since one may now draw upon the theory for systems of ordinary differential equations. The approach may be generalized to integral kernels different from the Gamma distribution (Ponosov and Shindiapin, 2003).

4.2 Validation against data and discussion

In order to test whether the proposed lag formulation can match real data, we used experimental data from Chen et al. (1992) for the transport and biodegradation of benzene in laboratory sand columns. They built a numerical model of coupled PDEs for this system that did not match the experimental data unless they assumed that only 1/8 of the biomass was able to degrade benzene. This shortcoming was what motivated Wood et al. (1995) to incorporate a lag formulation into the model of Chen et al. The full model is presented in **Paper V**. Briefly,

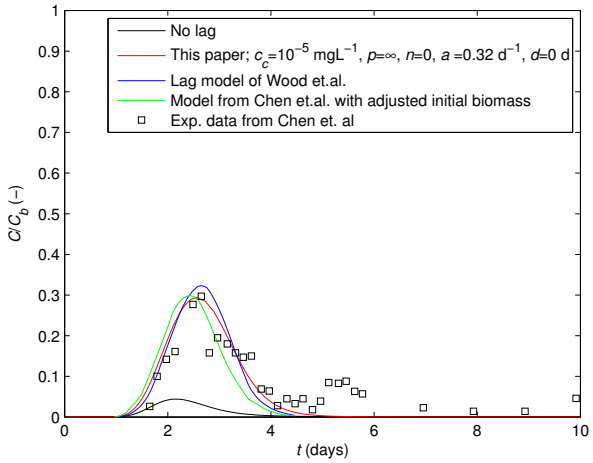

Figure 4.3: Performance of the lag formulation in a biodegradation experiment. From **Paper V**.

it involved advection/dispersion of benzene and hydrogenperoxide (the final electron acceptor) in a mobile aqueous phase, equilibrium adsorption for benzene, mass exchange of both compounds between the mobile phase and an immobile biomass phase, and biodegradation in the biomass phase described by Monod kinetics. All parameters except those associated with our lag formulation were known. We used a simple method-of-lines approach for the numerical implementation, which involved discretization of spatial derivatives using finite-differences and yielded a system of ordinary differential equations in the time variable that were solved using built-in solvers in MATLAB. The numerical implementation was verified graphically against data presented by Wood et al. (1995).

The results of the simulations are shown in Figure 4.3, where the vertical axis represents effluent benzene concentrations normalized to the constant influent benzene concentration. With no lag formulation included, the model overestimates the benzene degradation. For the parameters of the Hill function (eq. (4.5)), s_c was taken from Wood et al. and results were found to be insensitive to the steepness parameter p. For the Gamma kernel (4.6), it was found that having $n > 0$ did not improve the fit as compared to $n = 0$. Hence, there is only one fitting parameter left, a, which was adjusted manually to produce a good fit. This is one less parameter than the lag model of Wood et al. (1995), but these authors used parameters that were estimated from independent data and not during fitting. A comparison with another set of experimental data from Park et al. (2001), using a slightly less complicated transport model, is given in **Paper V**.

It is interesting to note that Huang (2015), in investigating the distribution of lag times among individual bacterial cells, found that the data could be fitted well by many probability distributions, including the Gamma distribution. It is also worth noting that some previous models for lag phenomena in response to changes in substrate levels (not only switching from absence to presence of substrate), as presented by Haas et al. (2014, pp. 255-256), have the

structure

$$\begin{aligned} \frac{\mathrm{d}M_{\mathrm{b}}}{\mathrm{d}t} &= \kappa M_{\mathrm{b}} \\ k_{\mathrm{e}}(s) &= \mu \frac{s}{K_s + s} \\ \frac{\mathrm{d}\kappa}{\mathrm{d}t} &= a(k_{\mathrm{e}}(s) - \kappa) \end{aligned} \tag{4.8}$$

Comparing with equations (4.3) - (4.7), the system (4.8) is equivalent to identifying κ with λ_{m}, setting $\Psi_{\max} = M_{\mathrm{b}}$, $H(s) = k_{\mathrm{e}}(s)$ (the Monod specific growth rate) and $n = 0$. It seems that the interpretation of this system as reflecting an exponentially decaying weight function of past values of k_{e} has not been made, though.

Although the lag formulation was presented here in a setting of biodegradation in a porous medium, we may speculate that it may be useful in settings more relevant to microbial risk assessment. Specifically, one could investigate whether it may be useful for modeling growth of environmental pathogens (Ashbolt, 2015). Furthermore, widely used compartmental SIR-models (susceptible-infected-recovered; Eisenberg et al., 1996; Kermack and McKendrick, 1927) in epidemiology describe distributions of incubation times using convolution integrals. Finally, it could be interesting to investigate whether it could be useful for modeling biological treatment processes, such as biofiltration or slow sand filtration for drinking water or activated sludge processes for waste water.

5. Conclusions and Outlook

The main conclusions emanating from this thesis may be stated as follows, with recommendations for further research and practical implications in bullet points:

Host/pathogen properties in single-hit models. Equation (2.6) provides a general expression for the single-hit probability R as a function of host/pathogen random variables.

- This expression may possibly guide future efforts to develop dose-response models that take pathogen and host properties as parameters.

Risk from repeated exposures. The model-consistent expression for the risk from repeated exposures deviates from the conventional expression, and is obtained by interpreting the dose-distribution in the general single-hit model (2.5) as the distribution of the *accumulated dose* from multiple exposures.

- The model-consistent expression for risk from repeated exposures should be used for risk characterization, including Monte-Carlo simulations.
- The full practical relevance of this result should be explored for a range of exposure scenarios and pathogens with known dose-response parameters.

Dose overdispersion and risk. The single-hit risk computed with stuttering or mixed Poisson distributions is lower than that computed with a Poisson distribution, assuming identical mean doses. Overdispersion from moderate clustering of pathogens in the form of a Hermite distribution is unlikely to significantly affect the risk estimate under most conditions. However, extensive overdispersion significantly reduces the risk estimate.

- If management decisions are based on *mean* risk estimates, using point estimates of the mean dose λ_{d} rather than a distribution of λ_{d}-values may be a conservative approach.

Improved bound on risk. Equation (2.21) gives an improved bound on the single-hit risk and appears to be close to exact computations when doses are extensively overdispersed. It takes the probability of zero dose as a parameter, in addition to the mean dose.

- The bound may be useful for applications since it doesn't require a full dose-distribution.
- In a single-hit framework, efforts should be directed at estimating these two parameters with precision.

Filtration dynamics. Spatio-temporal removal patterns of viruses and bacteria were in qualitative agreement with expectations, based on their respective sizes. However, peak observed removal rates within the filter bed were higher than expected from filtration theory. Overall removal efficiencies were observed to be highly variable, even during periods of stable effluent turbidity.

- Further pilot-scale experiments with high-resolution sampling should be performed under a range of conditions to corroborate these experimental results.
- The role of microorganism detachment in extrapolating log-removal values from high-spike experiment to real-world settings should be explored.

Filtration dynamics and mean removal efficiency. The peak *mean* removal efficiency of a microorganism in a filter run occurs *after* breakthrough of that organism, a result which appears robust. Time differences of 2-4 hours were observed. The mean removal efficiency may deteriorate drastically if filtration is continued past turbidity breakthrough, e.g. until typical regulatory limits of 0.1, 0.2 or 0.3 NTU are reached.

- At the very latest, filtration should be stopped at turbidity breakthrough, i.e. the time when effluent turbidity starts to increase.
- As a basis for comparison, results from filtration experiments should be reported as mean removal efficiency as a function of produced water volume per unit filter area.

Filtration dynamics and risk. *In isolation*, filtration dynamics is unlikely to affect single-hit risk estimates except in a situation with extremely high pathogen concentrations, assuming that the correct mean removal efficiency of the filter is known. The main challenge presented to QMRA by filtration dynamics is therefore to obtain correct mean removal efficiencies. However, filtration dynamics does represent a vulnerability when coupled with other short-term variations in pathogen concentrations or removal efficiencies.

- The effect of realistic concurrent short-term fluctuations in filtration performance, disinfection performance and raw water pathogen concentrations should be explored.
- Proper consideration of time-scales of variation in different parts of the water supply system should be a focus of QMRA.

Microbial metabolic lag. The microbial metabolic lag model presented in Chapter 4 is simple to implement numerically and was shown to simulate the example biodegradation system as well as previous models.

- The possibility of using the metabolic lag model in population disease transmission, growth of environmental pathogens or biological treatment processes may be explored.

References

Abbaszadegan, M. et al. (2007). "Efficacy of removal of CCL viruses under enhanced coagulation conditions." *Environmental Science and Technology* **41** (3), pp. 971–977. DOI: 10.1021/es061517z.

Abbaszadegan, M. et al. (2008). "Removal of adenovirus, calicivirus, and bacteriophages by conventional drinking water treatment." *Journal of Environmental Science and Health, Part A: Toxic/Hazardous Substances and Environmental Engineering* **43** (2), pp. 171–177. DOI: 10.1080/10934520701781541.

Abramowitz, M. and I. A. Stegun, eds. (1964). *Handbook of Mathematical Functions with Formulas, Graphs, and Mathematical Tables*. National Bureau of Standards - Applied Mathematics Series, p. 958. DOI: 10.1119/1.15378.

Adamczyk, Z. and P. Weroński (1999). "Application of the DLVO theory for particle deposition problems." *Advances in Colloid and Interface Science* **83** (1), pp. 137–226. DOI: 10.1016/S0001-8686(99)00009-3.

Adin, A. and M. Rebhun (1987). "Deep-bed filtration: Accumulation-detachment model parameters." *Chemical Engineering Science* **42** (5), pp. 1213–1219. DOI: 10.1016/0009-2509(87)80072-6.

Adin, A. and M. Rebhun (1974). "High-rate contact flocculation—filtration with cationic polyelectrolytes." *Journal (American Water Works Association)* **66** (2), pp. 109–117. URL: http://www.jstor.org/stable/41266974.

Agbalika, F et al. (1985). "Study of Indigenous Virus Removal at Different Stages in a Drinking Water Plant Treating River Water." *Water Science & Technology* **17** (10), pp. 211–218. URL: http://wst.iwaponline.com/content/17/10/211.abstract.

Allen, M. J., S. C. Edberg, and D. J. Reasoner (2004). "Heterotrophic plate count bacteria—what is their significance in drinking water?" *International Journal of Food Microbiology* **92** (3), pp. 265–274. DOI: 10.1016/j.ijfoodmicro.2003.08.017.

Alvarez, A. C. et al. (2013). "Analytic regularization of an inverse filtration problem in porous media." *Inverse Problems* **29** (2), p. 025006. DOI: 10.1088/0266-5611/29/2/025006.

Alvarez, A. C. (2005). "Inverse problems for deep bed filtration in porous media." PhD. Instituto Nacional de Matemática Pura e Aplicada, Rio de Janeiro, Brasil, p. 152. URL: http://goo.gl/KYVdUJ.

Alvarez, A. C. et al. (2006). "A fast inverse solver for the filtration function for flow of water with particles in porous media." *Inverse Problems* **22** (1), pp. 69–88. DOI: 10.1088/0266-5611/22/1/005.

Alvarez, A. C. et al. (2007). "The inverse problem of determining the filtration function and permeability reduction in flow of water with particles in porous media." *Transport in Porous Media* **70** (1), pp. 43–62. DOI: 10.1007/s11242-006-9082-3.

Amirtharajah, A. (1985). "The interface between filtration and backwashing." *Water Research* **19** (5), pp. 581–588. DOI: 10.1016/0043-1354(85)90063-6.

Amirtharajah, A. and K. Mills (1982). "Rapid mix design for mechanisms of alum coagulation." *American Water Works Association* **74** (4), pp. 210–216. URL: http://www.jstor.org/stable/41271001.

Amirtharajah, A. (1988). "Some Theoretical and Conceptual Views of Filtration." *Journal (American Water Works Association)* **80** (12), pp. 36–46. URL: http://www.jstor.org/stable/41292090.

Armitage, P. (1959). "Host Variability in Dilution Experiments." *Biometrics* **15** (1), pp. 1–9. DOI: 10.2307/2527597.

Armitage, P. and C. C. Spicer (1956). "The detection of variation in host susceptibility in dilution counting experiments." *Journal of Hygiene* **54** (3), pp. 401–414. DOI: 10.1017/S0022172400044661.

Armitage, P., G. G. Meynell, and T. Williams (1965). "Birth–Death and other Models for Microbial Infection." *Nature* **207** (4997), pp. 570–572. DOI: 10.1038/207570a0.

Asami, T. et al. (2016). "Evaluation of virus removal efficiency of coagulation-sedimentation and rapid sand filtration processes in a drinking water treatment plant in Bangkok, Thailand." *Water Research*. DOI: 10.1016/j.watres.2016.05.012.

Ashbolt, N. (2015). "Environmental (Saprozoic) Pathogens of Engineered Water Systems: Understanding Their Ecology for Risk Assessment and Management." *Pathogens* **4** (2), pp. 390–405. DOI: 10.3390/pathogens4020390.

Ashbolt, N. J. (2004). "Risk analysis of drinking water microbial contamination versus disinfection by-products (DBPs)." *Toxicology* **198** (1-3), pp. 255–262. DOI: 10.1016/j.tox.2004.01.034.

Assavasilavasukul, P. et al. (2008). "Effect of pathogen concentrations on removal of Cryptosporidium and Giardia by conventional drinking water treatment." *Water Research* **42** (10-11), pp. 2678–2690. DOI: 10.1016/j.watres.2008.01.021.

Åström, J et al. (2007). "Evaluation of the microbial risk reduction due to selective closure of the raw water intake before drinking water treatment." *Journal of Water and Health* **5** (S1), pp. 81–97. DOI: 10.2166/wh.2007.139.

Auset, M. and A. A. Keller (2006). "Pore-scale visualization of colloid straining and filtration in saturated porous media using micromodels." *Water Resources Research* **42** (12), W12S02. DOI: 10.1029/2005WR004639.

Aw, T. G. and J. B. Rose (2012). "Detection of pathogens in water: from phylochips to qPCR to pyrosequencing." *Current Opinion in Biotechnology* **23** (3), pp. 422–430. DOI: 10.1016/j.copbio.2011.11.016.

Bache, D. H. and R. Gregory (2010). "Flocs and separation processes in drinking water treatment: a review." *Journal of Water Supply: Research and Technology—AQUA* **59** (1), pp. 16–30. DOI: 10.2166/aqua.2010.028.

Bai, R. and C. Tien (1997). "Particle Detachment in Deep Bed Filtration." *Journal of colloid and interface science* **186** (2), pp. 307–317. DOI: 10.1006/jcis.1996.4663.

Bai, R. and C. Tien (2000). "Effect of Deposition in Deep-Bed Filtration: Determination and Search of Rate Parameters." *Journal of colloid and interface science* **231** (2), pp. 299–311. DOI: 10.1006/jcis.2000.7130.

Berg, G. (1973). "Removal of viruses from sewage, effluents, and waters. 1. A review." *Bulletin of the World Health Organization* **49** (5), pp. 461–469. URL: http://www.ncbi.nlm.nih.gov/pmc/articles/PMC2480995/.

Bergendahl, J. a. and D. Grasso (2003). "Mechanistic basis for particle detachment from granular media." *Environmental Science & Technology* **37** (10), pp. 2317–2322. DOI: 10.1021/es0209316.

Besner, M.-C., M. Prévost, and S. Regli (2011). "Assessing the public health risk of microbial intrusion events in distribution systems: Conceptual model, available data, and challenges." *Water Research* **45** (3), pp. 961–979. DOI: 10.1016/j.watres.2010.10.035.

Bichai, F. and P. W. M. H. Smeets (2013). "Using QMRA-based regulation as a water quality management tool in the water security challenge: Experience from the Netherlands and Australia." *Water Research* **47** (20), pp. 7315–7326. DOI: 10.1016/j.watres.2013.09.062.

Birkhead, G and R. L. Vogt (1989). "Epidemiologic surveillance for endemic Giardia lamblia infection in Vermont. The roles of waterborne and person-to-person transmission." *American journal of epidemiology* **129** (4), pp. 762–768. URL: http://aje.oxfordjournals.org/content/129/4/762.short.

Bocharov, G. a. and F. a. Rihan (2000). "Numerical modelling in biosciences using delay differential equations." *Journal of Computational and Applied Mathematics* **125** (1-2), pp. 183–199. DOI: 10.1016/S0377-0427(00)00468-4.

Boorman, G. A. (1999). "Drinking Water Disinfection Byproducs: Review and Approach to Toxicity Evaluation." *Environmental Health Perspectives* **107** (Suppl. 1), pp. 207–217. URL: http://www.ncbi.nlm.nih.gov/pubmed/10229719.

Bosch, A (1998). "Human enteric viruses in the water environment: a minireview." *International microbiology: the official journal of the Spanish Society for Microbiology* **1** (3), pp. 191–196. URL: http://www.ncbi.nlm.nih.gov/pubmed/10943359.

Bosch, A., ed. (2007). *Human Viruses in Water*. Vol. 17. Perspectives in Medical Virology. Elsevier, p. 306. URL: https://www.elsevier.com/books/human-viruses-in-water/bosch/978-0-444-52157-6.

Boudaud, N. et al. (2012). "Removal of MS2, Qβ and GA bacteriophages during drinking water treatment at pilot scale." *Water Research* **46** (8), pp. 2651–2664. DOI: 10.1016/j.watres.2012.02.020.

Bradford, S. a. et al. (2006). "Significance of straining in colloid deposition: Evidence and implications." *Water Resources Research* **42** (12), W12S15. DOI: 10.1029/2005WR004791.

Bradford, S. a. et al. (2014). "Modeling microorganism transport and survival in the subsurface." *Journal of environmental quality* **43** (2), pp. 421–440. DOI: 10.2134/jeq2013.05.0212.

Brock, T. D. (1999). *Robert Koch: A Life in Medicine and Bacteriology*. American Society of Microbiology, p. 364. DOI: 10.1128/9781555818272.

Buchanan, R. L., J. L. Smith, and W. Long (2000). "Microbial risk assessment: Dose-response relations and risk characterization." *International Journal of Food Microbiology* **58** (3), pp. 159–172. DOI: 10.1016/S0168-1605(00)00270-1.

Calderon, R. L. and G. F. Craun (2006). "Estimates of endemic waterborne risks from community-intervention studies." *Journal of Water and Health* **04** (Suppl. 2), pp. 89–99. DOI: 10.2166/wh.2006.019.

Calderon, R. L., G. Craun, and D. a. Levy (2006). "Estimating the infectious disease risks associated with drinking water in the United States." *Journal of Water and Health* **04** (Suppl. 2), pp. 1–2. DOI: 10.2166/wh.2006.026.

Caperon, J. (1969). "Time lag in population growth response of Isochrysis galbana to a variable nitrate environment." *Ecology* **50** (2), pp. 188–192. DOI: 10.2307/1934845.

Carlson, H. J., G. M. Ridenour, and C. F. McKhann (1942). "Efficacy of Standard Purification Methods in Removing Poliomyelitis Virus from Water." *American Journal of Public Health and the Nations Health* **32** (11), pp. 1256–1262. URL: http://www.ncbi.nlm.nih.gov/pubmed/18015702.

Center for Advancing Microbial Risk Assessment. *QMRA Wiki*. URL: http://qmrawiki.canr.msu.edu/ (visited on 11/20/2015).

Chen, Y.-M. et al. (1992). "Modeling transport and biodegradation of benzene and toluene in sandy aquifer material: Comparisons With experimental measurements." *Water Resources Research* **28** (7), pp. 1833–1847. DOI: 10.1029/92WR00667.

Clark, S. C., D. F. Lawler, and R. S. Cushing (1992). "Contact Filtration: Particle Size and Ripening." *Journal (American Water Works Association)* **84** (12), pp. 61–71. URL: http://www.jstor.org/stable/41293944.

Colford, J. M. et al. (2006). "A review of household drinking water intervention trials and an approach to the estimation of endemic waterborne gastroenteritis in the United States." *Journal of Water and Health* **04** (Suppl. 2), pp. 71–88. DOI: 10.2166/wh.2006.018.

Collier, S. A. et al. (2012). "Direct healthcare costs of selected diseases primarily or partially transmitted by water." *Epidemiology and Infection* **140** (11), pp. 2003–2013. DOI: 10.1017/S0950268811002858.

Cornforth, D. M. et al. (2015). "Bacterial cooperation causes systematic errors in pathogen risk assessment due to the failure of the independent action hypothesis." *Public Library of Science Pathogens* **11** (4), e1004775. DOI: 10.1371/journal.ppat.1004775.

Corso, P et al. (2003). "Costs of Illness in the 1993 Waterborne Cryptosporidium Outbreak, Milwaukee, Wisconsin." *Emerging Infectious Diseases* **9** (4), pp. 426 –431. DOI: 10.3201/eid0904.020417.

Council of the European Union (1998). "Council Directive 98/83/EC of 3 November 1998 on the quality of water intended for human consumption." *Official Journal of the European Communities* (L330), pp. 32–54. URL: http://eur-lex.europa.eu/legal-content/EN/TXT/?uri=CELEX:31998L0083.

Craun, G. F. et al. (2006). "Waterborne outbreaks reported in the United States." *Journal of Water and Health* **04** (Suppl. 2), pp. 19–30. DOI: 10.2166/wh.2006.016.

Crittenden, J. C. et al. (2005). *MWH's Water Treatment: Principles and Design*. 2nd ed. Hoboken, NJ, USA: John Wiley & Sons, Inc., p. 2000. DOI: 10.1002/9781118131473.

Crowther, J. (1924). "Some Considerations Relative to the Action of X-Rays on Tissue Cells." *Proceedings of the Royal Society of London. Series B, Containing Papers of a Biological Character* **96** (674), pp. 207–211. URL: http://www.jstor.org/stable/81217.

Cummins, E., R. Kennedy, and M. Cormican (2010). "Quantitative risk assessment of Cryptosporidium in tap water in Ireland." *Science of the Total Environment* **408** (4), pp. 740–753. DOI: 10.1016/j.scitotenv.2009.11.008.

Cushing, J. M. (1977). *Integrodifferential Equations and Delay Models in Population Dynamics*. Vol. 20. Lecture Notes in Biomathematics. Berlin, Heidelberg: Springer Berlin Heidelberg. DOI: 10.1007/978-3-642-93073-7.

Cutler, D. and G. Miller (2005). "The Role of Public Health Improvements In Health Advances: The Twentieth-Century United States." *Demography* **42** (1), pp. 1–22. DOI: 10.1353/dem.2005.0002.

Dábrowski, W. (1988). "Consequences of the mass balance simplification in modelling deep filtration." *Water Research* **22** (10), pp. 1219–1227. DOI: 10.1016/0043-1354(88)90108-X.

Damikouka, I., A. Katsiri, and C. Tzia (2007). "Application of HACCP principles in drinking water treatment." *Desalination* **210** (1-3), pp. 138–145. DOI: 10.1016/j.desal.2006.05.039.

Davidson, A. et al. (2005). *Water Safety Plans: Managing drinking-water quality from catchment to consumer*. Geneva, Switzerland. URL: http://goo.gl/diV4EK.

DeFelice, N. B., J. E. Johnston, and J. M. Gibson (2015). "Acute Gastrointestinal Illness Risks in North Carolina Community Water Systems: A Methodological Comparison." *Environmental Science & Technology* **49** (16), pp. 10019–10027. DOI: 10.1021/acs.est.5b01898.

Derjaguin, B and L Landau (1941). "Theory of the stability of strongly charged lyophobic sols and of the adhesion of strongly charged particles in solutions of electrolytes." *Acta physicochim. URSS* **14** (6), pp. 633–662. DOI: 10.1016/0079-6816(93)90013-L.

Dika, C. et al. (2011). "Impact of internal RNA on aggregation and electrokinetics of viruses: Comparison between MS2 phage and corresponding virus-like particles." *Applied and Environmental Microbiology* **77** (14), pp. 4939–4948. DOI: 10.1128/AEM.00407-11.

Donald, M. et al. (2011). "Incorporating parameter uncertainty into Quantitative Microbial Risk Assessment (QMRA)." *Journal of Water and Health* **9** (1), pp. 10–26. DOI: 10.2166/wh.2010.073.

Donaldson, S. H. et al. (2015). "Developing a General Interaction Potential for Hydrophobic and Hydrophilic Interactions." *Langmuir* **31** (7), pp. 2051–2064. DOI: 10.1021/la502115g.

Dowd, S. E. et al. (1998). "Delineating the specific influence of virus isoelectric point and size on virus adsorption and transport through sandy soils." *Applied and environmental microbiology* **64** (2), pp. 405–410. URL: http://aem.asm.org/content/64/2/405.short.

Drikkevannsforskriften (2001). *Forskrift 04.12.2001 nr. 1372 om vannforsyning og drikkevann*. URL: https://lovdata.no/dokument/SF/forskrift/2001-12-04-1372.

Driver, R. D. (1977). *Ordinary and Delay Differential Equations*. Vol. 20. Applied Mathematical Sciences. New York, NY: Springer New York. DOI: 10.1007/978-1-4684-9467-9.

Druett, H. A. (1952). "Bacterial Invasion." *Nature* **170** (4320), pp. 288–288. DOI: 10.1038/170288a0.

Duncan, H. E. and S. C. Edberg (1995). "Host-Microbe Interaction in the Gastrointestinal Tract." *Critical Reviews in Microbiology* **21** (2), pp. 85–100. DOI: 10.3109/10408419509113535.

Duval, J. F. L. and F. Gaboriaud (2010). "Progress in electrohydrodynamics of soft microbial particle interphases." *Current Opinion in Colloid and Interface Science* **15** (3), pp. 184–195. DOI: 10.1016/j.cocis.2009.12.002.

Edberg, S. C. (1996). "Assessing health risk in drinking water from naturally occurring microbes." *Journal of Environmental Health* **58** (6), pp. 18–24. URL: http://search.proquest.com/docview/219708692?accountid=28244.

Edberg, S. et al. (2000). "Escherichia coli: the best biological drinking water indicator for public health protection." *Journal of Applied Microbiology* **88** (S1), 106S–116S. DOI: 10.1111/j.1365-2672.2000.tb05338.x.

Edberg, S. C. and M. J. Allen (2004). "Virulence and risk from drinking water of heterotrophic plate count bacteria in human population groups." *International Journal of Food Microbiology* **92** (3), pp. 255–263. DOI: 10.1016/j.ijfoodmicro.2003.08.012.

Edwards, V. H. (1970). "The influence of high substrate concentrations on microbial kinetics." *Biotechnology and Bioengineering* **12** (5), pp. 679–712. DOI: 10.1002/bit.260120504.

Edzwald, J. K. and J. E. Tobiason (1999). "Enhanced coagulation: US requirements and a broader view." *Water Science and Technology* **40** (9), pp. 63–70. DOI: 10.1016/S0273-1223(99)00641-1.

Eikebrokk, B., R. D. Vogt, and H. Liltved (2004a). "NOM increase in Northern European source waters: discussion of possible causes and impacts on coagulation/contact filtration processes." *Water Science & Technology: Water Supply* **4** (4), pp. 47–54. URL: http://ws.iwaponline.com/content/4/4/47.abstract.

Eikebrokk, B. (2012). *Veiledning for drift av koaguleringsanlegg*. Tech. rep. Norsk Vann, p. 155. URL: http://norskvann.no/kompetanse/va-bokhandelen/rapporter.

Eikebrokk, B. (2014). *Håndbok for driftsoptimalisering av koaguleringsanlegg*. Tech. rep. Norsk Vann, p. 59. URL: http://norskvann.no/kompetanse/va-bokhandelen/rapporter.

Eikebrokk, B. and T. Saltnes (2001). "Removal of natural organic matter (NOM) using different coagulants and lightweight expanded clay aggregate filters." *Water Science & Technology: Water Supply* **1** (2), pp. 131–140. URL: http://ws.iwaponline.com/content/1/2/131.abstract.

Eikebrokk, B. and T. Saltnes (2002). "NOM removal from drinking water by chitosan coagulation and filtration through lightweight expanded clay aggregate filters." *Journal of Water Supply: Research and Technology-AQUA* **51** (6), pp. 323–332. URL: http://www.iwaponline.com/jws/051/jws0510323.htm.

Eikebrokk, B., R. D. Vogt, and H. Liltved (2004b). "NOM increase in Northern European Source Waters: Impacts on coagulation/contact filtration processes." In: *NOM Innovations and Applications*. Adelaide.

Eikebrokk, B. et al. (2006). *Giardia-utbruddet i Bergen høsten 2004: Rapport fra det eksterne evalueringsutvalget*. Tech. rep. Byrådet i Bergen, p. 220. URL: https://goo.gl/ULRIhN.

Eisenberg, J. N. et al. (1996). "Quantifying water pathogen risk in an epidemiological framework." *Risk Analysis* **16** (4), pp. 549–563. DOI: 10.1111/j.1539-6924.1996.tb01100.x.

Ekvall, A. (2010). *Utbrott av calicivirus i Lilla Edet - händelseförlopp och lärdomar*. Tech. rep. Svenskt Vatten AB, p. 56. URL: http://www.svensktvatten.se/globalassets/dricksvatten/riskanalys-och-provtagning/svu-2010-13.pdf.

Elimelech, M. et al. (1995). *Particle Deposition and Aggregation: Measurement, Modelling and Simulation*. Oxford: Butterworth-Heinemann, p. 448. URL: http://www.sciencedirect.com/science/book/9780750670241.

Emelko, M. B., P. J. Schmidt, and J. A. Roberson (2008). "Quantification of uncertainity in microbial data - reporting and regulatory implications." *Journal (American Water Works Association)* **100** (3), pp. 94–104. URL: http://www.jstor.org/stable/41312998.

Emelko, M. B., P. J. Schmidt, and P. M. Reilly (2010). "Particle and microorganism enumeration data: Enabling quantitative rigor and judicious interpretation." *Environmental Science and Technology* **44** (5), pp. 1720–1727. DOI: 10.1021/es902382a.

Emelko, M. B. (2001). "Removal of Cryptosporidium parvum by granular media filtration." PhD. University of Waterloo, p. 374. URL: http://hdl.handle.net/10012/614.

Englehardt, J, J Swartout, and C Loewenstine (2009). "A New Theoretical Discrete Growth Distribution with Verification for Microbial Counts in Water." *Risk Analysis* **29** (6), pp. 841–856. DOI: 10.1111/j.1539-6924.2008.01194.x.

Englehardt, J. D. and R. Li (2011). "The Discrete Weibull Distribution: An Alternative for Correlated Counts with Confirmation for Microbial Counts in Water." *Risk Analysis* **31** (3), pp. 370–381. DOI: 10.1111/j.1539-6924.2010.01520.x.

Englehardt, J. D. et al. (2012). "Methods for assessing long-term mean pathogen count in drinking water and risk management implications." *Journal of water and health* **10** (2), pp. 197–208. DOI: 10.2166/wh.2012.142.

FAO/WHO (2003). *Hazard Characterisation for Pathogens in Food and Water: Guidelines*. Tech. rep. Food and Agriculatural Organization, World Health Organization, p. 61. URL: http://www.fao.org/docrep/006/y4666e/y4666e00.htm.

Fazekas de St Groth, S. (1955). "Production of Non-Infective Particles among Influenza Viruses: Do Changes in Virulence Accompany the von Magnus phenomenon?" *Journal of Hygiene* **53** (03), pp. 276–296. DOI: 10.1017/S0022172400000760.

Fazekas de St Groth, S. and P. A. P. Moran (1955). "Appendix: A Mathematical Model of Virus-Cell Interaction." *Journal of Hygiene* **53** (03), pp. 291–296. DOI: 10.1017/S0022172400000760.

Fewtrell, L. and J. Bartram, eds. (2001). *Water Quality. Guidelines, Standards and Health: Assessment of risk and risk management for water-related infectious disease*. Geneva, Switzerland: World Health Organization, p. 424. URL: http://apps.who.int//iris/handle/10665/42442.

Fiksdal, L. and T. Leiknes (2006). "The effect of coagulation with MF/UF membrane filtration for the removal of virus in drinking water." *Journal of Membrane Science* **279** (1-2), pp. 364–371. DOI: 10.1016/j.memsci.2005.12.023.

Fiksdal, L., H. Ødegaard, and S. W. Østerhus (2008). "Risiko og sårbarhet i vannforsyningen." *Vann* **43** (2), pp. 95–104. URL: http://vannforeningen.no/dokumentarkiv/risiko-og-sarbarhet-i-vannforsyningen/.

Foliguet, J.-M. and F Doncoeur (1975). "Elimination des enterovirus au cours du traitement des eaux d'alimentation par coagulation-floculation-filtration." *Water Research* **9** (11), pp. 953–961. URL: http://www.sciencedirect.com/science/article/pii/0043135475901232.

Folkehelseinstituttet (2014). *Folkehelserapporten 2014 - Helsetilstanden i Norge*. Tech. rep. Nasjonalt folkehelseinstitutt, p. 272. URL: http://www.fhi.no/publikasjoner-og-haandboker/folkehelserapporten.

Ford, T. E. (1999). "Microbiological safety of drinking water: United States and global perspectives." *Environmental Health Perspectives* **107** (Suppl. 1), pp. 191–206. DOI: 10.2307/3434483.

Fraser, G. G. and K. R. Cooke (1991). "Endemic Giardiasis and Municipal Water Supply." *American Journal of Public Health* **81** (6), pp. 760–762. DOI: 10.2105/AJPH.81.6.760.

Frost, F. J. et al. (2000). "A serological survey of college students for antibody to Cryptosporidium before and after the introduction of a new water filtration plant." *Epidemiology and infection* **125** (01), pp. 87–92. DOI: 10.1017/S0950268899004148.

Frost, F. J., G. F. Craun, and R. L. Calderon (1996). "Waterborne disease surveillance." *Journal (American Water Works Association)* **88** (9), pp. 66–75. URL: http://www.jstor.org/stable/41295856.

Frost, F. J. et al. (2009). "Enteric illness risks before and after water treatment improvements." *Journal of Water and Health* **07** (4), pp. 581–589. DOI: 10.2166/wh.2009.116.

Furumoto, W. A. and R. Mickey (1967a). "A mathematical model for the infectivity-dilution curve of tobacco mosaic virus: Experimental tests." *Virology* **32** (2), pp. 224–233. DOI: 10.1016/0042-6822(67)90272-3.

Furumoto, W. A. and R. Mickey (1967b). "A mathematical model for the infectivity-dilution curve of tobacco mosaic virus: Theoretical considerations." *Virology* **32** (2), pp. 216–223. DOI: 10.1016/0042-6822(67)90271-1.

Gale, P., P. van Dijk, and G. Stanfield (1997). "Drinking water treatment increases micro-organism clustering; The implications for microbiological risk assessment." *Journal of Water Supply: Research and Technology-AQUA* **46** (3), pp. 117–126.

Gale, P., R. Pitchers, and P. Gray (2002). "The effect of drinking water treatment on the spatial heterogeneity of micro-organisms: implications for assessment of treatment efficiency and health risk." *Water Research* **36** (6), pp. 1640–1648. DOI: 10.1016/S0043-1354(01)00350-5.

GBD 2013 Risk Factors Collaborators (2015). "Global, regional, and national comparative risk assessment of 79 behavioural, environmental and occupational, and metabolic risks or clusters of risks in 188 countries, 1990-2013: a systematic analysis for the Global Burden of Disease Study 2013." *Lancet* **386** (10010), pp. 2287–2323. DOI: 10.1016/S0140-6736(15)00128-2.

Gerba, C. P., J. B. Rose, and C. N. Haas (1996a). "Sensitive populations: who is at the greatest risk?" *International journal of food microbiology* **30** (1-2), pp. 113–123. URL: http://www.ncbi.nlm.nih.gov/pubmed/8856378.

Gerba, C. P. (1984). "Applied and theoretical aspects of virus adsorption to surfaces." In: *Advances in applied microbiology*. Vol. 30. Orlando, Florida: Academic Press, pp. 133–168. DOI: 10.1016/S0065-2164(08)70054-6.

Gerba, C. P. et al. (1996b). "Waterborne rotavirus: A risk assessment." *Water Research* **30** (12), pp. 2929–2940. DOI: 10.1016/S0043-1354(96)00187-X.

Gerba, C. P. et al. (2003). "Removal of Encephalitozoon intestinalis, Calicivirus, and Coliphages by Conventional Drinking Water Treatment." *Journal of Environmental Science and Health, Part A* **38** (7), pp. 1259–1268. DOI: 10.1081/ESE-120021124.

Gerba, C. and C. Haas (1988). "Assessment of Risks Associated with Enteric Viruses in Contaminated Drinking Water." In: *Chemical and Biological Characterization of Municipal Sludges, Sediments, Dredge Spoils, and Drilling Muds. ASTM STP 976.* Ed. by J. Lichtenberg et al. Vol. 976. Philadelphia, US: ASTM International, pp. 489–494. DOI: 10.1520/STP26732S.

Gibson, K. E. (2014). "Viral pathogens in water: occurrence, public health impact, and available control strategies." *Current Opinion in Virology* **4**, pp. 50–57. DOI: 10.1016/j.coviro.2013.12.005.

Gilbert, M.-L., P. Levallois, and M. J. Rodriguez (2006). "Use of a health information telephone line, Info-sante CLSC, for the surveillance of waterborne gastroenteritis." *Journal of water and health* **4** (2), pp. 225–232. DOI: 10.2166/wh.2006.005.

Gilcreas, F. W. and S. M. Kelly (1955). "Relation of Coliform-Organism Test to Enteric-Virus Pollution." *Journal (American Water Works Association)* **47** (7), pp. 683–694. URL: http://www.jstor.org/stable/41254146.

Gitis, V. et al. (2002). "Fluorescent dye labeled bacteriophages–a new tracer for the investigation of viral transport in porous media: 2. Studies of deep-bed filtration." *Water Research* **36** (17), pp. 4235–4242. DOI: 10.1016/S0043-1354(02)00164-1.

Grant, S. B. (1994). "Virus coagulation in aqueous environments." *Environmental science & technology* **28** (5), pp. 928–933. DOI: 10.1021/es00054a026.

Grasso, D. et al. (2002). "A review of non-DLVO interactions in environmental colloidal systems." *Reviews in Environmental Science and Biotechnology* **1** (1), pp. 17–38. DOI: 10.1023/A:1015146710500.

Greenwood, M and G. U. Yule (1917). "On the Statistical Interpretation of Some Bacteriological Methods Employed in Water Analysis." *The Journal of Hygiene* **16** (1), pp. 36–54. DOI: 10.1017/S0022172400006501.

Gregory, J and V Dupon (2001). "Properties of flocs produced by water treatment coagulants." *Water Science & Technology* **44** (10), pp. 231–236. URL: http://wst.iwaponline.com/content/44/10/231.abstract.

Grøndahl-Rosado, R. C. et al. (2014a). "A One Year Study on the Concentrations of Norovirus and Enteric Adenoviruses in Wastewater and A Surface Drinking Water Source in Norway." *Food and environmental virology* **6** (4), pp. 232–245. DOI: 10.1007/s12560-014-9161-5.

Grøndahl-Rosado, R. C. et al. (2014b). "Detection of Microbial Pathogens and Indicators in Sewage Effluent and River Water During the Temporary Interruption of a Wastewater Treatment Plant." *Water Quality, Exposure and Health* **6** (3), pp. 155–159. DOI: 10.1007/s12403-014-0121-y.

Guy, M. D., J. D. Mciver, and M. J. Lewis (1977). "The removal of virus by a pilot treatment plant." *Water Research* **11** (7), pp. 421–428. DOI: 10.1016/0043-1354(77)90083-5.

Guzman-Herrador, B et al. (2015). "Waterborne outbreaks in the Nordic countries, 1998 to 2012." *Eurosurveillance* **20** (24), p. 21160. DOI: 10.2807/1560-7917.ES2015.20.24.21160.

Haas, C. N. (1983). "Estimation of risk due to low doses of microorganisms: a comparison of alternative methodologies." *American journal of epidemiology* **118** (4), pp. 573–582. URL: http://aje.oxfordjournals.org/content/118/4/573.short.

Haas, C. N. and B Heller (1988). "Test of the validity of the Poisson assumption for analysis of most-probable-number results." *Applied and environmental microbiology* **54** (12), pp. 2996–3002. URL: http://aem.asm.org/content/54/12/2996.short.

Haas, C. N. et al. (2000). "Development of a dose-response relationship for Escherichia coli O157:H7." *International journal of food microbiology* **56** (2-3), pp. 153–159. DOI: 10.1016/S0168-1605(99)00197-X.

Haas, C. N. (1996a). "Acceptable microbial risk." *Journal (American Water Works Association)* **88** (12), p. 8. URL: http://www.jstor.org/stable/41295647.

Haas, C. N. (1996b). "How to average microbial densities to characterize risk." *Water Research* **30** (4), pp. 1036–1038. DOI: 10.1016/0043-1354(95)00228-6.

Haas, C. N. (2002). "Conditional Dose-Response Relationships for Microorganisms: Development and Application." *Risk Analysis* **22** (3), pp. 455–463. DOI: 10.1111/0272-4332.00035.

Haas, C. N. et al. (1993). "Risk Assessment of Virus in Drinking Water." *Risk Analysis* **13** (5), pp. 545–552. DOI: 10.1111/j.1539-6924.1993.tb00013.x.

Haas, C. N., J. B. Rose, and C. P. Gerba (2014). *Quantitative Microbial Risk Assessment*. 2nd ed. Hoboken, New Jersey: John Wiley & Sons, Inc, p. 440. DOI: 10.1002/9781118910030.

Halvorson, H. (1935). "The Effect of Chance on the Mortality of Experimentally Infected Animals." *Journal of bacteriology* **30** (3), pp. 330–331. URL: http://jb.asm.org/content/30/3/329.short.

Hamaker, H. (1937). "The London—van der Waals attraction between spherical particles." *Physica* **4** (10), pp. 1058–1072. DOI: 10.1016/S0031-8914(37)80203-7.

Hamouda, M. A. et al. (2016). "Scenario-based quantitative microbial risk assessment to evaluate the robustness of a drinking water treatment plant." *Water Quality Research Journal of Canada*. DOI: 10.2166/wqrjc.2016.034.

Happel, J. (1958). "Viscous flow in multiparticle systems: Slow motion of fluids relative to beds of spherical particles." *AIChE Journal* **4** (2), pp. 197–201. DOI: 10.1002/aic.690040214.

Harrington, G. W. et al. (2003). "Effect of Filtration Conditions on Removal of Emerging Pathogens." *Journal (American Water Works Association)* **95** (12), pp. 95–104. URL: http://www.jstor.org/stable/41311407.

Harwood, V. J. et al. (2005). "Validity of the Indicator Organism Paradigm for Pathogen Reduction in Reclaimed Water and Public Health Protection." *Applied and Environmental Microbiology* **71** (6), pp. 3163–3170. DOI: 10.1128/AEM.71.6.3163-3170.2005.

Hassan, J. et al. (2014). "Low Probability of Initiating nirS Transcription Explains Observed Gas Kinetics and Growth of Bacteria Switching from Aerobic Respiration to Denitrification." *PLoS Computational Biology* **10** (11), e1003933. DOI: 10.1371/journal.pcbi.1003933.

Havelaar, A. H. (1994). "Application of HACCP to drinking water supply." *Food Control* **5** (3), pp. 145–152. DOI: 10.1016/0956-7135(94)90074-4.

Havelaar, A. and J. Melse (2003). *Quantifying public health risk in the WHO Guidelines for Drinking-Water Quality: a burden of disease approach*. Tech. rep. Bilthoven, The Netherlands: National Institute of Public Health and the Environment (RIVM), p. 49. URL: http://hdl.handle.net/10029/9098.

Havelaar, A. H. and A. N. Swart (2014). "Impact of Acquired Immunity and Dose-Dependent Probability of Illness on Quantitative Microbial Risk Assessment." *Risk Analysis* **34** (10), pp. 1807–1819. DOI: 10.1111/risa.12214.

Havelaar, A. H. et al. (2000). "Balancing the risks and benefits of drinking water disinfection: Disability adjusted life-years on the scale." *Environmental Health Perspectives* **108** (4), pp. 315–321. DOI: 10.1289/ehp.00108315.

Heerden, J. van et al. (2005). "Risk assessment of adenoviruses detected in treated drinking water and recreational water." *Journal of Applied Microbiology* **99** (4), pp. 926–933. DOI: 10.1111/j.1365-2672.2005.02650.x.

Heistad, A. et al. (2009a). "Virus removal by unsaturated wastewater filtration: effects of biofilm accumulation and hydrophobicity." *Water Science & Technology* **60** (2), pp. 399–407. DOI: 10.2166/wst.2009.343.

Heistad, A. et al. (2009b). "Long-term Hygienic Barrier Efficiency of a Compact On-site Wastewater Treatment System." *Journal of Environment Quality* **38** (6), pp. 2182–2188. DOI: 10.2134/jeq2008.0407.

Hendricks, D. W. et al. (2006). "Filtration Removals of Microorganisms and Particles." *Journal of Environmental Engineering* **131** (12), pp. 1621–1632. DOI: 10.1061/(ASCE)0733-9372(2005)131:12(1621).

Hermansson, M. (1999). "The DLVO theory in microbial adhesion." *Colloids and Surfaces B: Biointerfaces* **14** (1-4), pp. 105–119. DOI: 10.1016/S0927-7765(99)00029-6.

Herzig, J. P., D. M. Leclerc, and P. L. Goff (1970). "Flow of suspensions through porous media—application to deep filtration." *Industrial & Engineering Chemistry* **62** (5), pp. 8–35. DOI: 10.1021/ie50725a003.

Hijnen, W. A. and G. Medema (2010). *Elimination of Microorganisms by Water Treatment Processes*. IWA Publishing, p. 160.

Horner, R., R. Jarvis, and R. Mackie (1986). "Deep bed filtration: A new look at the basic equations." *Water Research* **20** (2), pp. 215–220. DOI: 10.1016/0043-1354(86)90011-4.

Hrudey, S. E., E. J. Hrudey, and S. J. T. Pollard (2006). "Risk management for assuring safe drinking water." *Environment International* **32** (8), pp. 948–957. DOI: 10.1016/j.envint.2006.06.004.

Hsieh, J. L. et al. (2015). "Drinking Water Turbidity and Emergency Department Visits for Gastrointestinal Illness in New York City, 2002-2009." *Plos One* **10** (4), e0125071. DOI: 10.1371/journal.pone.0125071.

Huang, L. (2015). "Simulation and evaluation of different statistical functions for describing lag time distributions of a bacterial growth curve." *Microbial Risk Analysis* **1**, pp. 1–9. DOI: 10.1016/j.mran.2015.08.002.

Huang, Y. and C. N. Haas (2009). "Time-Dose-Response Models for Microbial Risk Assessment." *Risk Analysis* **29** (5), pp. 648–661. DOI: 10.1111/j.1539-6924.2008.01195.x.

Huck, P. M. et al. (2001). *Filter operation effects on pathogen passage*. AWWA Research Foundation, p. 285.

Hunter, P. R. (2003). "Climate change and waterborne and vector-borne disease." *Journal of applied microbiology* **94** (s1), 37S–46S. DOI: 10.1046/j.1365-2672.94.s1.5.x.

Hunter, P. R. and L. Fewtrell (2001). "Acceptable risk." In: *Water Quality. Guidelines, Standards and Health: Assessment of risk and risk management for water-related infectious disease*. Ed. by L. Fewtrell and J. Bartram. Geneva, Switzerland: World Health Organization. Chap. 10, pp. 207–228. URL: http://goo.gl/4u9H2.

Ikner, L. A., C. P. Gerba, and K. R. Bright (2012). "Concentration and Recovery of Viruses from Water: A Comprehensive Review." *Food and Environmental Virology* **4** (2), pp. 41–67. DOI: 10.1007/s12560-012-9080-2.

ILSI Risk Science Institute (2000). *Revised Framework for Microbial Risk Assessment*. Tech. rep. ILSI Risk Science Institute, p. 29.

ILSI Risk Science Institute Pathogen Risk Assessment Working Group (1996). "A Conceptual Framework to Assess the Risks of Human Disease Following Exposure to Pathogens." *Risk Analysis* **16** (6), pp. 841–847. DOI: 10.1111/j.1539-6924.1996.tb00835.x.

Iversen, S. and N. Arley (1950). "ON THE MECHANISM OF EXPERIMENTAL CARCINOGENESIS." *Acta Pathologica Microbiologica Scandinavica* **27** (6), pp. 773–803. DOI: 10.1111/j.1699-0463.1950.tb00081.x.

Ives, K. J. (1969). "Modern theory of filtration. Special Subject No. 7." In: *International Water Supply Congress, Vienna 1969*. London: International Water Supply Association.

Ives, K. J. (1964). "Progress in Filtration." *Journal (American Water Works Association)* **56** (9), pp. 1225–1232. URL: http://www.jstor.org/stable/41263989.

Ives, K. (1970). "Rapid filtration." *Water Research* **4** (3), pp. 201–223. DOI: 10.1016/0043-1354(70)90068-0.

Ives, K. and J. L. Cleasby (1972). "Filtration of water and wastewater." *C R C Critical Reviews in Environmental Control* **2** (1-4), pp. 293–335. DOI: 10.1080/10643387109381584.

Iwasaki, T. (1937). "SOME NOTES ON SAND FILTRATION." *Journal (American Water Works Association)* **29** (10), pp. 1591–1602. URL: http://www.jstor.org/stable/41231759.

Jakopanec, I. et al. (2008). "A large waterborne outbreak of campylobacteriosis in Norway: The need to focus on distribution system safety." *BMC infectious diseases* **8** (128). DOI: 10.1186/1471-2334-8-128.

Jegatheesan, V. and S. Vigneswaran (2005). "Deep Bed Filtration: Mathematical Models and Observations." *Critical Reviews in Environmental Science and Technology* **35** (6), pp. 515–569. DOI: 10.1080/10643380500326432.

Johansen, T. A. (2001). *Under byens gater: Oslos vann- og avløpshistorie*. Oslo kommune, Vann- og avløpsetaten, p. 239.

Johansen, T. A. (2004). *Det viktige vannet: Norsk vann- og avløpshistore*. Interconsult ASA, p. 245.

Johnson, W. P., M. Tong, and X. Li (2007). "On colloid retention in saturated porous media in the presence of energy barriers: The failure of α, and opportunities to predict η." *Water Resources Research* **43** (12), W12S13. DOI: 10.1029/2006WR005770.

Johnson, W. P., H. Ma, and E. Pazmino (2011). "Straining Credibility: A General Comment Regarding Common Arguments Used to Infer Straining As the Mechanism of Colloid Retention in Porous Media." *Environmental Science & Technology* **45** (9), pp. 3831–3832. DOI: 10.1021/es200868e.

Jones, M. K. et al. (2014). "Enteric bacteria promote human and mouse norovirus infection of B cells." *Science* **346** (6210), pp. 755–759. DOI: 10.1126/science.1257147.

Joret, J. C. et al. (1986). "Two Year Survey of Indicator Bacteria and Enteroviruses during the Preparation of Drinking Water from Three Water Treatment Plants in Paris Suburbs." *Water Science & Technology* **18** (10), p. 107. URL: http://wst.iwaponline.com/content/18/10/107.abstract.

Keller, A. A. and M. Auset (2007). "A review of visualization techniques of biocolloid transport processes at the pore scale under saturated and unsaturated conditions." *Advances in Water Resources* **30** (6-7), pp. 1392–1407. DOI: 10.1016/j.advwatres.2006.05.013.

Kemp, C. D. (1967). ""Stuttering - Poisson" distributions." *Journal of the Statistical and Social Inquiry Society of Ireland* **XXI** (V), pp. 151–157. URL: http://www.tara.tcd.ie/handle/2262/6987.

Kemp, C. D. and A. W. Kemp (1965). "Some Properties of the 'Hermite' Distribution." *Biometrika* **52** (3/4), pp. 381–394. DOI: 10.2307/2333691.

Kempf, J. E. et al. (1942). "Effect of Aluminum Hydroxide Sedimentation, Sand Filtration and Chlorination on the Virus of Poliomyelitis." *American Journal of Public Health and the Nations Health* **32** (12), pp. 1366–1370. URL: http://www.ncbi.nlm.nih.gov/pmc/articles/PMC1527256/.

Kermack, W. O. and A. G. McKendrick (1927). "A Contribution to the Mathematical Theory of Epidemics." *Proceedings of the Royal Society A: Mathematical, Physical and Engineering Sciences* **115** (772), pp. 700–721. DOI: 10.1098/rspa.1927.0118.

Keswick, B. H. et al. (1984). "Detection of Enteric Viruses in Treated Drinking-Water." *Applied and Environmental Microbiology* **47** (6), pp. 1290–1294. URL: http://aem.asm.org/content/47/6/1290.short.

Keswick, B. H. et al. (1985). "Detection of Rotavirus in Treated Drinking Water." *Water Science & Technology* **17** (10), pp. 1–6. URL: http://wst.iwaponline.com/content/17/10/1.abstract.

Kim, J. K. and D. F. Lawler (2006). "Particle detachment during hydraulic shock loads in granular media filtration." *Water Science & Technology* **53** (7), pp. 177–184. DOI: 10.2166/wst.2006.222.

Kim, J. and J. E. Tobiason (2004). "Particles in filter effluent: the roles of deposition and detachment." *Environmental Science & Technology* **38** (22), pp. 6132–6138. DOI: 10.1021/es0352698.

Kim, J. and D. F. Lawler (2008). "Influence of particle characteristics on filter ripening." *Separation Science and Technology* **43** (7), pp. 1583–1594. DOI: 10.1080/01496390801974688.

Kim, J. and D. F. Lawler (2012). "The influence of hydraulic loads on depth filtration." *Water Research* **46** (2), pp. 433–441. DOI: 10.1016/j.watres.2011.10.059.

Kirkwood, J. P. (1869). *Report on the Filtration of River Waters, for the Supply of Cities, as Practised in Europe, Made to the Board of Water Commissioners of the City of St. Louis*. New York: D. Van Nostrand, p. 178. URL: https://goo.gl/IoUG1V.

Koch, R. (1893). "Wasserfiltration und Cholera." *Zeitschrift für Hygiene und Infektionskrankheiten* **14** (1), pp. 393–426. DOI: 10.1007/BF02284326.

Koch, R. (1894). *Professor Koch on the bacteriological diagnosis of cholera, water-filtration and cholera, and the cholera in Germany during the winter of 1892-93*. Edinburgh: David Douglas, p. 150. URL: http://nrs.harvard.edu/urn-3:HMS.COUNT:1063478.

Kodell, R. L., S.-H. Kang, and J. J. Chen (2002). "Statistical models of health risk due to microbial contamination of foods." *Environmental and Ecological Statistics* **9** (3), pp. 259–271. DOI: 10.1023/A:1016240210061.

Koutinas, M. et al. (2011). "Linking genes to microbial growth kinetics - An integrated biochemical systems engineering approach." *Metabolic Engineering* **13** (4), pp. 401–413. DOI: 10.1016/j.ymben.2011.02.001.

Kreißel, K. et al. (2014). "Inactivation of F-specific bacteriophages during flocculation with polyaluminum chloride - A mechanistic study." *Water Research* **51**, pp. 144–151. DOI: 10.1016/j.watres.2013.12.026.

Kunkel, L. O. (1934). "Tobacco and aucuba-mosaic infections by single units of virus." *Phytopathology* **24** (3). URL: http://apsjournals.apsnet.org/loi/phyto.

Kuusi, M. et al. (2003). "Incidence of gastroenteritis in Norway – a population-based survey." *Epidemiology and Infection* **131** (1), pp. 591–597. DOI: 10.1017/S0950268803008744.

Kvitsand, H. M. L. and L. Fiksdal (2010). "Waterborne disease in Norway: emphasizing outbreaks in groundwater systems." *Water Science & Technology* **61** (3), pp. 563–571. DOI: 10.2166/wst.2010.863.

La Rosa, G. et al. (2012). "Emerging and potentially emerging viruses in water environments." *Annali dell'Istituto Superiore di Sanità* **48** (4), pp. 397–406. DOI: 10.4415/ANN_12_04_07.

Laine, J. et al. (2011). "An extensive gastroenteritis outbreak after drinking-water contamination by sewage effluent, Finland." *Epidemiology and Infection* **139** (07), pp. 1105–1113. DOI: 10.1017/S0950268810002141.

Landvik, T. (2015). "Giardia outbreak in Bergen 2004 – what was the source of infection?" *Tidsskrift for Den norske legeforening* **135** (16), pp. 1435–1436. DOI: 10.4045/tidsskr.15.0348.

Lang, J. S. et al. (1993). "Investigating filter performance as a function of the ratio of filter size to media size." *Journal / American Water Works Association* **85** (10), pp. 122–130. URL: http://www.jstor.org/stable/41294403.

Langlet, J., F. Gaboriaud, and C. Gantzer (2007). "Effects of pH on plaque forming unit counts and aggregation of MS2 bacteriophage." *Journal of Applied Microbiology* **103** (5), pp. 1632–1638. DOI: 10.1111/j.1365-2672.2007.03396.x.

Langlet, J. et al. (2008). "Impact of chemical and structural anisotropy on the electrophoretic mobility of spherical soft multilayer particles: the case of bacteriophage MS2." *Biophysical journal* **94** (8), pp. 3293–3312. DOI: 10.1529/biophysj.107.115477.

Larsson, C et al. (2014). "Epidemiology and estimated costs of a large waterborne outbreak of norovirus infection in Sweden." *Epidemiology and infection* **142** (03), pp. 592–600. DOI: 10.1017/S0950268813001209.

Lawler, D. F. and J. A. Nason (2006). "Granular media filtration: Old process, new thoughts." *Water Science & Technology* **53** (7), pp. 1–7. DOI: 10.2166/wst.2006.201.

Leclerc, H., L. Schwartzbrod, and E. Dei-Cas (2002). "Microbial Agents Associated with Waterborne Diseases." *Critical Reviews in Microbiology* **28** (4), pp. 371–409. DOI: 10.1080/1040-840291046768.

Leong, L. Y. C. (1983). "Removal and Inactivation of Viruses by Treatment Processes for Potable Water and Wastewater – A Review." *Water Science & Technology* **15** (5), pp. 91–114. URL: http://wst.iwaponline.com/content/15/5/91.abstract.

Lieverloo, J. H. M. van, E. J. M. Blokker, and G. Medema (2007). "Quantitative microbial risk assessment of distributed drinking water using faecal indicator incidence and concentrations." *Journal of Water and Health* **5** (S1), pp. 131–149. DOI: 10.2166/wh.2007.134.

Lilleengen, K. (1948). "Typing of Salmonella typhimurium by means of bacteriophage: an experimental bacteriologic study for the purpose of devising a phago-typing method to be used an an aid in epidemiologic and epizootologic investigations in outbreaks of typhimurium infection." PhD. Royal Veterinary College, Stockholm.

Lim, S. S. et al. (2012). "A comparative risk assessment of burden of disease and injury attributable to 67 risk factors and risk factor clusters in 21 regions, 1990–2010: a systematic analysis for the Global Burden of Disease Study 2010." *The Lancet* **380** (9859), pp. 2224–2260. DOI: 10.1016/S0140-6736(12)61766-8.

Logan, B. E. et al. (1995). "Clarification of Clean-Bed Filtration Models." *Journal of Environmental Engineering* **121** (12), pp. 869–873. DOI: 10.1061/(ASCE)0733-9372(1995)121:12(869).

Logan, J. D. (2001). *Transport Modeling in Hydrogeochemical Systems*. Vol. 15. Interdisciplinary Applied Mathematics. New York, NY: Springer New York. DOI: 10.1007/978-1-4757-3518-5.

Logsdon, G. S. (1982). "The role of filtration in preventing waterborne disease." *Journal (American Water Works Association)* **74** (12), pp. 649–655. URL: http://www.jstor.org/stable/41271441.

Long, W. and M. Hilpert (2009). "A Correlation for the Collector Efficiency of Brownian Particles in Clean-Bed Filtration in Sphere Packings by a Lattice-Boltzmann Method." *Environmental Science & Technology* **43** (12), pp. 4419–4424. DOI: 10.1021/es8024275.

Long, W. et al. (2010). "Pore-scale study of the collector efficiency of nanoparticles in packings of nonspherical collectors." *Colloids and Surfaces A: Physicochemical and Engineering Aspects* **358** (1-3), pp. 163–171. DOI: 10.1016/j.colsurfa.2010.01.043.

Loret, J. F. et al. (2013). "Assessment and management of health risks related to the recycling of filter backwash water in drinking water production." *Water Practice & Technology* **8** (2), pp. 166–179. DOI: 10.2166/wpt.2013.019.

Lundberg Abrahamsson, J., J. Ansker, and G. Heinicke (2009). *MRA – Ett modellverktyg för svenska vattenverk*. Tech. rep. Svenskt Vatten AB, p. 78. URL: http://goo.gl/Q8Ydl1.

Lytle, D. a., C. H. Johnson, and E. W. Rice (2002). "A systematic comparison of the electrokinetic properties of environmentally important microorganisms in water." *Colloids and Surfaces B: Biointerfaces* **24** (2), pp. 91–101. DOI: 10.1016/S0927-7765(01)00219-3.

Ma, H. et al. (2009). "Hemispheres-in-Cell Geometry to Predict Colloid Deposition in Porous Media." *Environmental Science & Technology* **43** (22), pp. 8573–8579. DOI: 10.1021/es901242b.

Mac Kenzie, W. R. et al. (1994). "A massive outbreak in Milwaukee of cryptosporidium infection transmitted through the public water supply." *The New England journal of medicine* **331** (3), pp. 161–167. DOI: 10.1056/NEJM199407213310304.

MacDonald, N. (1978). *Time Lags in Biological Models*. Vol. 27. Lecture Notes in Biomathematics. Berlin, Heidelberg: Springer Berlin Heidelberg. DOI: 10.1007/978-3-642-93107-9.

Macler, B. A. and S. Regli (1993). "Use of microbial risk assessment in setting US drinking water standards." *International Journal of Food Microbiology* **18** (4), pp. 245–256. DOI: 10.1016/0168-1605(93)90148-A.

Mann, A. G. et al. (2007). "The association between drinking water turbidity and gastrointestinal illness: a systematic review." *BMC Public Health* **7** (256). DOI: 10.1186/1471-2458-7-256.

Masago, Y et al. (2002). "Assessment of risk of infection due to Cryptosporidium parvum in drinking water." *Water Science & Technology* **46** (11-12), pp. 319–324. URL: http://wst.iwaponline.com/content/46/11-12/319.abstract.

Masago, Y. et al. (2006). "Quantitative risk assessment of noroviruses in drinking water based on qualitative data in Japan." *Environmental science & technology* **40** (23), pp. 7428–7433. DOI: 10.1021/es060348f.

Matilainen, A., M. Vepsäläinen, and M. Sillanpää (2010). "Natural organic matter removal by coagulation during drinking water treatment: A review." *Advances in Colloid and Interface Science* **159** (2), pp. 189–197. DOI: 10.1016/j.cis.2010.06.007.

Matsui, Y. et al. (2003). "Virus inactivation in aluminum and polyaluminum coagulation." *Environmental science & technology* **37** (22), pp. 5175–5180. DOI: 10.1021/es0343003.

Matsushita, T, Y Matsui, and T Inoue (2004). "Irreversible and reversible adhesion between virus particles and hydrolyzing-precipitating aluminium: a function of coagulation." *Water Science & Technology* **50** (12), pp. 201–206. URL: http://wst.iwaponline.com/content/50/12/201.abstract.

Matsushita, T. et al. (2011). "Virus inactivation during coagulation with aluminum coagulants." *Chemosphere* **85** (4), pp. 571–576. DOI: 10.1016/j.chemosphere.2011.06.083.

Mattilsynet (2011). *Veiledning til Drikkevannsforskriften*. URL: http://goo.gl/4QPw4B.

Mayer, B. T. et al. (2011). "A dynamic dose-response model to account for exposure patterns in risk assessment: a case study in inhalation anthrax." *Journal of The Royal Society Interface* **8** (57), pp. 506–517. DOI: 10.1098/rsif.2010.0491.

McConnell, S et al. (2001). "Changes in the incidence of gastroenteritis and the implementation of public water treatment." *International Journal of Environmental Health Research* **11** (4), pp. 299–303. DOI: 10.1080/09603120120070919.

McDowell-Boyer, L. M., J. R. Hunt, and N. Sitar (1986). "Particle transport through porous media." *Water Resources Research* **22** (13), pp. 1901–1921. DOI: 10.1029/WR022i013p01901.

Medema, G. and N. Ashbolt (2006). *QMRA: its value for risk management*. Tech. rep. Microrisk, p. 36.

Medema, G. and P. Smeets (2009). "Quantitative risk assessment in the Water Safety Plan: case studies from drinking water practice." *Water Science & Technology: Water Supply* **9** (2), pp. 127–132. DOI: 10.2166/ws.2009.297.

Mehta, D. and M. C. Hawley (1969). "Wall effect in packed columns." *Industrial & Engineering Chemistry Process Design and Development* **8** (2), pp. 280–282. DOI: 10.1021/i260030a021.

Mena, K. D. et al. (2003). "Risk assessment of waterborne coxsackievirus." *Journal (American Water Works Association)* **95** (7), pp. 122–131. URL: http://www.jstor.org/stable/41311136.

Mesquita, M. M. and M. B. Emelko (2012). "Bacteriophages as Surrogates for the Fate and Transport of Pathogens in Source Water and in Drinking Water Treatment Processes." In: *Bacteriophages*. Ed. by I. Kurtboke. 2006. InTech. Chap. 4, pp. 57–80. DOI: 10.5772/34024.

Messner, M. et al. (2006). "An approach for developing a national estimate of waterborne disease due to drinking water and a national estimate model application." *Journal of Water and Health* **04** (Suppl. 2), pp. 201–240. DOI: 10.2166/wh.2006.024.

Messner, M. J., P. Berger, and S. P. Nappier (2014). "Fractional Poisson-A Simple Dose-Response Model for Human Norovirus." *Risk Analysis* **34** (10), pp. 1820–1829. DOI: 10.1111/risa.12207.

Meynell, G. G. (1957a). "Inherently Low Precision of Infectivity Titrations Using a Quantal Response." *Biometrics* **13** (2), pp. 149–163. DOI: 10.2307/2527798.

Meynell, G. G. (1957b). "The applicability of the hypothesis of independent action to fatal infections in mice given Salmonella typhimurium by mouth." *Journal of general microbiology* **16** (2), pp. 396–404. DOI: 10.1099/00221287-16-2-396.

Meynell, G. G. and B. A. D. Stocker (1957). "Some Hypotheses on the Aetiology of Fatal Infections in Partially Resistant Hosts and their Application to Mice Challenged with Salmonella paratyphi-B or Salmonella typhimuriurn by Intraperitoneal Injection." *Journal of general Microbiology* **16** (1), pp. 38–58. DOI: 10.1099/00221287-16-1-38.

Michen, B. and T. Graule (2010). "Isoelectric points of viruses." *Journal of Applied Microbiology* **109** (2), pp. 388–397. DOI: 10.1111/j.1365-2672.2010.04663.x.

Microrisk (2006). *Microbiological risk assessment: a scientific basis for managing drinking water safety from source to tap*. URL: http://www.microrisk.com.

Mints, D. M. (1966). "Modern theory of filtration. Special Subject No. 10." In: *International Water Supply Congress, Barcelona 1966*. London: International Water Supply Association.

Monod, J (1949). "The Growth of Bacterial Cultures." *Annual Review of Microbiology* **3** (1), pp. 371–394. DOI: 10.1146/annurev.mi.03.100149.002103.

Moon, H. et al. (2004). "A comparison of microbial dose–response models fitted to human data." *Regulatory Toxicology and Pharmacology* **40** (2), pp. 177–184. DOI: 10.1016/j.yrtph.2004.07.003.

Moran, D. C. et al. (1993a). "Particle Behavior in Deep-Bed Filtration: Part 1—Ripening and Breakthrough." *Journal (American Water Works Association)* **85** (12), pp. 69–81. URL: http://www.jstor.org/stable/41294461.

Moran, M. C. et al. (1993b). "Particle Behavior in Deep-Bed Filtration: Part 2—Particle Detachment." *Journal (American Water Works Association)* **85** (12), pp. 82–93. URL: http://www.jstor.org/stable/41294462.

Moran, P. A. P. (1954a). "The dilution assay of viruses. II." *Journal of Hygiene* **52** (04), pp. 444–446. DOI: 10.1017/S0022172400036913.

Moran, P. (1954b). "The dilution assay of viruses." *Journal of Hygiene* **52** (02), pp. 189–193. DOI: 10.1017/S002217240002739X.

Morgan, B. J. (1992). *Analysis of Quantal Response Data*. Chapman & Hall/CRC, p. 512. URL: https://www.crcpress.com/Analysis-of-Quantal-Response-Data/Morgan/9780412317507.

Morris, R. D., E. N. Naumova, and J. K. Griffiths (1998). "Did Milwaukee experience waterborne cryptosporidiosis before the large documented outbreak in 1993?" *Epidemiology* **9** (3), pp. 264–270. URL: http://www.jstor.org/stable/3703055.

Murphy, H. M. et al. (2014). "A systematic review of waterborne disease burden methodologies from developed countries." *Journal of Water and Health* **12** (4), pp. 634–655. DOI: 10.2166/wh.2014.049.

Myrstad, L., C. F. Nordheim, and K. Janak (2015). *Rapport fra Vannverksregisteret Drikkevannsstatus (data 2011)*. Tech. rep. 122. Nasjonalt folkehelseinstitutt, p. 57. URL: http://www.fhi.no/artikler/?id=114525.

Nasser, A et al. (1995). "Removal of hepatitis A virus (HAV) poliovirus, and MS2 coliphage by coagulation and high rate filtration." *Water Science & Technology* **31** (5-6), pp. 63–68. DOI: 10.1016/0273-1223(95)00242-F.

National Research Council (1983). *Risk Assessment in the Federal Government: Managing the Process*. Washington, D.C.: National Academies Press, p. 191. DOI: 10.17226/366.

Neefe, J. R. et al. (1947). "Inactivation of the Virus of Infectious Hepatitis in Drinking Water." *American Journal of Public Health and the Nations Health* **37** (4), pp. 365–372. URL: http://www.ncbi.nlm.nih.gov/pubmed/18016503.

Nelson, K. E. and T. R. Ginn (2005). "Colloid filtration theory and the happel sphere-in-cell model revisited with direct numerical simulation of colloids." *Langmuir* **21** (6), pp. 2173–2184. DOI: 10.1021/la048404i.

Nelson, K. E. and T. R. Ginn (2011). "New collector efficiency equation for colloid filtration in both natural and engineered flow conditions." *Water Resources Research* **47** (5), W05543. DOI: 10.1029/2010WR009587.

Nilsen, V. (2016). "Some aspects of deep-bed filtration dynamics in QMRA for drinking water." Manuscript in preparation.

Nilsen, V. and J. Wyller (2016a). "QMRA for drinking water: 1. Revisiting the mathematical structure of single-hit dose-response models." *Risk Analysis* **36** (1), pp. 145–162.

Nilsen, V. and J. Wyller (2016b). "QMRA for drinking water: 2. The effect of pathogen clustering in single-hit dose-response models." *Risk Analysis* **36** (1), pp. 163–181.

Nilsen, V., J. A. Wyller, and A. Heistad (2012). "Efficient incorporation of microbial metabolic lag in subsurface transport modeling." *Water Resources Research* **48** (9), W09519.

Nilsen, V. et al. (2016). "Spatio-temporal dynamics of virus removal in dual-media contact-filtration for drinking water: Experimental results and inverse modeling." Manuscript in preparation.

Nilsson, P. et al. (2007). "SCADA data and the quantification of hazardous events for QMRA." *Journal of Water and Health* **5** (S1), pp. 99–105. DOI: 10.2166/wh.2007.138.

Norwegian Institute of Public Health. *Norwegian Surveillance System for Communicable Diseases*. URL: http://www.msis.no/.

Nwachcuku, N. and C. P. Gerba (2004). "Emerging waterborne pathogens: can we kill them all?" *Current Opinion in Biotechnology* **15** (3), pp. 175–180. DOI: 10.1016/j.copbio.2004.04.010.

Nygård, K., B. Gondrosen, and V. Lund (2003). "Sykdomsutbrudd forårsaket av drikkevann i Norge." *Tidsskrift For Den Norske Lægeforening* **123** (23), pp. 3410–3413. URL: http://tidsskriftet.no/article/933966.

Nygård, K. et al. (2006). "A large community outbreak of waterborne giardiasis-delayed detection in a non-endemic urban area." *BMC public health* **6** (141). DOI: 10.1186/1471-2458-6-141.

Nygård, K. et al. (2007). "Breaks and maintenance work in the water distribution systems and gastrointestinal illness: A cohort study." *International Journal of Epidemiology* **36** (4), pp. 873–880. DOI: 10.1093/ije/dym029.

Ødegaard, H. et al. (2010). "NOM removal technologies – Norwegian experiences." *Drinking Water Engineering and Science* **3**, pp. 1–9. DOI: 10.5194/dwes-3-1-2010.

Ødegaard, H., J. Fettig, and H. Ratnaweera (1990). "Coagulation with Prepolymerized Metal Salts." In: *Chemical water and wastewater treatment. Proceedings of the 4th Gothenburg Symposium 1990 October 1–3, 1990 Madrid, Spain*. Ed. by H. Hahn and R. Klute. Springer-Verlag, pp. 189–220. DOI: 10.1007/978-3-642-76093-8_14.

Ødegaard, H., B. Eikebrokk, and R. Storhaug (1999). "Processes for the Removal of Humic Substances from Water - an Overview Based on Norwegian Experiences." *Water Science & Technology* **40** (9), pp. 37–46. DOI: 10.1016/S0273-1223(99)00638-1.

Ødegaard, H., L. Fiksdal, and S. Østerhus (2006). *Optimal desinfeksjonspraksis for drikkevann*. Tech. rep. NORVAR, p. 136. URL: http://norskvann.no/kompetanse/va-bokhandelen/rapporter.

Ødegaard, H., S. Østerhus, and E. Melin (2009). *Veiledning til bestemmelse av god desinfeksjonspraksis - Sluttrapport fra prosjektet Optimal desinfeksjonspraksis*. Tech. rep. Norsk Vann, p. 99. URL: http://norskvann.no/kompetanse/va-bokhandelen/rapporter.

Ødegaard, H., S. W. Østerhus, and B.-M. Pott (2016a). *Microbial Barrier Analysis (MBA) - a guideline*. Tech. rep. Norsk Vann, p. 74. URL: http://norskvann.no/kompetanse/va-bokhandelen/rapporter.

Ødegaard, H., S. W. Østerhus, and B.-M. Pott (2016b). *Veiledning i mikrobiell barriere analyse (MBA)*. Tech. rep. Norsk Vann. URL: http://norskvann.no/kompetanse/va-bokhandelen/rapporter.

O'Melia, C. R. (1985). "Particles, Pretreatment, and Performance in Water Filtration." *Journal of Environmental Engineering* **111** (6), pp. 874–890. DOI: 10.1061/(ASCE)0733-9372(1985)111:6(874).

O'Melia, C. R. and W. Ali (1979). "THE ROLE OF RETAINED PARTICLES IN DEEP BED FILTRATION." In: *Proceedings of the 9th International Conference on Water Pollution Research, Stockholm, Sweden, 1978*. Ed. by S. Jenkins. Elsevier, pp. 167–182. DOI: 10.1016/B978-0-08-022939-3.50019-2.

Pacini, F. (1854). "Osservazioni microscopiche e deduzioni patologiche sul cholera asiatico (Microscopic observations and pathological deductions on asiatic cholera)." *Gazzetta Medica Italiana* **4**, pp. 405–412. URL: https://goo.gl/2qCpHN.

Park, J et al. (2001). "Influence of substrate exposure history on biodegradation in a porous medium." *Journal of Contaminant Hydrology* **51** (3-4), pp. 233–256. DOI: 10.1016/S0169-7722(01)00125-5.

Payatakes, A. C., R. Rajagopalan, and C. Tien (1974). "Application of Porous Media Models to the Study of Deep Bed Filtration." *The Canadian Journal of Chemical Engineering* **52** (6), pp. 722–731. DOI: 10.1002/cjce.5450520605.

Payment, P. and E. Franco (1993). "Clostridium perfringens and somatic coliphages as indicators of the efficiency of drinking water treatment for viruses and protozoan cysts." *Applied and Environmental Microbiology* **59** (8), pp. 2418–2424. URL: http://aem.asm.org/content/59/8/2418.short.

Payment, P., M. Trudel, and R. Plante (1985). "Elimination of viruses and indicator bacteria at each step of treatment during preparation of drinking water at seven water treatment plants." *Applied and Environmental Microbiology* **49** (6), pp. 1418–1428. URL: http://aem.asm.org/content/49/6/1418.short.

Payment, P. et al. (1991). "A randomized trial to evaluate the risk of gastrointestinal disease due to consumption of drinking water meeting current microbiological standards." *American Journal of Public Health* **81** (6), pp. 703–708. DOI: 10.2105/AJPH.81.6.703.

Payment, P. and R. Armon (1989). "Virus removal by drinking water treatment processes." *Critical Reviews in Environmental Control* **19** (1), pp. 15–31. DOI: 10.1080/10643388909388357.

Payment, P. et al. (1997). "A prospective epidemiological study of gastrointestinal health effects due to the consumption of drinking water." *International Journal of Environmental Health Research* **7** (1), pp. 5–31. DOI: 10.1080/09603129773977.

Pearson, J. W. (2009). "Computation of Hypergeometric Functions." MSc. University of Oxford, p. 118. URL: https://goo.gl/IJSGoR.

Pearson, J. W., S. Olver, and M. A. Porter (2015). "Numerical Methods for the Computation of the Confluent and Gauss Hypergeometric Functions." URL: http://arxiv.org/abs/1407.7786.

Persson, F. et al. (2005). "Characterisation of the behaviour of particles in biofilters for pre-treatment of drinking water." *Water Research* **39** (16), pp. 3791–3800. DOI: 10.1016/j.watres.2005.07.007.

Peto, S (1953). "A Dose-Response Equation for the Invasion of Micro-Organisms." *Biometrics* **9** (3), pp. 320–335. DOI: 10.2307/3001707.

Petterson, S. R. and N. J. Ashbolt (2016). "QMRA and water safety management: review of application in drinking water systems." *Journal of Water and Health*. DOI: 10.2166/wh.2016.262.

Petterson, S. et al. (2013). *Work Package 5. Case Study Report. Quantitative Microbial Risk Assessment for Evaluation and Management of Drinking Water Systems*. Tech. rep. VISK, p. 87. URL: http://visk.nu/resultat/rapporter/.

Petterson, S. et al. (2015). "Variability in the recovery of a virus concentration procedure in water: Implications for QMRA." *Water Research* **87**, pp. 79–86. DOI: 10.1016/j.watres.2015.09.006.

Petterson, S. R., R. S. Signor, and N. J. Ashbolt (2007). "Incorporating method recovery uncertainties in stochastic estimates of raw water protozoan concentrations for QMRA." *Journal of Water and Health* **5** (S1), pp. 51–65. DOI: 10.2166/wh.2007.142.

Petterson, S. R., T. A. Stenström, and J. Ottoson (2016). "A theoretical approach to using faecal indicator data to model norovirus concentration in surface water for QMRA: Glomma River, Norway." *Water Research* **91**, pp. 31–37. DOI: 10.1016/j.watres.2015.12.037.

Pintar, K. D. M. et al. (2012). "Considering the Risk of Infection by Cryptosporidium via Consumption of Municipally Treated Drinking Water from a Surface Water Source in a Southwestern Ontario Community." *Risk Analysis* **32** (7), pp. 1122–1138. DOI: 10.1111/j.1539-6924.2011.01742.x.

Ponosov, A. and A. Shindiapin (2003). "Azbelev'S W-Transform and its Applications in Mathematical Modeling." *Differential Equations and Control Processes* (4), pp. 52–72. URL: http://www.math.spbu.ru/diffjournal/EN/numbers/2003.4/article.1.4.html.

Pouillot, R. et al. (2004). "A Quantitative Risk Assessment of Waterborne Cryptosporidiosis in France Using Second-Order Monte Carlo Simulation." *Risk Analysis* **24** (1), pp. 1–17. DOI: 10.1111/j.0272-4332.2004.00407.x.

Powell, E. O. (1967). "The Growth Rate of Microorganisms as a Function of Substrate Concentration." In: *Microbial Physiology and Continuous Culture. Proc. 3rd International Symposium on Continuous Culture*. Ed. by E. O. Powell et al. London: H. M. Stationary Office.

Prasanthi, H., S. Vigneswaran, and H. Dharmappa (1997). "Effect of particle concentration on the entire cycle of filtration." *Water Science & Technology* **35** (8), pp. 91–102. DOI: 10.1016/S0273-1223(97)00155-8.

Pujol, J. M. et al. (2009). "The Effect of Ongoing Exposure Dynamics in Dose Response Relationships." *PLoS Computational Biology* **5** (6), e1000399. DOI: 10.1371/journal.pcbi.1000399.

Rajagopalan, R and C Tien (1976). "Trajectory analysis of deep-bed filtration with the sphere-in-cell porous media model." *AIChE Journal* **22** (3), pp. 523–533. DOI: 10.1002/aic.690220316.

Rao, V. C. et al. (1988). "Removal of Hepatitis A Virus and Rotavirus by Drinking Water Treatment." *Journal (American Water Works Association)* **80** (2), pp. 59–67. URL: http://www.jstor.org/stable/41290917.

Raymond, B. et al. (2012). "The Dynamics of Cooperative Bacterial Virulence in the Field." *Science* **337** (6090), pp. 85–88. DOI: 10.1126/science.1218196.

Regli, S et al. (1991). "Modeling the Risk from Giardia and Viruses in Drinking Water." *Journal American Water Works Association* **83** (11), pp. 76–84. URL: http://www.jstor.org/stable/41293556.

Reynolds, K. a., K. D. Mena, and C. P. Gerba (2008). "Risk of waterborne illness via drinking water in the United States." *Reviews of Environmental Contamination and Toxicology* **192**, pp. 117–158. DOI: 10.1007/978-0-387-71724-1_4.

Rice, G. et al. (2006). "The role of disease burden measures in future estimates of endemic waterborne disease." *Journal of Water and Health* **04** (Suppl. 2), pp. 187–199. DOI: 10.2166/wh.2006.023.

Robeck, G., N. Clark, and K. Dostal (1962). "Effectiveness of water treatment processes in virus removal." *Journal (American Water Works Association)* **54** (10), pp. 1275–1292. URL: http://www.jstor.org/stable/41256904.

Robertson, L. J. et al. (2015). "Dogs as the source of Giardia in Bergen in 2004 – barking up the wrong tree?" *Tidsskrift for Den norske legeforening* **135** (19), pp. 1718–1720. DOI: 10.4045/tidsskr.15.0883.

Rose, J. B., C. N. Haas, and S. Regli (1991). "Risk assessment and control of waterborne giardiasis." *American Journal of Public Health* **81** (6), pp. 709–713. DOI: 10.2105/AJPH.81.6.709.

Rose, J. B. and C. P. Gerba (1991). "Use of risk assessment for development of microbial standards." *Water Science & Technology* **24** (2), pp. 29–34. URL: http://wst.iwaponline.com/content/24/2/29.abstract.

Rose, J. B. et al. (1986). "Isolating Viruses From Finished Water." *Journal (American Water Works Association)* **78** (1), pp. 56–61. URL: http://www.jstor.org/stable/41273408.

Roy, S. L., M. J. Beach, and E. Scallan (2006). "The rate of acute gastrointestinal illness in developed countries." *Journal of Water and Health* **04** (Suppl. 2), pp. 31–69. DOI: 10.2166/wh.2006.017.

Rubin, L. G. (1987). "Bacterial Colonization and Infection Resulting from Multiplication of a Single Organism." *Clinical Infectious Diseases* **9** (3), pp. 488–493. DOI: 10.1093/clinids/9.3.488.

Rusin, P. A. et al. (1997). "Risk Assessment of Opportunistic Bacterial Pathogens in Drinking Water." In: *Reviews of Environmental Contamination and Toxicology*. Ed. by G. W. Ware. Springer New York, pp. 57–83. DOI: 10.1007/978-1-4612-1964-4_2.

Ryan, J. N. and M. Elimelech (1996). "Colloid mobilization and transport in groundwater." *Colloids and Surfaces A: Physicochemical and Engineering Aspects* **107**, pp. 1–56. DOI: 10.1016/0927-7757(95)03384-X.

Saltnes, T., B. Eikebrokk, and H. Ødegaard (2002a). "Coagulation optimisation for NOM removal by direct filtration in clay aggregate filters." *Journal of Water Supply: Research and Technology-AQUA* **51** (2), pp. 125–134. URL: http://www.iwaponline.com/jws/051/jws0510125.htm.

Saltnes, T., B. Eikebrokk, and H. Ødegaard (2002b). "Contact filtration of humic waters: performance of an expanded clay aggregate filter (Filtralite) compared to a dual anthracite/sand filter." *Journal of Water Supply: Research and Technology-AQUA* **2** (5-6), pp. 17–23. URL: http://www.iwaponline.com/ws/00205/ws002050017.htm.

Saxena, G. et al. (2015). "Microbial indicators, pathogens and methods for their monitoring in water environment." *Journal of Water and Health* **13** (2), pp. 319–339. DOI: 10.2166/wh.2014.275.

Schijven, J. F. and S. M. Hassanizadeh (2000). "Removal of Viruses by Soil Passage: Overview of Modeling, Processes, and Parameters." *Critical Reviews in Environmental Science and Technology* **30** (1), pp. 49–127. DOI: 10.1080/10643380091184174.

Schijven, J. F. et al. (2011). "QMRAspot: A tool for Quantitative Microbial Risk Assessment from surface water to potable water." *Water Research* **45** (17), pp. 5564–5576. DOI: 10.1016/j.watres.2011.08.024.

Schmidt, P. J. and M. B. Emelko (2011). "QMRA and decision-making: are we handling measurement errors associated with pathogen concentration data correctly?" *Water Research* **45** (2), pp. 427–438. DOI: 10.1016/j.watres.2010.08.042.

Schmidt, P. J., M. B. Emelko, and M. E. Thompson (2013a). "Analytical recovery of protozoan enumeration methods: Have drinking water QMRA models corrected or created bias?" *Water Research* **47** (7), pp. 2399–2408. DOI: 10.1016/j.watres.2013.02.001.

Schmidt, P. J., M. B. Emelko, and M. E. Thompson (2014). "Variance decomposition: a tool enabling strategic improvement of the precision of analytical recovery and concentration estimates associated with microorganism enumeration methods." *Water Research* **55**, pp. 203–214. DOI: 10.1016/j.watres.2014.02.015.

Schmidt, P. J. (2014). "Norovirus Dose-Response: Are Currently Available Data Informative Enough to Determine How Susceptible Humans Are to Infection from a Single Virus?" *Risk Analysis* **35** (7), pp. 1364–1383. DOI: 10.1111/risa.12323.

Schmidt, P. J. et al. (2013b). "Harnessing the theoretical foundations of the exponential and beta-poisson dose-response models to quantify parameter uncertainty using markov chain monte carlo." *Risk Analysis* **33** (9), pp. 1677–1693. DOI: 10.1111/risa.12006.

Schwartz, J, R Levin, and R Goldstein (2000). "Drinking water turbidity and gastrointestinal illness in the elderly of Philadelphia." *Journal of epidemiology and community health* **54** (1), pp. 45–51. DOI: 10.1136/jech.54.1.45.

Schwartz, J., R. Levin, and K. Hodge (1997). "Drinking Water Turbidity and Pediatric Hospital Use for Gastrointestinal Illness in Philadelphia." *Epidemiology* **8** (6), pp. 615–620. URL: http://www.jstor.org/stable/3702652.

Seidu, R. (2013). "Norwegian drinking water supply systems and risk management: guidelines, directives and microbial risk assessment." *VANN* **48** (4), pp. 519–528. URL: http://vannforeningen.no/dokumentarkiv/norwegian-drinking-water-supply-systems-and-risk-management-guidelines-directves-and-microbial-risk-assessment/.

Seidu, R. et al. (2007). "Integrating Quantitative Microbial Risk Assessment into Health Risk Management of Water Supply Systems in Norway." *VANN* **42** (4), pp. 329–336. URL: http://vannforeningen.no/dokumentarkiv/integrating-quantitative-microbial-risk-assessment-into-health-risk-management-of-water-supply-systems-in-norway-2/.

Semenza, J. C. et al. (2012). "Climate Change Impact Assessment of Food- and Waterborne Diseases." *Critical Reviews in Environmental Science and Technology* **42** (8), pp. 857–890. DOI: 10.1080/10643389.2010.534706.

Sen, T. K. and K. C. Khilar (2006). "Review on subsurface colloids and colloid-associated contaminant transport in saturated porous media." *Advances in Colloid and Interface Science* **119** (2-3), pp. 71–96. DOI: 10.1016/j.cis.2005.09.001.

Sharma, S, P Sachdeva, and J. S. Virdi (2003). "Emerging water-borne pathogens." *Applied Microbiology and Biotechnology* **61** (5-6), pp. 424–428. DOI: 10.1007/s00253-003-1302-y.

Shirasaki, N et al. (2010). "Estimation of norovirus removal performance in a coagulation–rapid sand filtration process by using recombinant norovirus VLPs." *Water Research* **44** (8), pp. 1307–1316. DOI: 10.1016/j.watres.2009.10.038.

Signor, R. S. and N. J. Ashbolt (2006). "Pathogen monitoring offers questionable protection against drinking-water risks: A QMRA (Quantitative Microbial Risk Analysis) approach to assess management strategies." *Water Science & Technology* **54** (3), pp. 261–268. DOI: 10.2166/wst.2006.478.

Signor, R. S. and N. J. Ashbolt (2009). "Comparing probabilistic microbial risk assessments for drinking water against daily rather than annualised infection probability targets." *Journal of Water and Health* **7** (4), pp. 535–543. DOI: 10.2166/wh.2009.101.

Silva, A. K. da et al. (2011). "Adsorption and aggregation properties of norovirus GI and GII virus-like particles demonstrate differing responses to solution chemistry." *Environmental science & technology* **45** (2), pp. 520–526. DOI: 10.1021/es102368d.

Sinclair, M. I. and C. K. Fairley (2000). "Drinking water and endemic gastrointestinal illness." *Journal of Epidemiology & Community Health* **54** (10), pp. 728–728. DOI: 10.1136/jech.54.10.728.

Sinclair, R. G. et al. (2012). "Criteria for Selection of Surrogates Used To Study the Fate and Control of Pathogens in the Environment." *Applied and Environmental Microbiology* **78** (6), pp. 1969–1977. DOI: 10.1128/AEM.06582-11.

Smeets, P. W. M. H., G. J. Medema, and J. C. van Dijk (2009). "The Dutch secret: how to provide safe drinking water without chlorine in the Netherlands." *Drinking Water Engineering and Science* **2** (1), pp. 1–14. DOI: 10.5194/dwes-2-1-2009.

Smeets, P. W. M. H. et al. (2010). "Practical applications of quantitative microbial risk assessment (QMRA) for water safety plans." *Water Science & Technology* **61** (6), pp. 1561–1568. DOI: 10.2166/wst.2010.839.

Smeets, P. W. M. H. et al. (2008). "Improved methods for modelling drinking water treatment in quantitative microbial risk assessment; a case study of Campylobacter reduction by filtration and ozonation." *Journal of Water and Health* **6** (3), pp. 301–314. DOI: 10.2166/wh.2008.066.

Snow, J. (1855). *On the mode of transmission of cholera*. 2nd ed. London: John Churchill, p. 162. URL: https://goo.gl/cEI8QQ.

Sobsey, M. D. et al. (1993). "Using a Conceptual Framework for Assessing Risks to Health From Microbes in Drinking Water." *Journal (American Water Works Association)* **85** (3), pp. 44–48. URL: http://www.jstor.org/stable/41294332.

Sokolova, E. et al. (2012). "Estimation of pathogen concentrations in a drinking water source using hydrodynamic modelling and microbial source tracking." *Journal of Water and Health* **10** (3), pp. 358–370. DOI: 10.2166/wh.2012.183.

Soller, J. A. (2006). "Use of microbial risk assessment to inform the national estimate of acute gastrointestinal illness attributable to microbes in drinking water." *Journal of Water and Health* **04** (Suppl. 2), pp. 165–186. DOI: 10.2166/wh.2006.022.

Steinmeyer, D. and M. Shuler (1989). "Structured model for Saccharomyces cerevisiae." *Chemical Engineering Science* **44** (9), pp. 2017–2030. DOI: 10.1016/0009-2509(89)85138-3.

Stenström, T. A. et al. (1994). *Vattenburna infektioner i Norden: epidemiologiskt uppföljningsarbete och hälsoproblem relaterade till förekomst av mikroorganismer i vatten*. Tech. rep. København: Nordisk Ministerråd, p. 91.

Sterk, A. et al. (2013). "Direct and Indirect Effects of Climate Change on the Risk of Infection by Water-Transmitted Pathogens." *Environmental Science & Technology* **47** (22), pp. 12648–12660. DOI: 10.1021/es403549s.

Stetler, R. E., R. L. Ward, and S. C. Waltrip (1984). "Enteric Virus and Indicator Bacteria Levels in a Water Treatment System Modified to Reduce Trihalomethane Production." *Applied and environmental microbiology* **47** (2), pp. 319–324. URL: http://aem.asm.org/content/47/2/319.short.

Straub, T. M. and D. P. Chandler (2003). "Towards a unified system for detecting waterborne pathogens." *Journal of Microbiological Methods* **53** (2), pp. 185–197. DOI: 10.1016/S0167-7012(03)00023-X.

Strauss, J. H. and R. L. Sinsheimer (1963). "Purification and properties of bacteriophage MS2 and of its ribonucleic acid." *Journal of Molecular Biology* **7** (1), pp. 43–54. DOI: 10.1016/S0022-2836(63)80017-0.

Svenskt Vatten (2015). *Introduktion till Mikrobiologisk BarriärAnalys, MBA*. Tech. rep. Svenskt Vatten, p. 68. URL: http://www.svensktvatten.se/vattentjanster/dricksvatten/riskanalys-och-provtagning/riskanalyser-och-ravattenskydd/mba/.

Svenson, S. B. et al. (1979). "Salmonella bacteriophage glycanases: endorhamnosidases of Salmonella typhimurium bacteriophages." *Journal of virology* **32** (2), pp. 583–592. URL: http://jvi.asm.org/content/32/2/583.abstract.

Tanneru, C. T., J. D. Rimer, and S. Chellam (2013). "Sweep flocculation and adsorption of viruses on aluminum flocs during electrochemical treatment prior to surface water microfiltration." *Environmental Science and Technology* **47** (9), pp. 4612–4618. DOI: 10.1021/es400291e.

Templeton, M. R., R. C. Andrews, and R Hofmann (2007). "Removal of particle-associated bacteriophages by dual-media filtration at different filter cycle stages and impacts on subsequent UV disinfection." *Water Research* **41** (11), pp. 2393–2406. DOI: 10.1016/j.watres.2007.02.047.

Templeton, M. R., R. C. Andrews, and R. Hofmann (2008). "Particle-Associated Viruses in Water: Impacts on Disinfection Processes." *Critical Reviews in Environmental Science and Technology* **38** (3), pp. 137–164. DOI: 10.1080/10643380601174764.

Teunis, P. F., N. J. Nagelkerke, and C. N. Haas (1999a). "Dose response models for infectious gastroenteritis." *Risk Analysis* **19** (6), pp. 1251–1260. DOI: 10.1023/A:1007055316559.

Teunis, P. F. M. and A. H. Havelaar (2000). "The Beta Poisson dose-response model is not a single-hit model." *Risk Analysis* **20** (4), pp. 513–520. DOI: 10.1111/0272-4332.204048.

Teunis, P. F. M. et al. (2005). "Mixed plaques: statistical evidence how plaque assays may underestimate virus concentrations." *Water Research* **39** (17), pp. 4240–4250. DOI: 10.1016/j.watres.2005.08.012.

Teunis, P. F. M. et al. (2009). "Characterization of drinking water treatment for virus risk assessment." *Water Research* **43** (2), pp. 395–404. DOI: 10.1016/j.watres.2008.10.049.

Teunis, P. F. M. et al. (2010). "Enteric virus infection risk from intrusion of sewage into a drinking water distribution network." *Environmental Science and Technology* **44** (22), pp. 8561–8566. DOI: 10.1021/es101266k.

Teunis, P. F. M., C. L. Chappell, and P. C. Okhuysen (2002a). "Cryptosporidium dose-response studies: Variation between hosts." *Risk Analysis* **22** (3), pp. 475–485. DOI: 10.1111/0272-4332.00046.

Teunis, P. F. M., C. L. Chappell, and P. C. Okhuysen (2002b). "Cryptosporidium dose response studies: variation between isolates." *Risk Analysis* **22** (1), pp. 175–183. DOI: 10.1111/0272-4332.00014.

Teunis, P. F. (1997). *Infectious gastro-enteritis - opportunities for dose response modelling*. Tech. rep. Bilthoven, The Netherlands: National Institute of Public Health and the Environment (RIVM), p. 49. URL: http://hdl.handle.net/10029/9967.

Teunis, P. F. et al. (1996). *The dose-response relation in human volunteers for gastro-intestinal pathogens*. Tech. rep. Bilthoven, The Netherlands: National Institute of Public Health and the Environment (RIVM), p. 87. URL: http://hdl.handle.net/10029/9966.

Teunis, P. F. et al. (2008). "Norwalk virus: How infectious is it?" *Journal of Medical Virology* **80** (8), pp. 1468–1476. DOI: 10.1002/jmv.21237.

Teunis, P. and A. Havelaar (1999). *Cryptosporidium in drinking water: Evaluation of the ILSI quantitative risk assessment framework*. Tech. rep. Bilthoven, The Netherlands: National Institute of Public Health and the Environment (RIVM), p. 100. URL: http://hdl.handle.net/10029/9968.

Teunis, P. et al. (1997). "Assessment of the risk of infection by Cryptosporidium or Giardia in drinking water from a surface water source." *Water Research* **31** (6), pp. 1333–1346. DOI: 10.1016/S0043-1354(96)00387-9.

Teunis, P., E. Evers, and W Slob (1999b). "Analysis of variable fractions resulting from microbial counts." *Quantitative Microbiology* **1** (1), pp. 63–88. DOI: 10.1023/A:1010028411716.

Tfaily, R. et al. (2015). "Application of Quantitative Microbial Risk Assessment at 17 Canadian Water Treatment Facilities." *Journal - American Water Works Association* **107** (10), E497–E508. DOI: 10.5942/jawwa.2015.107.0141.

Thebault, A. et al. (2013). "Infectivity of GI and GII noroviruses established from oyster related outbreaks." *Epidemics* **5** (2), pp. 98–110. DOI: 10.1016/j.epidem.2012.12.004.

Tien, C. and A. C. Payatakes (1979). "Advances in deep bed filtration." *AIChE Journal* **25** (5), pp. 737–759. DOI: 10.1002/aic.690250502.

Tien, C. and B. Ramaro (2007). *Granular Filtration of Aerosols and Hydrosols*. 2nd ed. Elsevier, p. 512. URL: http://www.sciencedirect.com/science/book/9781856174589.

Tillett, H. E., J de Louvois, and P. G. Wall (1998). "Surveillance of outbreaks of waterborne infectious disease: categorizing levels of evidence." *Epidemiology and infection* **120** (1), pp. 37–42. URL: http://goo.gl/6y4KxN.

Tinker, S. C. et al. (2009). "Drinking water residence time in distribution networks and emergency department visits for gastrointestinal illness in Metro Atlanta, Georgia." *Journal of Water and Health* **07** (2), pp. 332–343. DOI: 10.2166/wh.2009.022.

Tinker, S. C. et al. (2010). "Drinking water turbidity and emergency department visits for gastrointestinal illness in Atlanta, 1993–2004." *Journal of Exposure Science and Environmental Epidemiology* **20** (1), pp. 19–28. DOI: 10.1038/jes.2008.68.

Tufenkji, N and M Elimelech (2004). "Correlation Equation For Predicting Single-Collector Efficiency in Physiochemical Filtration in Saturated Porous Media." *Environmental Science & Technology* **38** (2), pp. 529–536. DOI: 10.1021/es034049r.

Tufenkji, N. (2007). "Modeling microbial transport in porous media: Traditional approaches and recent developments." *Advances in Water Resources* **30** (6-7), pp. 1455–1469. DOI: 10.1016/j.advwatres.2006.05.014.

Tufenkji, N. and M. Elimelech (2005). "Breakdown of Colloid Filtration Theory: Role of the Secondary Energy Minimum and Surface Charge Heterogeneities." *Langmuir* **21** (3), pp. 841–852. DOI: 10.1021/la048102g.

UNECE (1999). *Protocol on Water and Health to the 1992 Convention on the Protection and Use of Transboundary Watercourses and International Lakes*. URL: http://goo.gl/8IR4q1.

USDA/FSIS and USEPA (2012). *Microbial Risk Assessment Guideline: Pathogenic Microorganisms with Focus on Food and Water*. Tech. rep. U.S. Department of Agriculture/Food Safety, Inspection Service (USDA/FSIS), and U.S. Environmental Protection Agency (USEPA), p. 207. DOI: EPA/100/J-12/001.

USEPA (2014). *Microbiological Risk Assessment (MRA): Tools, Methods, and Approaches for Water Media*. Tech. rep. Washington, D.C.: United States Environmental Protection Agency, Office of Science and Technology, p. 184. URL: https://www.epa.gov/wqc/microbiological-risk-assessment-mra-tools-methods-and-approaches-water-media.

Verwey, E. and J. Overbeek (1948). *Theory of the stability of lyophobic colloids*. Amsterdam: Elsevier, p. 108. URL: https://goo.gl/xlGgL0.

VISK (2013). *Virus i vatten - skandinavisk kunskapsbank*. URL: http://visk.nu/.

Vivier, J. C. et al. (2002). "Assessment of the risk of infection associated with Coxsackie B viruses in drinking water." *Water Science & Technology: Water Supply* **2** (3), pp. 1–8. URL: http://ws.iwaponline.com/content/2/3/1.

Vrale, L. and R. M. Jorden (1971). "RAPID MIXING IN WATER TREATMENT." *Journal (American Water Works Association)* **63** (1), pp. 52–58. URL: http://www.jstor.org/stable/41266237.

Wahl, E. (2005). *Kartlegging av mulig helserisiko for abonnenter berørt av trykkløs vann- ledning ved arbeid på ledningsnettet*. Tech. rep. NORVAR, p. 62. URL: http://norskvann.no/kompetanse/va-bokhandelen/rapporter.

Wensaas, K.-A. (2011). "Giardiasis in Bergen. Outbreak and clinical consequences." PhD. University of Bergen, p. 82. URL: https://bora.uib.no/handle/1956/5614.

Werf, W. van der et al. (2011). "Heterogeneous host susceptibility enhances prevalence of mixed-genotype micro-parasite infections." *PLoS computational biology* **7** (6), e1002097. DOI: 10.1371/journal.pcbi.1002097.

Weroński, P., J. Y. Walz, and M. Elimelech (2003). "Effect of depletion interactions on transport of colloidal particles in porous media." *Journal of Colloid and Interface Science* **262** (2), pp. 372–383. DOI: 10.1016/S0021-9797(03)00174-7.

Westrell, T et al. (2003). "A theoretical approach to assess microbial risks due to failures in drinking water systems." *International journal of environmental health research* **13** (2), pp. 181–197. DOI: 10.1080/0960312031000098080.

Westrell, T., Y. Andersson, and T. A. Stenström (2006). "Drinking water consumption patterns in Sweden." *Journal of water and health* **4** (4), pp. 511–522. DOI: 10.2166/wh.2006.030.

Widerström, M. et al. (2014). "Large outbreak of Cryptosporidium hominis infection transmitted through the public water supply, Sweden." *Emerging infectious diseases* **20** (4), pp. 581–589. DOI: 10.3201/eid2004.121415.

Williams, T. (1965). "The Basic Birth-Death Model for Microbial Infections." *Journal of the Royal Statistical Society. Series B (Methodological)* **27** (2), pp. 338–360. URL: http://www.jstor.org/stable/2984203.

Willumsen, A. (2015). "Undersøkelse av virusfjerning i modning- og gjennombruddsperiodene i et pilotskala to-media sandfilter for drikkevann [Pilot-Scale Investigations of Virus Removal During the Ripening and Breakthrough Phases in a Dual-Media Sand Filter for Drinking Water]." MSc. Norwegian University of Life Sciences, p. 104. URL: http://hdl.handle.net/11250/286191.

Wood, B. D., T. R. Ginn, and C. N. Dawson (1995). "Effects of Microbial Metabolic Lag in Contaminant Transport and Biodegradation Modeling." *Water Resources Research* **31** (3), pp. 553–563. DOI: 10.1029/94WR02533.

World Health Organization (2003). *Assessing Microbial Safety of Drinking Water - Improving Approaches and Methods*. OECD Publishing, p. 296. URL: http://goo.gl/H8MONy.

World Health Organization (2011). *Guidelines for Drinking-water Quality*. 4th ed. Geneva, Switzerland: World Health Organization, p. 564. URL: http://goo.gl/EdFKSb.

Wu, J. et al. (2011). "Are microbial indicators and pathogens correlated? A statistical analysis of 40 years of research." *Journal of Water and Health* **9** (2), pp. 265–278. DOI: 10.2166/wh.2011.117.

Yang, J. et al. (2011). "Managing risks from virus intrusion into water distribution systems due to pressure transients." *Journal of Water and Health* **9** (2), pp. 291–305. DOI: 10.2166/wh.2011.102.

Yao, K.-m., M. T. Habibian, and C. R. O'Melia (1971). "Water and Waste Water Filtration: Concepts and Applications." *Environmental Science & Technology* **5** (11), pp. 1105–1112. DOI: 10.1021/es60058a005.

Zamani, A. and B. Maini (2009). "Flow of dispersed particles through porous media — Deep bed filtration." *Journal of Petroleum Science and Engineering* **69** (1-2), pp. 71–88. DOI: 10.1016/j.petrol.2009.06.016.

Zmirou-Navier, D, L Gofti-Laroche, and P. Hartemann (2006). "Waterborne microbial risk assessment: a population-based dose-response function for Giardia spp. (E.MI.R.A study)." *BMC Public Health* **6** (122). DOI: 10.1186/1471-2458-6-122.

Zwart, M. P. et al. (2009). "An experimental test of the independent action hypothesis in virus-insect pathosystems." *Proceedings. Biological sciences / The Royal Society* **276** (1665), pp. 2233–2242. DOI: 10.1098/rspb.2009.0064.

Zwart, M. P., J.-A. Daròs, and S. F. Elena (2011). "One is enough: in vivo effective population size is dose-dependent for a plant RNA virus." *PLoS pathogens* **7** (7), e1002122. DOI: 10.1371/journal.ppat.1002122.

Appended Papers

Paper I

Nilsen, V. and J. Wyller (2016a). "QMRA for drinking water: 1. Revisiting the mathematical structure of single-hit dose-response models." *Risk Analysis* **36** (1), pp. 145–162.

Risk Analysis, Vol. 36, No. 1, 2016 DOI: 10.1111/risa.12389

QMRA for Drinking Water: 1. Revisiting the Mathematical Structure of Single-Hit Dose-Response Models

Vegard Nilsen* and John Wyller

Dose-response models are essential to quantitative microbial risk assessment (QMRA), providing a link between levels of human exposure to pathogens and the probability of negative health outcomes. In drinking water studies, the class of semi-mechanistic models known as *single-hit* models, such as the exponential and the exact beta-Poisson, has seen widespread use. In this work, an attempt is made to carefully develop the general mathematical single-hit framework while explicitly accounting for variation in (1) host susceptibility and (2) pathogen infectivity. This allows a precise interpretation of the so-called single-hit probability and precise identification of a set of statistical independence assumptions that are sufficient to arrive at single-hit models. Further analysis of the model framework is facilitated by formulating the single-hit models compactly using probability generating and moment generating functions. Among the more practically relevant conclusions drawn are: (1) for any dose distribution, variation in host susceptibility always reduces the single-hit risk compared to a constant host susceptibility (assuming equal mean susceptibilities), (2) the model-consistent representation of complete host immunity is formally demonstrated to be a simple scaling of the response, (3) the model-consistent expression for the total risk from repeated exposures deviates (gives lower risk) from the conventional expression used in applications, and (4) a model-consistent expression for the mean per-exposure dose that produces the correct total risk from repeated exposures is developed.

KEY WORDS: Dose response; microbial risk; QMRA; single hit

1. INTRODUCTION

Dose-response models are at the core of quantitative microbial risk assessment (QMRA) since they provide a quantitative relationship between microbial exposure (the dose) and the resulting health consequences (the response) in exposed populations. However, determining the appropriate mathematical form of such models is not an easy task. First, the host-pathogen interaction is complex and not easily observed or modeled. Second, due to the difficulty of quantifying the low-probability responses to low doses, the dose levels in available data (either from feeding trials or epidemiological outbreak data) for fitting dose-response model parameters are usually orders of magnitude above the typical background dose levels in drinking water. Therefore, drinking water risk assessments often require a rather bold extrapolation assumption that can only be strictly justified if the mathematical form of the dose-response model is appropriate for the whole range of doses, including the low-dose range, and if the available data allow reliable model fitting.

Department of Mathematical Sciences and Technology, Norwegian University of Life Sciences, N-1432 Aas, Norway.
*Address correspondence to Vegard Nilsen, Department of Mathematical Sciences and Technology, Norwegian University of Life Sciences, P.O. Box 5003, N-1432 Aas, Norway; vegard.nilsen@nmbu.no.

The above remarks motivate the development of *(semi)mechanistic* dose-response models, as opposed to any arbitrary best-fitting model, to provide a rationale for the extrapolation. So-called single-hit models[1–5] provide the most important example, as they have dominated QMRA applications for drinking water. It is the purpose of this article to take a closer look at their derivation and general properties. In short, they are based on the main assumptions that (1) a single pathogen may be capable of causing an infection and (2) pathogens act independently of each other. They represent a simple semi-mechanistic dose-response framework, but a good understanding of the models' origins and structure may provide hints to the mechanistic underpinnings in cases of poor fits to data, as well as suggest strategies to construct improved semi-mechanistic models.

The microbial quality of drinking water is an ever-present concern in the promotion of public health. The regulatory practice in many countries has been to prescribe maximum allowable concentrations of fecal indicator microorganisms in drinking water, with the assumption that elevated levels of fecal indicators signal the presence of fecal contamination, a condition for the presence of fecal *pathogens*. In recent years, QMRA has emerged as an alternative theoretical framework for evaluating the microbial safety of drinking water supply systems.[6] By keeping account of the concentration of pathogenic organisms from the raw water source to the tap, by measurements and/or modeling, an estimate of a population's exposure to pathogens in drinking water is obtained. This estimate forms the input to the dose-response model that allows the probability of infection, and possibly disease, to be estimated. Thus, QMRA aims to provide a framework for a more rational, detailed, and quantitative analysis of microbial drinking water quality. It may serve as a management tool to optimize the design and operation of a drinking water system with respect to microbial quality,[7] and form the basis for risk-based regulations[8] and guidelines.[9]

Three main sources of variation are usually considered in conventional dose-response modeling: (1) variation in infectivity between individual pathogens, (2) variation between individual hosts in their susceptibility to infection by the pathogens, and (3) randomness (e.g., Poisson) in the exact number of pathogens ingested. Many authors have developed the single-hit framework[1–5] and it has been shown previously[4,5,10] that under single-hit assumptions, the variation between individual pathogens gets integrated out of the model and is not a source of variation in the so-called single-hit probability; only variation in host susceptibility is. The purpose of the present work was to introduce slightly more detail to the analysis; i.e., carefully develop the single-hit framework by introducing random variables to explicitly represent all three sources of variation; essentially a generalization in a QMRA context of the host-pathogen interation model of Fazekas de st Groth and Moran.[10] This allows precise identification of a minimal set of sufficient statistical independence assumptions for arriving at single-hit models, and a precise expression for the single-hit probability as a certain function of pathogen- and host-related variables. Further specification of this function and variables may provide interesting extended single-hit models and opportunities for interpretation, particularly as tools and data to characterize relevant host and pathogen properties become more available.

As mentioned above, it has been demonstrated previously that variation in host susceptibility is the only source of variation in single-hit probabilities. This conclusion leads to some interpretive consequences that are developed in this work, regarding risks in homogeneous versus heterogeneous host populations, representation of complete host immunity, and the correct treatment of repeated exposures. The analysis of single-hit models is greatly facilitated by formulating them compactly using probability generating (pgf) and moment generating functions (mgf). The mgf formulation can be used to place a useful theoretical restriction on the class of functions that can serve as a single-hit model when doses are Poisson distributed. The pgf formulation is utilized in full in the companion article,[11] where the effect of (spatial) pathogen clustering on health risk estimates is studied.

2. PROBLEM FORMULATION AND NOMENCLATURE

Suppose there is a population of human hosts and that, for each individual host, the susceptibility to infection from a particular type of pathogen may be characterized by a set of properties, collected in a vector of variables **s**. Suppose further that there is a population of the particular type of pathogen and that, for each individual pathogen, its infectivity may be characterized by a set of properties, collected in a vector of variables **t**. Vectors are used here because it seems too restrictive to characterize such complex properties as susceptibility and infectivity by scalar

Table I. Random Variables Used in the Model Development (Some Variables Have Indexed Versions in the Text)

Symbol	Support	Meaning (See Text for Precise Definitions)
Y	$\{0, 1\}$	Host infection state in the experiment of Section 2 ($Y = 1$ if infected, $Y = 0$ if not)
P_{I}	$[0, 1]$	$\Pr(Y = 1)$
W	$\{0, 1, \ldots, n\}$	The sum of n iid variables Y
X	$\mathbb{N}_0 = \{0, 1, 2, \ldots\}$	Dose, i.e., the total number of pathogens ingested by a host
$\mathbf{S}$	Not specified	A vector of variables that characterizes the susceptibility of an individual host
$\mathbf{T}$	Not specified	A vector of variables that characterizes the infectivity of an individual pathogen
I	[0,1]	I characterizes the fate of a pathogen ($I = 1$ if it establishes infection, $I = 0$ if not)
R	[0,1]	Equation (12): The conditional expected probability that a single pathogen infects a random host

variables. Finally, assume that the population of pathogens is dispersed in a drinking water source from which we take a small volume sample. For the purposes of this article, we are concerned with the *total number* of pathogens contained in the sample, which will be denoted x. Table I gives an overview of the random variables used in developing the dose-response framework.

In formulating the single-hit framework, we will be concerned with the outcome of a particular hypothetical, probabilistic experiment described by:

(1) Randomly select one host from the population of hosts.
(2) Take a random sample from the water source; this will contain a random number of pathogens from the population of pathogens.
(3) Let the host ingest the water sample.

This means we obtain one instance $\mathbf{s}$ of the random variable[1] $\mathbf{S}$, one instance x of the random variable X, and x instances $\mathbf{t}_1, \ldots, \mathbf{t}_x$ of the random variables $\mathbf{T}_1, \ldots, \mathbf{T}_x$ (or, more precisely, one instance of each of the x variables). We need the indexing here to allow for statistical dependence between the infectivity of individual pathogens.

In the experiment, there are two outcomes of interest. First, there is the establishment or not of an infection (or, alternatively, illness) by the pathogens in the host. In conventional single-hit models, this outcome is a binary random variable Y that takes the value 1 if infection is established and 0 if not. For enteric pathogens, the presence of an infection is usually operationally defined as the detection of the pathogen in stool samples. Second, we are also interested in the *probability* of infection for the host selected in the experiment, P_{I}, a random variable assumed to be some (deterministic) function of the underlying random variables $\mathbf{S}$, X, and $\mathbf{T}_{\mathbf{X}}$, where $\mathbf{T}_{\mathbf{X}}$ is a matrix collecting $\mathbf{T}_1, \ldots, \mathbf{T}_x$:

$$P_{\mathrm{I}} = h(\mathbf{S}, X, \mathbf{T}_{\mathbf{X}}). \tag{1}$$

P_{I} will have some probability density function (pdf)[2] $f_{P_{\mathrm{I}}}(p_{\mathrm{I}})$ that depends on the function h and the joint distribution of its arguments.

The joint distribution $f_{Y,P_{\mathrm{I}}}$ of the two experimental outcomes Y and P_{I} may be written using the probability mass function (pmf) $p_Y(y)$ of a Bernoulli variable, conditioned on the random parameter P_{I} (i.e., the *success probability* is random):

$$\begin{aligned} f_{Y,P_{\mathrm{I}}}(y, p_{\mathrm{I}}) &= p_{Y|P_{\mathrm{I}}}(y|p_{\mathrm{I}})\, f_{P_{\mathrm{I}}}(p_{\mathrm{I}}) \\ &= {p_{\mathrm{I}}}^{y}(1 - p_{\mathrm{I}})^{1-y}\, f_{P_{\mathrm{I}}}(p_{\mathrm{I}}). \end{aligned} \tag{2}$$

The pmf of Y is then obtained by marginalizing over P_{I}:

$$\begin{aligned} p_Y(y) &= \int_0^1 f_{Y,P_{\mathrm{I}}}(y, p_{\mathrm{I}})\, \mathrm{d}p_{\mathrm{I}} \\ &= [\mathrm{E}(P_{\mathrm{I}})]^y [1 - \mathrm{E}(P_{\mathrm{I}})]^{1-y}, \end{aligned} \tag{3}$$

where $\mathrm{E}(\cdot)$ is the expectation operator. We recognize Equation (3) as the pmf of a Bernoulli variable with constant success probability $\mathrm{E}(P_{\mathrm{I}})$. Thus, the fact that the success probability is a random variable instead of a constant does not affect the distribution of the Bernoulli variable Y (or a binomial variable derived from it); it merely requires an interpretation of the success probability as an expectation value. This is a basic fact of probability, but it is highlighted here since essentially the same argument leads to the conclusion[4,5] that variation in pathogen infectivity is "averaged out" of the single-hit dose-response

[1] Throughout this article, strict adherence is made to the convention of denoting random variables with uppercase letters and particular instances of the same variables with the corresponding lowercase letters.

[2] Actually, because X is discrete, it will be a mixed discrete and continuous distribution, as explained in the Appendix.

model, a fact that seems to not be universally recognized in the single-hit literature. The single-hit dose-response model is given as the expression for $\mathrm{E}(P_\mathrm{I})$ as a function of the parameters of the dose distribution, and is developed in Section 3.

One is usually interested in performing the experiment above many times. If we restrict our interest to infections that are the direct result of ingesting contaminated drinking water and exclude secondary infections from the count, it is reasonable to assume that the outcome of Y and P_I in any single experiment is independent of the outcomes in every other experiment. Thus, the total number W of infected hosts after n experiments is:

$$W = \sum_{j=1}^{n} Y_j, \tag{4}$$

where the Y_j,s are independent and identically (iid) distributed as Y. W is therefore binomially distributed with success probability $\mathrm{E}(P_\mathrm{I})$ and number of trials n.

3. SINGLE-HIT MODELS

3.1. General Framework

In this section, we obtain expressions for $\mathrm{E}(P_\mathrm{I})$ by applying a sequence of statistical independence assumptions on $\mathbf{S}$, X, and $\mathbf{T}_1, \ldots, \mathbf{T}_x$. Our goal in the end is to arrive at the single-hit dose-response model, which has the form:

$$\mathrm{E}(P_\mathrm{I}) = \mathrm{E}_X[\mathrm{E}_R(P_\mathrm{I})]\,. \tag{5}$$

Here, R is the so-called single-hit probability and it is independent of X. It is a function of $\mathbf{S}$ and the $\mathbf{T}$,s, defined more precisely below. The notation E_X (E_R) denotes expectation with respect to X (R).

3.1.1. Model Derivation

By assumption in a single-hit model, a single pathogen may have a nonzero probability of establishing infection in a host. The probability of infection P_I may then be expressed as the complement to the probability that none of the pathogens establishes an infection. Let I_i ($i = 0, \ldots, X$) denote the fate of pathogen i ($I_i = 1$ if pathogen i establishes infection, $I_i = 0$ if not) with $I_0 \equiv 0$. Using the chain rule of probability, we then have:

$$\begin{aligned} P_\mathrm{I} &= 1 - \Pr\left(I_0 = I_1 = I_2 = \cdots = I_X = 0\right) \\ &= 1 - \prod_{i=1}^{X} \Pr\left(I_i = 0 \mid I_0 = \cdots = I_{i-1} = 0\right) \\ &= 1 - \prod_{i=1}^{X} \left[1 - \Pr\left(I_i = 1 \mid I_0 = \cdots = I_{i-1} = 0\right)\right], \end{aligned} \tag{6}$$

where the number of factors in the product, X, is random. For $X = 0$, the product becomes the empty product (which is 1, by definition) so in the absence of any ingested pathogens, no infection will occur. Note that no independence assumptions are needed for Equation (6).

The independence assumptions that are sequentially employed in the derivation below are summarized in Table II. The first of them (IA1) is the following. We fix a set of host properties $\mathbf{S} = \mathbf{s}$, a dose $X = x$, and a set of pathogen properties $\mathbf{T}_1 = \mathbf{t}_1, \ldots, \mathbf{T}_x = \mathbf{t}_x$. Then, $\Pr(I_i = 1)$ is assumed to be independent of both the number and "identity" of individual pathogens that *fail* ($I_j = 0$ for $j \neq i$) to establish infection. This means that $\Pr(I_i = 1)$ is completely determined by $\mathbf{s}, x,$ and $\mathbf{t}_1, \ldots, \mathbf{t}_x$. Note that IA1 is not equivalent to making the slightly stronger assumption that all the I_i,s are mutually independent since we do not have to worry about the situation where more than one pathogen infects the host; i.e., conditional probabilities like $\Pr(I_i = 1 | \sum_{j<i} I_j \geq 1)$ do not enter the problem. IA1 implies that Equation (6) may be written:

$$P_\mathrm{I} = h(\mathbf{S}, \mathbf{T}_\mathbf{X}, X) = 1 - \prod_{i=1}^{X} [1 - g(\mathbf{S}, \mathbf{T}_i, X)], \tag{7}$$

where the function $g(\mathbf{S}, \mathbf{T}_i, X)$ maps $\mathbf{S}$, $\mathbf{T}_i$, and X onto the unit interval $[0, 1]$ and equals the probability that an individual pathogen indexed by i initiates an infection in a host. For generality, we have included X as an argument of the function g. Following Fazekas de St Groth and Moran,[10] the functions g and h may be termed *interaction* functions.

Put another way, IA1 implies that the knowledge that the host has successfully defeated one or more pathogens in a given dose does not provide information on the probability that the other pathogens will establish an infection; this probability is fixed once we fix the host, the dose, and the individual pathogens. IA1 would be violated if the immune system and/or pathogens mobilize/employ some sort of signaling in response to the fate of an individual pathogen, which changes the probability

Table II. Independence Assumptions Employed Sequentially in Developing the Single-Hit Dose-Response Framework

Name	Description
IA1	If $\mathbf{s}, x,$ and $\mathbf{t}_1, \ldots, \mathbf{t}_x$ are given, $\Pr(I_i = 1 \mid I_0 = \cdots = I_{i-1} = 0) = g(\mathbf{S}, \mathbf{T}_i, X)$ for all i *In words*: Given a host, a dose, and particular pathogens, the number and identity of pathogens that fail to establish infection does not affect the probability that other pathogens will establish infection
IA2	If $\mathbf{s}$ and x are given, the $\mathbf{T}_i$,s are mutually independent *In words*: Given a host and a dose, the infectivities of individual pathogens are mutually independent
IA3	If $\mathbf{s}$ is given, X and every $\mathbf{T}_i$ are mutually independent *In words*: Given a host, the dose and the infectivity of every pathogen are mutually independent
IA4	$\mathbf{S}$ and X are mutually independent *In words*: The host susceptibility and the dose are mutually independent
IAnet	IA1 + pair-wise independence between all variables ($\mathbf{T}_i$ iid as $\mathbf{T}$), except possibly between $\mathbf{S}$ and $\mathbf{T}$

of infection for the other pathogens. This assumes that the fate of each pathogen may be determined sequentially in time even if the ingestion of the dose is instantaneous.

There is also a practical, clinical aspect to the single-hit assumption that deserves mentioning: pathogen detection/enumeration methods have a detection limit (or perhaps a probability of detection for a given concentration of pathogens), and clinical symptoms may exist without an observed infection.[12,13] If there are enough pathogens in a given stool sample to exceed the detection limit and these pathogens stem from more than one infectious focus in the intestinal system, single-hit theory can be strictly correct only if at least one of the infectious foci produced enough pathogens on its own to exceed the detection limit. Otherwise, there would be instances where two or more infectious foci (originating from at least two pathogens) would be required to produce an observable infection. The interesting scientific question in this regard is, of course, the relationship between clinically relevant infections (i.e., levels of multiplication that increase the probability of illness) and infections that can be detected in stool samples. It would also be interesting to see if one could develop dose-response models that explicitly estimate the probability of pathogen counts exceeding the detection limit in stool samples. One could still assume independent pathogen action in the host, but one would have to somehow account for the total numbers shedded.

As stated above, the conventional dose-response models of QMRA will be derived by taking the expectation value of the random variable $P_I = h(\mathbf{S}, \mathbf{T}_\mathbf{X}, X)$ as expressed in Equation (7). By the law of total expectation, we may decompose the expectation operation using conditional expectations:

$$\begin{aligned} \mathrm{E}(P_I) &= 1 - \mathrm{E}\left\{\prod_{i=1}^{X}[1 - g(\mathbf{S}, \mathbf{T}_i, X)]\right\} \\ &= 1 - \mathrm{E}_X\left[\mathrm{E}_{\mathbf{S}|X}\left(\mathrm{E}_{\mathbf{T}_\mathbf{X}|\mathbf{S},X}\left\{\prod_{i=1}^{X}[1 - g(\mathbf{S}, \mathbf{T}_i, X)]\right\}\right)\right]. \end{aligned} \tag{8}$$

The notation $\mathrm{E}_{A|B,C}$ denotes expectation with respect to A while holding B and C constant (conditional expectation). We could have used another ordering in the sequence of conditional expectations, but the choice made above will be convenient.

The second independence assumption (IA2) will now be imposed, namely, that the vectors $\mathbf{T}_i$ contained in the matrix $\mathbf{T}_\mathbf{X}$ are mutually independent, conditioned on $\mathbf{S} = \mathbf{s}$ and $X = x$. This means that knowledge of the infectivity properties $\mathbf{t}_i$ for pathogen i does not provide information about $\mathbf{t}_j$ for pathogen j ($i \neq j$), i.e., there is no tendency for pathogens with particular infectivity properties to occur simultaneously (i.e., be included in the same sample). IA2 implies that the innermost expectation in Equation (8), which is with respect to $\mathbf{T}_\mathbf{X}$, may be written as a product of expectations taken with respect to the $\mathbf{T}_i$'s:

$$\begin{aligned} \mathrm{E}(P_I) &= 1 - \mathrm{E}_X\left[\mathrm{E}_{\mathbf{S}|X}\left(\prod_{i=1}^{X}\{1 - \mathrm{E}_{\mathbf{T}_i|\mathbf{S},X}[g(\mathbf{S}, \mathbf{T}_i, X)]\}\right)\right] \\ &= 1 - \mathrm{E}_X\left[\mathrm{E}_{\mathbf{S}|X}\left(\{1 - \mathrm{E}_{\mathbf{T}|\mathbf{S},X}[g(\mathbf{S}, \mathbf{T}, X)]\}^X\right)\right]. \end{aligned} \tag{9}$$

Here, $\mathbf{T}$ denotes a random variable whose distribution is the common distribution of the $\mathbf{T}_i$'s.

The third independence assumption (IA3) is that $\mathbf{T}$ and X are mutually independent if $\mathbf{S} = \mathbf{s}$ is given. This means that there is no correlation between the number of pathogens ingested and their individual

infectivity properties. With this assumption, we may write:

$$\mathrm{E}(P_{\mathrm{I}}) = 1 - \mathrm{E}_X\left[\mathrm{E}_{\mathbf{S}|X}\left(\{1 - \mathrm{E}_{\mathbf{T}|\mathbf{S}}[g(\mathbf{S}, \mathbf{T}, X)]\}^X\right)\right]. \tag{10}$$

The last independence assumption (IA4) is that **S** and X must be mutually independent, i.e., there is no correlation between host susceptibility and the number of ingested pathogens. This may be a questionable assumption, since those members of the host population with a weakened immune system (e.g., infants, elderly, and hospitalized people) may also reasonably be expected to drink less water and hence experience lower doses. It is also plausible that ingesting a higher dose of pathogens may trigger a stronger immune response, which could effectively alter the host susceptibility **s**. However, ignoring these possible correlations seems to constitute a conservative approach (overestimation of risk) and we find:

$$\mathrm{E}(P_{\mathrm{I}}) = 1 - \mathrm{E}_X\left[\mathrm{E}_{\mathbf{S}}\left(\{1 - \mathrm{E}_{\mathbf{T}|\mathbf{S}}[g(\mathbf{S}, \mathbf{T}, X)]\}^X\right)\right]. \tag{11}$$

It will also be assumed that g does not depend deterministically on X, i.e., $g(\mathbf{S}, \mathbf{T}, X) \equiv g(\mathbf{S}, \mathbf{T})$.[3] This implies that the only place X appears as a parameter when taking the expectation with respect to **S** is in the exponent. The quantity $\mathrm{E}_{\mathbf{T}|\mathbf{S}}[g(\mathbf{S}, \mathbf{T})]$ may be considered a random variable in its own right, and is a function of **S** alone since **T** has been integrated out. It is known as the single-hit infection probability and denoted by R:

$$R = R(\mathbf{S}) = \mathrm{E}_{\mathbf{T}|\mathbf{S}}[g(\mathbf{S}, \mathbf{T})]. \tag{12}$$

With this, Equation (11) is written:

$$\mathrm{E}(P_{\mathrm{I}}) = 1 - \mathrm{E}_X(\mathrm{E}_{\mathbf{S}}\{[1 - R(\mathbf{S})]^X\}). \tag{13}$$

Assuming that **S** has a pdf $f_{\mathbf{S}}(\mathbf{s})$ and X a pmf $p_X(x)$, Equation (13) may be written explicitly as:

$$\mathrm{E}(P_{\mathrm{I}}) = 1 - \sum_{x=0}^{\infty} p_X(x) \int_{\mathbf{S}} [1 - r(\mathbf{s})]^x f_{\mathbf{S}}(\mathbf{s})\, \mathrm{d}\mathbf{s}, \tag{14}$$

where the integration is over the whole support of **S**, and r is a particular instance of the random variable R. The only thing that is needed now to arrive at a conventional single-hit dose-response formulation is a multivariate substitution in Equation (14) to allow an integration over r instead of **s**. Assuming that there exists such a substitution, we may write:

$$\mathrm{E}(P_{\mathrm{I}}) = 1 - \sum_{x=0}^{\infty} p_X(x) \int_0^1 (1 - r)^x f_R(r)\, \mathrm{d}r. \tag{15}$$

If **S** can be assumed to be a scalar S, i.e., S is *the* susceptibility of the hosts, we can easily perform the substitution explicitly. Then, we have:

$$r(s) = \mathrm{E}_{\mathbf{T}|S=s}[g(s, \mathbf{T})] \tag{16}$$

and, assuming r is a differentiable function of s, let $r'(s) = \frac{\mathrm{d}r}{\mathrm{d}s}$. It is reasonable to assume that r must be a monotonically increasing function of s so that its inverse $s(r)$ exists. Substituting in Equation (14), we again arrive at Equation (15), now with:

$$f_R(r) \equiv \frac{f_S[s(r)]}{r'[s(r)]}, \tag{17}$$

which is guaranteed to be a well-defined probability density if $r'(s)$ is nonzero and smooth. Finally, this may be written:

$$\begin{aligned}\mathrm{E}(P_{\mathrm{I}}) &= \sum_{x=0}^{\infty} p_X(x) \int_0^1 [1 - (1 - r)^x] f_R(r)\, \mathrm{d}r \\ &= \sum_{x=0}^{\infty} p_X(x) \mathrm{E}_R(P_{\mathrm{I}}) = \mathrm{E}_X[\mathrm{E}_R(P_{\mathrm{I}})]. \end{aligned} \tag{18}$$

This is the form in which the single-hit dose-response model structure has been given previously.[4] The integral expression $\mathrm{E}_R(P_{\mathrm{I}})$ has been termed a "conditional" dose-response model, as it gives the (expected) probability of infection given that exactly x pathogens have been ingested.[4] The model in Equation (18) may be parameterized by specific choices of distributions for p_X and $f_R(r)$ (Section 3.2). Usually p_X is taken to be the Poisson distribution, which has a single parameter that equals its expected value, $\mathrm{E}(X)$. One could therefore argue that a more precise term for the single-hit models would be "mean dose-mean response."

To sum up the most important points: in the framework laid out above, (IA1)–(IA4) constitute sufficient assumptions to arrive at the single-hit dose-response model in Equation (18). It is not clear whether they are necessary assumptions, since specific choices of some of the distributions

[3]This is not a very strong additional assumption, as we have already assumed X is independent of **S** and **T**. If g is required to somehow depend on X, a more plausible approach would probably be to introduce statistical dependence by relaxing IA3 and/or IA4.

[4]Note that this does not mean that the distribution of R depends on X; they are independent variables.

involved could possibly produce a similar form. The only possible statistical dependence that is left after employing (IA1)–(IA4) is the dependence between **S** and **T**. This is convenient since it could be difficult to make a sharp distinction between host susceptibility and pathogen infectivity in practice. In fact, this dependence makes it impossible to distinguish pathogen infectivity from host susceptibility only based on fitting a conventional single-hit model to data. It could, however, become possible with further specification of the function g and variables **S** and **T** (an example is given in Section 3.2.3), possibly together with some kind of additional recorded data (*covariables*) on pathogens and/or hosts. If the response variable is treated not as binary, but instead as a quantitative variable[14] (discrete or continuous), so that we may speak of "degrees of infection," pathogen and host effects could possibly be more easily identified based on model fitting alone, but such models are beyond the scope of this article.

Equation (12) gives a precise expression for the single-hit probability R as a conditional expectation value, where the expectation is with respect to pathogen infectivity **T**. Thus, we may say, as has been shown previously,[4,5,10] that variation in pathogen infectivity is "integrated out" and the random variable R derives its variation (randomness) from the variation in the host susceptibility **S**. In other words, if we fix $\mathbf{S} = \mathbf{s}$, we also fix $R = r$. The basic explanation for this is essentially the same as that following Equation (3): in a sequence of independent Bernoulli trials where the success probability (i.e., infectivity) is randomly and individually selected for each trial, only the *expected* success probability matters. Consequently, if a data set can be adequately described by a dose-response model with a constant R (such as the exponential model; see Section 3.2), this would indicate, in a single-hit framework, that the host population is relatively homogeneous with respect to its susceptibility to infection.

We note that our variables **S** and **T** are very closely related to the concept of *covariables* that are employed in some dose-response papers, where the single-hit probability is expressed as a certain function of such covariables. Covariables represent properties that can be measured on hosts (more often) or pathogens and are treated as independent variables in the dose-response model in addition to the mean dose (in case of Poisson distributed doses). Hosts' score on a test for anti-*Cryptosporidium* immunoglobulin G has, for example, been used as a covariable.[13] Translating the term to the terminology of this article, a host covariable would simply be equivalent to a parameter of the distribution of **S**, in much the same way that the mean dose is a parameter of the distribution of X. These parameters become independent variables in the dose-response model.

It is also noted that, frequently,[15,16] the mean dose input to a dose-response model is obtained using only those pathogens that are viable (often termed "infectious") by some culturing method (but not always, as when pathogens are enumerated using quantitative polymerase chain reaction (PCR)). This does not, however, eliminate the need to consider infectivity in the development of dose-response models, since the relationship between *in vitro* viability, as measured by some laboratory method, and *in vivo* infectivity is usually not clear. The important thing is that the enumeration method used for the mean dose when generating data for dose-response parameter fitting is consistent with the method that is used for the mean dose in subsequent risk assessments that rely on the fitted model.

Finally, it is made explicit that the distributions of **S**, **T**, and X may in principle incorporate temporal variation, with the understanding that the experiment in Section 2 then effectively involves sampling a random point in time as well. However, temporal variation is usually considered external to the dose-response model itself (for X, this is done during the *exposure assessment*). What cannot be accounted for in single-hit models is the dynamics of the host-pathogen interaction, and this renders the connection between any single dose and the response somewhat obscure. This is less of a problem when there is an isolated (in time), instantaneous exposure since an observed infection during the period that follows has a clear connection to the exposure. For repeated exposures within a time interval that is on the order of the incubation time, the problem is more serious: What is the effect of ingesting an additional dose while the host is still in the process of responding to the first dose? This problem has been studied[17] and the dynamic effects were found to be significant under plausible assumptions (there is very little experimental data available to test such dynamic models). As is shown in detail in Section 3.3, the single-hit framework dictates that for repeated exposures, it is only the accumulated dose that is important.

3.1.2. A Useful Simplification

Consider the general expression for $\mathrm{E}(P_{\mathrm{I}})$ in Equation (15), and assume that we may interchange the order of summation and integration, i.e., the order (with respect to the variables R and X) in which we take expectations is immaterial:

$$\mathrm{E}(P_{\mathrm{I}}) = 1 - \int_0^1 \sum_{x=0}^{\infty} (1-r)^x p_X(x) f_R(r) \, \mathrm{d}r. \quad (19)$$

If the series (the integrand) converges uniformly on the interval $r \in [0,1]$ and $(1-r)^x p_X(x) f_R(r)$ is continuous in r for every x, the interchange is justified. These properties can usually be established for distributions f_R of practical interest by employing Weierstrass's M-test, possibly with some tweaking to handle the endpoints of the interval. For example, the beta distribution (Table III, Section 3.2) with parameter values $\alpha, \beta < 1$ requires this tweaking to establish the validity of the interchange in Equation (19).

It is possible to make a quite useful simplification in Equation (19): the sum in the integrand is, by definition, the pgf G_X of the dose distribution X, evaluated at 1-r. Formulations using pgfs have appeared in the hit-theory literature previously, for example, in Turner[18] in the context of radiation induced damage. We therefore have:

$$\mathrm{E}(P_{\mathrm{I}}) = 1 - \int_0^1 G_X(1-r) f_R(r) \, \mathrm{d}r. \quad (20)$$

As explained in the Appendix, the pgf is an alternative representation of the distribution of a count random variable and possesses some nice properties. Simple expressions exist for the pgf of most dose distributions of theoretical and practical interest (Section 3.2). The pgf formulation can also facilitate the analysis of general properties of single-hit models. For example, we may formulate the following proposition about single-hit models in a compact way. It states that the risk computed with a constant single-hit probability r_c is always greater than the risk computed with a variable single-hit probability R with mean $\mathrm{E}(R) = r_c$.

Proposition 1. *For any dose distribution, host heterogeneity reduces the risk in a single-hit model in the following sense:*

$$\mathrm{E}(P_{\mathrm{I}}) \leq 1 - G_X[1 - \mathrm{E}(R)]. \quad (21)$$

Proof. We need Jensen's inequality, which says that for a random variable R and convex function ϕ,

$$\phi[\mathrm{E}(R)] \leq \mathrm{E}[\phi(R)]. \quad (22)$$

The inequality is reversed for concave functions, and becomes a strict inequality if ϕ is strictly convex/concave and R does not have a point mass distribution (i.e., is not a constant). Differentiating $G_X(1-r)$ term by term twice with respect to r shows that $G''_X(1-r) \geq 0$ for $r \in [0,1]$ and hence $G_X(1-r)$ is convex in r. This gives Equation (21). It becomes a strict inequality if $\Pr(X=2) > 0$ and R is not a constant. □

3.2. Parameterized Dose-response Models

Table III gives an overview of some (classes of) dose-response models that may result when we partially or fully specify the probability distributions of X and R. They are discussed below.

3.2.1. f_R with Point Masses and Host Immunity

Since the variation of R stems from variation in host susceptibility (for a given population of pathogens), R may be considered a property of a host. Hence, if a host is completely immune, we must have $R = 0$ for this particular host. However, when R is constructed as a continuous random variable on $[0,1]$, then $\Pr(R=0) = 0$ and the distribution f_R will not strictly be able to represent complete immunity in part of the host population. It is worth noting that the commonly used beta distribution (Table III) with support on the unit interval does have some ability to approximate variables that have a point mass of probability at 0. This happens when the parameter α is close to zero, and this is indeed what is often observed when the beta distribution is used to fit dose-response models to data. However, in some cases it may be that better fits can be obtained by defining R as a mixed random variable, in which case the distribution of R has both a continuous and a discrete part (some point masses of probability).

Formally, we may define a probability "density" f_R for a mixed random variable R using Dirac's delta functions.[5] In general, if the distribution of R has k point masses, we have:

$$f_R(r) = \sum_{i=1}^{k} \phi_i \delta(r - r_i) + \phi_c f_{R,c}(r), \quad (23)$$

[5]Strictly, the notion of generalized functions is needed for defining Dirac's delta function, and more general notions than the Riemann integral for its integration. However, it can be formally manipulated as a function for our purposes.

Table III. Inventory of Single-Hit Models, Expressed Using Probability Generating and Moment Generating Functions

$$\mathrm{E}(P_1) = 1 - \int_0^1 G_X(1-r)\, f_R(r)\, \mathrm{d}r$$

$G_X(1-r)$	$f_R(r)$	$\mathrm{E}(P_1)$	Comment
	$\sum_{i=1}^{k} \phi_i \delta(r - r_i) + \phi_c f_{R,c}(r)$	$1 - \sum_{i=1}^{k} \phi_i G_X(1-r_i) - \phi_c \int_0^1 G_X(1-r) f_{R,c}(r)\, \mathrm{d}r$	$f_R(r)$ is general mixed continuous-discrete
Any	$R \sim$ Degenerate(r_1): $\delta(r - r_1)$	$1 - G_X(1-r_1)$	$f_R(r)$ has a single point mass
	$\phi_{\mathrm{im}}\delta(r) + (1-\phi_{\mathrm{im}}) f_{R,\mathrm{sus}}(r)$	$(1-\phi_{\mathrm{im}})\left(1 - \int_0^1 G_X(1-r) f_{R,\mathrm{sus}}(r)\, \mathrm{d}r\right)$	For a population with proportion of immune hosts ϕ_{im}
$X \sim$ Degenerate(N): $(1-r)^N$	Any	$1 - \int_0^1 (1-r)^N f_R(r)\, \mathrm{d}r$	Conditional dose-response model for N pathogens
	Any	$1 - M_R(-\lambda)$	Moment generating function of R, evaluated at $-\lambda$
	$R \sim$ Degenerate(r_1): $\delta(r - r_1)$	$1 - e^{-\lambda r_1}$	Exponential model
	$R \sim$ Beta(α, β): $\frac{r^{\alpha-1}(1-r)^{\beta-1}}{B(\alpha,\beta)}$	$1 - {}_1F_1(\alpha, \alpha+\beta, -\lambda)$	Exact Beta-Poisson model (eBP)
$X \sim$ Poisson(λ): $e^{-\lambda r}$	$R \sim$ Gamma(α, β): $\frac{\beta^\alpha}{\Gamma(\alpha)} r^{\alpha-1} e^{-\beta r}$	$\approx 1 - \left(1 + \frac{\lambda}{\beta}\right)^{-\alpha}$	Approximate Beta-Poisson model (aBP); $\beta \gg 1, \beta \gg \alpha$
	$R \sim$ Uniform(a, b): $\frac{1}{b-a}$	$1 - \frac{e^{-\lambda b} - e^{-\lambda a}}{-\lambda(b-a)}$	$0 \le a < b \le 1$
	$R \sim$ Triangular(a, c, b)	$1 - 2\frac{(b-c)e^{-a\lambda} - (b-a)e^{-c\lambda} + (c-a)e^{-b\lambda}}{(b-a)(c-a)(b-c)\lambda^2}$	$0 \le a < b \le 1, \quad a \le c \le b$
	$\frac{f_S[r/\mathrm{E}(T)]}{\mathrm{E}(T)}$	$1 - M_S[-\mathrm{E}(T)\lambda]$	f_R has a scale parameter $\mathrm{E}(T)$ (see Section 3.2.3)
$X \sim$ Neg.bin.(λ, b): $(1+br)^{-\lambda/b}$	$R \sim$ Degenerate(r_1): $\delta(r - r_1)$	$1 - (1+br_1)^{-\lambda/b}$	Interpretation of the clustering parameter b in Section 3.2.2.
	$R \sim$ Beta(α, β): $\frac{r^{\alpha-1}(1-r)^{\beta-1}}{B(\alpha,\beta)}$	$1 - {}_2F_1(\frac{\lambda}{b}, \alpha; \alpha+\beta, -b)$	Gauss hypergeometric function;[19] interpretation of b in Section 3.2.2
$X \sim$ 0-infl.Poiss(λ, π): $\pi + (1-\pi)e^{-\lambda r}$	Any	$(1-\pi)[1 - M_R(-\lambda)]$	Parametrically identical to a model with some immune hosts

where $\phi_i = \Pr(R = r_i)$ and δ is Dirac's delta function. The function $f_{R,c}$ represents the continuous part of f_R and may be any properly normalized pdf on [0, 1]. This f_R has $2k + 1$ parameters in addition to those associated with $f_{R,c}$. We have the normalization requirement $\sum_{i=1}^{k} \phi_i + \phi_c = 1$. Using Equation (23) in Equation (20), we find:

$$\mathrm{E}(P_\mathrm{I}) = 1 - \sum_{i=1}^{k} \phi_i G_X(1 - r_i) - \phi_c \int_0^1 G_X(1 - r) f_{R,c}(r)\,\mathrm{d}r. \quad (24)$$

If there is a point mass at 0 (some immune hosts), we may write:

$$f_R(r) = \phi_\mathrm{im}\delta(r) + (1 - \phi_\mathrm{im}) f_{R,\mathrm{sus}}(r), \quad (25)$$

where $\phi_\mathrm{im} = \Pr(R = 0)$ and corresponds to the proportion of hosts that are immune. $f_{R,\mathrm{sus}}$ is the pdf for R in the susceptible part of the population. Using this in Equation (20), it is found that:

$$\mathrm{E}(P_\mathrm{I}) = (1 - \phi_\mathrm{im}) \left(1 - \int_0^1 G_X(1 - r) f_{R,\mathrm{sus}}(r)\,\mathrm{d}r\right), \quad (26)$$

where we used $G_X(1) = 1$. We see that the formally correct representation of host immunity in a single-hit model is a simple scaling, which agrees with intuition and is indeed how it typically has been represented in practice.[20,21] One may speculate that by introducing a point mass at 0, the density function $f_{R,\mathrm{sus}}$ may take a simpler form since it no longer has to incorporate an approximate representation of complete immunity. We note that, recently, models incorporating complete host immunity have been found relevant for Norovirus dose-response assessment.[21,22]

For modeling acquired immunity, assume that a population of hosts is exposed to a pathogen, or may be vaccinated, so that the proportion with complete immunity changes to ϕ'_im. If the hosts that develop immunity after this exposure can be assumed to be randomly drawn from the population of non-immune hosts and the remaining hosts have an unchanged susceptibility to infection, only ϕ_im needs to be changed to ϕ'_im in Equation (26); the parameters of $f_{R,\mathrm{sus}}$ remain unchanged. An analogous situation occurs when extending a dose-response model that was developed for nonimmune hosts[19] to a population including some immune hosts; one only needs to know the proportion of immune hosts in the population to perform the extension.

3.2.2. Specifying G_X and f_R

The baseline assumption in QMRA is that X is Poisson distributed with parameter λ (equal to both the mean and variance of the dose), which gives a useful expression for the single-hit model for any f_R (see, e.g., Moran[23] for an early reference in a similar setting):

$$\mathrm{E}(P_\mathrm{I}) = 1 - \int_0^1 e^{-\lambda r} f_R(r)\,\mathrm{d}r = 1 - M_R(-\lambda). \quad (27)$$

Here, $M_R(-\lambda)$ is the moment generating function (mgf; see Appendix) of R, evaluated at $-\lambda$. The mgf expression facilitates the use of alternative distributions for R when X is Poisson distributed (example with the uniform and triangular distribution in Table III) since closed-form expressions for the mgf are readily available for most distributions of interest. Conversely, the only functions that strictly can serve as single-hit models when X is Poisson distributed are of the form of Equation (27), where M_R is the mgf of a variable supported on [0, 1]. The general properties of the moment sequence of such a random variable are studied in the *Hausdorff moment problem*.[24] The theory developed for this problem could therefore be useful if one has an empirical dose-response model and wishes to check whether it conforms to single-hit assumptions. For a useful low-dose approximation, one can use the series representation of the mgf (Equation (A.6)), to arrive at:

$$\mathrm{E}(P_\mathrm{I}) = \lambda\mathrm{E}(R) - \frac{\lambda^2\mathrm{E}(R^2)}{2!} + \frac{\lambda^3\mathrm{E}(R^3)}{3!} + \cdots \approx \lambda\mathrm{E}(R), \quad (28)$$

where the latter approximation applies at low doses for *any* f_R.

The most commonly used single-hit models are the exponential model, the exact beta-Poisson (eBP) model, and the approximate beta-Poisson (aBP) model. The differences between the two formulations of the beta-Poisson model have been studied,[3,5] and the criteria $\beta \gg 1$ and $\beta \gg \alpha$ were proposed for ensuring their similarity. A contour plot of the ratio of the aBP to the eBP is given in Fig. 1 and provides a convenient graphical comparison of the two models. It is clear from the figure that the proposed criteria mentioned above are sufficient for a good approximation. It is also clear that the closeness of the approximation is dose dependent. At low doses, the approximation is particularly poor (overestimation) for small β and large α while at higher

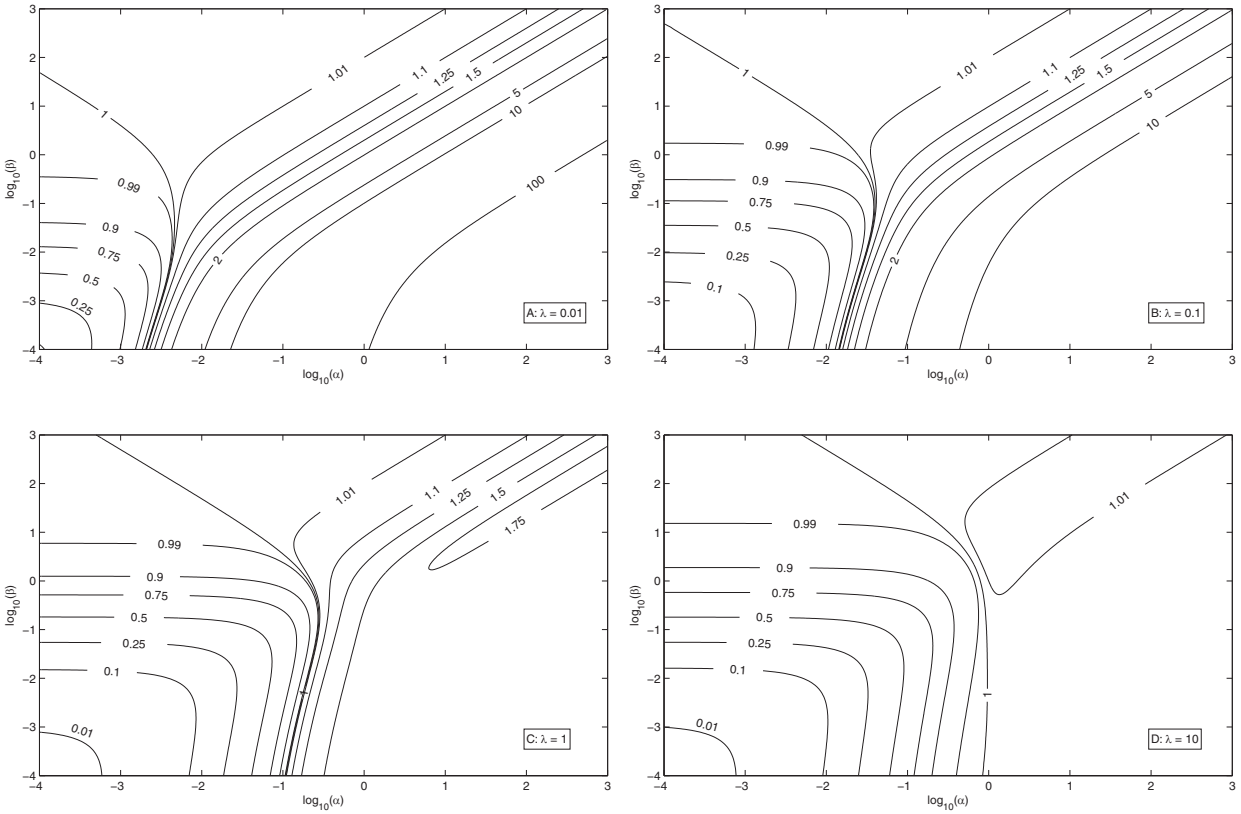

Fig. 1. Comparison of the exact and approximate beta-Poisson models for a range of parameter values and mean doses. Each contour represents a constant ratio of the approximate to the exact model. The hypergeometric function was evaluated in R[25–27] and the contours were generated with MATLAB.[28,29]

doses, the approximation is poor (underestimation) for small β and small α.

Many authors[3–5,30] have noted that the aBP may be derived by letting $f_R(r)$ in Equation (27) be the Gamma distribution and integrating over its support on $[0, \infty)$, although probabilities cannot exceed 1. One might ask if there exists some other (possibly obscure) f_R with support on $[0, 1]$ that gives the aBP when used in Equation (27). By appealing to the uniqueness of the mgf, the following proposition establishes formally that this is not the case. Hence, the aBP is not strictly a single-hit model, as has been asserted previously.[3]

PROPOSITION 2. *The aBP model is inadmissible as a single-hit model when the dose X is Poisson distributed.*

Proof. The term that is subtracted in the aBP is the mgf of a Gamma distribution, which is inadmissible as f_R in single-hit theory. By the uniqueness property of mgfs (see the Appendix), no other mgf exists that can turn Equation (27) into the aBP. □

Finally, to accommodate a larger variance (because of pathogen clustering, for example) than can be afforded by the one-parameter Poisson distribution, the two-parameter negative binomial distribution has sometimes been invoked.[2,19,31] If pathogen cluster sizes are logarithmic series distributed (with parameter a) and the number of clusters in a sample is Poisson distributed, the number of pathogens in a sample is negative binomial distributed.[11,19] For dose-response modeling, the negative binomial should be parameterized in terms of its mean, λ, and the cluster parameter a, or conveniently, $b = a/(1 - a)$ (Table III). Another way of parameterizing it is to set $k = \lambda/b$ and eliminate b. With a constant single-hit probability, we then get the same parametric form as the aBP model (Table III: $k = \alpha; k/r_1 = \beta$). However, choosing the independent variable λ freely while holding the other parameter $k = \alpha$ constant implies a systematic

change in b (the clustering state) with changes in the mean dose, which seems implausible in a dose-response model. Thus, parameterization in terms of λ and a or b seems preferable.

3.2.3. Specifying $g(\mathbf{S}, \mathbf{T})$

In order to illustrate how the function g from Section 3.1.1 may be constructed to possibly make it useful, let us choose the simplest possible functional form we may think of, namely, $g(S, T) = ST$ with support on $[0, 1] \times [0, 1]$. This means that S is to be interpreted as *the* susceptibility of a random host and T as *the* infectivity of a random pathogen. We may also say that S equals the single-hit probability for a maximally infective pathogen $T = 1$ and T equals the single-hit probability for a maximally susceptible host $S = 1$. Then, we find from Equation (12):

$$R = \mathrm{E}_{T|S}(ST) = S\int_0^1 t f_{T|S}(t|S)\,\mathrm{d}t. \qquad (29)$$

When it is further assumed that S and T are independent properties, we get:

$$R = S\int_0^1 t f_T(t)\,\mathrm{d}t = S\mathrm{E}(T), \qquad (30)$$

which gives, according to Equation (17):

$$f_R(r) = \frac{f_S[r/\mathrm{E}(T)]}{\mathrm{E}(T)}. \qquad (31)$$

Thus, in this very simple example the expected infectivity of the pathogens, $\mathrm{E}(T)$, acts (by definition) as a scale parameter in the distribution of single-hit infection probabilities. By a simple property of mgfs, we have:

$$M_R(-\lambda) = M_{S\mathrm{E}(T)}(-\lambda) = M_S[-\mathrm{E}(T)\lambda]. \qquad (32)$$

This means that for any single-hit model where doses are Poisson distributed (Equation (27)), $\mathrm{E}(T)$ translates directly into a scale factor on the dose. Parenthetically, it is noted that any function $g(S, \mathbf{T}) = Sg_{\mathbf{T}}(\mathbf{T})$ will give the same result with $\mathrm{E}[g_{\mathbf{T}}(\mathbf{T})]$ replacing $\mathrm{E}(T)$.

If the parameter $\mathrm{E}(T)$ can be reliably estimated, it appears that one may distinguish between pathogen infectivity and host susceptibility based on parameter estimation alone. We stress, however, that this result requires the specific functional form $g(ST) = ST$ and an independence assumption on S and T, in addition to ordinary single-hit assumptions. Fazekas de St Groth and Moran[10] dismissed this possibility in the special case of egg-influenza virus systems since log(dose)-response curves had been shown to change shape (as opposed to shifting along the dose axis) upon serial passage of the virus in similar host eggs, contradicting the scale-parameter expression in Ref. 32. The beta distribution in its most common form does not have a scale parameter, but it *can* be generalized and scaled on the interval $[0, \mathrm{E}(T)]$ (the ordinary beta is recovered by setting $\mathrm{E}(T) = 1$). For the exponential model and the aBP model, we can only ever estimate the product $r\mathrm{E}(T)$ and the quotient $\mathrm{E}(T)/\beta$, respectively, but for the eBP model it appears that $\mathrm{E}(T)$ may be estimated, in principle, if the data allow.

3.3. Repeated Exposure and Averaging Doses

3.3.1. Risk from Repeated Exposures

QMRA applications often require estimates of the expected probability of infection resulting from repeated exposures, for example, to obtain annual risk estimates. Most often,[32] the overall risk $\mathrm{E}(P_{\mathrm{I}}{}^{\mathrm{nh}})$ from n exposures, in which the doses are not necessarily identically distributed, is calculated as:

$$\begin{aligned}\mathrm{E}\left(P_{\mathrm{I}}{}^{\mathrm{nh}}\right) &= 1 - \prod_{i=1}^{n}[1 - \mathrm{E}(P_I)_i] \\ &= 1 - \prod_{i=1}^{n}\int_0^1 G_{X_i}(1-r)\,f_R(r)\,\mathrm{d}r, \qquad (33)\end{aligned}$$

where $\mathrm{E}(P_I)_i$ and G_{X_i} are the expected probability of infection and the pgf, respectively, associated with dose X_i. The assumptions stated along with Equation (33) are usually those of no acquired host immunity and independence between doses X_i. However, recalling that our probabilistic experiment in Section 2 started with selecting a random host, the consistent interpretation of $\mathrm{E}(P_{\mathrm{I}}{}^{\mathrm{nh}})$ is that it represents the expected probability that at least one host is infected when we randomly select *n hosts* (hence superscript nh) and expose each of them to *one* of the doses X_i (randomly allocated among the n hosts).

What we are instead actually interested in is the expected probability that *a single* randomly chosen host becomes infected if he is exposed to all the doses X_i. In the single-hit framework, R is fixed once we fix the host and is therefore the same for each exposure when there is no acquired immunity. With independence between doses X_i, the probability of infection from repeated exposures in a *given host* becomes:

$$P_{\mathrm{I}}^{\mathrm{ne}} = 1 - \prod_{i=1}^{n}(1-R)^{X_i} = 1 - (1-R)^{\sum_{i=1}^{n} X_i} = 1 - (1-R)^{X_{\mathrm{ne}}}, \quad (34)$$

where X_{ne} is the accumulated dose and the super-/subscript ne stands for *n exposures*. Taking the expectation value of Equation (34), we find:

$$\mathrm{E}\left(P_{\mathrm{I}}^{\mathrm{ne}}\right) = 1 - \int_0^1 G_{X_{\mathrm{ne}}}(1-r)\, f_R(r)\, \mathrm{d}r = 1 - \int_0^1 \prod_{i=1}^{n} G_{X_i}(1-r)\, f_R(r)\, \mathrm{d}r, \quad (35)$$

since the pgf of a sum of independent variables is the product of the corresponding pgfs (Equation (A.4)). Equation (35) gives the consistent way of calculating risk from repeated exposures within single-hit theory; simply use the distribution of the accumulated dose in place of the single dose. Whether this is a plausible description of the real world is, of course, another question.[17] Note that, when f_R has a single point mass (i.e., no variation in host susceptibility as, e.g., in the exponential model), there is no difference between Equations (33) and (35).

The following proposition shows that the conventional way of calculating risk from repeated exposures overestimates (i.e., is conservative) the model-consistent risk. This is useful since the conventional expression is arguably simpler to work with.

Proposition 3. *Equation* (35) *is bounded from above by Equation* (33) *when the individual doses are iid.*

Proof. The individual doses are iid with common pgf $G_X(z)$. We may compare the two expressions in Equations (33) and (35) using Jensen's inequality (see Proposition 1). Since the function $(\cdot)^n$ is convex, we get:

$$\left(\int_0^1 G_X(1-r)\, f_R(r)\, \mathrm{d}r\right)^n \le \int_0^1 \left[G_X(1-r)\right]^n f_R(r)\, \mathrm{d}r, \quad (36)$$

which implies that:

$$\mathrm{E}\left(P_{\mathrm{I}}^{\mathrm{nh}}\right) \ge \mathrm{E}\left(P_{\mathrm{I}}^{\mathrm{ne}}\right). \quad (37)$$

We have only shown this result for iid doses, but it is conjectured that it generalizes to the case of non-identically distributed doses.

An example of the relative difference between the two expressions for annual risk, using the eBP model for single exposure risk, is given in Fig. 2 in the form of a contour plot. It is apparent that the difference is small at low doses, which is usually the case in drinking water QMRA. However, for small α-values and intermediate β-values, the difference becomes significant as the dose increases.

We briefly give the most important special cases of Equation (35). When every dose is Poisson distributed, we have $G_{X_{\mathrm{ne}}}(1-r) = \prod_{i=1}^{n} G_{X_i}(1-r) = e^{-r\sum_{i=1}^{n}\lambda_i}$, which shows that the accumulated dose X_{ne} is also Poisson distributed with parameter $\sum_{i=1}^{n}\lambda_i$. Hence, if a single exposure is described by the eBP model, the expression for the risk from repeated exposures becomes:

$$\mathrm{E}\left(P_{\mathrm{I}}^{\mathrm{ne}}\right) = 1 - {}_1F_1\left(\alpha, \alpha+\beta, -\sum_{i=1}^{n}\lambda_i\right) = 1 - {}_1F_1(\alpha, \alpha+\beta, -n\lambda), \quad (38)$$

where the latter equality applies when all the doses X_i have the same Poisson parameter λ. For the aBP model, the correct expression for repeated exposures is:

$$\mathrm{E}\left(P_{\mathrm{I}}^{\mathrm{ne}}\right) = 1 - \left(1 + \frac{\sum_{i=1}^{n}\lambda_i}{\beta}\right)^{-\alpha}. \quad (39)$$

In contrast to the Poisson case, the product of negative binomial pgfs is not, in general, the pgf of a negative binomial distribution and the single-exposure expression does not easily generalize to the case of repeated exposures. However, for the special case when $X_i, \ldots, X_n$ are negative binomial variables with identical cluster parameter b, we get:

$$\mathrm{E}\left(P_{\mathrm{I}}^{\mathrm{ne}}\right) = 1 - \int_0^1 (1+br)^{-1/b\sum_{i=1}^{n}\lambda_i} \frac{r^{\alpha-1}(1-r)^{\beta-1}}{B(\alpha,\beta)}\, \mathrm{d}r = 1 - {}_2F_1\left(1/b\sum_{i=1}^{n}\lambda_i, \alpha; \alpha+\beta; -b\right). \quad (40)$$

3.3.2. Average Dose to Produce Consistent Total Risk

The average dose distribution $p_{\overline{X}}$ is the dose distribution that, when used to replace the actual dose distributions in repeated exposures, gives the same

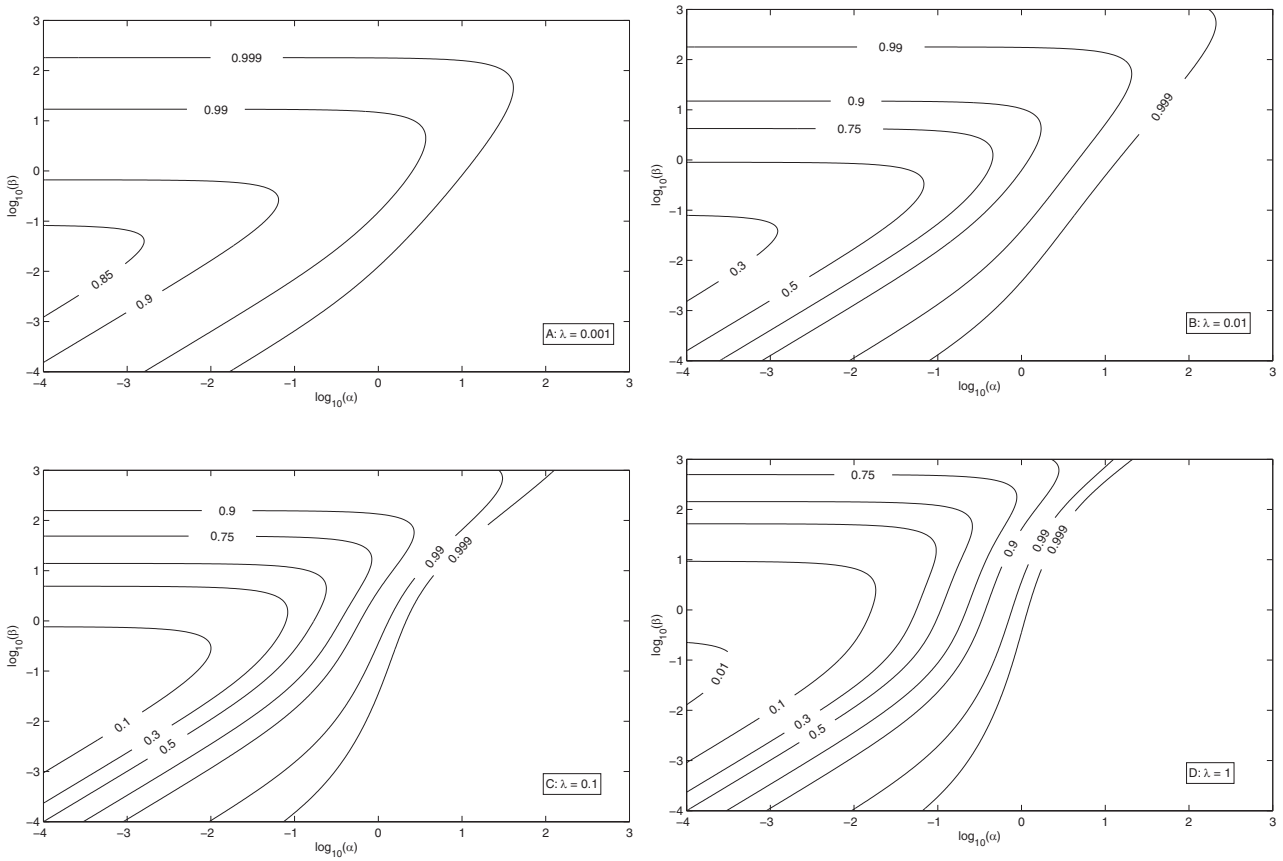

Fig. 2. Comparison of the single-hit consistent and the conventional expressions for the annual (365 exposures) risk, using a range of parameter values and mean doses (λ is the *per* exposure mean dose). Each contour represents a constant ratio of Equations (35) to (33), using the exact beta-Poisson model. The hypergeometric function was evaluated in R[25–27] and the contours were generated with MATLAB.[28,29]

risk estimate as the actual dose distributions. In terms of pgfs, it is given by the relation:

$$[G_{\overline{X}}(1-r)]^n = G_{X_{\mathrm{nc}}}(1-r) = \prod_{i=1}^{n} G_{X_i}(1-r). \quad (41)$$

In general, $G_{\overline{X}}(1-r)$ will not have a simple expression, but when the doses X_i are Poisson distributed, it becomes:

$$G_{\overline{X}}(1-r) = \left(\prod_{i=1}^{n} e^{-\lambda_i r}\right)^{\frac{1}{n}} = e^{-r\frac{1}{n}\sum_{i=1}^{n}\lambda_i}, \quad (42)$$

which is the pgf of a Poisson variable with mean $\frac{1}{n}\sum_{i=1}^{n}\lambda_i$. The implication is that, for any single-hit dose-response model that is based on a Poisson dose distribution, we may also speak of an average dose (not just an average dose distribution) and the average is an arithmetic average. This is consistent with what has been recommended previously,[32] although using Equation (33) as a starting point.

As a final point in this section, it is noted that Equations (33) and (35) lead to different conclusions regarding the mathematical connection between dose-response models and the *attack rate* in models for disease spread, as has been discussed earlier.[2] According to the above discussion, Equation (35) gives the correct expression for a consistent single-hit approach to this problem.

4. DISCUSSION AND CONCLUDING REMARKS

In this article, the single-hit dose-response model framework that has dominated QMRA-applications for drinking water has been reviewed by explicitly incorporating random variables to represent general pathogen and host properties as well as the dose. Sufficient statistical independence assumptions for arriving at single-hit models were identified. Essentially, the only possible mutual statistical

dependence left is that between pathogen properties and host properties. The so-called single-hit probability was precisely defined in Equation (12) and should be interpreted as a conditional expectation value, where the expectation is with respect to pathogen properties. Hence, variation in single-hit probabilities is due to variation in host properties, as has been demonstrated previously.[4,5] The single-hit framework can be formulated compactly in terms of pgf and mgf, as exemplified in Table III.

The fact that the randomness of R represents host variation relates directly to all of the conclusions highlighted in the abstract: Proposition 1 on constant versus variable host susceptibility, the formal representation of host immunity in f_R and $\mathrm{E}(P_1)$, mean pathogen infectivity as a scale parameter in f_R (Section 3.2.3), and the total and average risk in repeated exposures in Section 3.3. While the model-consistent estimate for the total risk from repeated exposures differs (gives lower risk; Proposition 3) from the conventional expression, the difference is quite small at low doses, which is more relevant for typical drinking water applications.

In Section 3.2.3, we assumed $g(S, T) = ST$ with S (host susceptibility) and T (pathogen infectivity) being two independent random variables on the unit interval. These may be strong assumptions, but they produce a very interesting result: $\mathrm{E}(T)$ becomes a scale parameter in the distribution of single-hit probabilities and translates into a scale factor on the mean dose in the dose-response model if doses are Poisson distributed. In a situation where there is between-host variation in susceptibility (i.e., f_S is not degenerate), this appears to open the possibility of distinguishing between pathogen effects (characterized by $\mathrm{E}(T)$) and host effects (characterized by f_S and its parameters) on the basis of model fitting alone, at least in principle. In practice, however, reliable parameter estimation would probably require a well-behaved data set and a highly appropriate choice of the distributional form for f_S (in addition to the appropriateness of the assumptions on $g(S, T)$). If f_S is degenerate, only the product $r = s\mathrm{E}(T)$ can be estimated.

Section 3.2.3 treats the problem of distinguishing between pathogen effects and host effects when there is a single pathogen population (and a single host population). This should be contrasted with attempts to account for varying infectivity between several pathogen populations or strains (and/or, equivalently, varying host susceptibility toward each of the pathogen populations) in one and the same dose-response model. For example, Teunis *et al.*[12] published such a study, where dose-response data from three different isolates of *Cryptosporidium* were used to construct a single model that allowed quantification of between-isolates variation (due to variation in infectivity/susceptibility) and within-isolates variation (due to variation in susceptibility, according to single-hit assumptions). Thus, experimental design and appropriate model building may allow distinction between certain aspects of host and pathogen properties based on model fitting alone, but in order to distinguish between pathogen infectivity and host susceptibility in a conventional single-hit dose-response experiment, further assumptions such as those employed in Section 3.2.3 seem to be needed.

Successful dose-response model choice, parameter estimation, and parameter interpretation, using single-hit models or other approaches, requires detailed knowledge of the conditions under which the dose-response data were obtained. Careful modeling and data collection may even allow applications of the model in other or more general settings than those used for data generation. This article did not aim to discuss the merits of single-hit models when fit to experimental data. However, it remains a scientific challenge to probe the appropriateness of single-hit models for low doses, since many experimental subjects are needed to obtain reliable estimates for the probability of infection. Very few such low-dose data exist and although single-hit models can be fit to many intermediate to high-dose data sets, applying single-hit theory in typical drinking water studies relies on an extrapolation in most cases. Furthermore, the differences between alternative models tend to become more important at low doses.[1,11,33] It should be mentioned that adequate fit of a model to a data set is in itself insufficient evidence to conclude that the assumptions behind the model are correct. In any case, a solid understanding of single-hit theory may provide hints to the underlying mechanistic causes in cases of poor model fits to data.

ACKNOWLEDGMENTS

Both authors would like to thank three anonymous reviewers for providing detailed and insightful reviews that greatly helped improve the article. The first author would like to thank Drs. Arve Heistad, Razak Seidu, and Susan Petterson for motivating his studies into QMRA.

APPENDIX: MATHEMATICAL DETAILS

For reasons of self-containment, the very basics of probability (pgf) and moment generating functions (mgf) are included here.[24,34] We also give a brief account of the moments and full distribution of P_{I}.

A.1. Probability Generating Functions

A random variable whose support is some subset of $\mathbb{N}_0$, the set of nonnegative integers, is called a *count* random variable. The pgf G_X of any count random variable X is defined by the power series:

$$G_X(z) = \mathrm{E}(z^X) = \sum_{x=0}^{\infty} p_X(x) z^x, \qquad \text{(A.1)}$$

whenever it exists, i.e., converges. Here, $p_X(x) = \Pr(X = x)$ denotes the probability mass function (pmf) of X. The series converges for at least all complex $|z| \leq 1$. By the uniqueness of the power series representation of a function, a pmf is uniquely identified by its pgf and most common distributions have nice closed-form expressions for $G_X(z)$. The coefficients of z^x are those of a Taylor series and thus the pmf can be recovered as:

$$p_X(x) = \frac{G_X^{(x)}(0)}{x!} = \frac{1}{x!} \left. \frac{d^x G_X}{dz^x} \right|_{z=0}. \qquad \text{(A.2)}$$

A new count random variable X may be constructed as a (possibly infinite) linear combination of *independent* count random variables X_i,

$$X = \sum_{i=1}^{n} a_i X_i = a_1 X_1 + a_2 X_2 + \cdots + a_n X_n, \qquad \text{(A.3)}$$

where $a_i \in \mathbb{N}_0$ and $\sum a_i \geq 1$. The problem of finding the distribution of X when the sequence $\{a_i\}$ and the distribution of every X_i are known, is simplified by the following result, which follows readily from the definition:

$$G_X(z) = G_{X_1}(z^{a_1}) G_{X_2}(z^{a_2}) \cdots G_{X_n}(z^{a_n}). \qquad \text{(A.4)}$$

In principle, the pmf of X can now be obtained by repeated differentiation of Equation (A.4) with respect to z and setting $z = 0$, as in Equation (A.2).

A.2. Moment Generating Functions

The mgf of a random variable R with support on some subset of the real line is defined by:

$$M_R(t) = \mathrm{E}(e^{tR}) = \int_{-\infty}^{\infty} e^{tR} f_R(r)\, \mathrm{d}r, \qquad \text{(A.5)}$$

whenever this expectation exists (it does for most distributions of practical interest). By performing a series expansion of the exponential function and taking term-by-term expectations, we find that:

$$M_R(t) = \sum_{n=0}^{\infty} \frac{t^n \mathrm{E}(R^n)}{n!}. \qquad \text{(A.6)}$$

The moments of R are recovered by:

$$\mathrm{E}(R^n) = M_R^{(n)}(0) = \left. \frac{d^n M_R}{dt^n} \right|_{t=0}. \qquad \text{(A.7)}$$

A uniqueness property holds for mgfs as well (although not as easily proved as for pgfs): any two variables whose mgfs exist and are equal have the same probability distribution.

A.3. The Moments and Full Distribution of P_{I}

$\mathrm{E}(P_{\mathrm{I}})$ is all we need for obtaining the distribution of W, the number of infected hosts, in Equation (4). It may still be of interest, though, to study the full distribution of P_{I} and its moments, in order to understand how risk is distributed in a population. The random variable P_{I} may be written:

$$P_{\mathrm{I}} = 1 - (1 - R)^X, \qquad \text{(A.8)}$$

where R has the interpretation given by Equation (12) and the joint distribution of the independent variables R and X is given by:

$$f_{R,X}(r, x) = f_R(r) p_X(x). \qquad \text{(A.9)}$$

To obtain the raw moments (moments about zero) of P_{I}, we first expand the kth power of P_{I} using the binomial formula:

$${P_{\mathrm{I}}}^k = \sum_{j=0}^{k} \binom{k}{j} (-1)^j [(1 - R)^j]^X. \qquad \text{(A.10)}$$

Then the raw moments are obtained by taking the expectation of Equation (A.10):

$$\begin{aligned} \mathrm{E}({P_{\mathrm{I}}}^k) &= \sum_{j=0}^{k} \binom{k}{j} (-1)^j \int_0^1 G_X[(1 - r)^j] f_R(r)\, \mathrm{d}r \\ &= \sum_{j=0}^{k} \binom{k}{j} (-1)^j I_j, \end{aligned} \qquad \text{(A.11)}$$

where

$$I_j = \int_0^1 G_X[(1-r)^j]\, f_R(r)\, \mathrm{d}r \;\; j = 1, 2, \ldots \quad \text{(A.12)}$$

with $I_0 = 1$ and $I_1 = 1 - \mathrm{E}(P_\mathrm{I})$. The central moments (moments about the mean) are then obtained as:

$$\mathrm{E}\{[P_\mathrm{I} - \mathrm{E}(P_\mathrm{I})]^n\} = \sum_{k=0}^{n} \binom{n}{k} [-\mathrm{E}(P_\mathrm{I})]^{n-k} \mathrm{E}\left({P_\mathrm{I}}^k\right)$$

$$= \sum_{k=0}^{n} \binom{n}{k} (I_1 - 1)^{n-k} \left(\sum_{j=0}^{k} \binom{k}{j} (-1)^j I_j \right). \quad \text{(A.13)}$$

After some algebra, the variance and third/fourth central moment can be expressed in terms of the integrals in Equation (A.12) as:

$$\mu_2 = \mathrm{var}(P_\mathrm{I}) = I_2 - I_1^2, \quad \text{(A.14)}$$

$$\mu_3 = -\left(I_3 - 3I_1 I_2 + 2I_1^3\right), \quad \text{(A.15)}$$

$$\mu_4 = I_4 - 4I_1 I_3 + 6I_1^2 I_2 - 3I_1^4. \quad \text{(A.16)}$$

The coefficient of variation is defined as $\mathrm{CV}(P_\mathrm{I}) = \sqrt{\mathrm{var}(P_\mathrm{I})}/\mathrm{E}(P_\mathrm{I})$.

Obtaining the full distribution of P_I analytically seems somewhat complicated since P_I in general will be mixed continuous/discrete (it always has a point mass corresponding to $X = 0$). However, a numerical approximation may be obtained by generating a set of random samples of R and X, and constructing a set of P_I-samples. Simulations (not shown) show that the shape of the distributions tend to resemble that of the underlying beta distribution, but with a shift that is controlled by the distribution of X.

REFERENCES

1. Haas CN. Estimation of risk due to low doses of microorganisms: A comparison of alternative methodologies. American Journal of Epidemiology, 1983; 118(4):573–582.
2. Haas CN, Rose JB, Gerba CP. Quantitative Microbial Risk Assessment. New York: John Wiley & Sons, 1999.
3. Teunis P, Havelaar A. The beta Poisson dose-response model is not a single-hit model. Risk Analysis, 2000; 20(4):513–520.
4. Haas CN. Conditional dose-response relationships for microorganisms: Development and application. Risk Analysis, 2002; 22(3):455–463.
5. Schmidt PJ, Pintar KDM, Fazil AM, Topp E. Harnessing the theoretical foundations of the exponential and beta-Poisson dose-response models to quantify parameter uncertainty using Markov chain Monte Carlo. Risk Analysis, 2013; 33(9):1677–1693.
6. Gale P. Developments in microbiological risk assessment for drinking water. Journal of Applied Microbiology, 2001; 91(2):191–205.
7. Smeets P, Rietveld L, van Dijk J, Medema G. Practical applications of quantitative microbial risk assessment (QMRA) for water safety plans. Water Science and Technology, 2010; 61(6):1561–1568.
8. Bichai F, Smeets PW. Using QMRA-based regulation as a water quality management tool in the water security challenge: Experience from the Netherlands and Australia. Water Research, 2013; 47(20):7315–7326.
9. World Health Organization. Guidelines for Drinking-Water Quality, 4th ed. Geneva, Switzerland: World Health Organization, 2011.
10. Fazekas de St Groth, S., and Moran, P.A.P. Appendix: A Mathematical Model of Virus-Cell Interaction. Journal of Hygiene, 1955; Doi: 10.1017/S0022172400000760. Available at: http://www.journals.cambridge.org/abstract_S0022172400000760. 53(3):291–296.
11. Nilsen V, Wyller J. QMRA for drinking water: 2. The effect of pathogen clustering in single-hit dose-response models. Risk Analysis, 2016; 36(1):163–181.
12. Teunis PF, Chappell CL, Okhuysen PC. *Cryptosporidium* dose response studies: Variation between isolates. Risk Analysis, 2002; 22(1):175–185.
13. Teunis PF, Chappell CL, Okhuysen PC. *Cryptosporidium* dose-response studies: Variation between hosts. Risk Analysis, 2002; 22(3):475–485.
14. Slob W. Dose-response modeling of continuous endpoints. Toxicological Sciences, 2002; 66(2):298–312.
15. Regli S, Rose JB, Haas CN, Gerba CP. Modeling the risk from Giardia and viruses in drinking water. Journal of the American Water Works Association, 1991; 83(11):76–84.
16. Teunis P, Medema G, Kruidenier L, Havelaar A. Assessment of the risk of infection by *Cryptosporidium* or *Giardia* in drinking water from a surface water source. Water Research, 1997; 31(6):1333–1346.
17. Pujol JM, Eisenberg JE, Haas CN, Koopman JS. The effect of ongoing exposure dynamics in dose response relationships. PLoS Computational Biology, 2009; 5(6):e1000399.
18. Turner Jr ME. Some classes of hit-theory models. Mathematical Biosciences, 1975; 23(3):219–235.
19. Teunis PF, Moe CL, Liu P, E Miller S, Lindesmith L, Baric RS, LePendu J, Calderon RL. Norwalk virus: How infectious is it? Journal of Medical Virology, 2008; 80(8):1468–1476.
20. Havelaar A, Swart A. Impact of acquired immunity and dose-dependent probability of illness on quantitative microbial risk assessment. Risk Analysis, 2014; 34(10):1807–1819.
21. Schmidt PJ. Norovirus dose-response: Are currently available data informative enough to determine how susceptible humans are to infection from a single virus? Risk Analysis, 2014; doi10.1111/risa.12323. Available at: http://dx.doi.org/10.1111/risa.12323.
22. Messner MJ, Berger P, Nappier SP. Fractional Poisson—A simple dose-response model for human norovirus. Risk Analysis, 2014; 34(10):1820–1829.
23. Moran P. The dilution assay of viruses. Journal of Hygiene, 1954; 52(2):189–193.
24. Feller W. An Introduction to Probability Theory and its Applications, Vol. 2, 2nd ed. New York: John Wiley & Sons, 1971.
25. R Core Team. R: A Language and Environment for Statistical Computing. Vienna, Austria: R Foundation for Statistical Computing, 2014. Available at: http://www.R-project.org/.
26. Hankin RKS. Special functions in R: Introducing the GSL package. R News, 2006; 6(4):24–26.
27. Bengtsson H. R.matlab: Read and write of MAT files together with R-to-MATLAB connectivity, 2014. Available at: http://CRAN.R-project.org/package=R.matlab, R Package Version 2.2.3.
28. MATLAB. Version 8.1.0.604 (R2013a). Natick, MA MathWorks Inc., 2013.

29. Woodford O. export_fig. MATLAB Central File Exchange, 2009. Available at: http://www.mathworks.com/matlabcentral/fileexchange/23629-export-fig, Accessed January 22, 2014.
30. Kodell RL, Kang SH, Chen JJ. Statistical models of health risk due to microbial contamination of foods. Environmental and Ecological Statistics, 2002; 9(3):259–271.
31. Gale P, Dijk Pv, Stanfield G. Drinking water treatment increases micro-organism clustering; The implications for microbiological risk assessment. Journal of Water Supply: Research and Technology-Aqua, 1997; 46(3):117–126.
32. Haas CN. How to average microbial densities to characterize risk. Water Research, 1996; 30(4):1036–1038.
33. Namata H, Aerts M, Faes C, Teunis P. Model averaging in microbial risk assessment using fractional polynomials. Risk Analysis, 2008; 28(4):891–905.
34. Feller W. An Introduction to Probability Theory and its Applications, Vol. 1, 3rd ed. New York: John Wiley & Sons, 1968.
35. Fazekas de St Groth, S. Production of Non-Infective Particles among Influenza Viruses: Do Changes in Virulence Accompany the von Magnus phenomenon?. Journal of Hygiene, 1955; Doi: 10.1017/S0022172400000760. Available at: http://www.journals.cambridge.org/abstract_S0022172400000760. 53(3):276–296.

Paper II

Nilsen, V. and J. Wyller (2016b). "QMRA for drinking water: 2. The effect of pathogen clustering in single-hit dose-response models." *Risk Analysis* **36** (1), pp. 163–181.

Risk Analysis, Vol. 36, No. 1, 2016 DOI: 10.1111/risa.12528

QMRA for Drinking Water: 2. The Effect of Pathogen Clustering in Single-Hit Dose-Response Models

Vegard Nilsen* and John Wyller

Spatial and/or temporal clustering of pathogens will invalidate the commonly used assumption of Poisson-distributed pathogen counts (doses) in quantitative microbial risk assessment. In this work, the theoretically predicted effect of *spatial* clustering in conventional "single-hit" dose-response models is investigated by employing the *stuttering Poisson* distribution, a very general family of count distributions that naturally models pathogen clustering and contains the Poisson and negative binomial distributions as special cases. The analysis is facilitated by formulating the dose-response models in terms of probability generating functions. It is shown formally that the theoretical single-hit risk obtained with a stuttering Poisson distribution is lower than that obtained with a Poisson distribution, assuming identical mean doses. A similar result holds for *mixed Poisson* distributions. Numerical examples indicate that the theoretical single-hit risk is fairly insensitive to moderate clustering, though the effect tends to be more pronounced for low mean doses. Furthermore, using Jensen's inequality, an upper bound on risk is derived that tends to better approximate the exact theoretical single-hit risk for highly overdispersed dose distributions. The bound holds with any dose distribution (characterized by its mean and *zero inflation index*) and any *conditional* dose-response model that is *concave* in the dose variable. Its application is exemplified with published data from Norovirus feeding trials, for which some of the administered doses were prepared from an inoculum of aggregated viruses. The potential implications of clustering for dose-response *assessment* as well as practical *risk characterization* are discussed.

KEY WORDS: Aggregation; clustering; dose-response; overdispersion; QMRA; stuttering Poisson

1. INTRODUCTION

In both natural and engineered systems, waterborne microbial pathogens such as viruses, bacteria, and protozoan parasites may, in principle, exist in aqueous suspensions as completely dispersed single pathogens or they may instead be spatially associated to some extent, in aggregates/clusters/clumps.[1–3] The extent and strength of the association will depend on the pathogen concentration, the processes that resulted in aggregation, the mechanisms by which pathogens are associated, and the physicochemical properties of the water. Some processes may introduce pathogens in the water in a clumped form, e.g., if a host sheds pathogens that are aggregated, if solids with accumulated pathogens detach from filter media, or if parts of biofilms separate. In the latter two cases, spatially associated pathogens are likely to be part of a large, complex particle that may not be easily dissociated. In other cases, it may be primarily electrostatic forces that hold pathogens together, and such interaction is likely to be more sensitive to changes in the environment of the pathogens.

Department of Mathematical Sciences and Technology, Norwegian University of Life Sciences, N-1432 Aas, Norway.
*Address correspondence to Vegard Nilsen, Department of Mathematical Sciences and Technology, Norwegian University of Life Sciences, P.O. Box 5003, N-1432 Aas, Norway; vegard.nilsen@nmbu.no; vgnils@gmail.com.

Within the field of quantitative microbial risk assessment (QMRA)[4] for drinking water, a baseline assumption is that pathogen numbers in water samples are Poisson distributed. In particular, this is a common assumption in the development and application of conventional semi-mechanistic *single-hit* dose-response models[4–9] that provide the probabilistic link between pathogen exposure levels (dose) and the resulting health consequences (response) for exposed individuals. The Poisson assumption is appropriate when pathogens are completely and randomly dispersed in the water source throughout the time period of interest.

However, in practice, it is most commonly observed that the variance in pathogen counts is larger than what can be accommodated by the one-parameter Poisson distribution.[10–13] This *overdispersion* will result if pathogens accumulate in space or time in excess of that which could occur by chance in a completely dispersed suspension. The phenomenon of *temporal* variation[13] in pathogen concentrations is well known, documented, and attempts are often made to account for it in applications. It can, e.g., be caused by relatively slow variation in raw water quality due to seasonal effects or could be the result of sudden changes such as treatment plant failures. *Spatial* accumulation of pathogens in the form of physical clusters, i.e., two or more pathogens sticking together or to the same suspended particle, is more difficult to document experimentally, and information on the pathogen clustering state is practically never available in applications.

Conventional water treatment (both drinking water and waste water) involving coagulation/flocculation processes is designed to promote particle aggregation in order to enhance downstream particle separation processes. This treatment is likely to affect pathogens (that are particles) to some extent as well, although difficult to verify and quantify experimentally. On the other hand, the generally low concentration of pathogens in drinking water implies that the average distance between pathogens is much larger than the pathogens themselves, reducing the chance of pathogens colliding and sticking together. Furthermore, colloid stability theory[1,14] predicts increasing dispersion of microorganisms at low ionic strength and pH-values away from their isoelectric points (typically less than neutral pH), which coincide with common conditions in drinking water.

Nevertheless, some empirical indications of clustering do exist. Gale and co-workers showed[10,11] that the variation between replicate counts of bacterial spores in water samples increased significantly after water treatment. Clustering would indeed produce such overdispersion, but independent confirmation of physical clustering is needed to fundamentally distinguish it from temporal variation in mean spore concentrations and/or variation in analytical recovery between samples. In another case of possible clustering,[15] polio virus plaques grown from sewage samples were shown to contain two different types of polio viruses, clashing with the standard assumption that each plaque arises from a single virus particle. Among several possible explanations, the authors found aggregation of viruses to be the more plausible. Clustering was also observed during electron microscopy in a protein-rich laboratory stock suspension of Norovirus that was used in human feeding trials for dose-response assessment.[16] The latter has motivated efforts to represent clustering in single-hit dose-response models.[16–18]

In general, at least four aspects of QMRA may be identified, in which the clustering state of pathogens may impact the analysis:

1. Clustering may obscure interpretation of microorganism counts from laboratory methods. First, it could possibly affect the recovery of concentration procedures. Second, some methods typically return results that relate to the total number of organisms, such as quantitative real-time polymerase chain reaction (qPCR) that measures the number of genome copies present. Other methods will tend to return results that relate more to the total number of clusters, such as plaque/colony counting methods where it is difficult to assess whether a macroscopic plaque/colony stems from a single organism or a cluster of organisms.[15] A dispersion step (e.g., using Tween[10]) may be added to the laboratory protocol of the latter methods to obtain the total numbers of organisms instead.
2. Clustering may play a role in the exposure assessment in a broad sense, since the transport properties of pathogens in nature and their removal and inactivation during water treatment and distribution may depend on the extent of clustering. For example, settling and filtration processes are size-sensitive, as well as disinfection processes such as chlorination (see, for example, Thurston-Enriquez *et al.*[19]) and ultraviolet radiation (where clustering of pathogens/particles may shield pathogens from radiation).

3. Clustering could affect pathogen infectivity upon entering a human host. That is, for a given number of pathogens ingested, is it relevant for the host-pathogen interaction whether they occur as single particles or are part of a cluster of a certain size? Any such dependence would induce a correlation between the dose and the infectivity of a single pathogen (since the dose and occurrence of certain cluster sizes would be correlated), which is inconsistent with traditional single-hit models (Section 2.1). If such effects exist and are important, dose-response models would require modification to account for them, which would complicate the modeling process. Designing an experiment that can detect and quantify such effects, if they are present, appears challenging.
4. Clustering affects the dose distribution. Even if the host is insensitive to the pathogen clustering state, clustering of pathogens will affect the probability distribution for the total number of pathogens included in a water sample (the *dose*), whether the "sample" is for human consumption or for laboratory analysis. The choice of a dose distribution (usually Poisson) is an integral part of the development of classical single-hit dose-response models, as well as in designing Monte Carlo simulations for practical risk characterization.

This article focuses on item 4 above; i.e., the effect of clustering on the dose distribution (total pathogen count) as it applies to single-hit dose-response models. Regarding item 3, it will be assumed that the host/pathogen interaction is insensitive to pathogen clustering state. This is potentially unrealistic, but has nevertheless been the assumption (tacitly or explicitly) in published work on Norovirus dose response[16–18] and it seems difficult to relax in a simple way. A primitive generalization of single-hit models to account for the effects mentioned in item 3 is provided in Section S.5 of the online appendix.

The introductory paragraphs above motivate the purpose of the present work, which is to

i. Investigate the theoretically predicted effect of pathogen clustering on single-hit dose-response models in QMRA; i.e., what is fundamentally built into the single-hit risk framework with respect to the effects of pathogen clustering (or more generally, overdispersion in the dose distribution)?
ii. Simulate the effects of moderate clustering on single-hit risk estimates, a situation that may be particularly relevant for background risk levels in drinking water. Are single-hit models robust with respect to unaccounted for clustering?
iii. Introduce a risk bound (the Jensen bound) that emerged during the investigation of bullet point i, which could be useful for many situations where one has an overdispersed dose distribution.

For some of the technical derivations, we will draw upon the dose-response model formulation in terms of probability generating functions (pgfs) presented in the companion paper.[9]

In discussing dose-response modeling, we should distinguish between *dose-response assessment* and dose-response models as employed in practical *risk characterization* studies. The purpose of dose-response assessment is to estimate dose-response parameters for a particular pathogen, which can subsequently be used in a dose-response model to estimate infection risk in a risk characterization study, possibly undertaken as a simulation study using Monte Carlo methods. The dose distributions need not be the same in the two cases, and if it is non-Poisson due to clustering, it will not be known in any detail. For dose-response assessment, it is very convenient[1] if the dose-response model can be expressed in closed form, which limits the choice of dose distribution to simple ones. For risk characterization, this is less important since a complicated dose distribution may easily be specified in a Monte Carlo study, in conjunction with a conditional[7] dose-response model (Section 2.1). The material presented in this article should be useful for both purposes.

2. MODEL DEVELOPMENT

The semi-mechanistic single-hit dose-response framework has been described by many authors.[4–9] We first recapitulate the essentials of this framework (Section 2.1) using the formulations of our companion paper,[9] before introducing some basic concepts of clustering in Section 2.2. Section 2.3 introduces the *stuttering Poisson* distribution, which forms the basis for the analysis presented in Section 3.1.

[1] Although not necessary if the required quantities can be computed numerically with sufficient precision.

2.1. Single-Hit Dose-Response Framework

In a single-hit model, it is assumed that a *single* pathogen may be capable of causing an infection, and that individual pathogens act *independently* of each other. Under more precise assumptions stated at the end of this section, a randomly selected host that ingests a random[2] number of pathogens X has a probability P_I of becoming infected, which equals the probability that at least one pathogen establishes infection:

$$P_I = 1 - (1 - R)^X. \tag{1}$$

Here, R is a random variable that equals the probability that a single pathogen establishes infection (the *single-hit probability*). We allow for the possibility that X (as in so-called conditional dose-response models) and/or R (as, e.g., in the exponential model) may degenerate to constants. It has been shown[7–9] that within single-hit theory, R derives its randomness from the variation in host susceptibility and that the variation in pathogen infectivity enters only indirectly through its modulating effect on the distribution of R.

The actual dose-response model is given by the marginal probability $\mathrm{E}(P_I)$ (the expected value of P_I) as a function of the dose distribution parameters. $\mathrm{E}(P_I)$ serves as a dose-dependent success probability in a binomial model for the number of infected hosts when one or more hosts are exposed. It can be written as:

$$\begin{aligned}\mathrm{E}(P_I) &= 1 - \int_0^1 \sum_{x=0}^{\infty} (1-r)^x \, p_X(x) \, f_R(r) \, \mathrm{d}r \\ &= 1 - \int_0^1 G_X(1-r) \, f_R(r) \, \mathrm{d}r,\end{aligned} \tag{2}$$

where $p_X(x)$ is the probability mass function (pmf) of X, $f_R(r)$ is the probability density function[3] (pdf) of R, and $G_X(1-r)$ is the pgf of X, evaluated at $1-r$. The pgf is an alternative representation of the distribution of a count random variable, and the basics of pgfs are reviewed in Section S.1 of the online appendix since they play a central role in our dose-response models.

[2]Throughout this article, strict adherence is made to the convention of denoting random variables with uppercase letters and particular instances of the same variables with the corresponding lowercase letters.

[3]R may also be represented as a mixed random variable[9] with both continuous and discrete parts (e.g., if some hosts are fully immune), in which case f_R is a mixed probability density/pmf.

The baseline assumption in QMRA is that X is Poisson distributed with pmf:

$$\Pr(X = x) = p_X(x) = \frac{\lambda^x e^{-\lambda}}{x!}, \tag{3}$$

which has a single parameter $\lambda > 0$ and $\mathrm{E}(X) = \mathrm{Var}(X) = \lambda$. The parameter λ can be interpreted as the product cv of the pathogen concentration c in the water source and the sample volume v. The pgf of a Poisson variable with mean λ is:

$$G_X(z) = e^{\lambda(z-1)}. \tag{4}$$

With this, Equation (2) reduces to:

$$\mathrm{E}(P_I) = 1 - \int_0^1 e^{-\lambda r} \, f_R(r) \, \mathrm{d}r. \tag{5}$$

Various parameterized dose-response models will result for different choices of f_R.[4,9]

Inherent in the simple formulation in Equation (2) are several statistical independence assumptions on random variables representing host susceptibility, pathogen infectivity, and the dose. For their precise formulation, the companion paper[9] should be consulted. They can be summarized briefly as follows:

1. The probability that any single pathogen establishes infection is independent of the failure of one or more other pathogens within the same dose to do so.
2. The infectivities of the individual pathogens in the water sample are mutually independent.
3. The dose and the infectivity of each individual pathogen in the water sample are mutually independent.
4. The dose and the susceptibility of the host are mutually independent.

2.2. Nomenclature and Basic Concepts

One of the axioms used in a rigorous development of the Poisson distribution says that, roughly, for a very small sample volume, the probability of observing more than one pathogen is zero.[20] The presence of pathogen clustering will obviously invalidate this assumption and the dose distribution will not be Poisson anymore. In practice, deviations from the Poisson distribution may be identified by a statistically significant difference between the sample mean and variance. A useful statistic in this respect is the dispersion index:

$$\delta = \frac{\mathrm{Var}(X)}{\mathrm{E}(X)}. \tag{6}$$

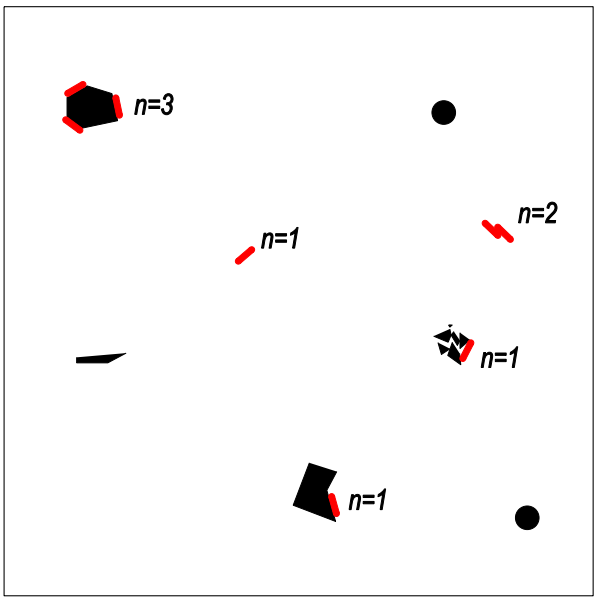

Fig. 1. Example of mild aggregation.

One may distinguish between the following situations:

- Underdispersion, i.e., $\delta < 1$. This can happen when there is a tendency toward special uniformity in the distribution of pathogens, and results in a pathogen count that is "less random" (its entropy is lower) than a Poisson variable.
- Poisson dispersion, i.e., $\delta = 1$.
- Overdispersion, i.e., $\delta > 1$. This is the type of deviation that is most commonly observed in practice,[10,11] and could be the effect of pathogen clustering.

Another useful measure of spread that will be employed below is the zero-inflation index, defined by:

$$\theta = 1 + \frac{\ln[p_X(0)]}{\mathrm{E}(X)}. \tag{7}$$

In general, $\theta < 1$. For a Poisson variable, $\theta = 0$, while $\theta > 0$ for a situation with clustering, as discussed in Section 2.3.

Assume now that a sample is taken from a water source in which some of the pathogens may be clustered. Fig. 1 shows a conceptual example of how pathogens may be distributed in a sample from such a water source with (moderate) clustering. Some pathogens exist as single particles, some are clustered together, and some are attached to other types of particles of various sizes. We will use the term *n-cluster* for any collection of particles that contains n ($n \geq 1$) pathogens, in which the association between the pathogens is sufficiently strong that the cluster behaves as a single unit during sampling. With this terminology, the simplest cluster is the one consisting of a single pathogen (a 1-cluster). Furthermore, clusters are characterized only by the number of pathogens they contain, and *not* by the number and size of other types of particles included in the cluster.

The number of n-clusters contained in the water sample is a random variable and will be denoted as X_n. The total number of pathogens contained in the sample, X, and the total number of *clusters*, X_{cl}, are functions of the X_ns and given, respectively, by:

$$X = \sum_{n=1}^{\infty} nX_n = X_1 + 2X_2 + 3X_3 + \cdots \tag{8}$$

$$X_{\mathrm{cl}} = \sum_{n=1}^{\infty} X_n = X_1 + X_2 + X_3 + \cdots \tag{9}$$

The sums are over all cluster sizes with the assumption that $\mathrm{E}(X) < \infty$ (and hence $\mathrm{E}(X_{\mathrm{cl}}) < \infty$).

Since X_n represents the count of a specific type of cluster, clustering itself is no longer a source of overdispersion in the distribution of X_n (e.g., if two n-clusters form a new cluster, they are instead counted as a $2n$-cluster). Hence, if clusters can be considered to move about essentially randomly and independently, it is natural to assume that the distribution of each X_n is Poisson with corresponding parameter $\lambda_n = c_n v$, where c_n represents the concentration (number per unit volume) of n-clusters in the water source. The general distribution of X under this assumption is considered in Section 2.3.

It is worth emphasizing again the similarities and differences between clustering as defined above and other sources of spatiotemporal heterogeneity in the distribution of pathogens. If some of the pathogens tend to stay close in space or time, without actually being physically clustered, this will also contribute to overdispersion in the dose distribution and can be difficult, if not impossible, to distinguish from clustering only on the basis of observing pathogen counts. Temporal variation in the mean pathogen concentration on larger time scales will also induce overdispersion. While these sources of overdispersion may possibly also be representable by a distribution of the form of Equation (8), the interpretation of the parameters in terms of clusters is lost. The main focus of this article is on suspensions that have a given mean pathogen concentration $\lambda = \mathrm{E}(X)$, for which some of

the pathogens are actually clustered, and the clusters themselves behave as Poisson particles.

2.3. A General Dose Distribution Accounting for Clustering

We are interested in the distribution of X as expressed in Equation (8), where the X_ns are assumed to be Poisson distributed. It is demonstrated in Section S.1 of the online appendix that the distribution of X is, in fact, a general *stuttering Poisson distribution*,[20–22] i.e., a Poisson-stopped sum of nonnegative discrete random variables. Special cases of this distribution have, for example, been used to model bulk arrivals in queuing theory[21] and the number of radiation-induced chromosome defects.[23] For the case where there is a fixed maximum cluster size $N > 1$, the distribution of X has been called the Nth-order (univariate) Hermite distribution.[24] For $N = 2$, it is known simply as the Hermite distribution.[25,26] This special case was used to model bacterial counts as early as 1926[27] (although the name "Hermite" distribution was coined later) and may be of particular importance for dilute suspensions, where larger clusters are unlikely to form. For the case where the only cluster sizes are 1 and N, it is known as the generalized Hermite distribution.[28]

The stuttering Poisson distribution may become very complicated (e.g., many modes), owing to the essentially combinatorial character of the problem of obtaining it (Section S.1 of the online appendix). Its pmf is generally not expressible in closed form, but can be obtained as a convenient recursive formula[22] that evaluates quite rapidly on an ordinary computer as long as the mean of the stuttering Poisson distribution is only moderately large. A proof of the following expression for the pmf is reproduced in Section S.1 of the online appendix (Lemma 1):

$$p_X(x) = \begin{cases} e^{-\sum_{n=1}^{\infty} \lambda_n} & \text{if } x = 0 \\ = \frac{1}{x} \sum_{n=1}^{x} n\lambda_n p_X(x-n) & \text{if } x \geq 1. \end{cases} \quad (10)$$

We may use Equation (10) to compute the dose distribution resulting from any given clustering state in the water source, which is specified by the set of parameters $\lambda_n = c_n v$, $n = 1, 2, \ldots$. Table S1 in Section S.1 of the online appendix gives expressions for δ and θ as a function of the parameters λ_n.

A special case of the stuttering Poisson is the two-parameter negative binomial distribution, which has been used to accommodate a larger than Poisson variance in QMRA studies.[10,16,18] For the negative binomial, the distribution of cluster sizes follows a logarithmic series distribution with parameter $0 < a < 1$. The details are given in Section S.1 of the online appendix. When parameterized in terms of the mean λ and a dispersion parameter $b = a/(1-a)$, the pmf is given by:

$$p_X(x) = \frac{\Gamma(x + \lambda/b)}{x!\Gamma(\lambda/b)} \left(\frac{b}{b+1}\right)^x \left(\frac{1}{b+1}\right)^{\lambda/b}. \quad (11)$$

The variance is $\mathrm{Var}(X) = \lambda(1+b)$. The negative binomial reduces to the Poisson distribution with mean λ as $b \to 0$. Its pgf is:

$$G_X(z) = [1 + b(1-z)]^{-\lambda/b}, \quad (12)$$

which we will use in Section 3.1.

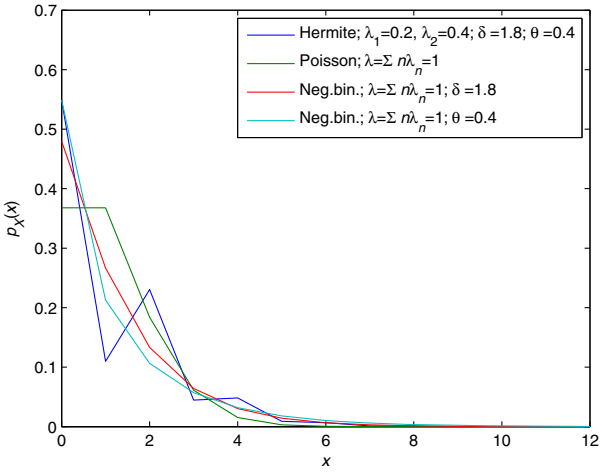

Fig. 2. Comparison of the Hermite distribution with the Poisson (equivalent λ) and the negative binomial (equivalent λ and δ, or λ and θ).

In Fig. 2, an example of the Hermite distribution ($N = 2$) is compared with the Poisson distribution (identical means) and the negative binomial distribution (identical means/dispersion indexes or means/zero inflation indexes). The example represents a situation where as much as 80% of the pathogens are contained in 2-clusters, which accentuates the jagged nature of the Hermite distribution. It is seen that, compared to the Poisson, the three other distributions give a higher probability of obtaining zero pathogens and lower probability of obtaining exactly 1.

It is interesting to compare some key general properties of the Poisson distribution with mean λ and a stuttering Poisson with the same mean, i.e., $\lambda = \sum_{n=1}^{\infty} n\lambda_n$ (in terms of pathogen concentrations,

$c = \sum_{n=1}^{\infty} nc_n$). The detailed expressions for the moments have been left to Table S1 in Section S.1 of the online appendix. The important fact is that the variance in the dose distribution will always increase after clustering, and therefore the dispersion index δ also increases. If there is a maximum cluster size N, it can easily be shown that $1 \leq \delta \leq N$, where $\delta = 1$ if and only if X is simple Poisson and $\delta = N$ if and only if all the pathogens are contained exclusively in N-clusters. Therefore, if a reliable estimate of δ can be obtained experimentally, it gives an indication of cluster sizes: there are at least some clusters greater than or equal to δ. However, obtaining a reliable δ estimate may be difficult in practice, requiring that we sample from a stationary distribution for X and that analytical procedures have a constant 100% recovery efficiency.

Since $p_X(0)$ increases as a result of clustering (which means that the zero-inflation index θ also increases), the probability of getting at least one pathogen always decreases. Slightly counterintuitive, the probability of getting exactly one pathogen may increase or decrease, even though the concentration of 1-clusters always decreases. The direction of change depends on details of the clustering state. However, for low pathogen concentrations ($\lambda < 1$), we can show that $p_X(1)$ always decreases after clustering. Consider the fraction:

$$\frac{\Pr(X=1)_{\text{cl}}}{\Pr(X=1)_{\text{disp}}} = \frac{\lambda_1 e^{-\sum_{n=1}^{\infty}\lambda_n}}{\lambda e^{-\lambda}} = \frac{\lambda_1 e^{-\lambda_1}}{\lambda e^{-\lambda}} e^{-\sum_{n=2}^{\infty}\lambda_n}. \quad (13)$$

The last exponential is always less than 1. Inspection of the function $\lambda e^{-\lambda}$ will show that it is strictly increasing for $0 < \lambda < 1$. Thus, since $\lambda > \lambda_1$, the fraction $(\lambda_1 e^{-\lambda_1})/(\lambda e^{-\lambda})$ will always be less than 1 for $0 < \lambda < 1$. Typically, the expected pathogen dose in a glass of water will rarely exceed 1.

3. ANALYTICAL RESULTS AND EXAMPLES

3.1. Dose Response with Stuttering Poisson Doses

Fortunately, the dose-response expression in Equation (2) requires not the complicated pmf of X, but instead the pgf, which has a simple expression. In Section S.1 of the online appendix, it is shown that it is given by:

$$G_X(z) = \exp\left(\sum_{n=1}^{\infty} \lambda_n (z^n - 1)\right). \quad (14)$$

For any given λ, we may reparameterize the stuttering Poisson distribution by letting $q_n = \frac{n\lambda_n}{\lambda}$, i.e., q_n denotes the fraction of the total pathogen count that is contained in n-clusters. With this, Equation (14) becomes:

$$G_X(z) = \exp\left(\lambda \sum_{n=1}^{\infty} \frac{q_n}{n}(z^n - 1)\right). \quad (15)$$

Using the pgf of the stuttering Poisson (Equation (14)) in the general single-hit expression in Equation (2) gives us the dose-response relation:

$$\mathrm{E}(P_{\text{I,sPo}}) = 1 - \int_0^1 \exp\left\{\sum_{n=1}^{\infty} \lambda_n [(1-r)^n - 1]\right\} f_R(r)\, \mathrm{d}r. \quad (16)$$

Thus, within the single-hit theoretical framework, we may specify the parameters of the stuttering Poisson distribution corresponding to any given clustering state, and use Equation (16) to compute the (expected) probability of infection. Given the generality of the above expression, it is conjectured that it may encompass most, if not all, plausible "single-hit" dose-response relationships unless the dose distribution is underdispersed ($\delta < 1$), but this seems to be rare for microbial counts. It reduces to the conventional dose-response relationships (exponential, beta-Poisson) for specific choices of the parameters λ_n and the distribution f_R.[4,9]

The dose-response formulation in Equation (16) enables us to show quite generally that clustering, as represented by a stuttering Poisson distribution, always decreases the (expected) probability of infection in a single-hit model. We formulate this main result as a proposition, with the proof left to the Appendix.

Proposition 1 (Risk with stuttering Poisson doses). *Let the dose X be stuttering Poisson distributed with $\lambda_N > 0$ for some $N > 1$ (i.e., there exists some clusters) and fix the mean $\mathrm{E}(X) = \lambda = \sum_{n=1}^{\infty} n\lambda_n$. Then, the corresponding single-hit risk $\mathrm{E}(P_{\text{I,sPo}})$ is bounded from above by $\mathrm{E}(P_{\text{I,Po}})$, the single-hit risk computed using a Poisson distribution with the same mean λ.*

Proposition 1 is illustrated in Fig. 3, which shows a contour plot of the following ratio:

$$\frac{\mathrm{E}(P_{\text{I}})}{\mathrm{E}(P_{\text{I,He}})} = \frac{1 - e^{-\lambda r}}{1 - e^{-\lambda r(1 - \frac{1}{2}q_2 r)}}. \quad (17)$$

This is the ratio of the risk computed with a Poisson distribution (i.e., the exponential model)

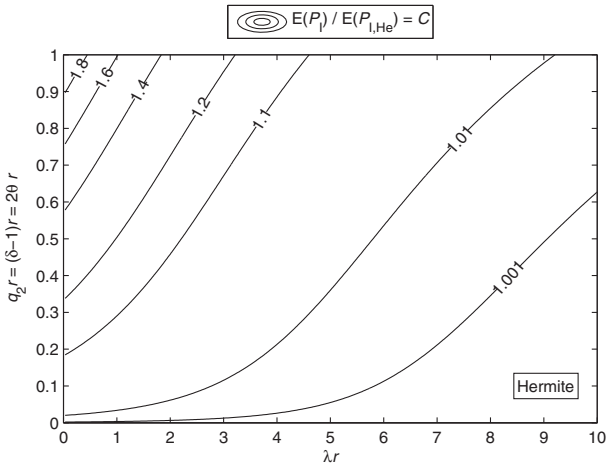

Fig. 3. Contour plot of the ratio in Equation (17), comparing the risk computed with the Poisson distribution (exponential model) to that computed with the Hermite distribution. q_2 is the proportion of pathogens in 2-clusters. A corresponding plot assuming beta-distributed R is given in Fig. S1 in the online appendix.

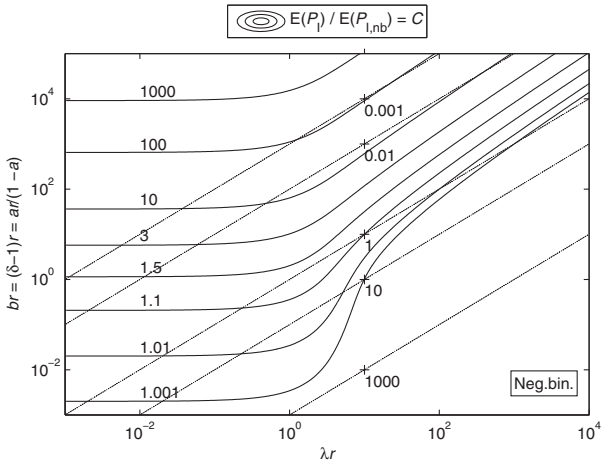

Fig. 4. Contour plot (solid lines) of the ratio in Equation (18), comparing the risk computed with the Poisson distribution (exponential model) to that computed with the negative binomial distribution. Dotted lines indicate a constant value of λ/b. A corresponding plot assuming beta-distributed R is given in Fig. S2 in the online appendix.

to the risk computed with the Hermite distribution, assuming a constant single-hit probability r. The denominator is obtained from Equation (16) with only λ_1 and λ_2 nonzero, r constant, and using $q_2 = 2\lambda_2/\lambda$. It is the simplest possible comparison between a clustered/nonclustered situation, but it may potentially be of practical relevance in dilute suspensions for pathogens that fit the exponential model. Furthermore, it uncovers some general tendencies of interest. First, for any r (single-hit probability) and q_2 (proportion of pathogens in 2-clusters), the effect of clustering becomes less important as the mean λ of the distributions increases. Second, for any λ and q_2, the effect of clustering becomes negligible when r becomes small since we are then approaching the lower-left corner of the plot. Third, even for small λ and large r, the effect of clustering is negligible unless q_2 is quite large. In summary, the effect of clustering only becomes important for jointly small λ, large r, and large q_2 ($rq_2 \gtrsim 0.2$ is required for a ratio of 1.1 or larger). The ratio in Equation (17) is bounded from above by 2. Fig. S1 in the online appendix generalizes Fig. 3 to the case of beta-distributed R, parameterized in terms of $\mathrm{E}(R) = \alpha/(\alpha+\beta)$ and α. The effect of clustering generally increases with $\mathrm{E}(R)$ and q_2 and decreases with α. For any given $\mathrm{E}(R)$ and q_2, the effect of clustering is relatively small unless both α *and* λ are small.

Fig. 4 is similar to Fig. 3 and shows a contour plot of:

$$\frac{\mathrm{E}(P_{\mathrm{I}})}{\mathrm{E}(P_{\mathrm{I,nb}})} = \frac{1-e^{-\lambda r}}{1-(1+br)^{-\lambda/b}}, \tag{18}$$

where the denominator is the risk computed using the negative binomial distribution (no host heterogeneity), obtained by using Equation (2) with Equation (12). Here, the extent of clustering increases with the dispersion parameter $b = \delta - 1$. The situation is a bit more complicated than in Fig. 3. It is still correct that clustering becomes negligible as r or b becomes very small. When holding r and b constant while decreasing λ, the ratio reaches a near steady state for $\lambda r < 1$. The ratio is above 1.1 if $\lambda r < 1$ and $br > 0.25$. The effect of increasing r while holding b and λ constant (moving along dotted lines) depends on whether λr is below (ratio increases) or above (ratio decreases) 1. For drinking water applications, it will usually be below 1. Fig. S2 in the online appendix generalizes Fig. 4 to the case of beta-distributed R. The effect of clustering generally increases with $\mathrm{E}(R)$ and b and decreases with α.

3.2. Dose Response with Mixed Poisson Doses

For completeness, we now consider an alternative generalization of the dose distribution known as mixed Poisson distributions. Here, the Poisson parameter λ is considered to be randomly drawn from a so-called mixing distribution that represents the variation in λ. Such distributions have, e.g., been used to

model seasonal variations in pathogen count in raw water (e.g., the Poisson log-normal distribution). In the case of mixed Poisson doses, the pmf $p_X(x)$ of the dose distribution is obtained by marginalizing the Poisson distribution over λ:

$$p_X(x) = \int_0^\infty p_{X_{\mathrm{Po}}}(x) f_\Lambda(\lambda)\,\mathrm{d}\lambda = \int_0^\infty \frac{\lambda^x e^{-\lambda}}{x!} f_\Lambda(\lambda)\,\mathrm{d}\lambda, \tag{19}$$

where $p_{X_{\mathrm{Po}}}$ is the pmf of a Poisson distribution with parameter λ and $f_\Lambda(\lambda)$ is the pdf of the mixing distribution. It can be demonstrated that the distribution in Equation (19) is indeed overdispersed relative to the Poisson distribution. By the law of total variance, we have $\mathrm{Var}(X) = \mathrm{Var}(\Lambda) + \mathrm{E}(\Lambda)$, which has a minimum when Λ is point mass distributed (i.e., X is Poisson and $\mathrm{Var}(\Lambda)=0$). When f_Λ is specified, p_X may be used in the general single-hit expression (Equation (2)) to obtain a (possibly closed-form) marginal dose-response model. However, variation in λ is often more relevant for risk characterization (as opposed to dose-response assessment), for which it may be easier to sample sequentially from f_Λ and p_X during Monte Carlo simulations than it is to use a marginal dose-response model.

By an advanced theorem of probability,[20,29] a mixed Poisson distribution that is constructed from a so-called *infinitely divisible* mixing distribution will also be a stuttering Poisson distribution, so in many cases, the two families of distributions overlap (e.g., the negative binomial affords both interpretations). For completeness, though, we include the following proposition, which is the equivalent to Proposition 1, but for Poisson mixtures (the proof is left to the Appendix).

Proposition 2 (Risk with mixed Poisson doses). *Let the dose X be mixed Poisson distributed with mixing distribution $f_\Lambda(\lambda)$ and pmf given by Equation* (19)*. Then, the corresponding single-hit risk* $\mathrm{E}(P_{\mathrm{I,mPo}})$ *is bounded from above by* $\mathrm{E}(P_{\mathrm{I,Po}})$*, the single-hit risk computed using a Poisson distribution with mean equal to the mean of the mixing distribution,* $\mathrm{E}(\Lambda)$.

In order to build some intuition for why Propositions 1 and 2 hold, note that the single-hit model in Equation (2) may be written:

$$\begin{aligned}\mathrm{E}(P_{\mathrm{I}}) &= \mathrm{E}_X[\mathrm{E}_R(P_{\mathrm{I}})] \\ &= \sum_{x=0}^{\infty} p_X(x) \int_0^1 [1-(1-r)^x] f_R(r)\,\mathrm{d}r, \end{aligned} \tag{20}$$

where the subscripts denote expectation with respect to the indicated random variables. The integral expression $\mathrm{E}_R(P_{\mathrm{I}})$ has been called a *conditional* dose-response model[7] since it gives the (expected) risk if exactly x pathogens are ingested. The essential property of $\mathrm{E}_R(P_{\mathrm{I}})$, which may be verified by twice differentiation under the integral sign, is that it is always *concave*[4] in x for $x \geq 0$. Furthermore, the variance of X increases when X is stuttering Poisson or mixed Poisson, as compared to a Poisson-distributed X with the same mean. Thus, in the weighted sum $\mathrm{E}_X[\mathrm{E}_R(P_{\mathrm{I}})]$ of conditional dose-response models, more weight is put on x-values far from the mean of X (on both sides of it). Since $\mathrm{E}_R(P_{\mathrm{I}})$ is concave in x (i.e., it becomes progressively flatter), the dispersion of weights may intuitively be expected to reduce the risk estimate. This property may be expected to not hold for a model that incorporates between-pathogen cooperation, which tends to introduce a convex region in the low-dose range of the conditional dose-response model (see Section S.4 of the online appendix).

While Propositions 1 and 2 agree with intuition, their strength is their generality: there exists no stuttering or mixed Poisson distribution, no matter how obscure, that increases the risk estimate compared to a Poisson distribution with the same mean. One may still ask how general these families of distributions are, and whether overdispersed count (dose) distributions that are not representable as stuttering or mixed Poisson lead to similar results as Propositions 1 and 2.[5] While we have not succeeded in finding a definitive answer, it has been shown[30] that any count random variable for which $\Pr(X=0) > 0.5$ follows a *generalized*[6] stuttering Poisson distribution, but it is not clear to us whether the proof of Proposition 1 can be modified to cover this case.

Finally, we want to briefly mention the concept of *stochastic dominance*,[31,32] widely used in expected utility theory in economics, and a potentially useful tool also for microbial risk analysis. In particular, for any concave conditional dose-response model, second-order stochastic dominance dictates that the risk from dose distribution X_A is higher than the risk from dose distribution X_B if X_B is a so-called

[4]Often, dose-response models are plotted on log-log or semi-log plots, which gives the appearance of a convexity in the low-dose region.

[5]Section S.3 in the online appendix shows that it also holds when the X_is in Equation (8) are binomial random variables with identical success probabilities.

[6]The generalized version allows for negative λ_ns.

mean-preserving spread[33] of X_A, i.e., if $X_B = X_A + Z$ for some random variable Z and $\mathrm{E}(Z|x_A) = 0$ for all x_A.

4. AN APPROXIMATE DOSE-RESPONSE MODEL FROM JENSEN'S INEQUALITY

From Propositions 1 and 2, it is clear that the single-hit risk obtained with an overdispersed dose distribution in the form of stuttering or mixed Poisson-distributed doses is bounded from above by the risk obtained with Poisson-distributed doses. As shown in Figs. 3 and 4 and Figs. S1 and S2 in the online appendix, the difference in risk between the Poisson case and the overdispersed case may become substantial for extreme overdispersion. The following proposition gives another bound on risk that appears to be significantly closer (shown below) to the exact single-hit risk for highly overdispersed dose distributions, and could be useful for practical purposes. It is valid for *any* dose distribution (not necessarily stuttering or mixed Poisson) and *any* conditional dose-response model that is concave in the dose variable (not necessarily single-hit), and it requires only one additional parameter (the zero-inflation index) of the dose distribution compared to the Poisson distribution. The proof is again left to the Appendix.

Proposition 3. *Introduce the notation* $P_{\mathrm{I}}^0(x) \equiv \mathrm{E}_R(P_{\mathrm{I}})|_{X=x}$ *for a general concave (in x) conditional dose-response model. Then, the risk* $\mathrm{E}(P_{\mathrm{I}}) = \sum_{x=0}^{\infty} p_X(x) P_{\mathrm{I}}^0(x)$ *is bounded from above by:*

$$\begin{aligned}\mathrm{E}(P_{\mathrm{I,J}}) &= [1 - p_X(0)] \cdot P_{\mathrm{I}}^0\left(\frac{\lambda}{1 - p_X(0)}\right) \\ &= \left(1 - e^{\lambda(\theta-1)}\right) \cdot P_{\mathrm{I}}^0\left(\frac{\lambda}{1 - e^{\lambda(\theta-1)}}\right), \end{aligned} \quad (21)$$

where θ *is the zero-inflation index of the distribution of X.*

It is readily verified that Equation (21) satisfies some fundamental requirements of a dose-response model:

$$\begin{aligned} &0 \le \mathrm{E}(P_{\mathrm{I,J}}) \le 1, \\ &\lim_{\lambda \to 0} \mathrm{E}(P_{\mathrm{I,J}}) = 0, \\ &\lim_{\lambda \to \infty} \mathrm{E}(P_{\mathrm{I,J}}) = 1. \end{aligned} \quad (22)$$

The latter property holds only if there are no completely immune hosts.[9] The Jensen bound takes particular forms depending on which conditional dose-response model P_{I}^0 we choose. If R has a single point mass, the Jensen bound becomes:

$$\mathrm{E}(P_{\mathrm{I,J}}) = \left(1 - e^{\lambda(\theta-1)}\right) \cdot \left(1 - (1-r)^{\lambda/\left(1-e^{\lambda(\theta-1)}\right)}\right). \quad (23)$$

If R is beta distributed, the Jensen bound is:

$$\mathrm{E}(P_{\mathrm{I,J}}) = \left(1 - e^{\lambda(\theta-1)}\right) \cdot \left(1 - \frac{B\left[\alpha, \beta + \lambda/\left(1 - e^{\lambda(\theta-1)}\right)\right]}{B(\alpha, \beta)}\right), \quad (24)$$

where B denotes the beta function.

As mentioned, Equation (21) seems to be a very good risk bound in the single-hit case, i.e., it is quite close to the exact single-hit risk. Figs. 5 and 6 illustrate this. Fig. 5 shows a contour plot for the following ratio of the risk from the Jensen bound to the risk computed with a Hermite distribution (no host heterogeneity, i.e., a constant $R = r$):

$$\frac{\mathrm{E}(P_{\mathrm{I,J}})}{\mathrm{E}(P_{\mathrm{I,He}})} = \frac{\left(1 - e^{\lambda(\theta-1)}\right) \cdot \left(1 - (1-r)^{\lambda/\left(1-e^{\lambda(\theta-1)}\right)}\right)}{1 - e^{-\lambda r\left(1 - \frac{1}{2}q_2 r\right)}}. \quad (25)$$

Also shown (red curves (color visible in on-line version)) is the ratio in Equation (17) for comparison. For all parameter values, the Jensen bound stays within about 10% of the exact risk. In those cases where the exponential model (red curves) severely overestimates risk, the Jensen bound is markedly closer to the exact risk from the Hermite model. In other cases, where clustering is less pronounced, the exponential model tends to give a slightly more precise estimate of the exact risk than the Jensen bound. Fig. S1 in the online appendix generalizes Fig. 5 to the case of beta-distributed R, and the trends are similar; the Jensen bound performs very well overall and particularly in those cases where the exact beta-Poisson model overestimates risk.

Fig. 6 shows a contour plot for the following ratio of the risk from the Jensen bound to the risk computed with a negative binomial distribution (again, no host heterogeneity):

$$\frac{\mathrm{E}(P_{\mathrm{I,J}})}{\mathrm{E}(P_{\mathrm{I,nb}})} = \frac{\left(1 - e^{\lambda(\theta-1)}\right) \cdot \left(1 - (1-r)^{\lambda/\left(1-e^{\lambda(\theta-1)}\right)}\right)}{1 - (1+br)^{-\lambda/b}}. \quad (26)$$

Also shown (red curves) is the ratio in Equation (18) for comparison. Again, the bound seems to be very good in those cases where the exponential model (red curves) severely overestimates risk; for some parameter values close to two orders of magnitude better. Fig. S2 in the online appendix generalizes Fig. 6 to the case of beta-distributed R, and the trends are

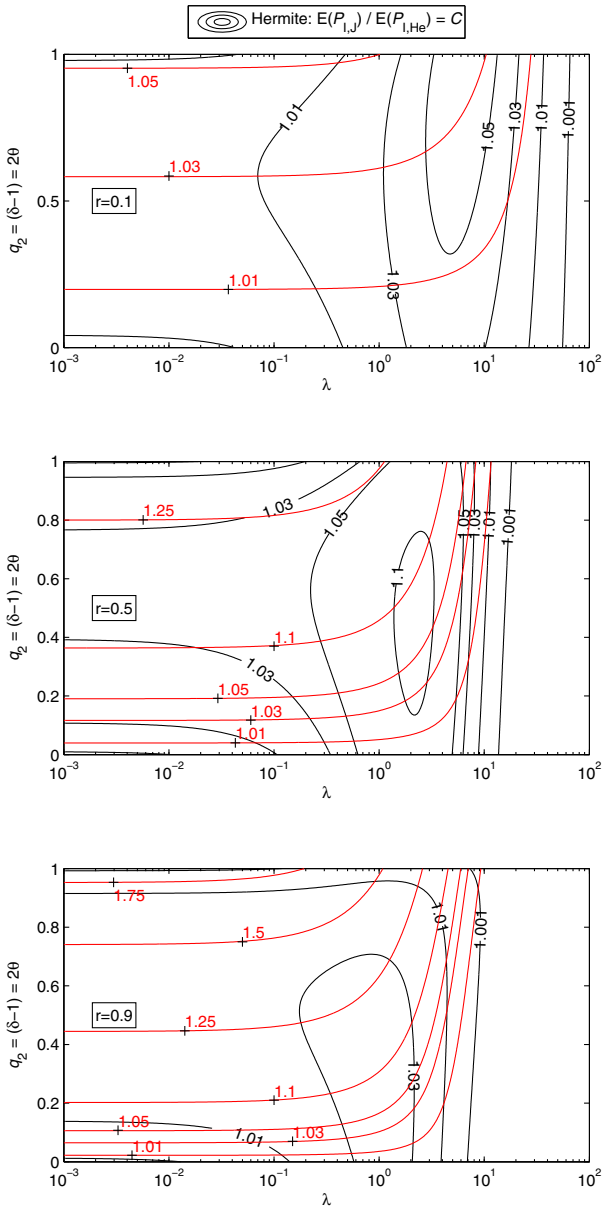

Fig. 5. Black curves are contours for the ratio in Equation (25), comparing the risk computed with the Jensen bound to that computed with the Hermite distribution. Red curves are contours for the ratio of risk computed with the Poisson distribution to that computed with the Hermite distribution. This figure is based on a constant $R = r$; Fig. S1 in the online appendix shows the case of beta-distributed R.

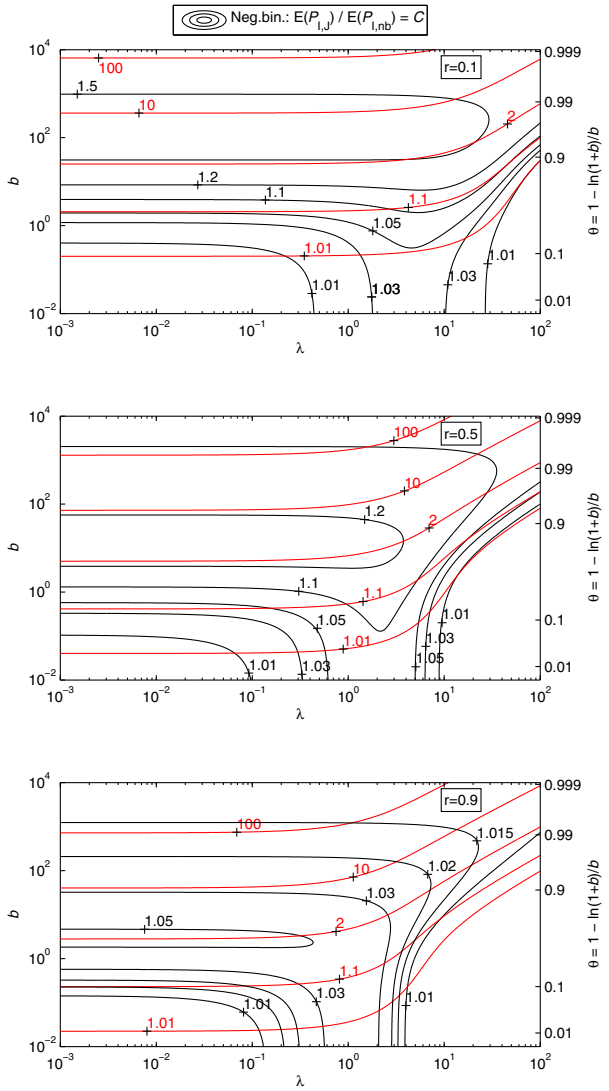

Fig. 6. Black curves are contours for the ratio in Equation (26), comparing the risk computed with the Jensen bound to that computed with the negative binomial distribution. Red curves are contours for the ratio of risk computed with the Poisson distribution to that computed with the neg.bin. distribution. This figure is based on a constant $R = r$; Fig. S2 in the online appendix shows the case of beta-distributed R.

similar; the Jensen bound performs very well overall and particularly in those cases where the exact beta-Poisson model overestimates risk.

Finally, we compare the Jensen bound risk to the risk computed with the discrete Weibull distribution.[34] This distribution has been suggested[12,13,35] as a natural model for long-term pathogen counts in drinking water with the ability to account for rare, high-consequence events such as treatment plant failures. Hence, it can potentially model pathogen counts that are subject to *temporal* clustering. Its pmf, mean, and zero-inflation index are given by, respectively:

$$p_X(x) = q^{x^\eta} - q^{(x+1)^\eta}, \tag{27}$$

$$\lambda = \sum_{x=1}^{\infty} q^{x^{\eta}}, \tag{28}$$

$$\theta = 1 + \frac{\ln(1-q)}{\lambda}, \tag{29}$$

with shape parameters $\eta > 0$ and $0 < q < 1$. The infinite sum for the mean was computed in this work by means of an approximation given by Englehardt and Li.[12] It can be shown that Equations (28) and (29) uniquely determine q and η for any given pair $\lambda > 0$ and $\theta < 1$; hence, we may reparameterize the distribution in terms of λ and θ. This was used in Figs. 7 (low θ values; θ on vertical axis) and 8 (high θ values; $1-\theta$ on vertical axis), which show contour plots of the following ratio:

$$\frac{\mathrm{E}(P_{\mathrm{I,J}})}{\mathrm{E}(P_{\mathrm{I,dW}})} = \frac{\left(1-e^{\lambda(\theta-1)}\right)\cdot\left(1-(1-r)^{\lambda/\left(1-e^{\lambda(\theta-1)}\right)}\right)}{1-\sum_{x=0}^{\infty} p_X(x)(1-r)^x}, \tag{30}$$

where X is discrete Weibull distributed. The denominator was computed to full numerical precision, i.e., until the term $p_X(x)(1-r)^x$ evaluated to 0. The trends in these figures are similar to those for the Hermite and negative binomial distribution; the Jensen bound performs very well in those cases where overdispersion causes a marked reduction in the exact risk, while it is also reasonably close to the exact risk when there is little overdispersion. Fig. S3 in the online appendix generalizes Figs. 7 and 8 to the case of beta-distributed R, and the trends are similar; the Jensen bound performs very well overall and particularly in those cases where the exact beta-Poisson model overestimates risk. In summary, the Jensen bound examples in this section appear to indicate that the single-hit risk is only moderately sensitive to the details of an overdispersed dose distribution, but quite sensitive to the overall *degree* of overdispersion, as expressed by the zero-inflation index.

5. APPLICATION OF THE APPROXIMATE MODEL: DOSE-RESPONSE FOR NOROVIRUS

Dose-response assessment for Norovirus[16–18] has been complicated by aggregation of viruses in the inoculum used for human feeding trials. Here, we fit the beta-Jensen bound (Equation (24)) to the available Norovirus dose-response data for the purposes of demonstrating its application, and for simple comparison with previous studies.

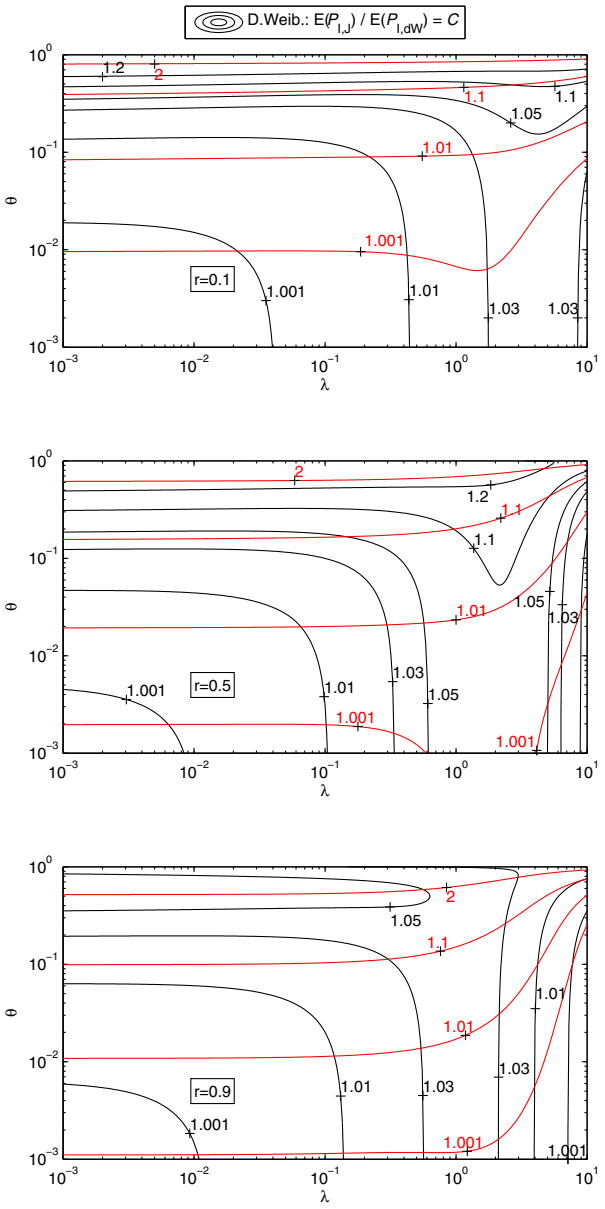

Fig. 7. Black curves are contours for the ratio in Equation (30), comparing the risk computed with the Jensen bound to that computed with the discrete Weibull distribution for low θ values. Red curves are contours for the ratio of risk computed with the Poisson distribution to that computed with the d.Wei. distribution. This figure is based on a constant $R = r$; Fig. S3 in the online appendix shows the case of beta-distributed R.

Several studies have reported Norovirus dose-response data from human feeding trials.[16,36–38] The essential data from those studies are given in Table I. In the study by Teunis *et al.*,[16] the suspension used as inoculum had been stored for a long time and, using electron microscopy, the viruses were observed to

Table I. Norovirus Dose-Response Data from Human Feeding Trials [16,36–38]

Designation	Aggregated	Source	Mean Dose (PCR Units)	Total Subjects	Infected Subjects
8fIIa GI.1	Y	Teunis *et al.*[16]			
			3.24×10^{0}	8	0
			3.24×10^{1}	9	0
			3.24×10^{2}	9	3
			3.24×10^{3}	3	2
			3.24×10^{5}	8	7
			3.24×10^{6}	7	3
			3.24×10^{7}	3	2
			3.24×10^{8}	6	5
8fIIb GI.1	N	Teunis *et al.*[16]			
			6.92×10^{5}	8	3
			6.92×10^{6}	18	14
			2.08×10^{7}	1	1
8fIIb GI.1	N (presumed)	Seitz *et al.*[36]			
			6.50×10^{7}	13	10
8fIIa GI.1	Y (presumed)	Atmar *et al.*[37]			
			1.92×10^{2}	13	1
			1.92×10^{3}	13	7
			1.92×10^{4}	8	7
			1.92×10^{6}	7	6
GII.4	Y (presumed)	Frenck *et al.*[38]			
			2.00×10^{7}	23	16

Note: 8fIIa: "Primary" inoculum from the original Norwalk isolate. 8fIIb: "Secondary" inoculum from stool samples of an infected individual. GI.1: Genogroup I/genotype 1. GII.4: Genogroup II/genotype 4.

be significantly clustered and could not be dispersed by sonication. The assumptions on aggregation in the other studies have been adopted here from Messner *et al.*[17] The dose levels in all these studies were determined by quantitative PCR. Recently, Norovirus was cultivated *in vitro* for the first time,[39] which may pave the way for quantification by culturing methods that will arguably be more relevant for dose-response assessment.

Table II gives an overview of the models that were fitted to the data in this work. The exact beta-Poisson model assumes completely dispersed pathogens and is included as a reference. The beta-negative binomial model was suggested and fitted by Teunis *et al.*[16] and refitted[7] to an extended data set by Messner *et al.*[17] Messner *et al.*[17] also suggested a model, termed *fractional Poisson*, in which R is Bernoulli distributed, i.e., hosts are either fully immune or fully susceptible. In that case, the model does not require the full dose distribution; only $p_X(0)$ is needed. The model contains two fitting parameters: the fraction of (fully) immune hosts, ϕ, and the mean aggregate size μ. Schmidt[18] investigated a range of models, including the previously mentioned ones, but extended all models to include a host immunity parameter and showed that the omission/inclusion of an immunity parameter may have a large effect on the results.

When fitting the Jensen bound, we have to assume that θ is constant across all dose levels, which is an assumption that warrants some attention. If we can assume that the only effect of dilution is to scale the concentration of each cluster size, it can be seen from the expression for θ in Table S1 (online appendix, Section S.1) that θ can be expected to be conserved across dilutions of a suspension, since every λ_n is scaled by the same (expected) factor. Equivalent assumptions have been made in the previously published models on Norovirus, either by stating the assumption explicitly[18] or implicitly by treating the aggregation parameter as a constant across all dose levels in a feeding trial.[16,17] In practice, however, the diluent may affect the colloidal stability and hence clustering state of the pathogens, and mechanical mixing procedures may also have an effect. Thus, there is some uncertainty

[7]Note that we arrive at parameter estimates for the beta-negative binomial model in this work that are different from those of Messner *et al.*,[17] using the same data set. We believe that the estimates reported here are correct, as our computed likelihood values agree to full reported precision with those of Schmidt.[18]

Table II. Dose-Response Models Fitted to Data in Table I

	Distr. of R	Dose distr. – agg.	E(P_I) – agg.	E(P_I) – disp.	θ
Exact beta-Poisson	Beta	Poisson	$1 - {}_1F_1(\alpha, \alpha+\beta, -\lambda)$	As for agg.	$\equiv 0$
Beta-neg.bin.	Beta	Neg.bin.	$1 - {}_2F_1(\lambda/b, \alpha; \alpha+\beta; -b)$	Ex. b.-Po.	$1 - \ln(b+1)/b$ $= 1 - 1/\mu$
Fractional Poisson	Bernoulli	$p_X(0) = e^{-\lambda/\mu}$	$(1-\phi)(1-e^{-\lambda/\mu})$	As for agg. with $\mu \equiv 1$	$1 - 1/\mu$
Beta-Jensen	Beta.	Not fully specified	Equation (24)	Ex. b.-Po.	$1 - 1/\mu$
Beta-Jensen with imm.	Beta.	Not fully specified	$(1-\phi)$ times Eq. (24)	Ex. b.-Po.	$1 - 1/\mu$

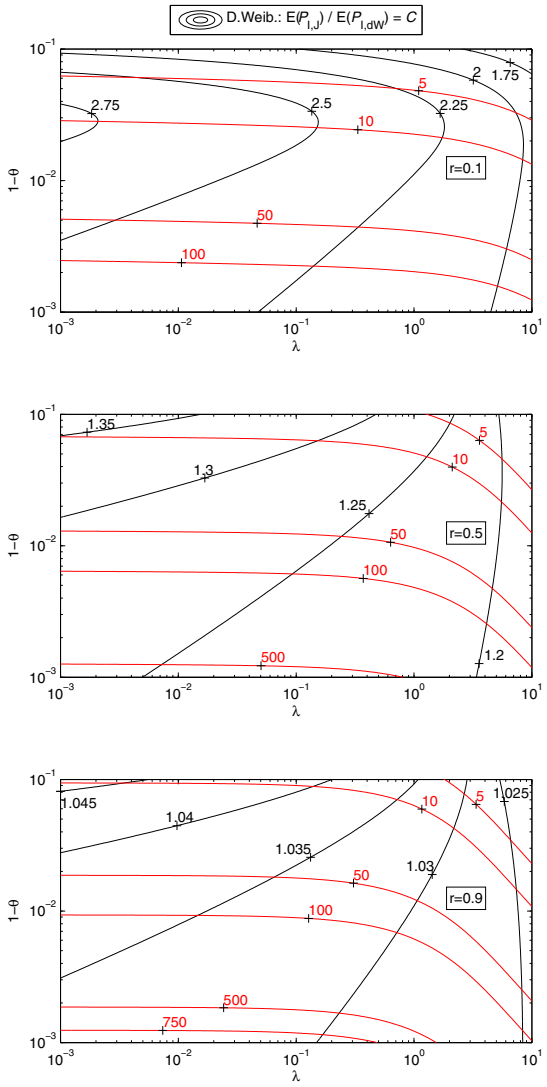

Fig. 8. Black curves are contours for the ratio in Equation (30), comparing the risk computed with the Jensen bound to that computed with the discrete Weibull distribution for high θ values. Red curves are contours for the ratio of risk computed with the Poisson distribution to that computed with the d.Wei. distribution. This figure is based on a constant $R = r$; Fig. S3 in the online appendix shows the case of beta-distributed R.

associated with treating the aggregation parameter as a constant.

For parameter fitting, maximum likelihood estimation was used. The likelihood function for this experimental setup is given by the product of binomial likelihood functions, where each factor corresponds to a certain dose level:

$$L(\omega) = \prod_{i=1}^{I} \binom{n_i}{w_i} \{\mathrm{E}(P_I)_i[\lambda_i, \omega]\}^{w_i} \{1 - \mathrm{E}(P_I)_i[\lambda_i, \omega]\}^{n_i - w_i}. \tag{31}$$

Here, ω is a parameter vector, I is the number of dose levels, λ_i, w_i, and n_i are the dose, number of positive (infected) subjects, and total number of subjects, respectively (at dose level indexed by i). $\mathrm{E}(P_I)_i[\lambda_i, \omega]$ is the dose-response model as a function of the mean dose and parameters to be fitted. Note that when constructing the likelihood function, we use different model formulations for data stemming from the use of aggregated and dispersed viruses, respectively (except in the case of the exact beta-Poisson model). Table II specifies which model formulation was used in each case. Thus, both the aggregated and dispersed data can be used simultaneously to estimate the parameters of the distribution of R, as well as the aggregation parameter. The maximum likelihood estimate of the unknown parameter vector ω is given by numerical optimization of Equation (31), which was performed in MATLAB.[40] The deviance, Y, also stated in Table III, is given by:

$$Y = -2 \ln \left(\frac{L(\omega)}{L^S} \right), \tag{32}$$

where L^S is the likelihood of the so-called saturated model:

$$L^S = \prod_{i=1}^{I} \binom{n_i}{w_i} \left(\frac{w_i}{n_i} \right)^{w_i} \left(1 - \frac{w_i}{n_i} \right)^{n_i - w_i}. \tag{33}$$

The p-value stated in Table III is for a chi-square goodness-of-fit test with the null hypothesis being

Table III. Parameter Estimates for the Dose-Response Models Fitted to Data in Table I

	$\hat{\alpha}$	$\hat{\beta}$	$\hat{\theta}$	$\hat{\phi}$	$\mathrm{E}(\hat{R})$	Deviance	p-Value
Exact beta-Poisson	0.1103	29.55	$\equiv 0$	$\equiv 0$	3.719×10^{-3}	21.030	0.136
Beta-neg.bin.	8.128×10^{-3}	3.756×10^{-3}	0.999024	$\equiv 0$	0.6840	13.270	0.505
Fractional Poisson	–	–	0.999096	0.2775	0.7225	13.288	0.580
Jensen-beta	7.663×10^{-3}	3.504×10^{-3}	0.999045	$\equiv 0$	0.6862	13.273	0.505
Jensen-beta with imm.	2.478	2,186	0.993140	0.2756	8.200×10^{-4}	13.080	0.442

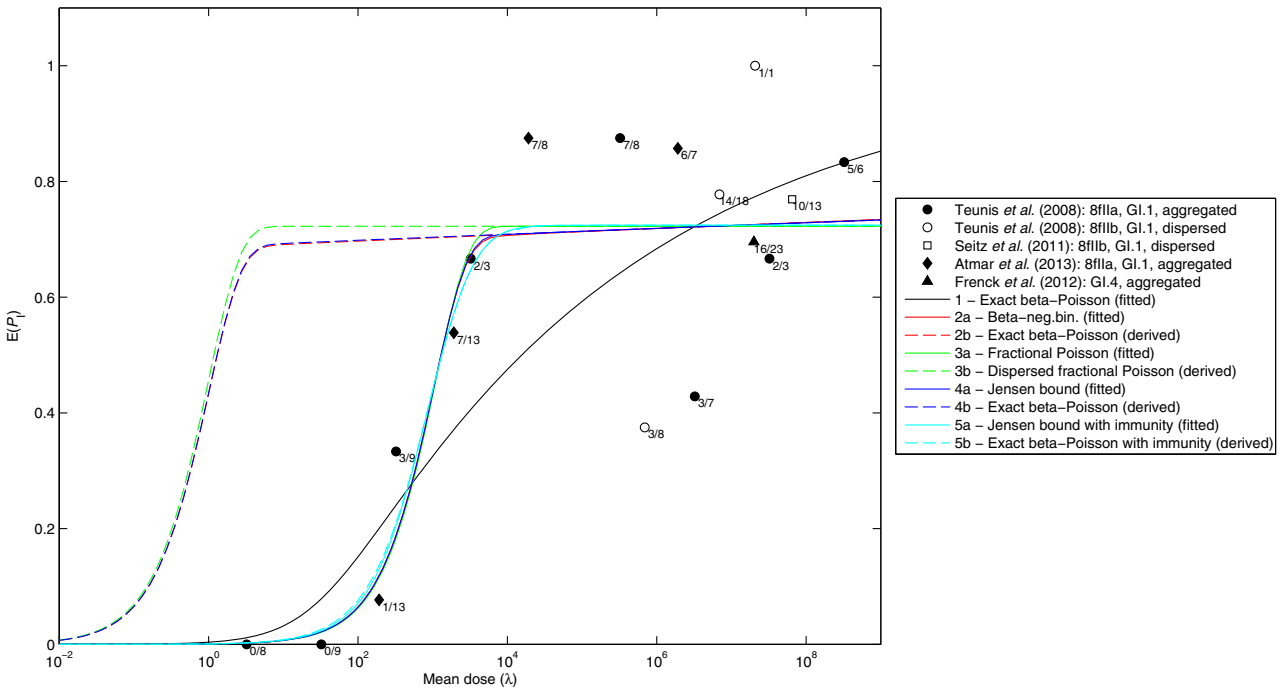

Fig. 9. Dose-response models (solid curves) in Table II fitted to the data in Table I. Dashed curves are derived from the respective fitted models by setting the value of the aggregation parameter to that corresponding to fully dispersed pathogens.

"acceptable fit" and the alternative hypothesis "lack of fit."

Table III and Fig. 9 give the results from parameter estimation. There are several points to note. First, the fitted models and their associated deviances are similar, except for the exact beta-Poisson model, which shows a somewhat poorer fit. Second, the fitted beta parameters of the beta-Jensen model (without immunity) are remarkably similar to those of the beta-negative binomial model. This result may not carry over to other cases, though, as the fitted beta distribution is quite extreme with almost all probability mass concentrated at 0 or 1.[17] Third, the mean single-hit probabilities of the exact beta-Poisson model and the beta-Jensen model with immunity deviate sharply from those in the three other models. Fourth, when eliminating the aggregation parameter from the fitted models (dashed curves in Fig. 9), the resulting dose-response curves are very different from their counterparts *with* the aggregation parameter, except for the beta-Jensen model with immunity, which almost does not change when compared with the exact beta-Poisson model (the corresponding dispersed model). This sensitivity to the inclusion/omission of an immunity parameter is consistent with what was reported by Schmidt.[18]

It should be noted, though, that the parameter estimates returned by the optimization routine for the beta-negative binomial model and the Jensen models seem quite sensitive to the initial guess that is supplied to the routine. The estimates reported here were obtained by maximizing the likelihood

over a range of initial values until the routine delivered consistent results. Worryingly, there seems to exist a wide range of parameter sets, corresponding to a "ridge" or "plateau" in the likelihood surface, that gives approximately the same likelihood (i.e., changes in one parameter may be compensated by corresponding changes in (an)other parameter(s) without affecting the likelihood significantly). Similar challenges with nearly nonunique maximum likelihood estimates were reported by Messner *et al.*[17] when refitting the model used by Teunis *et al.*,[16] and by Schmidt[18] for several models incorporating aggregation. There is significant nonmonotonicity in the data, and there may not be enough information to fit three parameters (or even four, as for the beta-Jensen model with immunity) reliably.

6. DISCUSSION AND CONCLUDING REMARKS

In this work, we have argued that the stuttering Poisson distribution (Equation (10)) is a general and natural model for the dose distribution in the presence of pathogen clustering. By formulating the single-hit dose-response model in terms of a pgf, the stuttering Poisson leads to a simple expression for the dose-response model (Equation (16)). It was shown formally that the single-hit risk computed with a stuttering Poisson distribution is bounded from above by the risk computed with a Poisson distribution (Proposition 1) with the same mean. An equivalent result was obtained for mixed Poisson distributions (Proposition 2). We derived another risk bound (the Jensen bound; Proposition 3), valid for *any* dose distribution and *any* concave conditional dose-response model, which appears to approximate the single-hit risk quite closely for highly overdispersed dose distributions. This bound may also serve as an approximate dose-response model and its application to a real data set was demonstrated in Section 5.

Throughout this article, we have maintained the single-hit assumption of independently acting pathogens, even in the presence of pathogen clustering, as has been assumed in the published work on Norovirus clustered dose response.[16–18] This is a potentially unrealistic assumption that deserves some further attention in future work, although it may be challenging to test it experimentally with sufficient rigor. Propositions 1 and 2, as well as the Jensen bound, suggest that reduced risk from overdispersion (assuming equivalent mean doses) is a property that is fundamentally built into the single-hit framework, and as such is a theoretical prediction that can possibly be tested against data. In the remaining paragraphs, we make an attempt to discuss some potential practical implications of the theoretical results in the event that they actually *do* coincide with real-world effects. We should distinguish between *risk characterization* using an already calibrated dose-response model and *dose-response assessment* or parameter estimation in dose-response models.

The figures in Section 3.1 and in Section S.2 of the online appendix indicate that the effects of clustering in a single-hit model tend to be more pronounced at low doses, coinciding with typical background dose levels in most cases of drinking water risk characterization. However, the effects seem to become relevant only when there is pronounced clustering and when r is simultaneously large (or $\mathrm{E}(R)$ large and α small in the case of beta-distributed R). Therefore, it appears that moderate unaccounted for clustering in drinking water, as exemplified by the Hermite distribution, is unlikely to introduce much additional uncertainty or error into a single-hit risk characterization study, given that QMRA studies often have to quantify uncertainties by order-of-magnitude estimates. In the case of significant temporal variation in pathogen concentrations, periods/events of high doses may dominate the long-term mean risk. Since the theoretical effects of clustering become smaller at larger doses, it appears relatively unimportant to account for any physical clustering during these events.

Given the (likely) modest importance of accounting for clustering in single-hit drinking water studies, and the theoretical prediction that the risk computed using a Poisson distribution forms an upper bound for the risk computed using overdispersed distributions (stuttering or mixed Poisson), we have compelling arguments to direct our efforts at obtaining a correct mean dose rather than characterizing the dose distribution in greater detail. That is, *provided* that we can obtain a reliable estimate of the mean pathogen concentration (and, of course, the single-hit probability, or its distribution), using a Poisson distribution for the single-hit dose-response model during *risk characterization* will produce a higher (more conservative) mean risk estimate than using an overdispersed distribution with the same mean. Note, however, that it may be very difficult in practice to obtain a good estimate of the pathogen concentration, in particular for clustered suspensions or when temporal variation[12,35] is important,

which may leave the risk estimate imprecise or even biased.

If one is interested in accounting for overdispersion, the Jensen bound in Equation (21) may prove useful. If a reliable estimate of both the mean concentration and the zero-inflation index (experimentally available from the proportion of zero counts) can be obtained, a significantly more precise single-hit risk estimate may be obtained for a situation with a highly overdispersed dose distribution without needing to consider further details of that dose distribution. For relatively dispersed suspensions, however, this bound may be more conservative than the risk obtained using a Poisson distribution, which means that the two should be compared before choosing which risk estimate to use.

When *fitting* a dose-response model to data, the implications of clustering are somewhat different. The risk computed with Poisson-distributed doses represents an upper bound on risk, so using the Poisson distribution when pathogens are, in fact, significantly clustered is likely to lead to an underestimation of the (mean) single-hit probability $\mathrm{E}(R)$, exemplified by the exact beta-Poisson parameters in Table III. This is because the parameters of the distribution for R will be chosen by the fitting procedure to compensate for the tendency toward increased risk enforced by the Poisson-distributed dose X. This problem may be somewhat counteracted by fitting the Jensen bound instead of a Poisson-based model, but only in those cases where the data allow reliable estimation of the additional parameter θ introduced in this model, which may represent a challenge.

The application of the Jensen bound in fitting dose-response data was illustrated in Section 5 with published data from human feeding trials on Norovirus. For this application, the Jensen bound model produced results that were very similar to the previously suggested beta-negative binomial model. However, like Schmidt,[18] we have some reservations regarding the possibility of reliably fitting three parameters to this data set. There appears to be a wide range of parameter values that gives roughly the same likelihood. Furthermore, Schmidt showed that the inclusion or omission of a host immunity parameter has a large effect on the results, which was also seen for the Jensen bound model in this work. Thus, there is still a need to obtain more dose-response data for Norovirus, preferably using nonaggregated viruses.

ACKNOWLEDGMENTS

The authors would like to thank four anonymous reviewers for their detailed and critical reviews.

APPENDIX

This appendix contains proofs of the three propositions that were presented in the main text. An overview of the contents of the online supplementary appendix can be found after the list of references.

A.1 Proofs of Propositions

Proposition 1 (Risk with stuttering Poisson doses). *Let the dose X be stuttering Poisson distributed with $\lambda_N > 0$ for some $N > 1$ (i.e., there exists some clusters) and fix the mean $\mathrm{E}(X) = \lambda = \sum_{n=1}^{\infty} n\lambda_n$. Then, the corresponding single-hit risk $\mathrm{E}(P_{\mathrm{I,sPo}})$ is bounded from above by $\mathrm{E}(P_{\mathrm{I,Po}})$, the single-hit risk computed using a Poisson distribution with the same mean λ.*

Proof. Consider the difference:

$$\mathrm{E}(P_{\mathrm{I,Po}}) - \mathrm{E}(P_{\mathrm{I,sPo}}) = \int_0^1 [G_X(1-r) - e^{-\lambda r}]\, f_R(r)\, \mathrm{d}r, \tag{A.1}$$

where we used the general expression of Equation (2) for $\mathrm{E}(P_{\mathrm{I,sPo}})$ and Equation (5) for $\mathrm{E}(P_{\mathrm{I,Po}})$. We need to show that Equation (A.1) is positive when X is stuttering Poisson. Since $f_R \geq 0$ for all $r \in [0, 1]$ and $f_R > 0$ on some subset of the unit interval, it will suffice to take $r > 0$ and show the positivity of the remaining factor in the integrand, ΔG:

$$\begin{aligned} \Delta G &= G_X(1-r) - e^{-\lambda r} \\ &= \left[G_X(1-r)e^{\lambda r} - 1\right] e^{-\lambda r} \\ &= \frac{\exp\left\{\sum_{n=1}^{\infty} \lambda_n \left[(1-r)^n - (1-nr)\right]\right\} - 1}{e^{\lambda r}}. \end{aligned} \tag{A.2}$$

Here, we used the pgf of a stuttering Poisson distribution (Equation (14)) and the identity (by assumption) $\lambda = \sum_{n=1}^{\infty} n\lambda_n$. We now show that the numerator in Equation (A.2) is positive. Let $h(n) = (1-r)^n - (1-nr)$. We have $h(1) = 0$ and for $n \geq 1$, we have the difference:

$$h(n+1) - h(n) = r[1 - (1-r)^n] > 0, \tag{A.3}$$

since $(1-r)^n < 1$ for $n \geq 1$. By mathematical induction, $h(n) > 0$ for $n \geq 2$. Since there exists some $N > 1$ such that $\lambda_N > 0$, we have $\exp[\sum_{n=1}^{\infty} \lambda_n h(n)] > 1$,

which shows that $\Delta G > 0$. This proves the proposition. □

Proposition 2 (Risk with mixed Poisson doses). *Let the dose X be mixed Poisson distributed with mixing distribution $f_\Lambda(\lambda)$ and pmf given by Equation* (19)*. Then, the corresponding single-hit risk* $\mathrm{E}(P_{\mathrm{I,mPo}})$ *is bounded from above by* $\mathrm{E}(P_{\mathrm{I,Po}})$*, the single-hit risk computed using a Poisson distribution with mean equal to the mean of the mixing distribution,* $\mathrm{E}(\Lambda)$.

Proof. We need the pgf of X, which is given by:

$$\begin{aligned} G_X(z) &= \sum_{x=0}^{\infty} z^x \int_0^\infty p_{X_{\mathrm{Po}}}(x)\, f_\Lambda(\lambda)\, \mathrm{d}\lambda \\ &= \int_0^\infty \sum_{x=0}^{\infty} z^x\, p_{X_{\mathrm{Po}}}(x)\, f_\Lambda(\lambda)\, \mathrm{d}\lambda \qquad \text{(A.4)} \\ &= \int_0^\infty e^{\lambda(z-1)}\, f_\Lambda(\lambda)\, \mathrm{d}\lambda, \end{aligned}$$

where we assumed that we may interchange integration and summation. Inserting Equation (A.4) in the general single-hit expression (Equation (2)), we get:

$$\mathrm{E}(P_{\mathrm{I,mPo}}) = 1 - \int_0^1 \int_0^\infty e^{-\lambda r}\, f_\Lambda(\lambda)\, \mathrm{d}\lambda f_R(r)\, \mathrm{d}r. \quad \text{(A.4)}$$

Since $e^{-\lambda r}$ is a strictly convex function of λ on $[0, \infty)$, we may use *Jensen's inequality* to conclude that:

$$\int_0^\infty e^{-\lambda r}\, f_\Lambda(\lambda)\, \mathrm{d}\lambda > e^{-\mathrm{E}(\Lambda) r}. \qquad \text{(A.6)}$$

This leads to:

$$\mathrm{E}(P_{\mathrm{I,mPo}}) < 1 - \int_0^1 e^{-\mathrm{E}(\Lambda) r}\, f_R(r)\, \mathrm{d}r, \qquad \text{(A.7)}$$

where the rhs. is recognized as $\mathrm{E}(P_{\mathrm{I,Po}})$, the single-hit risk computed with a Poisson distribution with mean $\mathrm{E}(\Lambda)$, which concludes the proof. □

Proposition 3 (The Jensen bound). *Introduce the notation $P_{\mathrm{I}}^0(x) \equiv \mathrm{E}_R(P_{\mathrm{I}})\big|_{X=x}$ for a general concave (in x) conditional dose-response model. Then, the risk $\mathrm{E}(P_{\mathrm{I}}) = \sum_{x=0}^\infty p_X(x) P_{\mathrm{I}}^0(x)$ is bounded from above by:*

$$\begin{aligned} \mathrm{E}(P_{\mathrm{I,J}}) &= [1 - p_X(0)] \cdot P_{\mathrm{I}}^0\left(\frac{\lambda}{1 - p_X(0)}\right) \\ &= \left(1 - e^{\lambda(\theta-1)}\right) \cdot P_{\mathrm{I}}^0\left(\frac{\lambda}{1 - e^{\lambda(\theta-1)}}\right), \qquad 21 \end{aligned}$$

where θ is the zero-inflation index of the distribution of X.

Proof. We need Jensen's inequality in the following form. Let ϕ be a concave function on $[0, \infty)$, u_x points in the domain of ϕ and $w_x \geq 0$ be weights such that $\sum w_x u_x < \infty$. Then, Jensen's inequality states (possibly involving infinite sums):

$$\frac{\sum w_x \phi(u_x)}{\sum w_x} \leq \phi\left(\frac{\sum w_x u_x}{\sum w_x}\right). \qquad \text{(A.8)}$$

Make the identifications $u_x = x$, $w_x = p_X(x)$, and $\phi(u_x) = \phi(x) = P_{\mathrm{I}}^0(x)$. Summing from $x = 1$ to infinity, inequality (A.8) becomes:

$$\frac{\sum_{x=1}^\infty p_X(x) P_{\mathrm{I}}^0(x)}{\sum_{x=1}^\infty p_X(x)} \leq P_{\mathrm{I}}^0\left(\frac{\sum_{x=1}^\infty x p_X(x)}{\sum_{x=1}^\infty p_X(x)}\right). \quad \text{(A.9)}$$

Using $P_{\mathrm{I}}^0(0) = 0$, we thus have:

$$\begin{aligned} \mathrm{E}(P_{\mathrm{I}}) &= \sum_{x=0}^\infty p_X(x) P_{\mathrm{I}}^0(x) = \sum_{x=1}^\infty p_X(x) P_{\mathrm{I}}^0(x) \\ &\leq \left(\sum_{x=1}^\infty p_X(x)\right) \cdot P_{\mathrm{I}}^0\left(\frac{\sum_{x=1}^\infty x p_X(x)}{\sum_{x=1}^\infty p_X(x)}\right) \\ &= [1 - p_X(0)] \cdot P_{\mathrm{I}}^0\left(\frac{\lambda}{1 - p_X(0)}\right) \\ &= \left(1 - e^{\lambda(\theta-1)}\right) \cdot P_{\mathrm{I}}^0\left(\frac{\lambda}{1 - e^{\lambda(\theta-1)}}\right) = \mathrm{E}(P_{\mathrm{I,J}}), \end{aligned} \qquad \text{(A.10)}$$

where we used Equation (7) to introduce the zero-inflation index. □

REFERENCES

1. Elimelech M, Gregory J, Jia X, Williams R. Particle Deposition and Aggregation: Measurement, Modelling and Simulation. Oxford: Butterworth-Heinemann, 1995.
2. Gale P. Developments in microbiological risk assessment models for drinking water—A short review. Journal of Applied Microbiology, 1996; 81(4):403–410.
3. Gale P. Developments in microbiological risk assessment for drinking water. Journal of Applied Microbiology, 2001; 91(2):191–205.
4. Haas CN, Rose JB, Gerba CP. Quantitative Microbial Risk Assessment. New York: John Wiley & Sons, 1999.
5. Haas CN. Estimation of risk due to low doses of microorganisms: A comparison of alternative methodologies. American Journal of Epidemiology, 1983; 118(4):573–582.
6. Teunis P, Havelaar A. The beta Poisson dose-response model is not a single-hit model. Risk Analysis, 2000; 20(4):513–520.
7. Haas CN. Conditional dose-response relationships for microorganisms: Development and application. Risk Analysis, 2002; 22(3):455–463.
8. Schmidt PJ, Pintar KDM, Fazil AM, Topp E. Harnessing the theoretical foundations of the exponential and beta-Poisson dose-response models to quantify parameter uncertainty using Markov chain Monte Carlo. Risk Analysis, 2013; 33(9):1677–1693,.

9. Nilsen V, Wyller J. QMRA for drinking water: 1. Revisiting the mathematical structure of single-hit dose-response models. Risk Analysis, 2016; 36(1):145–162.
10. Gale P, Dijk Pv, Stanfield G. Drinking water treatment increases micro-organism clustering; the implications for microbiological risk assessment. Journal of Water Supply: Research and Technology-Aqua, 1997; 46(3):117–126.
11. Gale P, Pitchers R, Gray P. The effect of drinking water treatment on the spatial heterogeneity of micro-organisms: Implications for assessment of treatment efficiency and health risk. Water Research, 2002; 36(6):1640–1648.
12. Englehardt JD, Li R. The discrete Weibull distribution: An alternative for correlated counts with confirmation for microbial counts in water. Risk Analysis, 2011; 31(3):370–381.
13. Englehardt JD, Ashbolt NJ, Loewenstine C, Gadzinski ER, Ayenu-Prah AY. Methods for assessing long-term mean pathogen count in drinking water and risk management implications. Journal of Water and Health, 2012; 10(2):197–208.
14. Grant SB. Virus coagulation in aqueous environments. Environmental Science & Technology, 1994; 28(5):928–933.
15. Teunis P, Lodder W, Heisterkamp S, de Roda Husman A. Mixed plaques: Statistical evidence how plaque assays may underestimate virus concentrations. Water Research, 2005; 39(17):4240–4250.
16. Teunis PF, Moe CL, Liu P, Miller SE, Lindesmith L, Baric RS, Le Pendu J, Calderon RL. Norwalk virus: How infectious is it? Journal of Medical Virology, 2008; 80(8):1468–1476.
17. Messner MJ, Berger P, Nappier SP. Fractional Poisson—A simple dose-response model for human norovirus. Risk Analysis, 2014; 34(10):1820–1829.
18. Schmidt PJ. Norovirus dose–response: Are currently available data informative enough to determine how susceptible humans are to infection from a single virus? Risk Analysis, 2014; 35(7):1364–1383.
19. Thurston-Enriquez JA, Haas CN, Jacangelo J, Gerba CP. Chlorine inactivation of adenovirus type 40 and feline calicivirus. Applied and Environmental Microbiology, 2003; 69(7):3979–3985.
20. Johnson NL, Kemp AW, Kotz S. Univariate Discrete Distributions, 3rd ed. Hoboken, NJ: John Wiley & Sons, 2005.
21. Adelson R. Compound poisson distributions. OR, 1966; 17(1):73–75.
22. Kemp C. "Stuttering-Poisson" distributions. Journal of the Statistical and Social Inquiry Society of Ireland, 1967; 21(5):151–157.
23. Puig P, Barquinero JF. An application of compound Poisson modelling to biological dosimetry. Proceedings of the Royal Society A, 2011; 467(2127):897–910.
24. Milne RK, Westcott M. Generalized multivariate Hermite distributions and related point processes. Annals of the Institute of Statistical Mathematics, 1993; 45(2):367–381.
25. Kemp C, Kemp AW. Some properties of the "Hermite" distribution. Biometrika, 1965; 52(3–4):381–394.
26. Kemp AW, Kemp C. An alternative derivation of the Hermite distribution. Biometrika, 1966; 53(3–4):627–628.
27. McKendrick A. Applications of mathematics to medical problems. Proceedings of the Edinburgh Mathematical Society, 1926; 44:98–130.
28. Gupta R, Jain G. A generalized Hermite distribution and its properties. SIAM Journal on Applied Mathematics, 1974; 27(2):359–363.
29. Feller W. An Introduction to Probability Theory and its Applications, vol. 2, 2nd ed. New York: John Wiley & Sons, 1971.
30. Zhang H, Liu Y, Li B. Notes on discrete compound poisson model with applications to risk theory. Insurance: Mathematics and Economics, 2014; 59(1):325–336.
31. Hadar J, Russell WR. Rules for ordering uncertain prospects. American Economic Review, 1969; 25–34.
32. Bawa VS. Optimal rules for ordering uncertain prospects. Journal of Financial Economics, 1975; 2(1):95–121.
33. Rothschild M, Stiglitz JE. Increasing risk: I. A definition. Journal of Economic Theory, 1970; 2(3):225–243.
34. Nakagawa T, Osaki S. The discrete Weibull distribution. IEEE Transactions on Reliability, 1975; 5:300–301.
35. Englehardt J, Swartout J, Loewenstine C. A new theoretical discrete growth distribution with verification for microbial counts in water. Risk Analysis, 2009; 29(6):841–856.
36. Seitz SR, Leon JS, Schwab KJ, Lyon GM, Dowd M, McDaniels M, Abdulhafid G, Fernandez ML, Lindesmith LC, Baric RS, Moe CL. Norovirus infectivity in humans and persistence in water. Applied and Environmental Microbiology, 2011; 77(19):6884–6888.
37. Atmar RL, Opekun AR, Gilger MA, Estes MK, Crawford SE, Neill FH, Ramani S, Hill H, Ferreira J, Graham DY. Determination of the 50 norwalk virus. Journal of Infectious Diseases, 2014; 209(7):1016–1022. Available at: http://jid.oxfordjournals.org/content/209/7/1016.abstract.
38. Frenck R, Bernstein DI, Xia M, Huang P, Zhong W, Parker S, Dickey M, McNeal M, Jiang X. Predicting susceptibility to norovirus gii. 4 by use of a challenge model involving humans. Journal of Infectious Diseases, 2012; 206(9):1386–1393.
39. Jones MK, Watanabe M, Zhu S, Graves CL, Keyes LR, Grau KR, Gonzalez-Hernandez MB, Iovine NM, Wobus CE, VinjÃ© J, Tibbetts SA, Wallet SM, Karst SM. Enteric bacteria promote human and mouse norovirus infection of b cells. Science, 2014; 346(6210):755–759. Available at: http://www.sciencemag.org/content/346/6210/755.abstract.
40. MATLAB. Version 8.1.0.604 (R2013a). Natick, MA: MathWorks Inc., 2013.

SUPPORTING INFORMATION

Additional supporting information may be found in the online version of this article at the publisher's website:

S.1. A compact review of the mathematical concepts, in particular probability generating functions, needed to fully understand the main article.
S.2. A collection of numerical examples to show how clustering may affect single-hit models when R is beta distributed, and how the Jensen bound performs in these examples.
S.3. A parallel to Propositions 1 and 2 for binomially distributed clusters.
S.4. A simple example to show that the conclusion from Proposition 1 (reduced risk from clustering) fails if the conditional dose-response model has a convex portion in the low-dose range, as in the 2-hit model.
S.5. A primitive generalization of the single-hit concept to account for the effects discussed in bullet point 3 in the introduction of the main article, i.e., if the host-pathogen interaction for each pathogen depends on that pathogen being part of a cluster or not.
S.6. A section to show how a single-hit risk estimate may be affected by misinterpreting clusters as single pathogen during enumeration, as discussed in bullet point 1 in the introduction to the main article.

Supporting Information to Paper II

SUPPORTING INFORMATION

This supplementary appendix contains the following:

S.1. A compact review of the mathematical concepts, in particular probability generating functions, needed to fully understand the main paper.
S.2. A collection of numerical examples to show how clustering may affect single-hit models when R is beta distributed, and how the Jensen bound performs in these examples.
S.3. A parallel to Propositions 1 and 2 for binomially distributed clusters.
S.4. A simple example to show that the conclusion from Proposition 1 (reduced risk from clustering) fails if the conditional dose-response model has a convex portion in the low-dose range, as in the 2-hit model.
S.5. A primitive generalization of the single-hit concept to account for the effects discussed in bullet point 3 in the introduction of the main paper, i.e. if the host-pathogen interaction for each pathogen depends on that pathogen being part of a cluster or not.
S.6. A section to show how a single-hit risk estimate may be affected by misinterpreting clusters as single pathogen during enumeration, as discussed in bullet point 1 in the introduction to the main paper.

S.1. Mathematical concepts

For reasons of self-containment, the very basics of probability generating functions and stuttering Poisson distributions is presented here. The material is covered in most mathematical statistics textbooks, e.g. the classics by Feller.[1,2]

Probability generating functions

A random variable whose support is $\mathbb{N}_0$, the set of non-negative integers, is called a *count* random variable. The probability generating function (pgf) G_X of any count random variable X is defined by the power series

$$G_X(z) = \mathrm{E}(z^X) = \sum_{x=0}^{\infty} p_X(x) z^x \tag{S.1}$$

whenever it exists, i.e. converges. Here $p_X(x) = \Pr(X = x)$ denotes the probability mass function (pmf) of X. The series converges for at least all complex $|z| \leq 1$. By the uniqueness of the power series representation of a function, a pmf is uniquely identified by its pgf. The coefficients $p_X(x)$ of z^x are those of a Taylor series and thus the pmf can be recovered as

$$p_X(x) = \frac{G_X^{(x)}(0)}{x!} = \frac{1}{x!} \left. \frac{d^x G_X}{dz^x} \right|_{z=0} \tag{S.2}$$

A new count random variable X may be constructed as a (possibly infinite) linear combination of *independent* count random variables X_n,

$$X = \sum_{n=1}^{\infty} a_n X_n = a_1 X_1 + a_2 X_2 + \cdots \tag{S.3}$$

where $a_n \in \mathbb{N}_0$ and $\sum a_n \geq 1$. The problem of finding the pmf of X when the sequence $\{a_n\}$ and the pmf of every X_n are known, is most easily tackled by means of pgfs. The utility of pgfs lies in the following result, which follows readily from the definition, for the pgf of the linear combination in (S.3):

$$G_X(z) = G_{X_1}(z^{a_1}) G_{X_2}(z^{a_2}) \cdots \tag{S.4}$$

In principle, the pmf of X can now be obtained by repeated differentiation of (S.4) with respect to z and setting $z = 0$, as in (S.2).

The pgf of a Poisson variable X_n with parameter λ_n is found by inserting the Poisson pmf from (3) into (S.1). The resulting series is easily recognized as

$$G_{X_n}(z) = e^{\lambda_n (z-1)} \tag{S.5}$$

Stuttering Poisson distributions

We begin with a definition:

Definition 1 (Compound and stuttering Poisson): Consider the sum

$$W = \sum_{m=1}^{M} Y_m \tag{S.6}$$

where the number of terms to be added is a Poisson distributed random variable M with parameter λ_M and Y_m, $m = 1, \ldots, M$, are independent and identically distributed variables that are also independent of M. For the case $M = 0$, W becomes the empty sum which is 0 by definition. The distribution of W is known as a *compound* Poisson distribution or Poisson-stopped sum. Furthermore, if the Y_m's are count random variables, the distribution of W is known as a *stuttering* Poisson distribution.

Assume from now that W is stuttering Poisson. By using the rule of total expectation, one can show that

the pgf of W is the pgf of M (which is Poisson) composed with the common pgf of the Y_m's:

$$\begin{aligned} G_W(z) =& \mathrm{E}(z^W) = \mathrm{E}(z^{\sum_{m=1}^{M} Y_m}) = \mathrm{E}\left(\prod_{m=1}^{M} z^{Y_m}\right) \\ =& \mathrm{E}_M\left[\mathrm{E}_{Y_1,\ldots,Y_M}\left(\prod_{m=1}^{M} z^{Y_m}\,|M\right)\right] \\ =& \mathrm{E}_M\left[\prod_{m=1}^{M} \mathrm{E}_Y\left(z^Y\right)\right] = \mathrm{E}_M\left\{[G_Y(z)]^M\right\} \\ =& G_M[G_Y(z)] = e^{\lambda_M[G_Y(z)-1]} \end{aligned} \tag{S.7}$$

where the subscript on E denotes expectation with respect only to the indicated variables and Y has the common distribution of the Y_m's.

Assume now that in (S.3), $a_n = n$ and every X_n is Poisson distributed with corresponding parameter λ_n. Equation (S.3) becomes

$$X = \sum_{n=1}^{\infty} nX_n = X_1 + 2X_2 + \cdots \tag{S.8}$$

which is the linear combination in equation (8) in Section 2.2. Using the Poisson pgf in (S.5) and the result from (S.4), the pgf of X in (S.8) becomes

$$\begin{aligned} G_X(z) =& e^{\lambda_1(z-1)}e^{\lambda_2(z^2-1)}\cdots \\ =& \exp\left(\sum_{n=1}^{\infty}\lambda_n(z^n-1)\right) \end{aligned} \tag{S.9}$$

In the following, we first obtain the pmf of this X before showing that X is actually a completely general stuttering Poisson distributed variable.

The pmf of stuttering Poisson distributions

Computing derivatives of (S.9) is cumbersome both analytically and numerically, and no general closed-form expression for the pmf exists. Fortunately, a more practically useful recurrence relation for the pmf can be derived. A simple proof of this was given by Kemp,[3] which we reproduce here with slightly more detail.

LEMMA 1: *The pmf of X in* (S.8) *can be expressed recursively as*

$$p_X(x) = \begin{cases} e^{-\sum_{n=1}^{\infty}\lambda_n} & \text{if } x = 0 \\ \dfrac{1}{x}\displaystyle\sum_{n=1}^{x} n\lambda_n p_X(x-n) & \text{if } x \geq 1 \end{cases} \tag{S.10}$$

Proof. For $x = 0$, we have simply $p_X(0) = G_X(0)$. For $x \geq 1$, we start by equating the definition of the pgf with the expression for G_X in (S.9):

$$\sum_{x=0}^{\infty} p_X(x)z^x = \exp\left(\sum_{n=1}^{\infty}\lambda_n(z^n-1)\right) \tag{S.11}$$

Taking logarithms and then differentiating with respect to z on both sides, we find

$$\left(\sum_{x=0}^{\infty} p_X(x)z^x\right)^{-1}\left(\sum_{x=0}^{\infty} xp_X(x)z^{x-1}\right) = \sum_{n=1}^{\infty} n\lambda_n z^{n-1} \tag{S.12}$$

We simplify, reorganize and relabel the index on one of the sums:

$$\left(\sum_{x=1}^{\infty} xp_X(x)z^{x-1}\right) = \left(\sum_{n=1}^{\infty} n\lambda_n z^{n-1}\right)\left(\sum_{s=0}^{\infty} p_X(s)z^s\right) \tag{S.13}$$

We equate the coefficients of terms of equal power with respect to z:

$$xp_X(x) = \sum_{s+n-1=x-1} n\lambda_n p_X(s) = \sum_{s=x-n} n\lambda_n p_X(s) \tag{S.14}$$

For any given $x \geq 1$, we may now express the latter sum by letting n run from 1 through x. This establishes the result:

$$p_X(x) = \frac{1}{x}\sum_{n=1}^{x} n\lambda_n p_X(x-n) \tag{S.15}$$

X in (S.8) *is stuttering Poisson*

LEMMA 2: *The distribution of X in equation* (S.8) *is that of a general stuttering Poisson distribution.*

Proof. The pgf in (S.9) may be rewritten

$$G_X(z) = \exp\left[\left(\sum_{n=1}^{\infty}\lambda_n\right)\left(\frac{\sum_{n=1}^{\infty}\lambda_n z^n}{\sum_{n=1}^{\infty}\lambda_n} - 1\right)\right] \tag{S.16}$$

The ratio is a power series with coefficients $\in [0,1]$ that sum to 1, i.e. it is a pgf. Comparing (S.16) with (S.7), we therefore find that X is stuttering Poisson distributed where M has Poisson parameter $\lambda_M = \sum_{n=1}^{\infty}\lambda_n$ and the pgf of Y is

$$G_Y(z) = \frac{\sum_{n=1}^{\infty}\lambda_n z^n}{\sum_{n=1}^{\infty}\lambda_n} \tag{S.17}$$

Note that in (S.9), the summation may be extended to include $n = 0$ without affecting the expression

since λ_0 cancels out. Thus, there is no loss of generality by summing from $n = 1$ above, and hence X is a *general* stuttering Poisson variable. The pmf of Y is easily derived by differentiating (S.17) repeatedly and using (S.2):

$$p_Y(y) = \begin{cases} 0 & \text{if } y = 0 \\ \dfrac{\lambda_y}{\sum_{n=1}^{\infty} \lambda_n} & \text{if } y \geq 1 \end{cases} \tag{S.18}$$

Moments of the stuttering Poisson distribution

We are interested in the expected value (μ), the variance (σ^2), the skewness (α_3) and the kurtosis (α_4) of X. These are most easily obtained using the *cumulant-generating function* (cgf) $g_X(t)$ of X. The reader may be more familiar with the moment-generating function (mgf) $M_X(t)$. The two are related through

$$g_X(t) = \ln[M_X(t)] \tag{S.19}$$

The mgf is also related to the pgf by

$$M_X(t) = G_X(e^t) \tag{S.20}$$

Combining (S.9), (S.19) and (S.20) yields the cgf for X:

$$g_X(t) = \sum_{n=1}^{\infty} \lambda_n (e^{nt} - 1) \tag{S.21}$$

The *cumulants* κ_i of X are obtained by

$$\kappa_i = \left. \frac{d^i g_X}{dt^i} \right|_{t=0} \tag{S.22}$$

After some algebra, the desired moments are obtained as

$$\mu = \kappa_1 = \sum_{n=1}^{\infty} n\lambda_n \tag{S.23}$$

$$\sigma^2 = \kappa_2 = \sum_{n=1}^{\infty} n^2\lambda_n \tag{S.24}$$

$$\alpha_3 = \frac{\kappa_3}{\kappa_2^{3/2}} = \frac{\sum_{n=1}^{\infty} n^3\lambda_n}{\left(\sum_{n=1}^{\infty} n^2\lambda_n\right)^{\frac{3}{2}}} \tag{S.25}$$

$$\alpha_4 = \frac{\kappa_4}{\kappa_2^2} = \frac{\sum_{n=1}^{\infty} n^4\lambda_n}{\left(\sum_{n=1}^{\infty} n^2\lambda_n\right)^2} \tag{S.26}$$

The negative binomial is stuttering Poisson

Finally it is ascertained that the negative binomial distribution is also stuttering Poisson. We do this by deriving the pgf of the negative binomial from the general expression for a stuttering Poisson pgf in (S.7). Assume that Y is logarithmic series distributed with parameter $0 < a < 1$. Its pgf is known as

$$G_Y(z) = \frac{\ln(1 - az)}{\ln(1 - a)} \tag{S.27}$$

Inserting this in (S.7), defining $b = a/(1 - a)$ and simplifying, we find

$$G_W(z) = (1 + b(1 - z))^{\frac{-\lambda_M}{\ln(b+1)}} \tag{S.28}$$

From a property of pgfs, we can find the mean λ of this W:

$$\lambda = \lim_{z \to 1^-} \frac{dG_W(z)}{dz} = \frac{\lambda_M b}{\ln(b + 1)} \tag{S.29}$$

Using this to eliminate λ_M from (S.28), we arrive at

$$G_W(z) = (1 + b(1 - z))^{\frac{-\lambda}{b}} \tag{S.30}$$

which is the pgf for the negative binomial distribution as parametrized in equation (12) in Section 2.3.

Combinatorial interpretation of stuttering Poisson distributions

We take a brief look at the problem of obtaining the pmf of a stuttering Poisson variable from a different perspective, in order to show more clearly why closed-forms are difficult. Let x denote an instance of the random variable X, x_n an instance of X_n and let n be finite, i.e. $n < N$. Instead of the pgf-approach, one can consider all possible combinations of x_n's that satisfy (S.8) for every x of interest. We have assumed that all the X_n's are mutually independent, so that the probability of seeing any given combination of x_n's can be written as $\prod_{n=1}^{N} \Pr(X_n = x_n)$. Since the occurrence of any two such combinations are disjoint events, $\Pr(X = x)$ is given by summing over all possible combinations:

$$\Pr(X = x) = \sum_{\text{all } \mathbf{x}_i} \left[\prod_{n=1}^{N} \Pr(X_n = x_n) \right] \tag{S.31}$$

where $\mathbf{x}_i$ is a non-negative integer solution $\{x_{n,i}\}_{n=1}^{N}$ of the equation

$$\sum_{n=1}^{N} n x_{n,i} = x_{1,i} + 2x_{2,i} + 3x_{3,i} + \cdots + N x_{N,i} = x \tag{S.32}$$

Solving this equation for $x = 0, 1, \ldots$ gives the pmf of X. The problem of solving it is known as

Table S1. Properties of the Poisson distribution compared with the stuttering Poisson. Note that $\lambda = \sum_{n=1}^{\infty} n\lambda_n$.

	Dispersed (Poisson)	Clustered (Stutt. Poisson)	Change
Key probabilities			
$\Pr(X = 0)$	$e^{-\lambda}$	$e^{-\sum_{n=1}^{\infty} \lambda_n}$	Increases
$\Pr(X = 1)$	$\lambda e^{-\lambda}$	$\lambda_1 e^{-\sum_{n=1}^{\infty} \lambda_n}$	Depends
$\Pr(X \geq 1)$	$1 - e^{-\lambda}$	$1 - e^{-\sum_{n=1}^{\infty} \lambda_n}$	Decreases
Moments			
Mean (μ)	λ	$\sum_{n=1}^{\infty} n\lambda_n$	None
Variance (σ^2)	λ	$\sum_{n=1}^{\infty} n^2\lambda_n$	Increases
Skewness (α_3)	$\lambda^{-1/2}$	$(\sum_{n=1}^{\infty} n^3\lambda_n)/(\sum_{n=1}^{\infty} n^2\lambda_n)^{\frac{3}{2}}$	Depends?
Kurtosis (α_4)	λ^{-1}	$(\sum_{n=1}^{\infty} n^4\lambda_n)/(\sum_{n=1}^{\infty} n^2\lambda_n)^2$	Depends?
Other spread measures			
Dispersion index (δ)	1	$(\sum_{n=1}^{\infty} n^2\lambda_n)/(\sum_{n=1}^{\infty} n\lambda_n)$	Increases
Zero inflation index (θ)	0	$1 - (\sum_{n=1}^{\infty} \lambda_n)/(\sum_{n=1}^{\infty} n\lambda_n)$	Increases

a *linear diophantine problem*. An attempt to apply Faa di Bruno's formula, which gives the higher-order derivatives of composite functions, to (S.9) leads to very similar problems. Obtaining the solutions to (S.32) numerically for moderately large x is a computationally intensive task. A recursive formula for the number of solutions has been published.[4]

Recursive formula to evaluate ${}_2F_1$ for large mean doses

In this work, we used the function *hypergeom* in the MATLAB Symbolic Math Toolbox[5] to compute the risk from the beta-neg.bin. model:

$$\mathrm{E}(P_1) = 1 - {}_2F_1(\lambda/b, \alpha; \alpha + \beta; -b) \tag{S.33}$$

For large values of the mean dose λ, *hypergeom* tends to be very slow or even fail. For this case, we used a recursive algorithm to compute ${}_2F_1$. We are thankful to user *uranix* on the mathematics section of StackExchange for pointing us to this solution, which is reproduced below. Introduce the notation ${}_2F_1(u_1, u_2; l_1; z)$. Our problem is thus with large u_1. A recursive formula exists that is useful for this situation (Abramowitz & Stegun,[6] formula 15.2.10):

$$\begin{aligned}&(l_1 - u_1){}_2F_1(u_1 - 1, u_2; l_1; z)\\ &+ (2u_1 - l_1 + (u_2 - u_1)z){}_2F_1(u_1, u_2; l_1; z)\\ &+ u_1(z - 1){}_2F_1(u_1 + 1, u_2; l_1; z) = 0\end{aligned} \tag{S.34}$$

If we define $G(u_1) = {}_2F_1(u_1, u_2; l_1; z)$, we may write

$$\begin{aligned}G(u_1 + 1) =& \frac{2u_1 - l_1 + (u_2 - u_1)z}{u_1(1 - z)} G(u_1)\\ &+ \frac{l_1 - u_1}{u_1(1 - z)} G(u_1 - 1)\end{aligned} \tag{S.35}$$

This may be used to compute $G(u_1)$ for large values of u_1 by starting from two initial values $G(u_1 - \lfloor u_1 \rfloor + 1)$ and $G(u_1 - \lfloor u_1 \rfloor + 2)$. These initial values could readily be computed by *hypergeom*. For comparison, the method were tested with parameter ranges that also allowed direct computation using *hypergeom* and results agreed to excellent precision.

S.2. Beta-distributed single-hit probabilities and clustering

The figures below are extensions of Figures 3 to 8 in the main article, included to show the effect of using a beta-distributed R in the respective risk comparisons. Since MATLABs *hypergeom* had difficulties tackling some combinations of parameter values that are integer powers of 10, the chosen parameter values have somewhat odd values. The number of parameter values were chosen to keep the computational time within reasonable bounds. The numerical precision in Figures S1 and S3 should not be trusted to be better than a couple of decimals.

The beta-Hermite model

The red numbers in Figure S1 are point values for the following ratio of the risk computed with the exact beta-Poisson to the risk computed with the

beta-Hermite model:

$$\frac{\mathrm{E}(P_{\mathrm{I}})}{\mathrm{E}(P_{\mathrm{I,He}})}=\frac{1-{}_1F_1(\alpha,\alpha+\beta,-\lambda)}{1-\frac{1}{B(\alpha,\beta)}\int_0^1 e^{-\lambda r(1-\frac{1}{2}q_2 r)}r^{\alpha-1}(1-r)^{\beta-1}\,\mathrm{d}r} \quad \text{(S.36)}$$

The integral in the denominator was difficult to evaluate numerically using available software because of the factor $e^{\frac{1}{2}\lambda q_2 r^2}$. Instead it was computed by truncating the following series expansion, usually requiring only a handful of terms to achieve excellent precision:

$$\begin{aligned}\mathrm{E}(P_{\mathrm{I,He}})&=1-\tfrac{1}{B(\alpha,\beta)}\int_0^1 e^{\frac{1}{2}\lambda q_2 r^2}e^{-\lambda r}r^{\alpha-1}(1-r)^{\beta-1}\,\mathrm{d}r\\ &=1-\tfrac{1}{B(\alpha,\beta)}\int_0^1\sum_{n=0}^{\infty}\tfrac{(\frac{1}{2}\lambda q_2)^n}{n!}r^{2n}e^{-\lambda r}r^{\alpha-1}(1-r)^{\beta-1}\,\mathrm{d}r\\ &=1-\tfrac{1}{B(\alpha,\beta)}\sum_{n=0}^{\infty}\tfrac{(\frac{1}{2}\lambda q_2)^n}{n!}\int_0^1 e^{-\lambda r}r^{2n+\alpha-1}(1-r)^{\beta-1}\,\mathrm{d}r\\ &=1-\tfrac{1}{B(\alpha,\beta)}\sum_{n=0}^{\infty}\tfrac{(\frac{1}{2}\lambda q_2)^n}{n!}B(2n+\alpha,\beta)\times\cdots\\ &\qquad\qquad {}_1F_1(2n+\alpha,2n+\alpha+\beta,-\lambda)\end{aligned} \quad \text{(S.37)}$$

The black numbers in Figure S1 are point values for the following ratio of the risk computed with the Jensen bound (with a beta-binomial conditional dose-response model) to the risk computed with the beta-Hermite model:

$$\frac{\mathrm{E}(P_{\mathrm{I,J}})}{\mathrm{E}(P_{\mathrm{I,He}})}=\frac{\left(1-e^{\lambda(\theta-1)}\right)\cdot\left(1-\frac{B\left[\alpha,\beta+\lambda/\left(1-e^{\lambda(\theta-1)}\right)\right]}{B(\alpha,\beta)}\right)}{1-\frac{1}{B(\alpha,\beta)}\int_0^1 e^{-\lambda r(1-\frac{1}{2}q_2 r)}r^{\alpha-1}(1-r)^{\beta-1}\,\mathrm{d}r} \quad \text{(S.38)}$$

The beta-neg.bin. model

The red numbers in Figure S2 are point values for the following ratio of the risk computed with the exact beta-Poisson to the risk computed with the beta-neg.bin. model:

$$\frac{\mathrm{E}(P_{\mathrm{I}})}{\mathrm{E}(P_{\mathrm{I,NB}})}=\frac{1-{}_1F_1(\alpha,\alpha+\beta,-\lambda)}{1-{}_2F_1(\lambda/b,\alpha;\alpha+\beta;-b)} \quad \text{(S.39)}$$

The black numbers in Figure S2 are point values for the following ratio of the risk computed with the Jensen bound (with a beta-binomial conditional dose-response model) to the risk computed with the beta-neg.bin. model:

$$\frac{\mathrm{E}(P_{\mathrm{I,J}})}{\mathrm{E}(P_{\mathrm{I,NB}})}=\frac{\left(1-e^{\lambda(\theta-1)}\right)\cdot\left(1-\frac{B\left[\alpha,\beta+\lambda/\left(1-e^{\lambda(\theta-1)}\right)\right]}{B(\alpha,\beta)}\right)}{1-{}_2F_1(\lambda/b,\alpha;\alpha+\beta;-b)} \quad \text{(S.40)}$$

The beta-discrete Weibull model

The red numbers in Figure S3 are point values for the following ratio of the risk computed with the exact beta-Poisson to the risk computed with the beta-discrete Weibull model

$$\frac{\mathrm{E}(P_{\mathrm{I}})}{\mathrm{E}(P_{\mathrm{I,dW}})}=\frac{1-{}_1F_1(\alpha,\alpha+\beta,-\lambda)}{1-\sum_{x=0}^{\infty}p_X(x)\frac{B(\alpha,\beta+x)}{B(\alpha,\beta)}} \quad \text{(S.41)}$$

where X is discrete Weibull distributed. The black numbers in Figure S3 are point values for the following ratio of the risk computed with the Jensen bound (with a beta-binomial conditional dose-response model) to the risk computed with the beta-discrete Weibull model

$$\frac{\mathrm{E}(P_{\mathrm{I,J}})}{\mathrm{E}(P_{\mathrm{I,dW}})}=\frac{\left(1-e^{\lambda(\theta-1)}\right)\cdot\left(1-\frac{B\left[\alpha,\beta+\lambda/\left(1-e^{\lambda(\theta-1)}\right)\right]}{B(\alpha,\beta)}\right)}{1-\sum_{x=0}^{\infty}p_X(x)\frac{B(\alpha,\beta+x)}{B(\alpha,\beta)}} \quad \text{(S.42)}$$

where X is discrete Weibull distributed. The numerical precision of the denominator in these equations was controlled by requiring the error bound $p_X(N)(1-P_X(N))$ on the truncation error ($x<N$) to be 1/1000 of the numerator (the Jensen bound). For $\theta=0.1$, the error bound was required to be less than 10^{-12}.

S.3. A result for binomially distributed clusters

The stuttering and mixed Poisson distributions considered in the main paper all prescribe a non-zero probability for any positive pathogen count. When taking a sample of volume v_{s} from a larger, fixed volume v that contains a finite number n_{b} of dispersed pathogens (e.g. a stock suspension in a laboratory), it can be argued that a natural model for the pathogen count is the binomial distribution with success probability $p=v_{\mathrm{s}}/v$ and number of trials n_{b}. The pgf of the binomial distribution is

$$G_{X_{\mathrm{b}}}(z)=[(1-p)+pz]^{n_{\mathrm{b}}} \quad \text{(S.43)}$$

If the suspension becomes clustered, the number of pathogens in a sample is given by

$$X=\sum_{i=1}^{k}iX_i=X_1+2X_2+\cdots+iX_i+\cdots+kX_k \quad \text{(S.44)}$$

where X_i is the number of i-clusters. The X_i's are independent and binomially distributed with equal p, but differing n_i's. The pgf of X is

$$G_X(z)=\prod_{i=1}^{k}[(1-p)+pz^i]^{n_i} \quad \text{(S.45)}$$

We assume that the means of X_{b} and X are equal, which implies that $n_{\mathrm{b}}=\sum_{i=1}^{k}in_i$. We want to

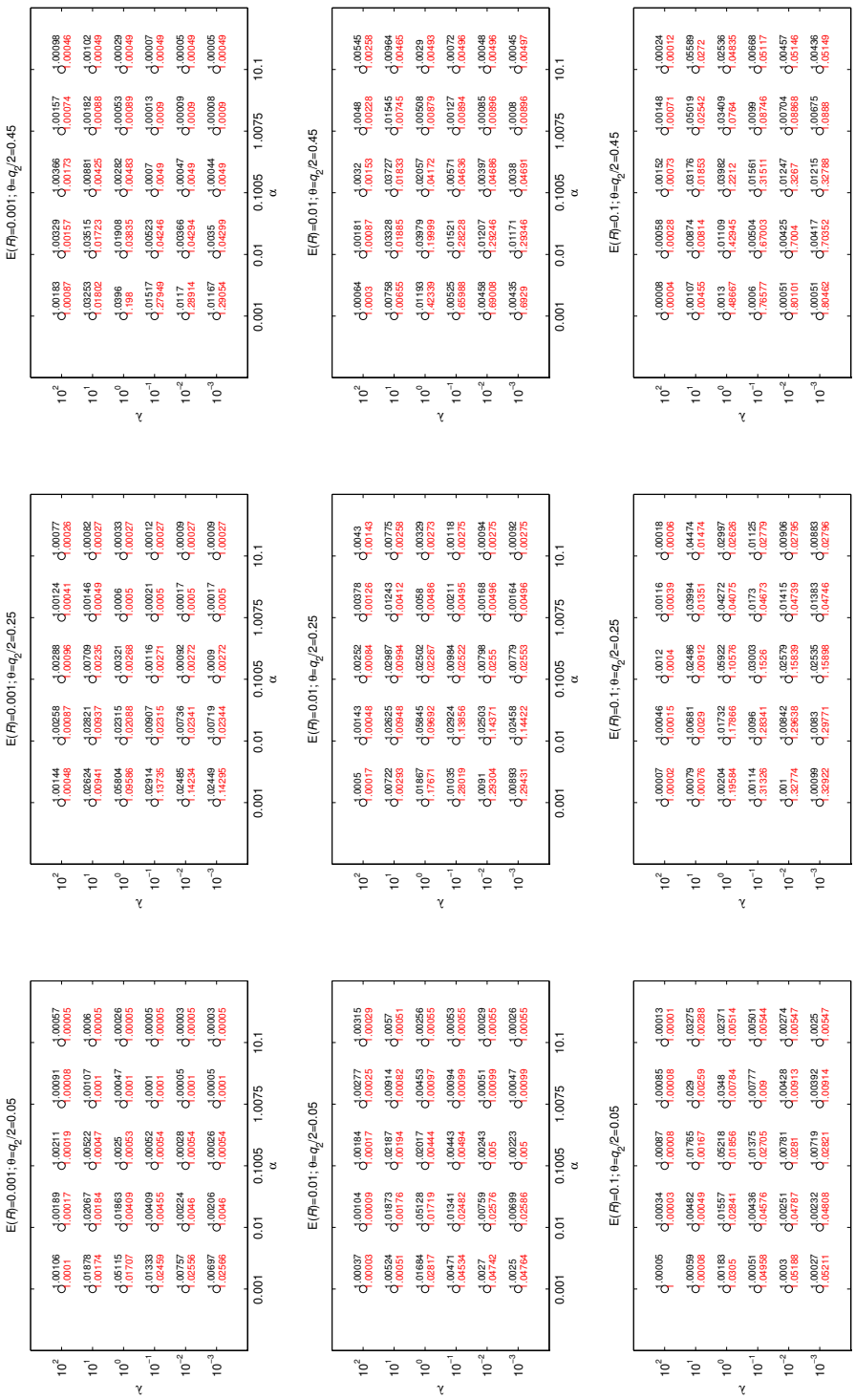

Fig. S1. Point values for the ratios in equations (S.36) and (S.38), respectively, comparing the risk computed with the exact beta-Poisson model (red numbers) and the Jensen bound (black numbers) to that computed with the Hermite model. q_2 is the proportion of pathogens in 2-clusters.

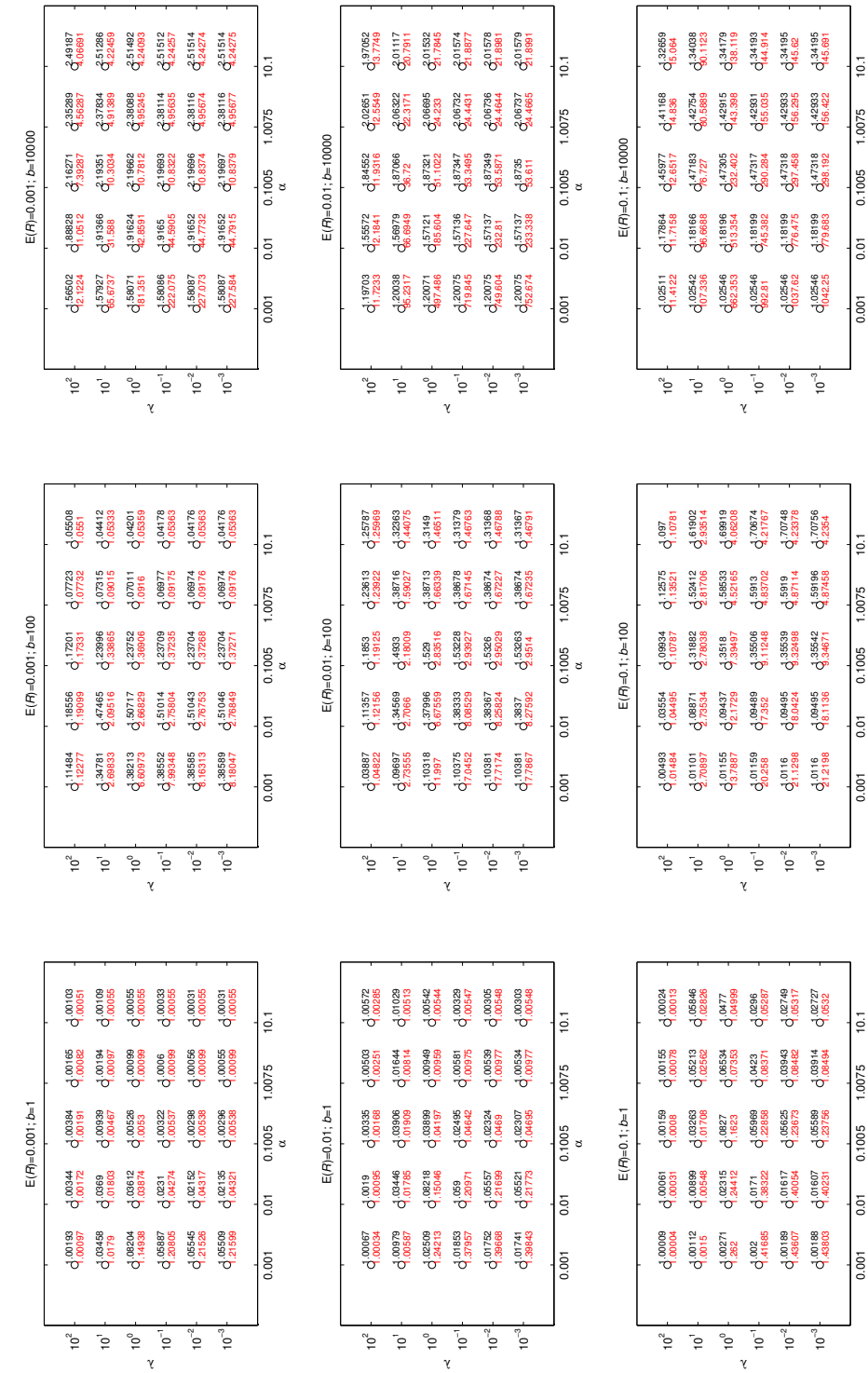

Fig. S2. Point values for the ratios in equations (S.39) and (S.40), respectively, comparing the risk computed with the exact beta-Poisson model (red numbers) and the Jensen bound (black numbers) to that computed with the neg.bin. model.

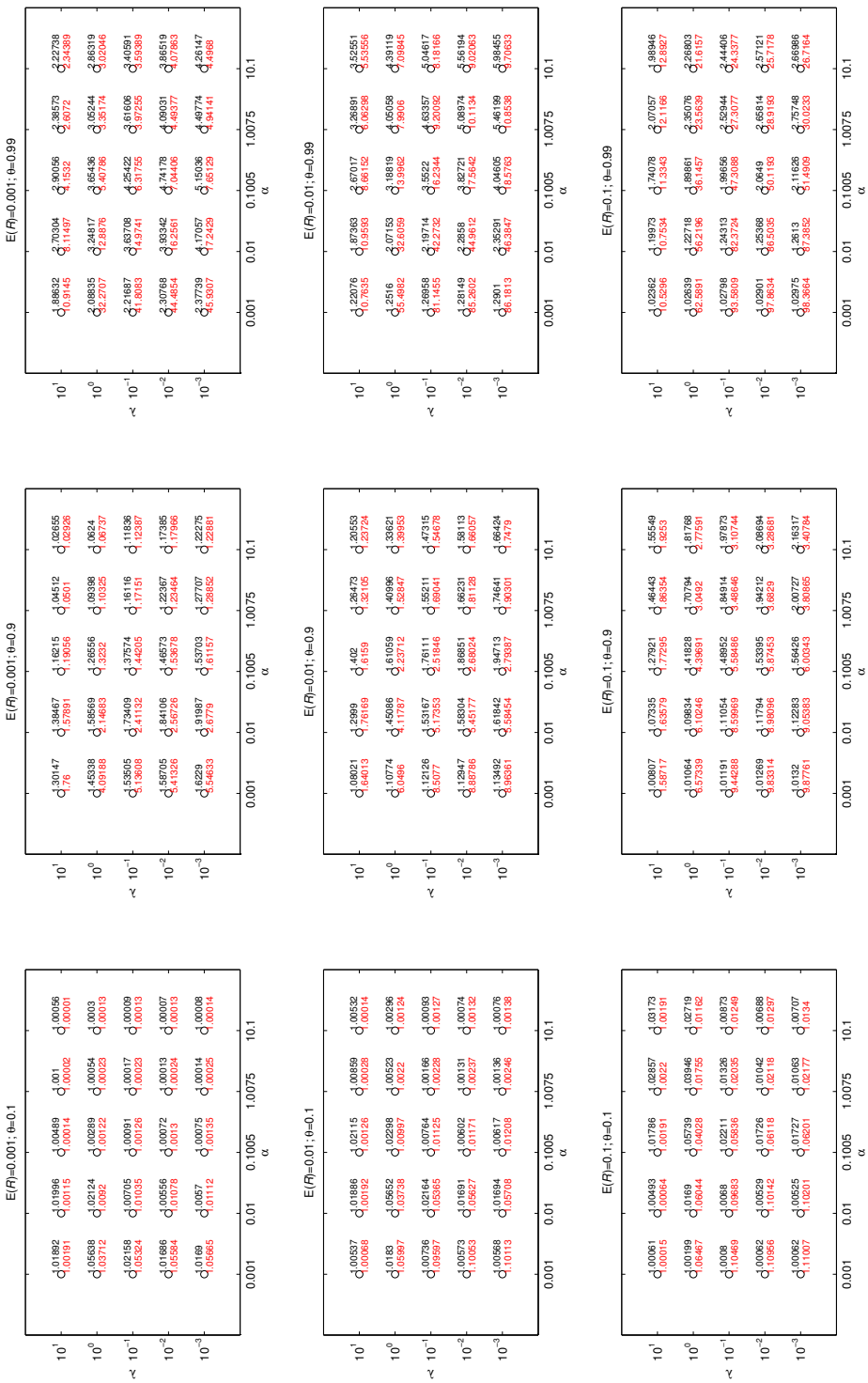

Fig. S3. Point values for the ratios in equations (S.41) and (S.42), respectively, comparing the risk computed with the exact beta-Poisson model (red numbers) and the Jensen bound (black numbers) to that computed with the discrete Weibull model.

show that the single-hit risk using X as the dose-distribution is less than the single-hit risk using X_{b} as the dose distribution. Proceeding as in the proof of Proposition 1, we need to show that the following quantity is positive for $0 \leq z < 1$ (corresponding to $0 < r \leq 1$ since $z = 1 - r$):

$$\begin{aligned}\Delta G &= G_X(z) - G_{X_{\mathrm{b}}}(z) \\ &= \prod_{i=1}^{k}[(1-p)+pz^i]^{n_i} - [(1-p)+pz]^{\sum_{i=1}^{k} in_i} \\ &= \prod_{i=1}^{k}[(1-p)+pz^i]^{n_i} - \prod_{i=1}^{k}[(1-p)+pz]^{in_i} \\ &= \prod_{i=1}^{k}[(1-p)+pf_i(z)]^{n_i} - \prod_{i=1}^{k}\{f_i[(1-p)+pz]\}^{n_i}\end{aligned} \tag{S.46}$$

Here, $f_i(z) = z^i$, which is a convex function on $[0, 1]$ for $i \geq 1$ and strictly convex for $i > 1$. The latter applies if there are some clusters. Therefore, by Jensen's inequality,

$$(1-p)+pf_i(z) > f_i[(1-p)+pz] \tag{S.47}$$

Thus, the first product in (S.46) is factor by factor larger than the second product and $\Delta G > 0$.

It may be noted that if n_{b} is itself a Poisson random variable with mean λ, then X_{b} becomes Poisson distributed with mean $p\lambda$. Also, in many cases the Poisson approximation to the binomial is very good. Thus, the difference between a binomially based model and a Poisson model may not be that relevant in practice.

S.4. Dependence between pathogens: Example

As the possibly simplest imaginable example of how clustering may impact the risk in a "non-single-hit" model, and how different this is from the single-hit case, we include Figure S4. This figure shows level curves for the following ratio (no host heterogeneity):

$$\begin{aligned}\frac{\mathrm{E}(P_{\mathrm{I}})}{\mathrm{E}(P_{\mathrm{I,cl}})} &= \frac{1 - G_{X_{\mathrm{Po}}}(1-r) + r\frac{\mathrm{d}}{\mathrm{d}r}G_{X_{\mathrm{Po}}}(1-r)}{1 - G_{X_{\mathrm{H}}}(1-r) + r\frac{\mathrm{d}}{\mathrm{d}r}G_{X_{\mathrm{H}}}(1-r)} \\ &= \frac{1 - e^{-\lambda r}(\lambda r + 1)}{1 - e^{-\lambda r(1-\frac{1}{2}q_2 r)}(\lambda r(1-q_2 r) + 1)}\end{aligned} \tag{S.48}$$

The numerator is the risk from a so-called 2-hit model[7] with Poisson distributed doses X_{Po},[7,8] and the denominator is the risk from the same model, but with Hermite distributed doses X_{H}. In such a 2-hit model, the host suffers an infection only if two or more pathogens succeed in establishing infectious foci, but the assumption of independent action is retained from the single-hit model. These are two somewhat contradictory and maybe implausible assumptions (generally not in agreement with human dose-response experimental data), but the resulting model may still serve as a primitive representation of *pathogen cooperation*, which tends to introduce a *convex* region in the low-dose range of the dose-response model. The figure shows a very different pattern compared to the single-hit model in Figure 3 in the main article. For the lowest doses, clustering *increases* the risk markedly. For high doses, clustering decreases the risk, although not by a large amount. For intermediate doses, there is a peak in the ratio, corresponding to a maximally decreased risk due to clustering. Intuitively, this happens when the mean of the dose distribution is close to the most concave region in the *conditional* dose-response model $\mathrm{E}_{R|X}(P_{\mathrm{I}})$.

The multiple-hit models, of which the 2-hit model above is a special case, may be formulated using pgfs in the following way. Let K, a random variable, be the number of pathogens that succeed in establishing infection after a given exposure event. Out of exactly x ingested pathogens, the probability that n or more (for an n-hit model) succeed in establishing infection is given by the binomial expression

$$\begin{aligned}\Pr(K \geq n) &= 1 - \sum_{k=0}^{n-1}\frac{x!}{k!(x-k)!}r^k(1-r)^{x-k} \\ &= 1 - \sum_{k=0}^{n-1}\frac{(-r)^k}{k!}\frac{\mathrm{d}^k}{\mathrm{d}r^k}(1-r)^x\end{aligned} \tag{S.49}$$

Marginalizing over the dose X, we find

$$\begin{aligned}\mathrm{E}(P_{\mathrm{I}}) &= \sum_{x=0}^{\infty}\Pr(K \geq n)p_X(x) \\ &= 1 - \sum_{k=0}^{n-1}\frac{(-r)^k}{k!}\frac{\mathrm{d}^k}{\mathrm{d}r^k}G_X(1-r)\end{aligned} \tag{S.50}$$

Generalizing to a variable hit-probability R is then straightforward in principle.

S.5. Generalization to independent clusters

Throughout our paper, we made the assumption of independently acting pathogens, even when the

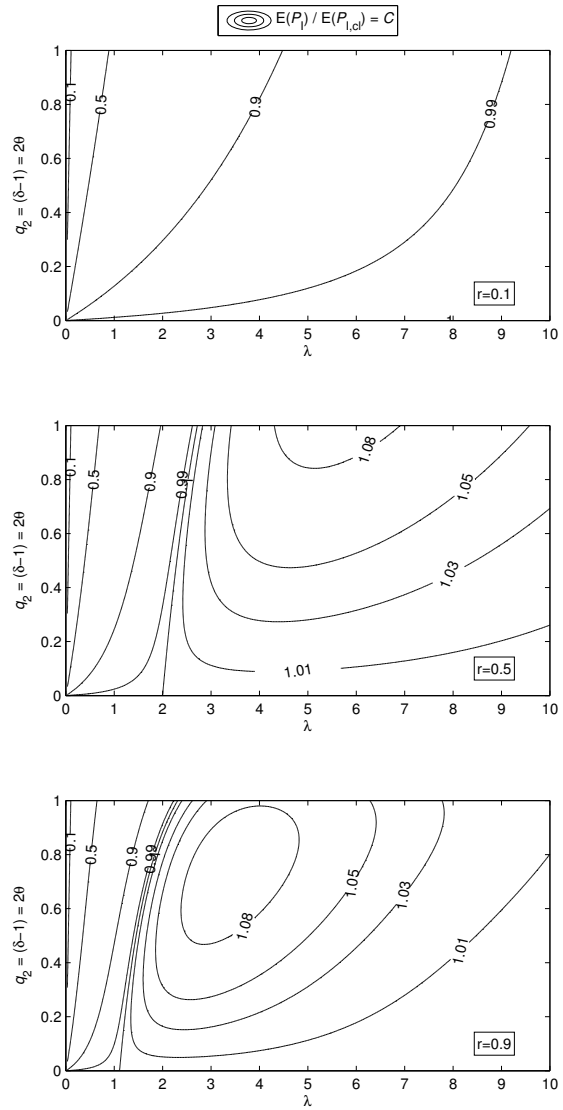

Fig. S4. Contour plot of the ratio in (S.48), comparing the risk computed with a 2-hit model with Poisson doses to that computed with the 2-hit model with Hermite doses. No host heterogeneity.

pathogens were part of a cluster of pathogens. As noted in the Introduction, this may not be a realistic assumption. In this section, we outline how the assumption can be generalized. Further work is needed to make this useful in practice, however, including specification of cluster-size distributions and specifying how the single-hit probability associated with a cluster depends on cluster size.

Equation (5), the single-hit risk with Poisson-distributed doses, may be written

$$\mathrm{E}(P_{\mathrm{I}}) = 1 - \int_0^1 e^{-\lambda r} f_R(r)\,\mathrm{d}r = 1 - M_R(-\lambda) \quad \text{(S.51)}$$

Here M_R is the moment-generating function (mgf) of R, defined by

$$M_R(t) \equiv \int_{-\infty}^{\infty} e^{tr} f_R(r)\,\mathrm{d}r = \int_0^1 e^{tr} f_R(r)\,\mathrm{d}r \quad \text{(S.52)}$$

where the latter equality is due to the compact support of R. In (S.51), the mgf is evaluated at the negative Poisson parameter.

The single-hit framework outlined in Section 2.1 may easily be generalized to a situation where pathogens are clustered by applying the list of assumptions to *individual clusters* instead of individual pathogens. Let R_n denote the probability that an individual n-cluster causes an infection and X_n the dose (number) of n-clusters in a water sample. Then we get for the general probability of infection, $P_{\mathrm{I,cl}}$

$$\begin{aligned} P_{\mathrm{I,cl}} =& 1 - (1-R_1)^{X_1}(1-R_2)^{X_2}(1-R_3)^{X_3}\cdots \\ =& 1 - \prod_{n=1}^{\infty}(1-R_n)^{X_n} \end{aligned} \quad \text{(S.53)}$$

where all the random variables involved are assumed to be mutually independent. The product in (S.53) is over all cluster sizes. The expectation value of (S.53) is

$$\begin{aligned} \mathrm{E}(P_{\mathrm{I,cl}}) =& 1 - \cdots \\ & \prod_{n=1}^{\infty}\int_0^1 \sum_{X_n=0}^{\infty}(1-r_n)^{X_n} p_{X_n}(x_n) f_{R_n}(r_n)\,\mathrm{d}r_n \\ =& 1 - \prod_{n=1}^{\infty}\int_0^1 G_{X_n}(1-r_n) f_{R_n}(r_n)\,\mathrm{d}r_n \end{aligned} \quad \text{(S.54)}$$

This is a general "single-hit" dose-response expression for a situation with clustering. It can serve as a starting point for analytical or numerical investigations (by postulating specific functions for f_{R_n} and G_{X_n}) on the effect of clustering on single-hit dose-response modeling, with allowance for cluster-size dependent single-hit probabilities.

With the natural assumption that every X_n is Poisson distributed with respective parameter λ_n,

equation (S.54) reduces to

$$\begin{aligned}\mathrm{E}(P_{\mathrm{I,cl}}) =& 1 - \prod_{n=1}^{\infty} \int_0^1 e^{-\lambda_n r_n} f_{R_n}(r_n)\,\mathrm{d}r_n \\ =& 1 - \prod_{n=1}^{\infty} M_{R_n}(-\lambda_n)\end{aligned} \tag{S.55}$$

This is to be compared with equation (5) for the completely dispersed situation, using a dose distribution with the same mean, i.e. $\lambda = \sum_{n=1}^{\infty} n\lambda_n$, and noting that $R = R_1$:

$$\mathrm{E}(P_{\mathrm{I}}) = 1 - M_{R_1}\left(-\sum_{n=1}^{\infty} n\lambda_n\right) \tag{S.56}$$

While equation (S.55) provides a starting point for theoretical analysis, it is less useful for real-world applications since it requires specification of the mean dose λ_n and corresponding distribution of single-hit probabilities f_{R_n} for *each* cluster size. In practice, we are restricted to working with either the total pathogen count X (with corresponding distribution f_R for *individual pathogens*) or the total cluster count X_{cl} (with corresponding distribution $f_{R_{\mathrm{cl}}}$ for *individual clusters* (regardless of cluster size)). Thus, there are only two practical options for the expression for $P_{\mathrm{I,cl}}$:

$$P_{\mathrm{I,cl}} = \begin{cases} 1-(1-R)^{X} & \text{for pathogens} \quad \text{(S.57)} \\ 1-(1-R_{\mathrm{cl}})^{X_{\mathrm{cl}}} & \text{for clusters} \quad \text{(S.58)} \end{cases}$$

The choice of which count (X or X_{cl}) to use and the possible effects of clustering on pathogen infectivity results in a range of possible dose-response models. Table S2 summarizes eight alternatives. In most cases, clustering necessarily induces a dependence relation between X and R, or between X_{cl} and R_{cl}, which complicates the dose-response expression significantly. Only two of the eight possibilities result in simple dose-response relationships where the dose and the single-hit probability are independent variables:

1. The single-hit probability of pathogens in a cluster is the same as if the pathogens were dispersed, i.e. $R_n = 1-(1-R)^n$. Inserting this in equation (S.53) gives equation (S.57):

$$\begin{aligned} P_{\mathrm{I,cl}} &= 1-(1-R)^{\sum_{n=1}^{\infty} nX_n} \\ &= 1-(1-R)^{X} \end{aligned} \tag{S.59}$$

$$\mathrm{E}(P_{\mathrm{I,cl}}) = 1 - \int_0^1 G_X(1-r) f_R(r)\,\mathrm{d}r \tag{S.60}$$

Thus, in this case, the only effect of clustering on the dose-response relationship is to alter the dose distribution so that it is not Poisson anymore. It is a priori non-trivial to predict what effect this will have on $\mathrm{E}(P_{\mathrm{I,cl}})$. It has been conjectured that $\mathrm{E}(P_{\mathrm{I,cl}})$ decreases[9] and this is confirmed analytically in Propositions 1 and 2 for stuttering Poisson and mixed Poisson dose distributions, respectively.

2. The single-hit probability of a cluster is the same as for a single dispersed pathogen, i.e. $R_n = R_{\mathrm{cl}} = R$. Inserting this in equation (S.53) gives equation (S.58) with $R_{\mathrm{cl}} = R$:

$$P_{\mathrm{I,cl}} = 1-(1-R)^{X_{\mathrm{cl}}} \tag{S.61}$$

$$\begin{aligned} \mathrm{E}(P_{\mathrm{I,cl}}) &= 1 - \int_0^1 G_{X_{\mathrm{cl}}}(1-r) f_R(r)\,\mathrm{d}r \\ &= 1 - M_R(-\lambda_{\mathrm{cl}}) \end{aligned} \tag{S.62}$$

Here, X_{cl} is Poisson distributed with parameter $\lambda_{\mathrm{cl}} = \sum_{n=1}^{\infty} \lambda_n$. Note also that, if equation (S.60) is the *correct* dose-response relationship, equation (S.62) can also be interpreted as the *erroneous* relationship that results if clusters are interpreted as single pathogens when microbes are enumerated, and vice versa.

S.6. Mistaking clusters as single pathogens

Figure 3 also applies to the following ratio

$$\frac{\mathrm{E}(P_{\mathrm{I}})}{\mathrm{E}(P_{\mathrm{I,err.}})} = \frac{1-e^{-\lambda r}}{1-e^{-\lambda r(1-\frac{1}{2}q_2)}} \tag{S.63}$$

when the vertical axis is interpreted as showing q_2 instead of $q_2 r$. The denominator in this expression is the risk obtained if the mean of the dose distribution is obtained by an enumeration error (interpreting clusters as single particles). It becomes significant for small r and λ, and large q_2. Since $q_2 > q_2 r$ (by a factor $1/r$), we see that, at least in this case, the enumeration error *underestimates* the true single-hit risk more than the failure to account for clustering *overestimates* it, i.e. $|\mathrm{E}(P_{\mathrm{I}}) - \mathrm{E}(P_{\mathrm{I,err.}})| > |\mathrm{E}(P_{\mathrm{I}}) - \mathrm{E}(P_{\mathrm{I,cl}})|$. In other words, for a precise (as well as conservative) risk estimate, it is more important to use a correct mean than accounting for clustering.

Table S2. Categorization of dose-response models for clustering, as expressed in equations (S.57) and (S.58).

			Count used	
			Total pathogens X X is not Poisson	Total clusters X_{cl} X_{cl} is Poisson
Infectivity postulate	Infectivities of individual clusters are mutually independent, but dependent on cluster-size; $R_n = g(n)$	Cluster infectivity as if pathogens were dispersed; $R_n = 1-(1-R)^n$	*R and X are independent.*	*R_{cl} and X_{cl} are dependent; joint distribution determined only by clustering state.*
		Increased cluster infectivity; $R_n > 1-(1-R)^n$	*R and X are dependent; joint distribution determined by $g(n)$ and clustering state.*	*R_{cl} and X_{cl} are dependent; joint distribution determined by $g(n)$ and clustering state.*
		Decreased cluster infectivity; $R_n < 1-(1-R)^n$	*R and X are dependent; joint distribution determined by $g(n)$ and clustering state.*	*R_{cl} and X_{cl} are dependent; joint distribution determined by $g(n)$ and clustering state.*
	Infectivities of individual clusters are mutually independent and independent of cluster-size; $R_n = R_{\mathrm{cl}} = R$		*R and X are dependent; joint distribution determined only by clustering state.*	*R_{cl} and X_{cl} are independent.*

REFERENCES

1. Feller W. An Introduction to Probability Theory and its Applications, vol. 1. 3rd ed., New York: John Wiley & Sons, 1968.
2. Feller W. An Introduction to Probability Theory and its Applications, vol. 2. 2nd ed., New York: John Wiley & Sons, 1971.
3. Kemp C. "Stuttering-Poisson" distributions. Journal of the Statistical and Social Inquiry Society of Ireland, 1967; 21(5):151–157.
4. Mahmoudvand R, Hassani H, Farzaneh A, Howell G. The exact number of nonnegative integer solutions for a linear diophantine inequality. IAENG International Journal of Applied Mathematics, 2010; 40(1):1–5.
5. MATLAB. Version 8.1.0.604 (R2013a). Natick, Massachusetts: The MathWorks Inc., 2013.
6. Abramowitz M, Stegun IA. Handbook of Mathematical Functions with Formulas, Graphs, and Mathematical Tables. No. 55 in National Bureau of Standards Applied Mathematics Series, New York: Dover Publications, 1964.
7. Haas CN, Rose JB, Gerba CP. Quantitative Microbial Risk Assessment. New York: John Wiley & Sons, 1999.
8. Nilsen V, Wyller J. QMRA for Drinking Water: 1. Revisiting the Mathematical Structure of Single-Hit Dose-Response Models. Risk Analysis, 2016; 36(1):145–162.
9. Haas CN. Conditional Dose-Response Relationships for Microorganisms: Development and Application. Risk Analysis, 2002; 22(3):455–463.

Paper III

Nilsen, V., E. Christensen, L. Molstad, M. Myrmel, and A. Heistad (2016). "Spatio-temporal dynamics of virus removal in dual-media contact-filtration for drinking water: Experimental results and inverse modeling." Manuscript in preparation.

Spatio-temporal dynamics of virus removal in dual-media contact-filtration for drinking water: Experimental results and inverse modeling

Vegard Nilsen[a,*], Ekaterina Christensen[b], Lars Molstad[c], Mette Myrmel[b], Arve Heistad[a]

[a]*Norwegian University of Life Sciences, Dept. of Mathematical Sciences and Technology, P.O.Box 5003, N-1432 Aas, Norway*
[b]*Norwegian University of Life Sciences, Dept. of Food Safety and Infection Biology, P.O.Box 8146 Dep, N-0033 Oslo, Norway*
[c]*Norwegian University of Life Sciences, Dept. of Environmental Sciences, P.O.Box 5003, N-1432 Aas, Norway*

Abstract

Microorganism removal rates in deep-bed filters vary with time and depth in the filter bed as the filter collects particles. Improved knowledge of such dynamics is relevant for the design, operation and microbial risk assessment of filtration processes for drinking water treatment. Here we report on a high-resolution spatio-temporal characterization of virus and bacteria removal in a pilot-scale dual-media filter, operated in contact-filtration mode. Bacteriophage *Salmonella* typhimurium 28B was enumerated by plaque assay (n=154), fRNA bacteriophage MS2 was enumerated both by plaque assay (n=17) and RT-qPCR (n=78), and a bacterial reference *E.coli* was enumerated by Colilert-18 (n=73). Microscopic and macroscopic filtration models were used to investigate and characterize the removal dynamics.

Results show that ripening and breakthrough fronts for turbidity, viruses and *E.coli* progressed in a wave-like manner down the filter column. Virus removal improved continuously throughout the filter cycle and broke through almost simultaneously with turbidity. *E.coli* removal continued to improve well past the turbidity ripening phase, but broke through mid-cycle. Instantaneous log-removal rates peaked at 3.2, 3.0 and 4.5 for 28B, MS2 and *E.coli*, respectively. However, true average log-removal rates throughout the cycle was significantly lower at 2.5, 2.3 and 3.6, respectively. Observed filter coefficients λ were significantly higher than predicted by ideal filtration theory and suggests that all microorganisms were to a large extent floc-bound. This study demonstrates the importance of carefully designed sampling regimes when characterizing microorganism removal efficiencies of deep-bed filters. The implications for microbial risk assessment are explored in parallel work.

Keywords:
drinking water, filtration, virus, dynamics, modeling

1. Introduction

Provision of hygienically safe drinking water is an essential part of public health protection across the world (World Health Organization, 2011). Waterborne microorganisms of concern include pathogenic viruses, bacteria and protozoan parasites, which may reach a point of consumption either by entering raw water sources and overcoming treatment barriers (Mac Kenzie et al., 1994) or by post-treatment introduction into a distribution system (Nygård et al., 2007). Treatment barriers include dedicated disinfection processes as well as general particle separation processes (Hijnen and Medema, 2010). Traditionally, most larger water treatment plants employ some combination of coagulation and deep-bed filtration for particle separation.

However, viruses may be relatively difficult to remove in particle separation processes (Hijnen and Medema, 2010) and some may be quite resistant to inactivation by disinfection (e.g. Thurston-Enriquez et al., 2003). In fact, enteric viruses have been found in finished drinking water on several occasions (Keswick et al., 1984; Rose et al., 1986; Payment and Armon, 1989). Therefore, in a multiple-barrier approach to microbial water quality, operational optimization and good estimates of virus removal efficiencies of each unit process are needed. Virus removal during filtration, and its relationship to turbidity, was recently identified as a knowledge gap in microbial risk assessment (Petterson and Ashbolt, 2016).

Since typical Norwegian surface waters are low in turbidity, but high in natural organic matter (NOM) most plants are designed as direct filtration or contact filtration plants (Ødegaard et al., 1999, 2010), i.e. filtration without a preceding sedimentation step. A coagulation-filtration system that meets specific regulatory requirements, mainly with respect to effluent turbidity, color and residual coagulant content, is recognized as a *hygienic barrier* in Norwegian regulations and assumed to be capable of removing viruses, bacteria and parasites by 3, 3 and 2 $\log_{10}$-units, respectively. However, guidelines issued by the Norwegian water industry association (Ødegaard et al., 2016), partly modeled on the USEPA Surface Water Treatment Rule (USEPA, 2006), only credit direct filtration systems with a log-removal capacity for viruses of 1.5 if effluent turbidity is < 0.2 NTU, or 2 if enhanced coagulation is used with effluent turbidity < 0.1 NTU and color removal is better than 70 %. A recent report (Eikebrokk, 2012) in Norway recommended that

*Corresponding author. Tel.: +47 930 94 406
Email address: vegard.nilsen@nmbu.no (Vegard Nilsen)

the virus removal efficiency of contact-filtration processes in particular be investigated in greater detail.

The deep-bed filtration process is inherently dynamic, even when the influent water quality is stable: filter performance vary with time and depth in the filter bed as the filter collects particles (Adin and Rebhun, 1974; Tien and Ramaro, 2007). Although there is usually a prolonged period of stable effluent turbidity after ripening and before breakthrough, the performance with respect to individual particle types, such as microorganisms, may be more dynamic than for turbidity (e.g. Clark et al. (1992)) and is important for determining optimal filter operation to minimize pathogen passage (Huck et al., 2001). The process is also periodic and discontinuous since regular backwashing is required to restore the particle removal capacity. Hence, average removal efficiencies during filtration may be challenging to estimate or, at worst, insufficient for characterizing health risks since the temporal variation in pathogen concentrations may be needed for a proper quantitative microbial risk assessment (QMRA; Haas et al., 2014).

The dynamic characteristics of the process imply that frequent sampling is needed in order to capture the full variation and allow true average removal efficiencies to be computed.[1] However, high-resolution spatio-temporal characterization of virus removal efficiency in deep-bed filters has hardly been undertaken, with most studies relying only on samples from the filter outlet at relatively coarse time intervals. Presumably, this is partly due to the cost and labor-intensive experiments that are needed for a detailed characterization. Obtaining more complete characterizations of the virus removal efficiency could lead to a better understanding of the virus removal dynamics, which could subsequently inform QMRA studies and decisions on the design and operation of deep bed filters.

Tables B.6 and B.7 in the online supporting material give a summary of 24 previous studies on virus removal in deep-bed filtration for drinking water where coagulation was employed at some point upstream of the filter (in general, very poor removal is observed if coagulation is not employed). The results vary significantly, from almost no removal to more than 5 log-removal. While it is difficult to pinpoint the exact reasons for this variation in each case, differences between virus types certainly may play a role, and it is obvious that the conditions under which the results were obtained also varied significantly. There appears to be a trend in that removal efficiencies obtained from full-scale studies are lower than those observed at pilot or bench scale. Workers who compared different filter configurations (depth, media, filtration rates) under otherwise similar conditions found only moderate differences in removal. Some workers investigated removal during ripening and/or breakthrough periods and found prolonged ripening for viruses compared to turbidity (Robeck et al., 1962) and reduced removal during these periods (Templeton et al., 2007). Templeton et al. (2007) also suggested that the degree of virus-particle-association, relevant for downstream disinfection processes, may vary during a filter cycle. Except for Templeton et al. (2007), which sampled mid-cycle from the interface between anthracite and sand media, none of the 24 studies that were found sampled from multiple levels of the filter column.

[1] Mean removal may also be obtained through continuous flow-proportional sampling, but this provides no information on temporal variation in removal efficiency.

Table 1: Filter material physical data, based on the respective manufacturer's information.

Parameter	**Filtralite**	**Rådasand**
Layer depth (m)	0.79	0.5
Grain size, nom. range (mm)	0.8-1.6	0.4-0.8
Effective grain size, d_{10} (mm)	0.95	0.4
Column diameter/d_{10} (-)	105	250
Uniformity coefficient, d_{60}/d_{10} (-)	< 1.5	< 1.8
Primary porosity (-)	0.58	0.45
Bulk porosity (-)	0.80	0.45
Grain density (kg/m^3)	1260	2600
Bulk density (kg/m^3)	530	1440

The purpose of the present study was therefore to undertake a detailed, high-resolution experimental investigation of a pilot-scale dual-media contact-filtration system with respect to virus removal throughout the entire filter column and the whole filtration cycle. A tailor-made automatic sampler was constructed to facilitate controlled, consistent and simultaneous sampling from eight levels of the filtration column without significantly disturbing the system hydraulics and thereby filtration behavior. Two model bacteriophages, *Salmonella* Typhimurium 28B and f-specific bacteriophage MS2 were used, while *E.coli* was also included as a bacterial reference. Measures were taken to characterize potential aggregation effects and account for known virucidal/inhibitory effects of the polyaluminium-chloride coagulant (Kreißel et al., 2014; Willumsen, 2015), which A subgoal of the project was to produce data that were suitable for fitting a dynamic filtration model through inverse modeling, and use this to characterize virus removal and the relationship between virus removal and overall particle removal, ideally providing opportunities for crude extrapolation to other experimental settings. Further implications of filtration dynamics for QMRA s explored in parallel work (Nilsen, 2016).

2. Materials and experimental methods

2.1. Pilot-plant design

An overview of the pilot-plant is given in Figure 1. The filter column was made from a transparent PVC cylinder with 10 cm inner diameter. A 10 cm deep support layer with graded gravel covered the outlet, a tapered plastic cone with slits. The bottom filter medium consisted of 50 cm of 0.4-0.8 mm silica sand (Rådasand AB, Sweden). The top filter medium consisted of 79 cm of 0.8-1.6 mm expanded clay aggregates (Filtralite NC - normal density, crushed; Weber Saint-Gobain, Norway). Filtralite has been shown to produce similar filtrate quality as anthracite, but with slightly slower headloss development (Eikebrokk and Saltnes, 2001). The physical characteristics of the filter media, as specified by the manufacturers, are given in Table 1. The ratio of column diameter to effective grain size was greater than 50, the recommended minimum ratio to minimize wall effects

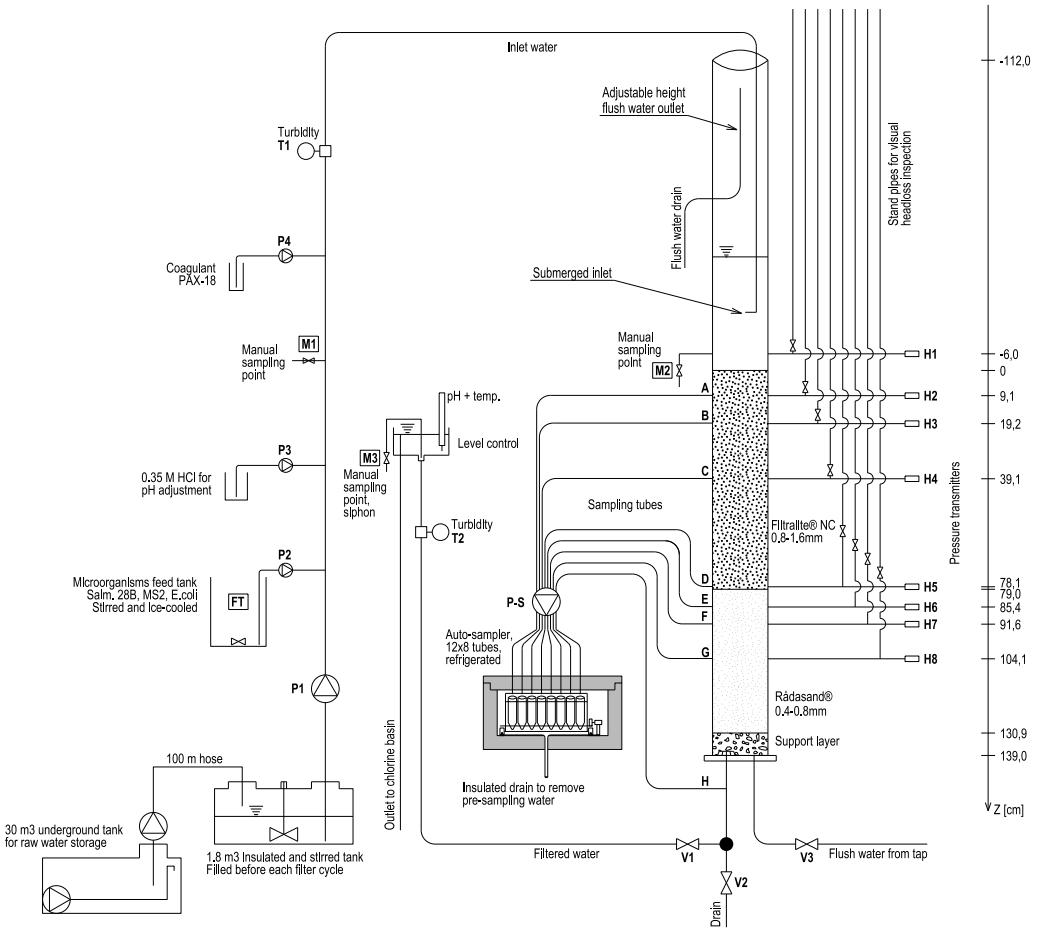

Figure 1: Schematic overview of the pilot-scale filtration plant. Manual sampling points are labeled with text boxes.

(Mehta and Hawley, 1969; Lang et al., 1993). This media configuration was chosen since it is used at the water treatment plant Nedre Romerike Vannverk (NRV), Strømmen, Norway, with whom we collaborated on this study.

Raw water was stored in a 30 m^3 underground tank equipped with a circulation pump. Prior to a filter run, a batch of raw water was pumped from the underground tank into a smaller steel tank (1.8 m^3, with a paddle stirrer) in the laboratory. Water was fed from the steel tank at a constant rate by feed pump P1 (Watson Marlow 620U hose pump with 620RE4 pump head and LoadSure 12 mm tubing) and entered the column through a (mostly) submerged pipe. The hydraulic head on the effluent side of the column was kept constant by a container with an overflow; thus the filter was operated in constant rate, rising head mode. Tap water was used for backwashing, with the flow rate controlled manually with a tap.

The microorganism suspension, hydrochloric acid (HCl, for pH adjustment) and polyaluminium chloride (PACl) coagulant (PAX-18, Kemira AS) were added with peristaltic dosing pumps (Watson Marlow 120U/DV with 114DV pump head) P2, P3 and P4, respectively. Venturi-type devices with sudden contraction and expansion were used to generate turbulence for rapid mixing. Online turbidimeters (WTW Visoturb 700 IQ) were installed on both the influent and effluent sides of the column, and calibrated for in-pipe-installation according to the manufacturer's instructions. An online pH-meter and temperature sensor (WTW SensoLyt 700 IQ) was installed on the effluent side in the overflow container. Eight online pressure transmitters H1-H8 (Impress IMP-LR 250 mbar) were installed with non-uniform spacing in order to focus data collection from the portions of the filter where the largest hydraulic gradients were expected to occur. Hydraulic head could also be visually inspected in eight standpipes. A LabView application (National Instruments, USA), communicating with sensors/valves/pumps through a micro-controller, was used for control, monitoring and logging of recorded data.

Ports for automated water sampling (A-H) were installed directly opposite the ports for pressure monitoring (A-G) and in the column outlet (H). Ports A-G contained a cylinder protruding about 15 mm into the filter media in order to minimize the influence of wall effects during sampling. The automatic sampler consisted of an 8-channel peristaltic pump (Ismatec ISM843A) that directed samples into a refrigerated (approx. 4 degrees Celsius), insulated box. The box contained a moving tube rack, controlled by an optical sensor and electrical motor, for sample collection and storage. Sampling tubes were cut to equal length and prior to each sampling event, three tube volumes would be drained to waste before actual sampling com-

menced. The insulated box could take 12 sets of samples, each consisting of eight 50 ml centrifuge tubes, i.e. 96 samples.

In addition to the automated samples, manual samples could be taken from locations M1 and M2 (before and after addition of coagulant, for assessment of possible aggregation and virucidal/inhibitory effects of the coagulant) as well as from the outlet M3. Manual samples could be taken more frequently than the automatic samples and allowed better monitoring of the ripening and breakthrough periods. Samples could also be taken from the microorganism feed tank (FT).

2.2. Microorganisms

2.2.1. MS2

F-specific bacteriophage MS2 is a 27 nm icosahedral single-stranded RNA virus (Strauss and Sinsheimer, 1963). It was included in this study since it is commonly used as a surrogate for pathogenic viruses when assessing the performance of water treatment processes. It was propagated according to ISO 10705-1 (ISO, 1995) against the host *Salmonella* Typhimurium WG49 (NCTC 12484). Most MS2 enumerations were performed using reverse transcription quantitative polymerase chain reaction (RT-qPCR), but a few samples were enumerated using a plaque assay.

Previous studies (Matsui et al., 2003; Matsushita et al., 2011; Kreißel et al., 2014) as well as preliminary investigations for this study have shown that PACl coagulants have a virucidal effect on f-specific phages like MS2, even at low doses, as measured by a reduced infectivity in plaque assays. Kreißel et al. (2014) attributed the effect to inactivation as a result of interaction between MS2-surfaces and dissolved polymeric aluminium species Al_{13}. In order to decrease the impact of this effect in the present study, the method of Matsushita et al. (2004) was performed prior to plaque assay, with some modifications. A solution of beef extract and urea (BE+U) was prepared by mixing solutions (1:1 v/v) of 13 % BE powder (211520, Becton, Dickinson and Company, USA) with 9.6 % sterile U (Merck, Germany) and adjusted to pH 9.5-10.0 with 5 N NaOH. The solution was stored at +4°C and used within three days. All MS2 samples were diluted 10-fold with BE+U and stirred at 1500 rpm at 4°C for a minimum of 5 hours. The plaque assay for MS2 was then performed on the treated samples as described by Debartolomeis and Cabelli (1991), using *Escherichia coli* Famp as the host.

For RT-qPCR, viral RNA was extracted from 140 μl water samples with the QIAamp Viral RNA Mini kit and QIAcube automated purification system according to the manufacturer's (Qiagen, Germany) instructions with minor modifications: the samples were stored in 560 μl lysis buffer at -80°C and were spiked with carrier-RNA (3.1 μg per sample) prior to RNA-extraction. RT-qPCR was performed in a Stratagene AriaMx Real-Time PCR System (Agilent Technologies, USA) using the RNA UltraSense One-Step Quantitative RT-PCR System kit (Invitrogen, USA). 3 μl RNA was used in a total volume of 20 μl, using primers and probe as listed in Table 2. The temperature sequence was 30 min at 55°C, 2 min at 95°C, 45 cycles of 15 sec at 95°C and 30 sec at 58°C. Each sample was run in duplicate. ROX was used as passive fluorescence reference and positive and negative (no template) controls were included on each plate. Aliquoted homologous RNA was also included on all plates and used as an inter-plate calibrator (IPC).

Table 2: Primers and probe sequences for MS2 RT-qPCR analyses. Retrieved from Dreier et al. (2005) with some modifications.

Primers and probe	**Sequence**
MS2-TM2-F (400 nM)	TGCTCGCGGATACCCG
MS2-TM2-R (400 nM)	AACTTGCGTTCTCGAGCGAT
MS2-TM2FAM (50 nM)	ACCTCGGGTTTCCGTCTTGCTCGT

Baseline correction was performed automatically by the Agilent AriaMx 1.1 Software (Agilent Technologies, USA). Interplate calibration (Hellemans et al., 2007) was performed by setting the threshold for each plate individually so as to make the mean C_q-values (quantification cycles) for the IPCs equal, while ensuring that all thresholds were in the exponential region of the amplification curves. One of the plates included a 10-fold serial dilution series of homologous viral RNA, run in triplicate, for determination of the amplification efficiency E ($E = 88.7\%; R^2 = 99.8\%$), which was assumed to be equal among plates. Under these conditions, the ratio of concentrations c_2/c_1 in any two samples (same or different plates), indexed by 1 and 2, is given by the qPCR equation

$$\frac{c_2}{c_1} = (1+E)^{C_{q,1}-C_{q,2}} \tag{1}$$

The absolute amount of RNA used for the serial dilution was not known, but only the ratios from (1) are needed to compute removal efficiencies as presented in Section 3.

Preliminary experiments were performed to test for potential interference effects of the coagulant with the PCR assay. Distilled water was spiked with MS2 (control) and also with coagulant (samples). No interference effects were observed for coagulant concentrations up to 10 mg/l.

2.2.2. Salmonella typhimurium 28B

Salmonella typhimurium phage 28B (Lilleengen, 1948) is an icosahedral double-stranded DNA bacteriophage with a baseplate that extends approximately 10 nm from its 50 nm diameter head (Svenson et al., 1979). The phage does not occur naturally in the environment and has been shown to be heat resistant (Sahlström et al., 2008). Also, stock suspensions can be kept for years at refrigeration temperatures without significantly loosing the titer. It was included in this study for its relatively simple and robust propagation and enumeration protocol.

The phage was propagated and enumerated according to an unpublished protocol from the Public Health Agency of Sweden, but essentially as described by Höglund et al. (2002) and equivalent to ISO (1999), using its host strain *Salmonella enterica* subsp. *enterica* Typhimurium type 5. The growth medium consisted of distilled water with nutrient broth (0.8 % w/v; 105443, Merck, Germany) and yeast extract (0.05 % w/v; 111926, Merck, Germany). For propagation, 10 ml/l of chloroform were added to kill and lyse the host cells after incubation.

The suspension was then centrifuged for 10 minutes at 3000rpm and filtered through a 0.45μm filter. The final concentration was determined to be $5 \cdot 10^9$ PFU/ml (plaque forming units/ml).

Enumeration was performed as a double-layer agar plaque assay. Petri dishes with 20 ml solid bottom-agar (growth medium with 1.5 % w/v agar) were prepared. Four ml molten top-agar (growth medium with 0.65 % w/v agar) was mixed with 0.5 ml sample (after serial dilution in 0.9 % NaCl, when required) and 0.5 ml exponential-phase host culture and poured over the solid agar. Samples were incubated at 37°C for approx. 18 hours and plaques were counted.

Preliminary investigations (Willumsen, 2015) revealed that samples from sampling point M1 (before coagulant addition) kept their titers during a few days of storage while samples from M2 and M3 (after coagulant addition) steadily lost their titers by up to 1.5-2 $\log_{10}$-units during one week. Thus, a slow virucidal and/or aggregation effect of the coagulant appears to be present. In order to reduce the impact of this effect, all samples were analyzed promptly after sampling (plated within 1-4 hours for all samples). Not all dilutions could be plated in replicates (due to hundreds of plates < 24 hours), but at least two plates were incubated for every sample (two dilutions and/or parallels of the same dilution). Figures with uncertainty estimates for each sample are included in the online supporting material.

The possibility of virus adsorption in the sampling tubes of the automatic sampler was assessed by pumping coagulated water containing viruses through one of the tubes, and enumerating phage 28B before and after tube passage. A reduction in phage concentration of 7% was observed (although not statistically significant) and considered acceptable.

2.2.3. Escherichia coli

E.coli was also included in this study for comparison with the viruses and because it is a widely used faecal indicator bacterium (Edberg et al., 2000). Cultures were prepared by inoculating brain-heart infusion broth (237500, Becton, Dickinson and Company, USA) with *E.coli* (CCUG 17620). Overnight cultures were centrifuged and washed twice with peptone saline diluent (CM0733, Oxoid, United Kingdom) and stored at 4°C for not longer than 5 days. Enumeration was performed using Colilert-18 with Quanti-Tray/2000 (IDEXX Laboratories, USA) according to the manufacturer's instructions. The method is equivalent to a most probable number (MPN) method with two dilutions and 48/49 tubes at each dilution. Samples were analyzed only once due to time constraints. Figures with uncertainty estimates for each sample are included in the online supporting material.

2.3. Water quality analyses

Manual turbidity measurements were performed with a HACH 2100N IS benchtop turbidimeter according to the manufacturer's instructions. Due to time constraints, turbidity measurements of the samples from ports A-H had to be performed during the days following the experiment. The mean turbidity in the samples from port H before breakthrough was 0.059 units higher than the mean logged turbidity. This difference was subtracted from all the turbidity values for ports A-H as a crude way of accounting for changes in turbidity as a result of storage.

Table 3: Raw water characteristics and operational conditions.

Parameter	**Value**
Raw water turbidity (NTU)	0.7-0.8
Raw water color (mg Pt/l)	26
Raw water TOC (mg/l)	3.03±0.61
Raw water UV absorption (1/m)	13.1
Raw water SUVA[a] (l/(m·mg))	> 4.3
Raw water pH (-)	7.3
Raw water alkalinity (mM)	0.28
Raw water temp. (°C)	15-16
Filtration rate (m/h)	5.9
Flow rate (l/min)	0.77
PAX-18 dose (mg Al/l)	1.5
HCl dose (mM)	0.12
Initial total headloss (cm)	26

[a]Specific UV absorption (UV abs./DOC)

Color and UV-absorption measurements were done on spectrophotometer HACH DR 3900 after filtering the samples through a 0.45 μm filter. Raw water alkalinity was determined by titration with HCl to pH 4.5, using the dosing pump and pH meter in the pilot plant. Raw water total organic carbon (TOC) was measured by an external lab (ALS Laboratory Group AS, Norway) according to NS-EN 1484:1997. The suspended solids content of the coagulated water was measured according to method NS-EN 872:2005. Total residual aluminium concentration was determined during a test run using HACH Aluminon method 8012, adapted from Standard Methods no. 3500-Al (APHA/AWWA/WEF, 2012). During the actual experiment, dissolved aluminium was determined by an external lab (Noranalyse AS, Norway) using ICP-OES according to method NS-EN ISO 11885:2009.

2.4. Raw water quality and coagulant dose determination

The raw water was collected from the river Glomma on two occasions (August 2014 and May 2015) and mixed in the storage tank at the university. After some initial sedimentation, turbidity remained stable. Raw water characteristics are listed in Table 3. The specific UV-absorption (SUVA) is relatively high, indicating that the NOM of this water is rich in aromatic compounds and well suited to treatment by coagulation (Matilainen et al., 2010).

PAX-18 (Kemira, Finland), a 42 % basicity polyaluminium chloride with an Al-content of 9 % (w/v), was chosen as the coagulant for this study as it is a commonly used coagulant in Norway. No filter aid was used. HCl was used for pH-adjustment prior to adding the coagulant. The filtration rate was kept constant at 5.9 m/h. The coagulant dose and coagulation-pH were determined by testing a range of doses and pH-values in the pilot plant, searching for the smallest dose (and the best-working pH at that dose) that resulted in outlet turbidity values less than 0.2 NTU, color less than 5 mg Pt/l and residual coagulant content < 0.15 mg Al/l, which are the main Norwegian regulatory requirements for an Al-based coagulation-filtration plant to be considered a hygienic barrier.

It was found that a coagulant dose of 1.5 mg Al/l and coagulation-pH of 5.8 constituted an optimal dosing regime, resulting in effluent turbidity of 0.03-0.04 NTU, color < 2 mg Pt/l and residual aluminium concentration of 0.031 mg Al/l during the optimization run. Subsequently, a full filtration cycle with this dose showed that the cycle was terminated by turbidity breakthrough after approx. 15 hours. The dose and the filter run length are in agreement with empirical models developed by Eikebrokk et al. (2004) based on numerous pilot filter runs with low-turbidity waters and a range of color values.

It should be noted that no microorganism suspension was added to the influent water during dose optimization. Thus, the particle content and water chemistry may have changed slightly during the actual experiment, but no significant changes in the process could be observed. Approximate net dilution factors for the addition of stock microorganism suspensions to the influent water were 26000 (28B), 6500 (MS2) and 11000 (*E.coli*).

2.5. Experimental protocol

Prior to a filter run, the column was backwashed for approximately 15 minutes at a rate of 50 - 60 m/h, resulting in a filter expansion of 50-60 %. The backwash rate was reduced gradually towards the end of the backwash in order to promote good separation of the two media, but some interfacial mixing was still observed. The system was then run with raw water for approximately 15 minutes in order to displace the tap water present in the filter from backwashing. This was considered to give a more realistic initial condition since the tap water came from a different raw water source than the one used for the experiments, and may also have contained some residual chlorine. After 15 minutes of running raw water, dosing of microorganisms, HCl and coagulant was initiated simultaneously.

Time, cost and raw-water availability meant that only a single filter-run with high-resolution sampling could be performed. An overview of the sampling regime employed for this study is given in Table B.5 in the online supporting material. Samples were taken uniformly spaced in time except for samples from point M3, which were taken more frequently during the ripening and breakthrough periods.

The automatic sampler was programmed to take samples with a total flow rate of 5 % of the flow rate through the filter i.e. 0.625 % per sampling port. This ensured that the water velocity through the sampling ports was lower than the pore water velocity, reducing the risk of eroding the deposit by sampling-induced shear forces. The sample collection duration was 10 minutes, which is still a short time compared to the time rate of changes in the local suspended concentrations. Prior to sample collection, the sampler drained the sampling tubes for 10 minutes, corresponding to approximately three tube volumes, using the same flow rate as during sampling.

2.6. Data presentation

Time points for all samples collected outside of the filter column (online turbidity, pH, temp., M1, M2 and M3) have been adjusted for the flow time in tubes/pipes, assuming plug-flow.

Table 4: Water quality results and influent microorganism concentrations.

Parameter	**Value**
Influent turbidity (-)	2.05
Influent SS (mg/l)	8.2
Influent coagulation pH (-)	5.8
Effluent pH (-)	5.9-6.0
Effluent color (mg Pt/l)	3
Effluent residual Al-content (mg Al/l)	0.031^a/$<0.010^b$
Influent mean 28B conc. (PFU/ml)	$2.57 \cdot 10^5$
Influent mean MS2 conc. (PFU/ml)	$1.96 \cdot 10^6$
Influent mean *E.coli* conc. (MPN/100ml)	$9.31 \cdot 10^5$

[a]During dose optimization, total (HACH method)
[b]During experiment, dissolved (external lab)

Time points for the automatic samples have been set to the midpoint of the 10-minute sampling duration. Time zero corresponds to the estimated arrival of the coagulated water at the filter surface.

3. Experimental results with discussion

3.1. Water quality

Water quality results are shown in Table 4. These were as expected based on trial runs. Effluent pH decreased initially to reach a stable value of 5.9-6.0 after 2-3 hours, which we suspect is due to a slightly pH-raising effect of the top Filtralite medium. Online effluent turbidity reached a stable level after approx. 3 hours and breakthrough started at approx. 14.2 hours. Online inlet turbidity (Figure 2d, "IN") showed a rising trend which we attribute to sludge blanket effects in the vertical pipe in which the sensor was installed. True influent turbidity likely remained stable around the initial value of ca. 2.05 NTU.

3.2. Spatio-temporal removal

No major differences in microorganism concentrations were found between sampling ports M1 (before coagulant) and port M2 (after coagulant dosing), suggesting that neither microorganism aggregation or inhibition effects from the coagulant were present to any appreciable extent. Mean influent concentrations c_{in} of each organism were calculated from all M1 and M2 samples and are given in Table 4. These were used to compute the passage probability $\pi = c/c_{\text{in}}$ for all sample ports, where c is the concentration in the sample port. The log-removal is simply $-\log_{10}(\pi)$. Figure 2 shows the results of all spatio-temporal sampling for phage 28B (2a), phage MS2 (2b), *E.coli* (2c) and turbidity (2d). Microorganism data is presented in terms of $\log_{10}(\pi)$.

3.2.1. Salm. typh. 28B

Figure 2a clearly shows the existence of ripening and breakthrough fronts that migrated down the filter as the cycle progressed. Overall removal continued to improve until breakthrough of 28B after approximately 13 hours, slightly before turbidity breakthrough. Log-removal remained below 2.5 for most of the cycle and peaked at about 3.2. It can be seen that

at the time of the first auto-sample, breakthrough of 28B had already occurred at ports A, B and C while the lower parts of the filter were still in a ripening phase. After breakthrough in a given port, the concentrations in that port rose and reached a plateau. At the end of the cycle there was still some removal, mainly between ports B and C, and between port G and the outlet.

Sampling from multiple depths effectively allows a study of the impact of media configuration and filter depths in a single-filter run. The peak removal in the upper layer (Filtralite, as measured by port D) was about 2.5, compared to the overall peak of 3.2. This is in line with previous research that found only moderate effects of filter depths and media configurations on virus removal (Hijnen and Medema, 2010; Harrington et al., 2003; Hendricks et al., 2006). This may be explained by the fact that only a relatively small part of the filter is responsible for the majority of the removal at any given time since ripening occurs progressively down the filter. However, breakthrough in the Filtralite occurred already after approx. 4 hours. Thus, while filter depth and media configurations may have a moderate effect on peak removal rates, a deeper filter will extend the useful operating period and decrease the number of breakthrough and initial ripening periods per unit time, thereby improving the overall mean log-removal. These effects may be investigated more quantitatively if a filtration model can be fitted to the data (Section 4).

There are some inconsistent results in Figure 2a. Early in the cycle, there is some removal between ports F and G, but not between ports D and F which is inconsistent with the assertion that ripening occurs progressively with depth. Also the concentrations in manual samples in the outlet (M3) are above those from ports G and H early in the cycle. We do not have a firm explanation for these results, although the early G and H concentrations may have been underestimated because of high plaque counts on some Petri dishes. In general, we trust the manual sampling data somewhat more than the auto-sampler data.

3.2.2. MS2

Sampling resolution for the MS2 data (Figure 2b) is coarser than for 28B, but the results for the auto-samples are qualitatively similar. Removal was slightly poorer for MS2 and peaked at about 3 $\log_{10}$-units after 12-13 hours (RT-qPCR). Data from plaque assays and RT-qPCR are largely consistent, with plaque assays indicating a slightly better removal. This may be due to some residual inhibitory effect of the coagulant even after the BE+U treatment, or possibly some non-infectious PCR-units that are more poorly removed than infectious MS2. However, there is a mid-cycle rise in outlet concentrations from RT-qPCR that was not observed for the plaque assay or any of the other organisms. While the data does not allow firm interpretations, we may speculate that this coudl be related to a breakthrough in the upper part of the filter before sufficient ripening for MS2 has occurred in the lower parts of the filter. Filtration modeling (Section 4) may possibly be used to support or dispel this hypothesis.

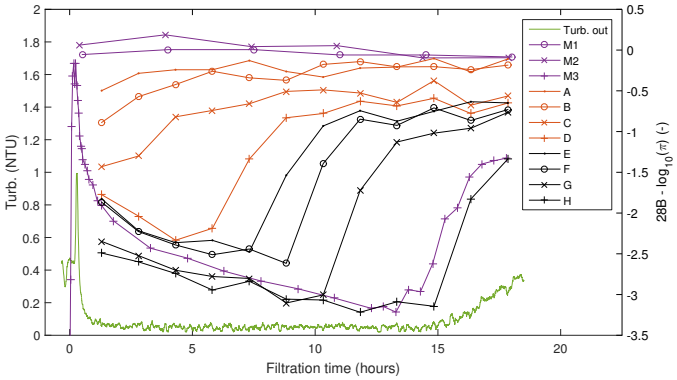

(a) Phage 28B concentrations normalized to influent concentrations.

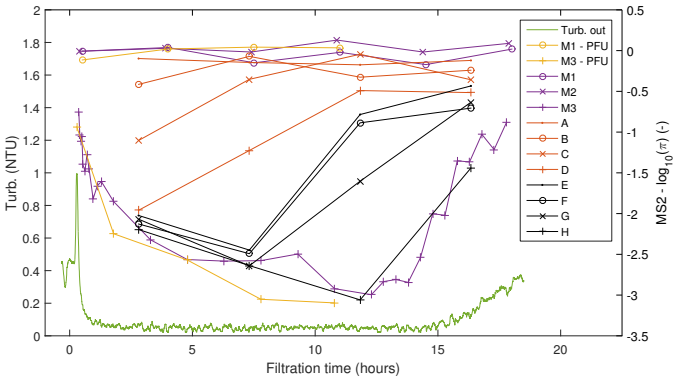

(b) Phage MS2 concentrations normalized to influent concentrations. All datapoints stem from RT-qPCR analyses except for the yellow lines/points which stem from the plaque assay.

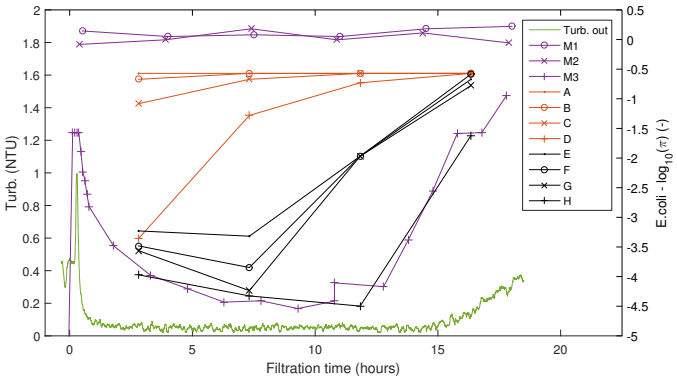

(c) *E.coli* concentrations normalized to influent concentrations. Note that several A-G samples were above enumeration limits (see Figure B.10 in online supporting material) and the data should be interpreted with care.

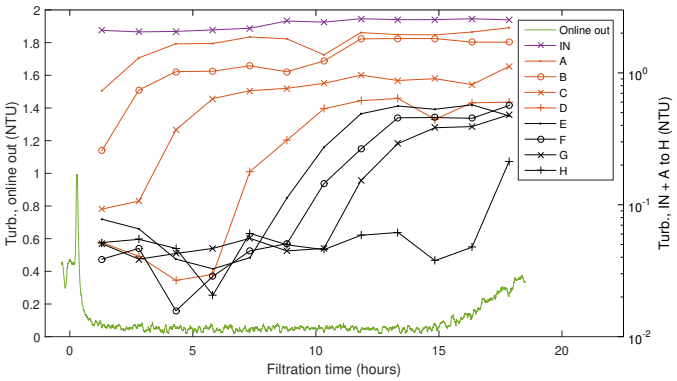

(d) Turbidity, online and manual measurements.

Figure 2: Spatio-temporal passage of microorganisms and turbidity.

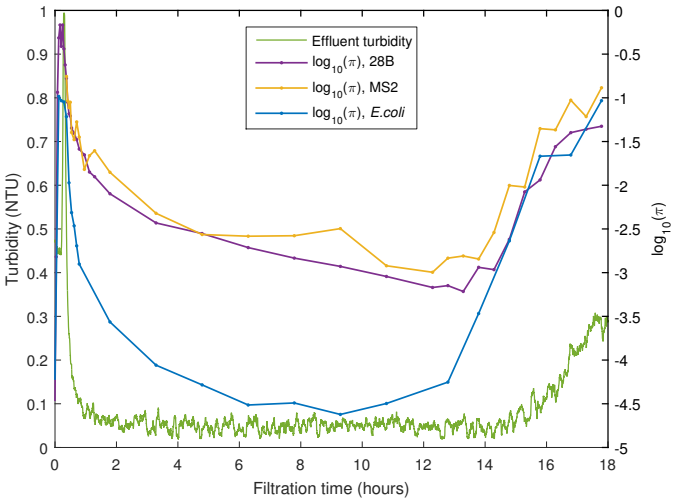

Figure 3: Overall log-removal compared. Note that we discarded one suspicious data point for *E.coli* at approx 11. hours (comp. Fig. 2c), where we had two data points.

3.2.3. *E.coli*

Sampling resolution for the *E.coli* data (Figure 2c) is also coarser than for 28B, but ripening and breakthrough fronts can be observed here as well. Note that all A-samples and several B- to G-samples were above the enumeration limit for the Colilert-18 method; hence $\log_{10}(\pi)$ is closer to zero for these samples than shown in Figure 2c. These samples are clearly identified in the online supporting material. Removal peaked at about 4.5 $\log_{10}$-units, but this occurred mid-cycle after approx. 9 hours and *E.coli* removal had deteriorated significantly by the time of turbidity breakthrough.

3.2.4. *Turbidity*

The turbidity data (Figure 2d) from within the filter column displays a pattern similar to that of the 28B data. At the time of the first auto-sample, breakthrough had already occurred at ports A, B and C. For ports D and E, it is possible to discern a ripening phase, but for the lower ports the noise drowns out the signal. After breakthrough, turbidity eventually stabilizes. Compared to the 28B data, the rising parts of the curves after breakthrough are slightly steeper in the Filtralite medium, but less steep than in the sand medium, indicating slightly different dynamics of turbidity and virus removal in the two media. The mechanistic interpretation of such a pattern is not presently clear to us.

3.2.5. *Removal compared*

Figure 3 shows the passage probability for all organisms in a single plot. The two viruses behave quite similarly while *E.coli* is both removed to a greater extent and shows faster ripening and earlier breakthrough than the viruses. These observations are qualitatively consistent with earlier observations on the ripening and breakthrough behavior of differently sized particles (Clark et al., 1992; Kim and Lawler, 2008; Moran et al., 1993). However, towards the end of the cycle the removal efficiencies appear to converge, which suggests that removal mechanisms that are independent of particle properties dominate at this stage.

By direct trapezoidal integration of these curves, the overall *mean* log-removal rate between 32 minutes (turbidity dropped below 0.2 NTU) and 14.2 hours (onset of turbidity breakthrough) was computed as 2.5, 2.3 and 3.6 for 28B, MS2 and *E.coli*, respectively. This is significantly lower than the corresponding peak removal rates of 3.2, 3.0 and 4.5, respectively, but higher than the log-credit values suggested by Ødegaard et al. (2016) (1.5/2.0 for viruses and 2.25/2.5 for bacteria). Hijnen and Medema (2010), in their review, reported much lower mean removal efficiencies, but their estimates included waste water studies and were also weighted strongly in favor of full-scale studies. The study in that comes closest to our study in terms of raw water characteristics and experimental setup is the one by Hendricks et al. (2006) (indexed 37 and 38 in the online supporting material), who reported a log-removal for MS2 of 2.9 (two-hour mean obtained mid-cycle).

The removal efficiency of phages MS2 and 28B appears to be quite similar under these experimental conditions. These are both nearly spherical viruses, but 28B is about twice as large as MS2. The isoelectric point of MS2 has been reported as between 3.1 and 3.9, with 3.9 most frequently reported (Michen and Graule, 2010)[2]. The isoelectric point of 28B has not been reported, but work on this is underway. In a single measurement, Heistad (2008) reported an electrophoretic mobility of -2.38 μm cm/(Vs) at pH 7.3 in 10 mM NaCl solution, compared to that of MS2 of approximately -0.7 μm cm/(Vs) under identical conditions (Penrod et al., 1995). Thus, it appears to be slightly more negatively charged than MS2 at higher pH. This might have contributed to a slightly higher affinity for positively charged aluminum hydroxide flocs, and a slightly better removal during filtration. The surface charge of *E.coli* appears to be between those of the viruses at this pH (Lytle et al., 2002) and thus cannot alone explain the better removal of *E.coli*.

3.3. *Headloss*

Figure 4 shows the Michau-diagram for the filter run, which confirms that most of the headloss increase occurred in the upper part of the Filtralite layer, but there was also some headloss development in the upper part of the sand layer.

4. Interpretations in terms of filtration modeling

Classical macroscopic filtration models that describe the dynamic behavior of the filtration process consist essentially of a particle volume conservation equation and a constitutive filtration rate equation (Iwasaki, 1937; Herzig et al., 1970; Tien and Ramaro, 2007), respectively:

$$\frac{\partial \sigma}{\partial t} + u\frac{\partial c}{\partial z} = 0 \tag{2}$$

$$\frac{\partial c}{\partial z} = -\lambda c \tag{3}$$

[2] A single measurement of 2.2 was also reported.

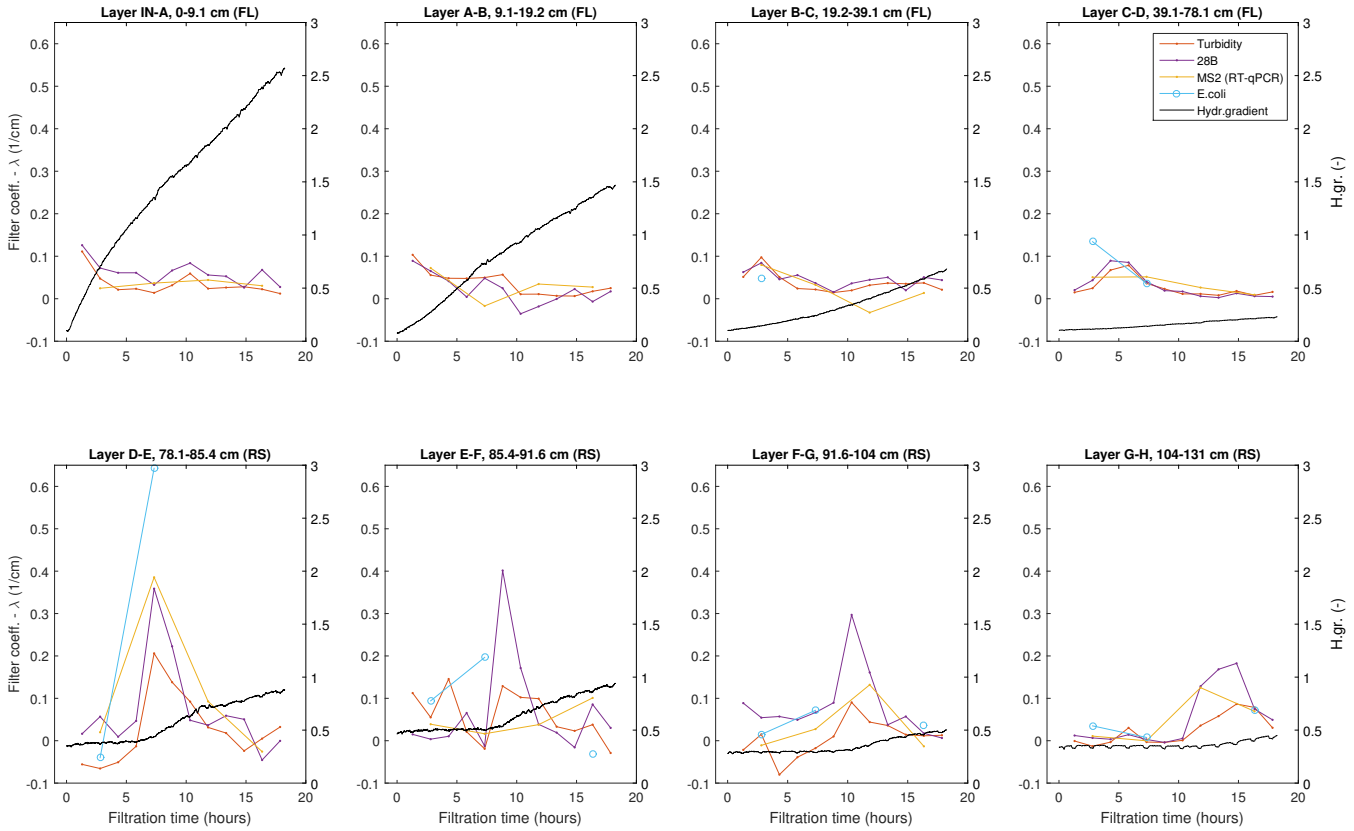

Figure 5: Estimated filter coefficients from equation (4), and hydraulic gradients. Filter coefficients for *E.coli* could not be computed for several layers/times because samples were above the enumeration limit. FL - Filtralite; RS - Rådasand.

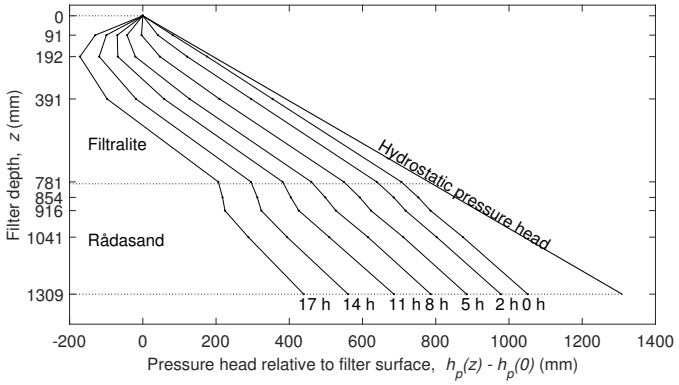

Figure 4: Michau-diagram.

Here c is the suspended particle concentration (volume of particles per unit volume of suspension, dim.less), σ is the specific deposit (volume of particles per unit volume of porous medium, dim.less), u is the Darcy velocity (L/T) and λ is the filter coefficient (1/L). The former equation assumes that dispersive transport is negligible as well as other simplifying approximations (Horner et al., 1986). The latter was first proposed by Iwasaki (1937) and remains a standard assumption. The system above does not consider particle detachment, which may be a limitation.

The main challenge in deep-bed filtration is that λ changes with time as the filter collects particles and it also changes with depth in the filter. Thus, λ is usually taken as a function of σ, and is called the *filtration function*. The final purpose of our modeling efforts will be to estimate this filtration function for both viruses and total particle content. The details of how the basic equations (2) - (3) may be refined to account for both particle and virus transport in both filter media, as well as the current status of the modeling efforts, are presented in the appendix. In the following, we rely on the data directly rather then model results.

4.1. Experimental filter coefficients

Here, crude estimates of the mean filter coefficient in each layer were determined directly from the experimental data by computing

$$\lambda_{i,i+1} = \frac{1}{z_{i+1} - z_i} \ln\left(\frac{c_i}{c_{i+1}}\right) \tag{4}$$

where c_i is the concentration/turbidity in port i and c_{i+1} is the concentration in the port below.

Figure 5 shows the results along with the hydraulic gradients for each layer. The data are noisy since we are estimating derivatives based on two data points that are both a little noisy, but the wave-like progression down the filter of the peak in λ can clearly be seen. The highest filter coefficients occurred in the upper part of the sand layer (which was partly mixed with

Filtralite after backwashing). Note the lower temporal resolution of the MS2/*E.coli* data, which masks some of their dynamics. Note also that the distance between sample ports varied so that one may expect that some peaks are "averaged down" as one moves the rightmost panels in Figure 5. The hydraulic gradient in the lower part of the sand layer started to rise after about 12 hours, thereby giving an "early" warning that turbidity breakthrough was imminent. The gradient increased some 30-fold in the upper part of the Filtralite, and there is a difference in initial hydraulic gradients between the various sand layers, another indication that there was some mixing of sand and Filtralite.

4.1.1. Comparison with ideal filtration theory

The filter coefficients in Figure 5 may be compared to those estimated from ideal filtration theory. Substantial research has been devoted to estimating λ from first-principles and has been largely successful under favorable conditions for filtration, i.e. no repulsive electrostatic interactions between particles and filter grains (Tufenkji, 2007). In this theory, the filter coefficient is given by:

$$\lambda = \frac{3}{2}\frac{(1-\epsilon)}{d_c}\alpha\eta_0 \tag{5}$$

Here ϵ is the porosity, d_c is the filter grain diameter, η_0 is the so-called single-collector contact efficiency and α the sticking efficiency. The latter is assumed to be 1 under favorable conditions. The currently most widely used equation for estimating η_0 was developed by Tufenkji and Elimelech (2004). Figure 6 compares peak values of λ taken from Figure 5 (assumed to correspond to complete ripening, hence $\alpha = 1$) with those predicted by equation (5), using the expression for η_0 from Tufenkji and Elimelech (2004). For size-graded porous media, as our filter media, it has been recommended to use a grain size that emphasizes the smaller grain fractions, such as d_{10} (Pazmino et al., 2011). The grey bands in Figure 6 corresponds to a wide range of input parameters, assumed to cover all plausible values, even accounting for the effect of the already retained particles (O'Melia and Ali, 1979).

From Figure 6, it is seen that the observed peak λ-values are inconsistent with the known microorganism sizes, and more consistent with a particle size of a few μm to a few dozens of μm. For both media, the best estimate of η implies a particle size of about 20 μm. If one accepts this application of filtration theory, this analysis therefore suggests that microorganism removal was largely controlled by floc-associated microorganisms, and that the dominating floc-size is around 20 μm.

4.1.2. Deposit distribution at end-of-cycle

Figure 7 shows the results of a simple numerical (trapezoidal) integration of equation (2) directly from the experimental data for c, and indicates how the deposit of particles (assumed proportional to turbidity) and 28B was distributed in the filter column at the end of the experiment. Most of the deposit is in the upper part of the Filtralite for both particles and 28B, but there is also a noticeable accumulation of deposit in the upper part of the sand layer. There is also some non-monotonicity

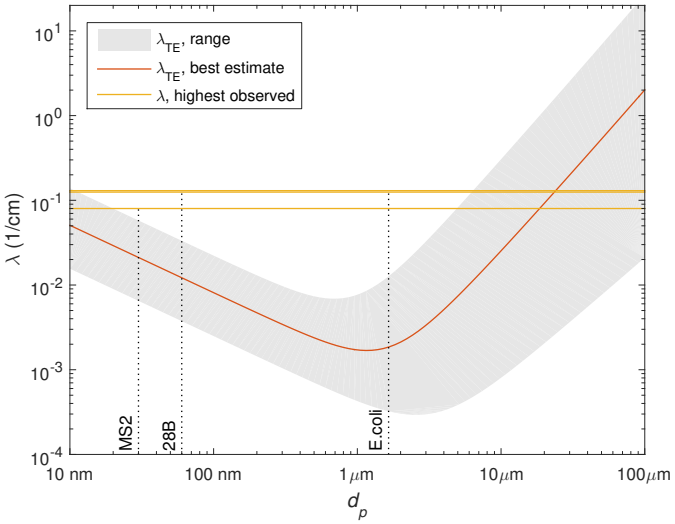

(a) Comparison for Filtralite. The grey area is the possible range of λ-values using the following parameters, with the parameters used for the best estimate in the middle: Porosity 0.48 - 0.58 - 0.63; Grain size 0.7 - 0.95 - 1.6 mm; Hamaker constant 1e-21 - 1e-20 - 1e-19 J; Density 1000 - 1250 - 2600 kg/m^3.

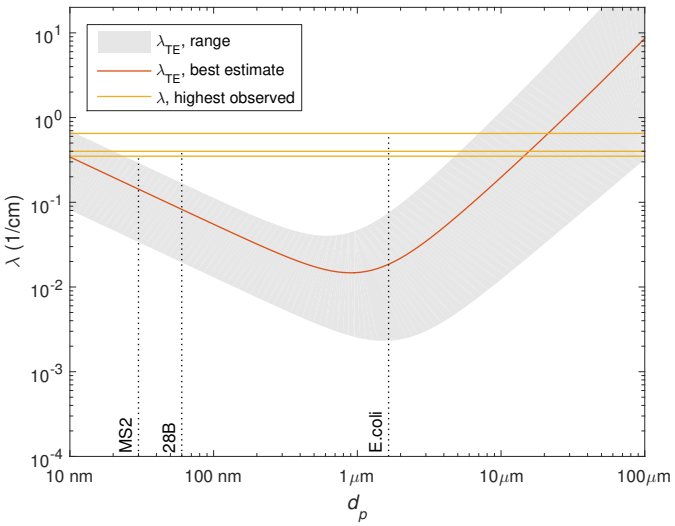

(b) Comparison for Rådasand. The grey area is the possible range of λ-values using the following parameters, with the parameters used for the best estimate in the middle: Porosity 0.35 - 0.45 - 0.50; Grain size 0.35 - 0.40 - 0.8 mm; Hamaker constant 1e-21 - 1e-20 - 1e-19 J; Density 1000 - 1250 - 2600 kg/m^3.

Figure 6: Comparison of peak values of λ from Figure 5 with those predicted by the TE correlation equation. All computations were carried out for water at 15°C.

within each filter medium which should disappear if the filtration model can be properly fitted to the data.

5. Overall discussion

Our results were obtained in a single filter run under a single set of conditions and, as such, generalizations of our computed removal efficiencies should be performed with care. The filtration performance may be affected by a range of factors such as e.g. raw water quality, coagulant type and dose, filtration rate, backwash strategies etc. (Hijnen and Medema, 2010). How-

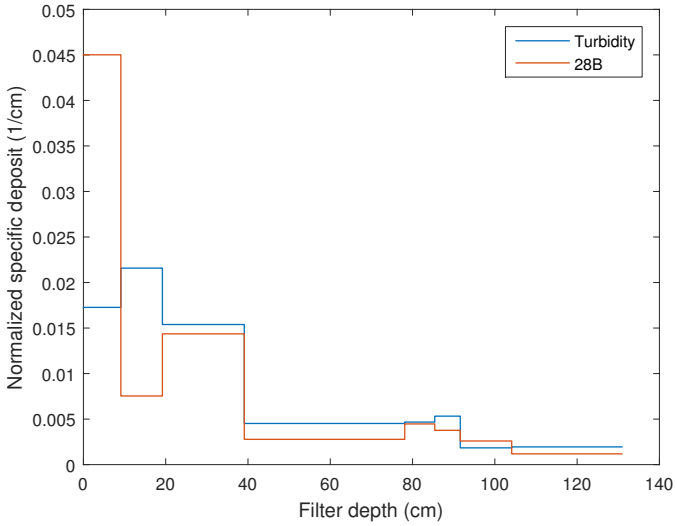

Figure 7: Estimated specific deposit distribution at the end of the cycle. The vertical axis is normalized with respect to the total deposit so that the area under the curves are 1.

ever, the dynamic microorganism removal observed here, even during the period of stable effluent turbidity, signals that care should be taken when characterizing microbial removal efficiencies during filtration. Either samples should be taken frequently, such as in this study, or at least flow-proportional continuous sampling should be employed.

The usefulness of surrogates, such as phages, for studying removal and inactivation of pathogenic viruses is a continuous concern (Mesquita and Emelko, 2012; Sinclair et al., 2012). Hijnen and Medema (2010) suggested that coliphages were appropriate surrogates for pathogenic viruses in deep-bed filtration. Since *Salmonella* typhimurium phage 28B is simple to work with, it would be a useful addition to the set of surrogate phages if it can be confirmed that it behaves similarly to MS2 and/or other coliphages under a wider range of conditions. We believe this study is the first to use this phage for deep-bed filtration experiments for drinking water. Examples of previous applications include waste water transport in soils (Carlander et al., 2000), small-scale waste water treatment systems (Heistad et al., 2009a,b) and biofilter performance in drinking water treatment (Persson et al., 2005).

A final concern regarding the applicability of these results, and those from most other pilot-scale studies, is the high influent concentrations used for the microorganisms; much higher than what occurs naturally. Assavasilavasukul et al. (2008) observed better removal of *Cryptosporidium* during conventional treatment with higher *Cryptosporidium* influent concentrations. Prasanthi et al. (1997) also observed better removal with higher influent concentrations in laboratory columns without coagulation. However, it is not clear if these results apply to viruses in our experiment. The virus volume is negligible compared to the total floc volume, virus aggregation was not observed, and according to standard flocculation theory the virus-floc aggregation rate is expected to scale linearly with virus concentrations. Further research is needed to clarify these issues. Finally, the role of virus detachment is also not clear (Kim and Tobiason, 2004). If virus detachment is not negligible compared to virus attachment, the observed removal efficiencies may be a function of the influent concentrations.

6. Conclusions

1. Both virus and E.coli filtration was dynamic, showing variations in removal performance during periods of stable effluent turbidity.
2. Ripening and breakthrough for E.coli occurred earlier than for viruses. Both deviated from turbidity.
3. Regulatory limits on turbidity appear not to ensure stable operation with respect to virus/E.coli removal.
4. True log-removal estimates over entire time periods of water production deviated significantly from instantaneous log-removal values.
5. Careful design of sampling regimes is needed to correctly estimate mean removal efficiencies in filtration experiments.
6. Reporting the removal efficiency of a deep-bed filter with a single number may be inappropriate, unless the single number is a properly computed mean removal efficiency.
7. While filter depth, in previous studies as well as this study, appears to be only moderately important for peak removal rates, deeper filters may postpone breakthrough and thus reduce the number of backwash cycle per unit time. The latter may be influential in controlling mean health risks since most of the pathogen passage may happen right before and right after backwashing.
8. Based on comparison of filter coefficients with ideal filtration theory, viruses and bacteria appeared to be largely associated with flocs.
9. Repeat studies should be performed in order to corroborate the results reported in this paper.

7. Acknowledgements

The authors would like to thank Arne Svendsen and Tom Ringstad for their invaluable role in designing and constructing the filtration column and automatic sampler. Anne Willumsen, MSc, and Torbjørn Friborg, MSc, provided much-needed assistance with the 28B analyses. Thanks also go to Jon Fredrik Hanssen, Else Aasen and Rannei Tjåland for assisting with microbiology laboratory preparations. The water treatment plant at Nedre Romerike Vannverk provided practical assistance with raw water for these experiments and helped finance the transport of raw water from the plant to the university. Tor Håkonsen, PhD, and Prof. Lars Hem provided advice on various aspects of the design and operation of the filtration system. Prof. John Wyller provided advice on the filtration model.

Appendix A. Dynamic modeling sketch

We will refine the model (2) - (3) by introducing concentration variables to represent (1) total particles and (2) viruses.

However, we will assume that the contribution of the viruses to the total particle volume (in suspension or deposited) is completely negligible, and hence that the filtration functions for total particles and viruses both depend only on the total particles specific deposit and not explicitly on the virus specific deposit. This partly decouples the system of equations and makes solution algorithms simpler, since the forward problem for particle volume can be solved independently from the forward problem for virus volume, but the problem for virus volume uses the solution from the particle volume problem as input to the virus filtration functions.

Fundamental unknowns to solve for in the forward problem: $c(z,t)$ - fluid phase particle volume fraction, $\sigma(z,t)$ - volume of particles per unit volume of filter, $c_v(z,t)$ - fluid phase virus volume fraction, $\sigma_v(z,t)$ - volume of viruses per unit volume of filter. Other quantities: u - filtration rate (constant). λ - filtration function for particle volume, λ_v - filtration function for virus volume. The filtration functions are specific to each medium (i.e four filtration functions in total) and contain a number of parameters to be determined in the inverse problem.

Experimental data is a grid in space-time of c and c_v values. Actually, at best, we can only hope that the turbidity measurements are proportional to c, which may be a reasonable assumption (Clark et al., 1992). The inverse problem is to determine functions λ and λ_v such that the experimental data is reproduced by the solutions to the forward problem. There exists various parametric forms for the filtration functions. At his point, we have only considered the following filtration function from Ives (1969), which is considered very general (assuming particle detachment is negligible):

$$\lambda(\sigma) = \lambda_0 \left(1 + \frac{b\sigma}{\epsilon_0}\right)^{n_1} \left(1 - \frac{\sigma}{\epsilon_0}\right)^{n_2} \left(1 - \frac{\sigma}{\sigma_\mathrm{ult}}\right)^{n_3} \tag{A.1}$$

Here, λ_0, b, n_1, n_2, n_3 and σ_ult are fitting parameters and ϵ_0 is the initial porosity, assumed to be known.

Appendix A.1. PDE formulation

The full system of equations is given below, where we have required continuity of fluid phase concentration at the boundary between the two filter media.

Initial conditions:

$$c(z,0) = \sigma(z,0) = 0 \tag{A.2}$$
$$c_\mathrm{v}(z,0) = \sigma_\mathrm{v}(z,0) = 0 \tag{A.3}$$

System of equations for **particle volume in upper medium**, $z \in [0, z_1]$:

$$\frac{\partial \sigma}{\partial t} + u\frac{\partial c}{\partial z} = 0 \tag{A.4}$$
$$\frac{\partial \sigma}{\partial t} = u\lambda_1(\sigma)c \tag{A.5}$$

Boundary conditions:

$$c(0,t) = c_\mathrm{in} \tag{A.6}$$
$$\sigma(0,t) \text{ from (A.5)} \tag{A.7}$$

System of equations for **particle volume in bottom medium**, $z \in [z_1, z_2]$:

$$\frac{\partial \sigma}{\partial t} + u\frac{\partial c}{\partial z} = 0 \tag{A.8}$$
$$\frac{\partial \sigma}{\partial t} = u\lambda_2(\sigma)c \tag{A.9}$$

Boundary conditions:

$$c(z_1,t) \text{ from (A.4)} - \text{(A.7)} \tag{A.10}$$
$$\sigma(z_1,t) \text{ from (A.4)} - \text{(A.7)} \tag{A.11}$$

System of equations for **virus volume in upper medium**, $z \in [0, z_1]$:

$$\frac{\partial \sigma_\mathrm{v}}{\partial t} + u\frac{\partial c_\mathrm{v}}{\partial z} = 0 \tag{A.12}$$
$$\frac{\partial \sigma_\mathrm{v}}{\partial t} = u\lambda_{\mathrm{v},1}(\sigma)c_\mathrm{v} \tag{A.13}$$

Boundary conditions:

$$c_\mathrm{v}(0,t) = c_{\mathrm{v,in}} \tag{A.14}$$
$$\sigma_\mathrm{v}(0,t) \text{ from (A.13)} \tag{A.15}$$

System of equations for **virus volume in bottom medium**, $z \in [z_1, z_2]$:

$$\frac{\partial \sigma_\mathrm{v}}{\partial t} + u\frac{\partial c_\mathrm{v}}{\partial z} = 0 \tag{A.16}$$
$$\frac{\partial \sigma_\mathrm{v}}{\partial t} = u\lambda_{\mathrm{v},2}(\sigma)c_\mathrm{v} \tag{A.17}$$

Boundary conditions:

$$c_\mathrm{v}(z_1,t) \text{ from (A.12)} - \text{(A.15)} \tag{A.18}$$
$$\sigma_\mathrm{v}(z_1,t) \text{ from (A.12)} - \text{(A.15)} \tag{A.19}$$

Appendix A.2. Preliminary results

The system in the previous section was implemented in MATLAB and C with filtration function (A.1). It soon became clear that the third factor in this filtration function forces λ towards 0 too rapidly. When λ becomes close to zero over an extended depth in the filter, there will be almost no removal across this depth. However, Figure 2a and 2d clearly demonstrates that there is stable removal over an extended period of time in the upper part of the filter in the latter half of the filter cycle. Hence, a filtration function is needed that doesn't tend to zero, but instead displays a plateau as σ becomes big. This will be the focus of upcoming investigations.

References

Abbaszadegan, M., Mayer, B.K., Ryu, H., Nwachuku, N., 2007. Efficacy of removal of CCL viruses under enhanced coagulation conditions. Environmental Science and Technology 41, 971–977. doi:10.1021/es061517z.

Abbaszadegan, M., Monteiro, P., Nwachuku, N., Alum, A., Ryu, H., 2008. Removal of adenovirus, calicivirus, and bacteriophages by conventional drinking water treatment. Journal of Environmental Science and Health, Part A: Toxic/Hazardous Substances and Environmental Engineering 43, 171–177. doi:10.1080/10934520701781541.

Adin, A., Rebhun, M., 1974. High-rate contact flocculation—filtration with cationic polyelectrolytes. Journal (American Water Works Association) 66, 109–117.

Agbalika, F., Hartemann, P., Joret, J.C., Hassen, A., Bourbigot, M.M., 1985. Study of Indigenous Virus Removal at Different Stages in a Drinking Water Plant Treating River Water. Water Science & Technology 17, 211–218.

APHA/AWWA/WEF, 2012. Standard methods for the examination of water and wastewater. 22 ed., American Public Health Association, American Water Works Association, Water Environment Federation.

Asami, T., Katayama, H., Torrey, J.R., Visvanathan, C., Furumai, H., 2016. Evaluation of virus removal efficiency of coagulation-sedimentation and rapid sand filtration processes in a drinking water treatment plant in Bangkok, Thailand. Water Research doi:10.1016/j.watres.2016.05.012.

Assavasilavasukul, P., Lau, B.L.T., Harrington, G.W., Hoffman, R.M., Borchardt, M.a., 2008. Effect of pathogen concentrations on removal of Cryptosporidium and Giardia by conventional drinking water treatment. Water Research 42, 2678–2690. doi:10.1016/j.watres.2008.01.021.

Boudaud, N., Machinal, C., David, F., Fréval-Le Bourdonnec, A., Jossent, J., Bakanga, F., Arnal, C., Jaffrezic, M.P., Oberti, S., Gantzer, C., 2012. Removal of MS2, Qβ and GA bacteriophages during drinking water treatment at pilot scale. Water Research 46, 2651–2664. doi:10.1016/j.watres.2012.02.020.

Carlander, A., Aronsson, P., Allestam, G., Stenström, T.A., Perttu, K., 2000. Transport and retention of bacteriophages in two types of willow-cropped lysimeters. Journal of Environmental Science and Health, Part A 35, 1477–1492. doi:10.1080/10934520009377048.

Clark, S.C., Lawler, D.F., Cushing, R.S., 1992. Contact Filtration: Particle Size and Ripening. Journal (American Water Works Association) 84, 61–71.

Debartolomeis, J., Cabelli, V.J., 1991. Evaluation of an Escherichia-Coli Host Strain for Enumeration of F-Male-Specific Bacteriophages. Applied and Environmental Microbiology 57, 1301–1305.

Dreier, J., Stormer, M., Kleesiek, K., 2005. Use of Bacteriophage MS2 as an Internal Control in Viral Reverse Transcription-PCR Assays. Journal of Clinical Microbiology 43, 4551–4557. doi:10.1128/JCM.43.9.4551-4557.2005.

Edberg, S., Rice, E., Karlin, R., Allen, M., 2000. Escherichia coli: the best biological drinking water indicator for public health protection. Journal of Applied Microbiology 88, 106S–116S. doi:10.1111/j.1365-2672.2000.tb05338.x.

Eikebrokk, B., 2012. Veiledning for drift av koaguleringsanlegg. Technical Report. Norsk Vann.

Eikebrokk, B., Saltnes, T., 2001. Removal of natural organic matter (NOM) using different coagulants and lightweight expanded clay aggregate filters. Water Science & Technology: Water Supply 1, 131–140.

Eikebrokk, B., Vogt, R.D., Liltved, H., 2004. NOM increase in Northern European Source Waters: Impacts on coagulation/contact filtration processes, in: NOM Innovations and Applications, Adelaide.

Foliguet, J.M., Doncoeur, F., 1975. Elimination des enterovirus au cours du traitement des eaux d'alimentation par coagulation-floculation-filtration. Water Research 9, 953–961.

Gerba, C.P., Riley, K.R., Nwachuku, N., Ryu, H., Abbaszadegan, M., 2003. Removal of Encephalitozoon intestinalis, Calicivirus, and Coliphages by Conventional Drinking Water Treatment. Journal of Environmental Science and Health, Part A 38, 1259–1268. doi:10.1081/ESE-120021124.

Gilcreas, F.W., Kelly, S.M., 1955. Relation of Coliform-Organism Test to Enteric-Virus Pollution. Journal (American Water Works Association) 47, 683–694.

Gitis, V., Adin, A., Nasser, A., Gun, J., Lev, O., 2002. Fluorescent dye labeled bacteriophages–a new tracer for the investigation of viral transport in porous media: 2. Studies of deep-bed filtration. Water Research 36, 4235–4242. doi:10.1016/S0043-1354(02)00164-1.

Guy, M.D., Mciver, J.D., Lewis, M.J., 1977. The removal of virus by a pilot treatment plant. Water Research 11, 421–428. doi:10.1016/0043-1354(77)90083-5.

Haas, C.N., Rose, J.B., Gerba, C.P., 2014. Quantitative Microbial Risk Assessment. 2 ed., John Wiley & Sons, Inc, Hoboken, New Jersey. doi:10.1002/9781118910030.

Harrington, G.W., Xagoraraki, I., Assavasilavasukul, P., Standridge, J.H., 2003. Effect of Filtration Conditions on Removal of Emerging Pathogens. Journal (American Water Works Association) 95, 95–104.

Heistad, A., 2008. Small scale wastewater treatment - design optimization, reduction efficiency and risk prediction. Phd. Norwegian University of Life Sciences.

Heistad, A., Scott, T., Skaarer, A.M., Seidu, R., Hanssen, J.F., Stenström, T.A., 2009a. Virus removal by unsaturated wastewater filtration: effects of biofilm accumulation and hydrophobicity. Water Science & Technology 60, 399–407. doi:10.2166/wst.2009.343.

Heistad, A., Seidu, R., Paruch, A.M., Hanssen, J.F., 2009b. Long-term Hygienic Barrier Efficiency of a Compact On-site Wastewater Treatment System. Journal of Environment Quality 38, 2182–2188. doi:10.2134/jeq2008.0407.

Hellemans, J., Mortier, G., De Paepe, A., Speleman, F., Vandesompele, J., 2007. qBase relative quantification framework and software for management and automated analysis of real-time quantitative PCR data. Genome biology 8, R19. doi:10.1186/gb-2007-8-2-r19.

Hendricks, D.W., Asce, F., Clunie, W.F., Sturbaum, G.D., Klein, D.A., Champlin, T.L., Asce, M., Kugrens, P., Hirsch, J., Mccourt, B., Nordby, G.R., Asce, M., Sobsey, M.D., Hunt, D.J., Allen, M.J., 2006. Filtration Removals of Microorganisms and Particles. Journal of Environmental Engineering 131, 1621–1632. doi:10.1061/(ASCE)0733-9372(2005)131:12(1621).

Herzig, J.P., Leclerc, D.M., Goff, P.L., 1970. Flow of suspensions through porous media—application to deep filtration. Industrial & Engineering Chemistry 62, 8–35. doi:10.1021/ie50725a003.

Hijnen, W.A., Medema, G., 2010. Elimination of Microorganisms by Water Treatment Processes. IWA Publishing.

Höglund, C., Ashbolt, N., Stenström, T.A., Svensson, L., 2002. Viral persistence in source-separated human urine. Advances in Environmental Research 6, 265–275. doi:10.1016/S1093-0191(01)00057-0.

Horner, R., Jarvis, R., Mackie, R., 1986. Deep bed filtration: A new look at the basic equations. Water Research 20, 215–220. doi:10.1016/0043-1354(86)90011-4.

Huck, P.M., Emelko, M.B., Coffee, B., Maurizio, D., O'Melia, C.R., 2001. Filter operation effects on pathogen passage. AWWA Research Foundation.

ISO, 1995. ISO 10705-1:1995. Water quality - Detection and enumeration of bacteriophages - Part 1: Enumeration of F-specific RNA bacteriophages. Technical Report. International Standards Organization.

ISO, 1999. ISO10705-2:2000. Water quality - Detection and enumeration of bacteriophages - Part 2: Enumeration of somatic coliphages. Technical Report. International Standards Organization.

Ives, K.J., 1969. Modern theory of filtration. Special Subject No. 7., in: International Water Supply Congress, Vienna 1969, International Water Supply Association, London.

Iwasaki, T., 1937. SOME NOTES ON SAND FILTRATION. Journal (American Water Works Association) 29, 1591–1602.

Joret, J.C., Dupin, T., Hassen, A., Agbalika, F., Hartemann, P., 1986. Two Year Survey of Indicator Bacteria and Enteroviruses during the Preparation of Drinking Water from Three Water Treatment Plants in Paris Suburbs. Water Science & Technology 18, 107.

Keswick, B.H., Gerba, C.P., Dupont, H.L., Rose, J.B., 1984. Detection of Enteric Viruses in Treated Drinking-Water. Applied and Environmental Microbiology 47, 1290–1294.

Keswick, B.H., Gerba, C.P., Rose, J.B., Toranzos, G.A., 1985. Detection of Rotavirus in Treated Drinking Water. Water Science & Technology 17, 1–6.

Kim, J., Lawler, D.F., 2008. Influence of particle characteristics on filter ripening. Separation Science and Technology 43, 1583–1594. doi:10.1080/01496390801974688.

Kim, J., Tobiason, J.E., 2004. Particles in filter effluent: the roles of deposition and detachment. Environmental Science & Technology 38, 6132–6138. doi:10.1021/es0352698.

Kreißel, K., Bösl, M., Hügler, M., Lipp, P., Franzreb, M., Hambsch, B., 2014. Inactivation of F-specific bacteriophages during flocculation with polyaluminum chloride - A mechanistic study. Water Research 51, 144–151. doi:10.1016/j.watres.2013.12.026.

Lang, J.S., Giron, J.J., Hansen, A.T., Trussell, R.R., Hodges, W.E., 1993. Investigating filter performance as a function of the ratio of filter size to media size. Journal / American Water Works Association 85, 122–130.

Lilleengen, K., 1948. Typing of Salmonella typhimurium by means of bacteriophage: an experimental bacteriologic study for the purpose of devising a phago-typing method to be used an an aid in epidemiologic and epizootologic investigations in outbreaks of typhimurium infection. Phd. Royal Veterinary College, Stockholm.

Lytle, D.a., Johnson, C.H., Rice, E.W., 2002. A systematic comparison of the electrokinetic properties of environmentally important microor-

ganisms in water. Colloids and Surfaces B: Biointerfaces 24, 91–101. doi:10.1016/S0927-7765(01)00219-3.

Mac Kenzie, W.R., Hoxie, N.J., Proctor, M.E., Gradus, M.S., Blair, K.A., Peterson, D.E., Kazmierczak, J.J., Addiss, D.G., Fox, K.R., Rose, J.B., 1994. A massive outbreak in Milwaukee of cryptosporidium infection transmitted through the public water supply. The New England journal of medicine 331, 161–167. doi:10.1056/NEJM199407213310304.

Matilainen, A., Vepsäläinen, M., Sillanpää, M., 2010. Natural organic matter removal by coagulation during drinking water treatment: A review. Advances in Colloid and Interface Science 159, 189–197. doi:10.1016/j.cis.2010.06.007.

Matsui, Y., Matsushita, T., Sakuma, S., Gojo, T., Mamiya, T., Suzuoki, H., Inoue, T., 2003. Virus inactivation in aluminum and polyaluminum coagulation. Environmental science & technology 37, 5175–5180. doi:10.1021/es0343003.

Matsushita, T., Matsui, Y., Inoue, T., 2004. Irreversible and reversible adhesion between virus particles and hydrolyzing-precipitating aluminium: a function of coagulation. Water Science & Technology 50, 201–206.

Matsushita, T., Shirasaki, N., Matsui, Y., Ohno, K., 2011. Virus inactivation during coagulation with aluminum coagulants. Chemosphere 85, 571–576. doi:10.1016/j.chemosphere.2011.06.083.

Mehta, D., Hawley, M.C., 1969. Wall effect in packed columns. Industrial & Engineering Chemistry Process Design and Development 8, 280–282. doi:10.1021/i260030a021.

Mesquita, M.M., Emelko, M.B., 2012. Bacteriophages as Surrogates for the Fate and Transport of Pathogens in Source Water and in Drinking Water Treatment Processes, in: Kurtboke, I. (Ed.), Bacteriophages. InTech. 2006. chapter 4, pp. 57–80. doi:10.5772/34024.

Michen, B., Graule, T., 2010. Isoelectric points of viruses. Journal of Applied Microbiology 109, 388–397. doi:10.1111/j.1365-2672.2010.04663.x.

Moran, D.C., Moran, M.C., Cushing, R.S., Luwler, D.F., 1993. Particle Behavior in Deep-Bed Filtration: Part 1—Ripening and Breakthrough. Journal (American Water Works Association) 85, 69–81.

Nasser, A., Weinberg, D., Dinoor, N., Fattal, B., Adin, A., 1995. Removal of hepatitis A virus (HAV) poliovirus, and MS2 coliphage by coagulation and high rate filtration. Water Science & Technology 31, 63–68. doi:10.1016/0273-1223(95)00242-F.

Nilsen, V., 2016. Some aspects of deep-bed filtration dynamics in qmra for drinking water Manuscript in preparation.

Nygård, K., Wahl, E., Krogh, T., Tveit, O.A., Bøhleng, E., Tverdal, A., Aavitsland, P., 2007. Breaks and maintenance work in the water distribution systems and gastrointestinal illness: A cohort study. International Journal of Epidemiology 36, 873–880. doi:10.1093/ije/dym029.

Ødegaard, H., Eikebrokk, B., Storhaug, R., 1999. Processes for the Removal of Humic Substances from Water - an Overview Based on Norwegian Experiences. Water Science & Technology 40, 37–46. doi:10.1016/S0273-1223(99)00638-1.

Ødegaard, H., Østerhus, S., Melin, E., Eikebrokk, B., 2010. NOM removal technologies – Norwegian experiences. Drinking Water Engineering and Science 3, 1–9. doi:10.5194/dwes-3-1-2010.

Ødegaard, H., Østerhus, S.W., Pott, B.M., 2016. Microbial Barrier Analysis (MBA) - a guideline. Technical Report. Norsk Vann.

O'Melia, C.R., Ali, W., 1979. THE ROLE OF RETAINED PARTICLES IN DEEP BED FILTRATION, in: Jenkins, S. (Ed.), Proceedings of the 9th International Conference on Water Pollution Research, Stockholm, Sweden, 1978. Elsevier, pp. 167–182. doi:10.1016/B978-0-08-022939-3.50019-2.

Payment, P., Armon, R., 1989. Virus removal by drinking water treatment processes. Critical Reviews in Environmental Control 19, 15–31. doi:10.1080/10643388909388357.

Payment, P., Franco, E., 1993. Clostridium perfringens and somatic coliphages as indicators of the efficiency of drinking water treatment for viruses and protozoan cysts. Applied and Environmental Microbiology 59, 2418–2424.

Payment, P., Trudel, M., Plante, R., 1985. Elimination of viruses and indicator bacteria at each step of treatment during preparation of drinking water at seven water treatment plants. Applied and Environmental Microbiology 49, 1418–1428.

Pazmino, E.F., Ma, H., Johnson, W.P., 2011. Applicability of Colloid Filtration Theory in Size-Distributed, Reduced Porosity, Granular Media in the Absence of Energy Barriers. Environmental science & technology 45, 10401–10407. doi:10.1021/es202203m.

Penrod, S.L., Olson, T.M., Grant, S.B., 1995. Whole Particle Microelectrophoresis for Small Viruses. Journal of Colloid and Interface Science 173, 521–523. doi:10.1006/jcis.1995.1354.

Persson, F., Långmark, J., Heinicke, G., Hedberg, T., Tobiason, J., Stenström, T.A., Hermansson, M., 2005. Characterisation of the behaviour of particles in biofilters for pre-treatment of drinking water. Water Research 39, 3791–3800. doi:10.1016/j.watres.2005.07.007.

Petterson, S.R., Ashbolt, N.J., 2016. QMRA and water safety management: review of application in drinking water systems. Journal of Water and Health doi:10.2166/wh.2016.262.

Prasanthi, H., Vigneswaran, S., Dharmappa, H., 1997. Effect of particle concentration on the entire cycle of filtration. Water Science & Technology 35, 91–102. doi:10.1016/S0273-1223(97)00155-8.

Rao, V.C., Symons, J.M., Ling, A., Wang, P., Metcalf, T.G., Hoff, J.C., Melnick, J., 1988. Removal of Hepatitis A Virus and Rotavirus by Drinking Water Treatment. Journal (American Water Works Association) 80, 59–67.

Robeck, G., Clark, N., Dostal, K., 1962. Effectiveness of water treatment processes in virus removal. Journal (American Water Works Association) 54, 1275–1292.

Rose, J.B., Gerba, C.P., Singh, S.N., Toranzos, G.A., 1986. Isolating Viruses From Finished Water. Journal (American Water Works Association) 78, 56–61.

Sahlström, L., Bagge, E., Emmoth, E., Holmqvist, A., Danielsson-Tham, M.L., Albihn, A., 2008. A laboratory study of survival of selected microorganisms after heat treatment of biowaste used in biogas plants. Bioresource Technology 99, 7859–7865. doi:10.1016/j.biortech.2007.09.071.

Shirasaki, N., Matsushita, T., Matsui, Y., Oshiba, A., Ohno, K., 2010. Estimation of norovirus removal performance in a coagulation–rapid sand filtration process by using recombinant norovirus VLPs. Water Research 44, 1307–1316. doi:10.1016/j.watres.2009.10.038.

Sinclair, R.G., Rose, J.B., Hashsham, S.A., Gerba, C.P., Haas, C.N., 2012. Criteria for Selection of Surrogates Used To Study the Fate and Control of Pathogens in the Environment. Applied and Environmental Microbiology 78, 1969–1977. doi:10.1128/AEM.06582-11.

Stetler, R.E., Ward, R.L., Waltrip, S.C., 1984. Enteric Virus and Indicator Bacteria Levels in a Water Treatment System Modified to Reduce Trihalomethane Production. Applied and environmental microbiology 47, 319–324.

Strauss, J.H., Sinsheimer, R.L., 1963. Purification and properties of bacteriophage MS2 and of its ribonucleic acid. Journal of Molecular Biology 7, 43–54. doi:10.1016/S0022-2836(63)80017-0.

Svenson, S.B., Lönngren, J., Carlin, N., Lindberg, a.a., 1979. Salmonella bacteriophage glycanases: endorhamnosidases of Salmonella typhimurium bacteriophages. Journal of virology 32, 583–592.

Templeton, M.R., Andrews, R.C., Hofmann, R., 2007. Removal of particle-associated bacteriophages by dual-media filtration at different filter cycle stages and impacts on subsequent UV disinfection. Water Research 41, 2393–2406. doi:10.1016/j.watres.2007.02.047.

Thurston-Enriquez, J.a., Haas, C.N., Jacangelo, J., Gerba, C.P., 2003. Chlorine inactivation of adenovirus type 40 and feline calicivirus. Applied and environmental microbiology 69, 3979–3985. doi:10.1128/AEM.69.7.3979.

Tien, C., Ramaro, B., 2007. Granular Filtration of Aerosols and Hydrosols. 2 ed., Elsevier.

Tufenkji, N., 2007. Modeling microbial transport in porous media: Traditional approaches and recent developments. Advances in Water Resources 30, 1455–1469. doi:10.1016/j.advwatres.2006.05.014.

Tufenkji, N., Elimelech, M., 2004. Correlation Equation For Predicting Single-Collector Efficiency in Physiochemical Filtration in Saturated Porous Media. Environmental Science & Technology 38, 529–536. doi:10.1021/es034049r.

USEPA, 2006. National Primary Drinking Water Regulations: Long Term 2 Enhanced Surface Water Treatment Rule. Federal Register 71, 654–786.

Willumsen, A., 2015. Undersøkelse av virusfjerning i modning- og gjennombruddsperiodene i et pilotskala to-media sandfilter for drikkevann [Pilot-Scale Investigations of Virus Removal During the Ripening and Breakthrough Phases in a Dual-Media Sand Filter for Drinking Water]. Msc. Norwegian University of Life Sciences.

World Health Organization, 2011. Guidelines for Drinking-water Quality. 4 ed., World Health Organization, Geneva, Switzerland.

Supporting Information to Paper III

Appendix B. Online supporting material

Table B.5 gives an overview of the number of samples taken from each sampling location and which parameters were analyzed. Figure B.8 - B.10 shows the microorganism data with uncertainty estimates. These uncertainty estimates are only associated with the statistics of microbial counts or qPCR-procedures and do not reflect variation that is inherent in the experimental procedures. Tables B.6 and B.7 give a summary of 24 previous studies on virus removal in deep-bed filtration for drinking water where coagulation was employed at some point upstream of the filter, and for which the removal efficiency across the filter could be estimated (at least roughly).

Table B.5: Sampling regime. Numbers in parenthesis represent the number of Petri plates incubated.

Sampling point	**No. of samples**	**No. of samples analysed for parameter**						
		28B	MS2:PFU	MS2:RT-qPCR	*E.coli*	Turbidity	Color	Al
RW	5	0	0	0	1	4	4	0
FT	4	4 (8)	0	4	4	0	0	0
M1	6	6 (12)	4 (8)	6	6	6	0	0
M2	7	6 (12)	0	6	6	7	0	0
A-H	96	96 (241)	0	32	32	96	0	0
M3	42	42 (120)	5 (18)	30	24	6	5	1
SUM	160	154 (393)	9 (26)	78	73	119	9	1

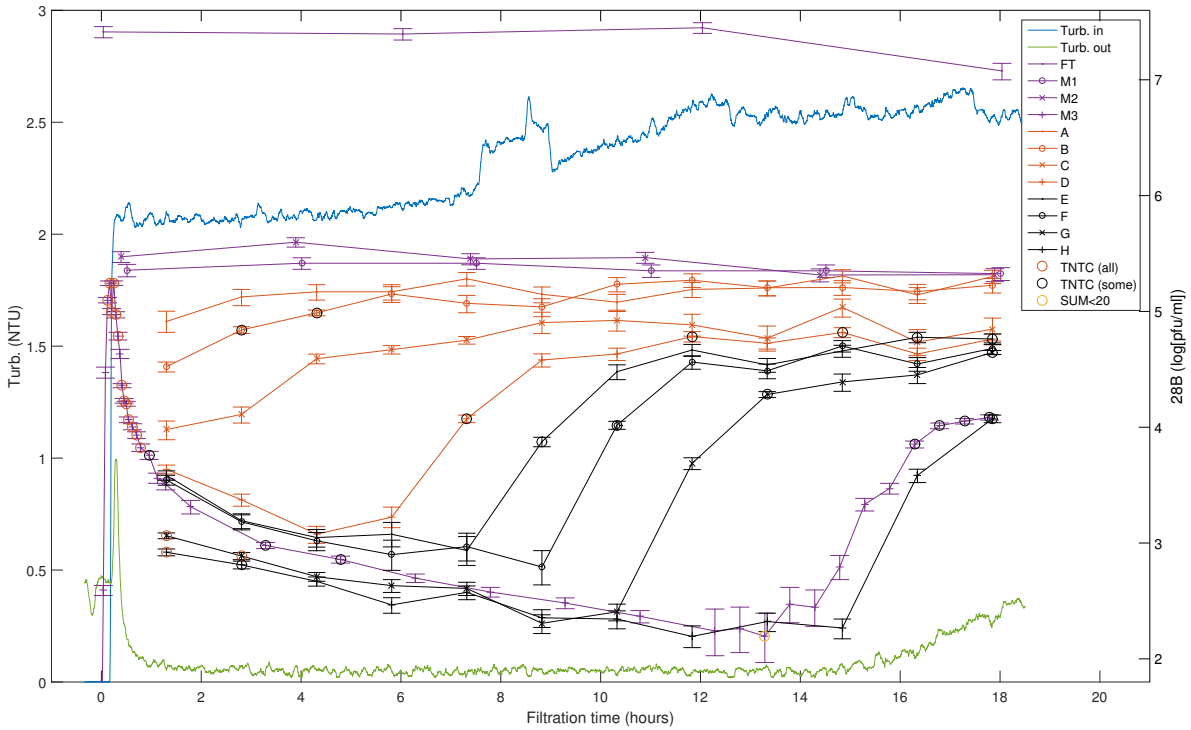

Figure B.8: Phage 28B concentrations with 95 % likelihood-ratio based confidence intervals, assuming that plaque counts are Poisson-distributed. Circles indicate whether some or all plates had plaques too numerous to count (TNTC) or whether the total count from all plates were less than 20.

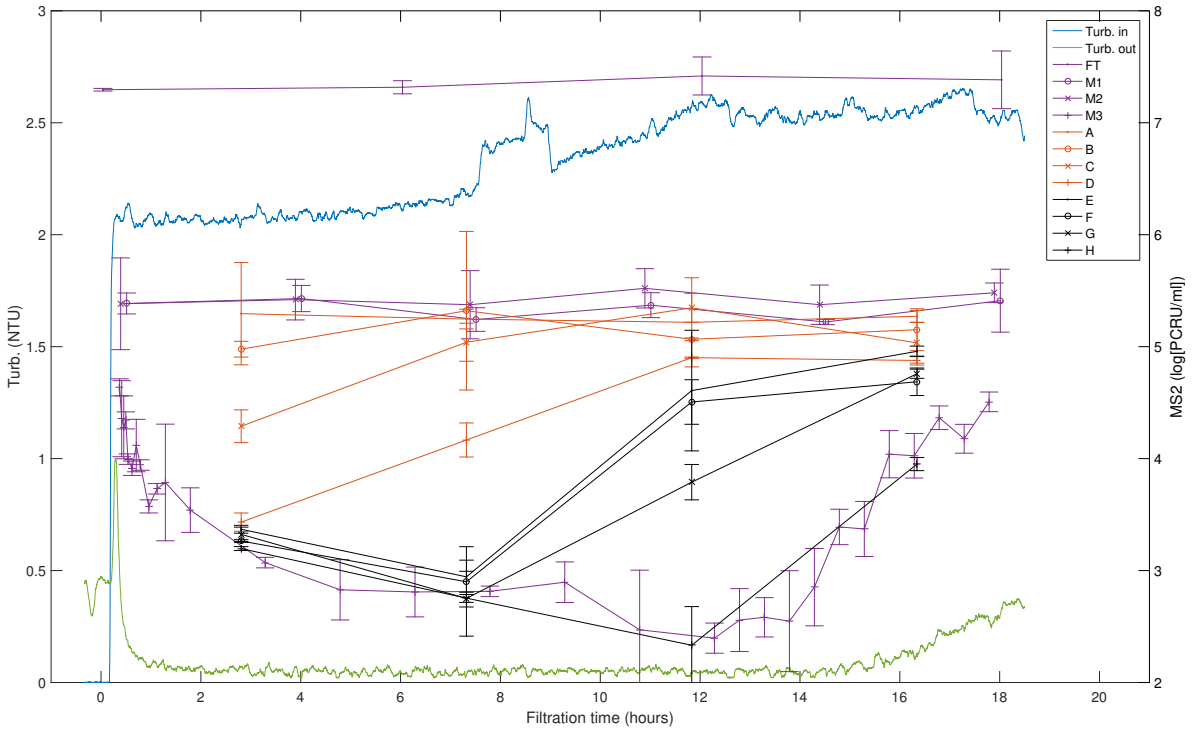

Figure B.9: MS2 RT-qPCR concentrations with uncertainty estimates derived from ± 3 standard deviations of replicate PCR C_q values.

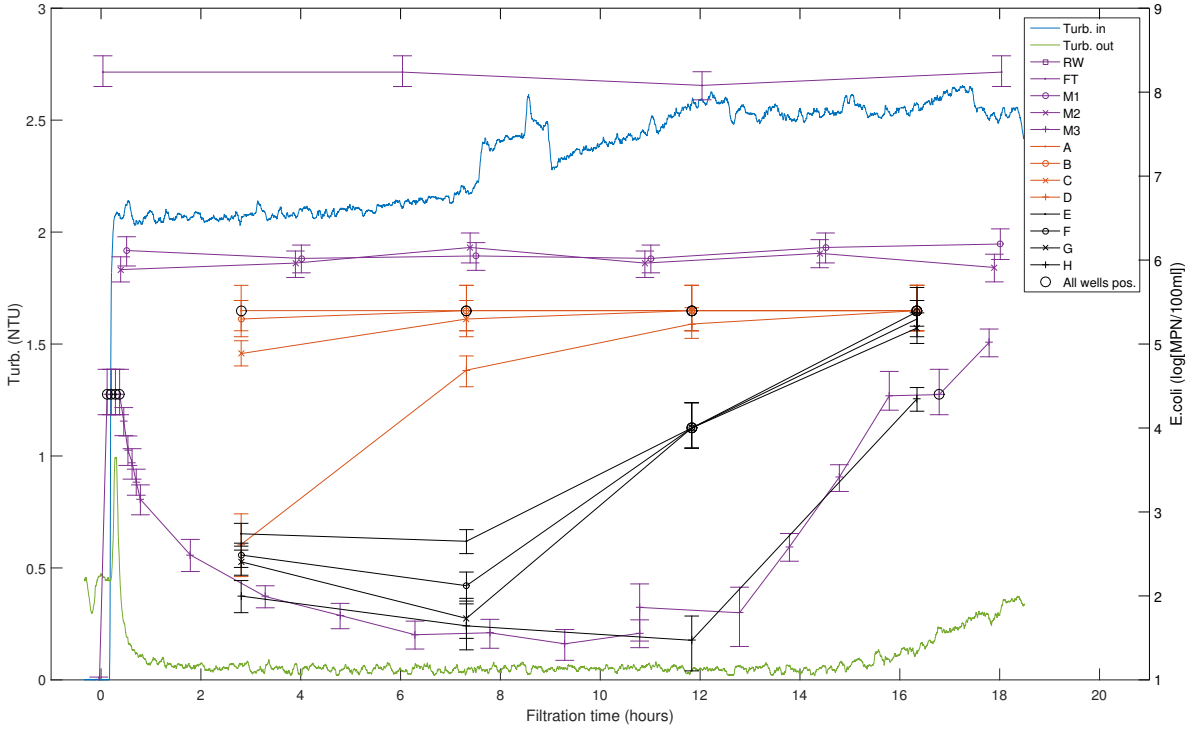

Figure B.10: *E.coli* concentrations with 95 % confidence intervals based on MPN-tables provided by IDEXX. Black circles indicate that all wells on the Quanti-Tray/2000 trays were positive.

Table B.6: Overview of results from previous studies on virus removal by rapid filtration: Experimental conditions.

Reference	Index	Scale — media[a] — type	F.rate [m/h]	Raw water	RW turb. [NTU]	RW org.mat.	RW pH	Coagulant[b] (dose)
This work	1	Pilot — F-S — contact	5.9	River	0.7-0.8	TOC=3.03 mg/l	7.3	PACl (1.5 mg Al/l)
Gilcreas and Kelly (1955)	2	Bench — S — conventional	4.8	Spring water	n/a	n/a	n/a	Alum (?)
Robeck et al. (1962)[c]	3	Pilot — A-S — contact	4.9	River	8	n/a	7.7-8.1	Alum (10 ppm)
”	4	Pilot — A-S — conventional	4.9	River	8	n/a	”	Alum (50 ppm)
”	5	Pilot — A-S — contact	4.9	River	27	n/a	”	Alum (n/a?)
”	6	Pilot — A-S — conventional	4.9	River	27	n/a	”	Alum (n/a?)
”	7	Pilot — A-S — contact	14.7	Tap	0.2	n/a	”	Alum (10 ppm)
”	8	Pilot — A-S — contact	14.7	Tap	0.2	n/a	”	Alum (5 ppm)
”	9	Pilot — A-S — contact	14.7	Synthetic	40	n/a	”	Alum (10 ppm)
”	10	Pilot — A-S — contact	4.9	Synthetic	12	n/a	”	Alum (10 ppm)
”	11	Pilot — A-S — contact	14.7	Synthetic	10	n/a	”	Alum (10 ppm)
Foliguet and Doncoeur (1975)	12	In French, no translation available to the author.						
Guy et al. (1977)	13	Pilot — A-S — conventional	n/a	River	n/a	n/a	n/a	Ferric sulphate (40 ppm)
”	14	Pilot — A-S — conventional	n/a	River	n/a	n/a	n/a	Ferric sulphate (40 ppm)
”	15	Pilot — A-S — conventional	n/a	River	n/a	n/a	n/a	Ferric sulphate (40 ppm)
Stetler et al. (1984)	16	Full (1 pl.) — n/a — conventional	n/a	River/poor	25.4 (mean)	n/a	n/a	Alum (n/a)
Keswick et al. (1984)	17	Full (1 pl.) — n/a — conventional	n/a	River/poor	26	n/a	7.4	Alum (n/a) + cat.pol.
Keswick et al. (1985)	18	Full (1 pl.) — n/a — conventional	n/a	Lake/poor	7.7	n/a	n/a	Alum (n/a) + cat.pol.
Payment et al. (1985)	19	Full (5 pl.) — n/a — conventional	n/a	Variable/poor	Var./high	Var./high	Var	n/a
Agbalika et al. (1985)[c]	20	Full (1 pl.) — n/a — conventional	3.6-5.1	River	12-36	COD=2.7-4.6 mg/l	8-8.1	Water alum. chloride (15-20 ppm)
Joret et al. (1986)	21	Full — n/a — conventional	5	River	n/a	n/a	n/a	n/a
Rose et al. (1986)	22	Full (3 pl.) — n/a — conventional	n/a	River/poor	3.4	n/a	n/a	Alum (31 mg/l) + cat. pol.
Rao et al. (1988)	23	Bench — CSG — conventional	4.7	Lake	42	n/a	n/a	Alum?
”	24	Bench — CSG — conventional	4.7	Lake	34	n/a	n/a	Alum?
”	25	Bench — S — conventional	4.7	Lake	34	n/a	n/a	Alum?
”	26	Bench — S — conventional	4.7	Lake	25	n/a	n/a	Alum?
”	27	Bench — CSG — conventional	4.7	Lake	12/14/26	n/a	n/a	Alum (15 mg/l) + cat.pol.
Payment and Franco (1993)	28	Full (3 pl.) — n/a — conventional	n/a	Variable/poor	n/a	n/a	n/a	Various
”	29	Full (3 pl.) — n/a — conventional	n/a	Variable/poor	n/a	n/a	n/a	Various
”	30	Full (3 pl.) — n/a — conventional	n/a	Variable/poor	n/a	n/a	n/a	Various
”	31	Full (3 pl.) — n/a — conventional	n/a	Variable/poor	n/a	n/a	n/a	Various
Nasser et al. (1995)	32	Pilot — S — contact	n/a	Kaolin+humic acid	~10	TOC=3.7 mg/l	n/a	Alum (30 ppm)
”	33	Pilot — S — contact	n/a	Kaolin+humic acid	~10	”	n/a	Alum (30 ppm) + pol.
Gitis et al. (2002)	34	Bench — S — contact	10	Synthetic	12.8	n/a	7.5?	Alum (10 mg/l)
Gerba et al. (2003)	35	Pilot — GAC-S — conventional	24	n/a	n/a	n/a	n/a	Alum (20-23 mg/l) + cat.pol.
Harrington et al. (2003)[d]	36	Pilot — 2M / 3M — conventional	5-20	Lake	~8.6	UV_{254}=0.074 cm^{-1}	~7.6	Alum (50-80 ppm)
Hendricks et al. (2006)	37	Pilot — A — contact	12.2	Lake	1.2-3.5	TOC=3 mg/l	n/a	Alum (26 mg/l)
”	38	Pilot — A-S — contact	12.2	Lake	1.2-3.5	”	n/a	Alum (26 mg/l)
”	39	Pilot — A — conventional	12.2	Lake	1.2-3.5	”	n/a	Alum (26 mg/l)
”	40	Pilot — A — contact	12.2	Lake	1.2-3.5	”	n/a	Alum (13 mg/l)
”	41	Pilot — A — contact	12.2	Lake	1.2-3.5	”	n/a	No coagulant
”	42	Pilot — A-S — contact	12.2	Lake	1.2-3.5	”	n/a	No coagulant
Abbaszadegan et al. (2007)	43	Pilot — GAC-S — conventional	12	Mix:surface+ground	13.2-17.7	DOC=4.86 mg/l	8.25	$FeCl_3$ (40 mg/l) + cat.pol.
”	44	Pilot — GAC-S — conventional	24	Mix:surface+ground	14-19	”	8.25	$FeCl_3$ (40 mg/l) + cat.pol.
Templeton et al. (2007)[e]	45	Bench — A-S — direct	1.9-6.8	Tap+kaolin clay	n/a	n/a	7.2	Alum (25mg/l)
”	46	Bench — A-S — direct	1.9-6.8	Tap+humic acids	n/a	n/a	”	Alum (50mg/l)
”	47	Bench — A-S — direct	1.9-6.8	Tap+kaolin clay	n/a	n/a	”	Alum (25mg/l)
”	48	Bench — A-S — direct	1.9-6.8	Tap+humic acids	n/a	n/a	”	Alum (50mg/l)
Abbaszadegan et al. (2008)	49	Pilot — GAC-S — conventional	12	Mix:surface+ground	<0.2	n/a	8	Ferric chloride (20 mg/l) + cat.pol.
”	50	Pilot — GAC-S — conventional	12	Mix:surface+ground	<0.2	n/a	”	Ferric chloride (40 mg/l) + cat.pol.
”	51	Pilot — GAC-S — conventional	24	Mix:surface+ground	<0.2	n/a	”	Ferric chloride (20 mg/l) + cat.pol.
”	52	Pilot — GAC-S — conventional	24	Mix:surface+ground	<0.2	n/a	”	Ferric chloride (40 mg/l) + cat.pol.
Shirasaki et al. (2010)	53	Bench — S — conventional	5	River	0.63	DOC=0.76mg/l	6.8	PACl (0.54 mg Al/l)
”	54	Bench — S — conventional	5	River	0.63	”	6.8	PACl (1.08 mg Al/l)
”	55	Bench — S — conventional	5	River	0.63	”	6.8	PACl (1.62 mg Al/l)
”	56	Bench — S — conventional	5	River	0.63	”	6.8	Alum (1.08 mg Al/l)
”	57	Bench — S — conventional	5	River	0.63	”	6.8	$FeCl_3$ (2.24 mg Fe/l)
”	58	Bench — S — conventional	5	River	0.63	”	5.8	$FeCl_3$ (2.24 mg Fe/l)
Boudaud et al. (2012)	59	Pilot — S — conventional	2.3	River	5.4-18.3	TOC=2.5-3.1 mg/l	7.6-8.2	PAX-XL7 (2.25 mg Al/l)
Asami et al. (2016)	60	Full (1 pl.) — A-S — conventional	12-20	River	51-185	n/a	6.8-7.2	Alum (45-60 mg/l)

[a] Filter media keys: A - anthracite; CSG - coal, sand and garnet mix; F - Filtralite; GAC - granular activated carbon; S - sand.
[b] PACl - poly-aluminium chloride; PAX-XL7 - aluminium polyhydroxychlorosulfate; cat. - cationic; pol. - polymer.
[c] Robeck et al. (1962) reported turbidity in Jackson turbidity units (JTU).
[d] Harrington et al. (2003) investigated a wide range of filter media and experimental conditions.
[e] Templeton et al. (2007) used declining rate filtration.

Table B.7: Overview of results from previous studies on virus removal by rapid filtration: Virus removal data.

Reference	Index	Virus[a]	Typical $\log_{10}$ removal	Note particularly
This work	1	S.t. 28B — MS2	2-3 — 2-3	Prolonged ripening, virus breakthrough shortly before turbidity breakthrough
Gilcreas and Kelly (1955)	2	Coxsackie A — Theiler — T4	1 — 1 — 1.7	Samples taken during initial ripening?
Robeck et al. (1962)	3	Polio I	1.7	Prolonged ripening
”	4	Polio I	>2	-
”	5	Polio I	1-1.3	Prolonged ripening
”	6	Polio I	>2	-
”	7	Polio I	ca. 2	Virus breakthrough, but no turbidity breakthrough
”	8	Polio I	ca. 1.2	-
”	9	Polio I	>2	Short run
”	10	Polio I	ca. 2	Long run, no virus breakthrough
”	11	Polio I	ca. 2	Virus and turbidity breakthrough coincided
Foliguet and Doncoeur (1975)	12	In French, no translation available to the author.		
Guy et al. (1977)	13	Natural phages	ca. 0.2	
”	14	T4	0-0.9	Time since last backwash important
”	15	Polio I,II,III	0.1-0.2	Time since last backwash important
Stetler et al. (1984)	16	Culturable enteric viruses	0.6	Large volume sampling
Keswick et al. (1984)	17	Coliphages — Enteroviruses — Rotavirus	1 — 0.3 — 0.7	Rainy season, large volume sampling
Keswick et al. (1985)	18	Rotavirus	Negative removal	Dry season (Mexico), large volume sampling
Payment et al. (1985)	19	Enteroviruses	1.2	Large volume sampling
Agbalika et al. (1985)	20	Enteroviruses	0.35	Large volume sampling
Joret et al. (1986)	21	Enteroviruses	0.6 - 2	Only abstract available
Rose et al. (1986)	22	Coliphages — Enteroviruses — Rotavirus	1.2 — >1 — -0.6	Large volume sampling
Rao et al. (1988)	23	Polio I	0.43	Samples taken during initial ripening?
”	24	Rotavirus	0.45-0.64	Samples taken during initial ripening?
”	25	Rotavirus	0.1-0.15	Samples taken during initial ripening?
”	26	Hepatitis A	0.5	Samples taken during initial ripening?
”	27	Polio I — Rotavirus — Hepatitis A	1.06 — 2.55 — 0.36	Samples taken during initial ripening?
Payment and Franco (1993)	28	Culturable human enteric viruses	>1.8 — 3.8 — -0.5	Large volume sampling
”	29	Somatic phages (E.coli host)	1.1 — 2.6 — -0.2	Large volume sampling
”	30	F-specific phages	n/a — 1.8 — -0.6	Large volume sampling
”	31	Somatic phages (Salmonella host)	n/a — 0.8 — -1.5	Large volume sampling
Nasser et al. (1995)	32	MS2 — Polio I — Hepatitis A	1.15 — 0.7 — n/a	
”	33	MS2 — Polio I — Hepatitis A	2 — 1.05 — >1.15	Worse with humic acids / early Polio I breakthrough
Gitis et al. (2002)	34	MS2	0.4 — 0.7	With 20 cm — 40 cm beds, respectively
Gerba et al. (2003)	35	MS2 — PRD1 — Fr — Feline calicivirus	0.68 — 1.07 — 1.24 — 0.56	
Harrington et al. (2003)	36	MS2	2-3.5	Combined removal of sedimentation+filtration.
Hendricks et al. (2006)	37	MS2 — Polio — ϕ-X174 — Echovirus-12	2.9 — 2.2 — 5.1 — 2.4	
”	38	MS2 — ϕ-X174	2.9 — 5.1	
”	39	MS2 — ϕ-X174	2.8 — 5.3	
”	40	MS2 — ϕ-X174	0.9 — 1.4	
”	41	MS2 — ϕ-X174	0 — 0.05	
”	42	MS2 — ϕ-X174	0.02 — 0.1	
Abbaszadegan et al. (2007)	43	MS2 — PRD1 — ϕ-X174 — Fr	0.66 — 2.94 — 0.66 — 0.57	
”	44	MS2 — PRD1 — ϕ-X174 — Fr	2.58 — 3.11 — 0.94 — 3.53	
Templeton et al. (2007)	45	T4	2.1 — 2.8 — 2.0	Ripening — stable period — breakthrough, respectively
”	46	T4	2.5 — 3.3 — 2.5	Ripening — stable period — breakthrough, respectively
”	47	MS2	2.8 — 3.3 — 2.8	Ripening — stable period — breakthrough, respectively
”	48	MS2	2.8 — 3.4 — 1.6	Ripening — stable period — breakthrough, respectively
Abbaszadegan et al. (2008)	49	MS2 — PRD1 — ϕ-X174 — Fr	2.9 — 0.7 — 0.3 — 2.0	
”	50	MS2 — PRD1 — ϕ-X174 — Fr	2.2 — 1.4 — 0.5 — 1.9	
”	51	MS2 — PRD1 — ϕ-X174 — Fr	3.0 — 1.1 — 0.3 — 3.4	
”	52	MS2 — PRD1 — ϕ-X174 — Fr	3.0 — 2.0 — 0.6 — 3.0	
Shirasaki et al. (2010)	53	Noro-VLP — MS2 — Qβ	~0	10 cm column
”	54	Noro-VLP — MS2 — Qβ	1.7 — 0.5 — 0.5	10 cm column
”	55	Noro-VLP — MS2 — Qβ	1.8 — 0.7 — 0.6	10 cm column
”	56	Noro-VLP — MS2 — Qβ	1.3 — 0.1 — 0.3	10 cm column
”	57	Noro-VLP — MS2 — Qβ	~0	10 cm column
”	58	Noro-VLP — MS2 — Qβ	1.5 — 1.5 — 2.0	10 cm column
Boudaud et al. (2012)	59	MS2 — Qβ — GA	4.24 — 2.74 — 1.03	Combined removal of sedimentation+filtration. RT-qPCR used.
Asami et al. (2016)	60	PMMoV — JC PyV	1.3 (0.8) — 0.5 (0.6)	RT-qPCR used.

[a] Noro-VLP - Noro-virus like particles; PMMoV - Pepper mild mottle virus; JC PyV - JC polyomavirus.

Paper IV

Nilsen, V. (2016). "Some aspects of deep-bed filtration dynamics in QMRA for drinking water." Manuscript in preparation.

Some aspects of deep-bed filtration dynamics in QMRA for drinking water

Vegard Nilsen*

Norwegian University of Life Sciences, Dept. of Mathematical Sciences and Technology, P.O.Box 5003, N-1432 Aas, Norway

Abstract

Unlike most unit processes in drinking water treatment, the performance of deep-bed filtration processes vary systematically on short time-scales; the particle removal capacity changes with elapsed time since the previous backwash, even when the influent water quality remains stable. For microorganisms, the removal efficiency may vary by orders of magnitude. In this work, we study the potential impact of such dynamics on microbial risk estimates and optimal filter operation, using representative experimental filtration data for viruses and bacteria. The data is used as input in a simplified conceptual model of a water supply system in conjunction with dose-response models for microbial infection.

Assuming that filtration is the only source of variation in pathogen concentrations on the time-scale of a single filter cycle, it is concluded that such variations are unlikely to substantially affect risk estimates, except possibly in an outbreak situation with extremely high pathogen concentrations; it generally suffices to know the *mean* pathogen concentrations. Future experimental work should focus on capturing the variation in performance in order to correctly estimate *mean* removal rates. Our results suggest that overall mean removal rates may differ substantially from typical mid-cycle removal rates, and it is demonstrated that the best *mean* removal rate actually occurs *after* breakthrough of an organism and closer to turbidity breakthrough. However, continuing filtration beyond turbidity breakthrough, even if turbidity remains below 0.1 NTU, may completely negate overall mean removal rates for the entire filter cycle. Future studies should include concurrent variation in the performance of other unit processes and raw water pathogen concentrations.

Keywords:
microbial risk, drinking water, filtration, dynamics

1. Introduction

A treatment train consisting of some combination of coagulation, flocculation, sedimentation/flotation and *deep-bed filtration* is common in water treatment plants throughout the world. While designed for removing particles and/or natural organic matter (NOM) in general, coagulation-filtration processes also account for a significant portion of the overall microorganism removal, including pathogens (Hijnen and Medema, 2010).

The microbial removal efficiency of the filtration process may vary between plants because of differences in design, raw water quality and operational practices. For a given plant, removal efficiency may also vary slowly in time, e.g. because of varying raw water composition throughout the year (Westrell et al., 2006), or it may change rapidly as a result of raw water contamination events (Signor et al., 2005; Åström et al., 2013) or upsets in the treatment processes (Hijnen and Medema, 2010; Huck et al., 2002; Emelko et al., 2003). Variations in removal rates have previously been modeled by fitting appropriate probability distributions to data from filter influent and effluent samples (Teunis et al., 1999, 2009; Smeets et al., 2008). In *quantitative microbial risk assessment* (QMRA; Haas et al., 2014), such fitted distributions may be used together with data on raw water quality as part of an effort to estimate the exposure of water consumers to pathogens. Data on exposure is subsequently used as input to dose-response models (Haas, 1983; Nilsen and Wyller, 2016a) for estimating microbial risks associated with drinking water consumption.

However, superimposed on the variations already mentioned, there may be *systematic* short-term variations in removal efficiency originating from the *inherently dynamic* character of the deep-bed filtration process during normal operation, even if influent water quality characteristics remain constant. Typically, as measured by filter effluent turbidity, there is an initial period of improvement in performance as the filter begins to collect particles (the ripening period), followed by a period of relatively stable performance until the performance eventually deteriorates (the breakthrough phase) when the particle collection capacity is exhausted, unless terminal head loss is reached earlier. The filter must then be taken out of service to be back washed so that the particle collection capacity can be restored to its initial state (i.e. the process is discontinuous and essentially periodic). These dynamic characteristics distinguish the filtration process from other typical unit processes in conventional treatment (sedimentation, flotation, chlorination, UV-irradiation), that are comparatively stable and uninterrupted during normal operation and when subjected to a constant in-

*Telephone: +47 930 94 406
Email address: vegard.nilsen@nmbu.no, vgnils@gmail.com (Vegard Nilsen)

fluent water quality.

Turbidity dynamics during filtration is not entirely representative for microbial filtration dynamics, though, since turbidity measurements lump the contribution of all particle types into a single parameter. Several studies have shown that the ripening and breakthrough behavior is dependent on particle size (Clark et al., 1992; Kim and Lawler, 2008; Moran et al., 1993), with smaller particles typically taking longer to both ripen and break through as compared to larger particles. Some studies have shown a marked reduction in microorganism removal early and late in the filter cycle (Robeck et al., 1962; Harrington et al., 2003; Emelko et al., 2003; Templeton et al., 2007). Still, studies that aim to characterize microbial removal rates of filtration processes are usually focused on "typical" removal rates, or removal rates during periods of stable effluent turbidity, often employing sampling regimes that are unable to capture the full variation in treatment efficiency throughout the filter cycle.

Recently, we undertook a pilot-scale dual-media contact-filtration study in an attempt to generate a high-resolution sample of such microbial filtration dynamics during an entire filter cycle (Nilsen et al., 2016). The instantaneous removal efficiency of model viruses and bacteria varied by a factor of about 50 and 200, respectively, within the period when effluent turbidity was less than 0.1 NTU, indicating that the dynamic character of filtration processes should not be overlooked in risk assessment.

The effect of such short-term systematic variations in microbial filtration efficiency, that are present during normal operation, has received comparatively little attention in the microbial risk literature, and is the topic of this paper. We will make an attempt to develop simplified conceptual models that account for such variation and analyze its effects when paired with typical dose-response models. Data from our filtration experiments will be used to exemplify and demonstrate the type of computations that can be performed when data of sufficiently high resolution is available. We will draw some preliminary conclusions on the relevance of filtration dynamics for QMRA and optimal filter operation.

2. Example data

The filtration experiment that generated the example data is reported in full elsewhere (Nilsen et al., 2016); here a brief summary is given. The purpose was to undertake a detailed characterization of virus and bacterial removal during a full filtration cycle and at several depths of the filter, in a setup representative of Norwegian filtration practice (Ødegaard et al., 2010). A pilot-scale circular (10 cm diameter) dual-media filter consisting of Rådasand (0.4-0.8 mm grains; 50 cm depth) above Filtralite (0.8-1.6 mm grains; 80 cm depth) was run with a constant filtration rate of 5.9 m/h. Raw water (turbidity 0.7-0.8 NTU, color 26 mg Pt/l) was collected from a river and coagulated inline with 1.5 mg Al/l of a 42 % basicity polyaluminum chloride coagulant at pH 5.9; no dedicated flocculation step was used (i.e. contact-filtration). Effluent turbidity is shown in Figure 1 (influent turbidity after coagulation was approx. 2.0-2.1 NTU), effluent color remained at around 3 mg Pt/l and a single sample taken mid-cycle showed a residual Al-content of 0.031 mg Al/l.

Bacteriophage MS2 (icosahedral, 27 nm), bacteriophage *Salmonella* Typhimurium 28B (icosahedral, 60 nm; Lilleengen, 1948; Svenson et al., 1979) and indicator bacterium *E.coli* (rod-shaped, approx. 1 μm x 3 μm) were continuously added inline, before coagulant addition, to provide a constant influent concentration of microorganisms. Microorganism concentrations were determined by RT-qPCR (MS2), plaque assay (28B) and Colilert-18 (*E.coli*). Figure 1 shows the logarithm of the estimated probability of passage, π_1, as a function of elapsed time in the filter cycle, t. More precisely,

$$\pi_1(t) = \frac{\dot{m}_1(t)}{\dot{m}_{\text{in}}(t)} = \frac{q_1(t)c_1(t)}{q_1(t)c_{\text{in}}(t)} = \frac{c_1(t)}{c_{\text{in}}(t)} \tag{1}$$

Here, c_1 and c_{in} are, respectively, the effluent and influent concentrations (as number of microorganisms/unit volume) from the filter; c_{in} was estimated from 12 influent samples and taken as constant. The flow rate is denoted by q_1, and the effluent and influent mass transport of microorganisms by $\dot{m}_1$ and $\dot{m}_{\text{in}}$, respectively. Our notation will not distinguish between organisms; it will be clear from context which organism is being discussed. Some computations in this paper have only been performed for phage 28B and *E.coli*. We use the subscript 1 here to denote this reference filter, to distinguish it from hypothetical copies of it introduced later. The commonly used log-removal rate is simply $-\log_{10}(\pi_1)$. Note that in formulating (1), we ignored the travel time between filter inlet and outlet, which is short relative to the duration of the filter cycle.

The strict interpretation of π_1 as the probability of passage of a single organism hinges on the assumption that organisms are removed independently of each other (otherwise $\pi_1(t)$ might depend on $c_{\text{in}}(t)$), and the assumption that detachment of organisms from filter grains is negligible compared to attachment (otherwise $c_1(t)$ will depend on the number of organisms available for detachment, i.e. the history of organism capture). Finally, it is assumed that $\pi_1(t)$ is determined by the amount and physico-chemical character of the particles that are already captured in the filter, of which the microorganisms themselves constitute a negligible proportion and therefore exert no influence on $\pi_1(t)$. In short: $\pi_1(t)$ is assumed to be independent of both influent and attached microorganism concentrations.

The data shows that bacteria were generally removed better than viruses, and the results are also consistent with expectations based on the size-difference between the organisms: ripening for bacteria occurred more rapidly than for viruses, and bacteria broke through before viruses. We define breakthrough here as the onset of persistently increasing passage.[1] Both organisms broke through before turbidity, though. It is noted that the breakthrough of viruses is rather abrupt compared to the more gradual breakthrough of bacteria. Each of the data series in Figure 1 has been fitted to a cubic smoothing spline with smoothing parameter 0.9 using the Curve Fitting Toolbox in

[1] For turbidity other definitions in terms of reaching a certain threshold value seem to be in use.

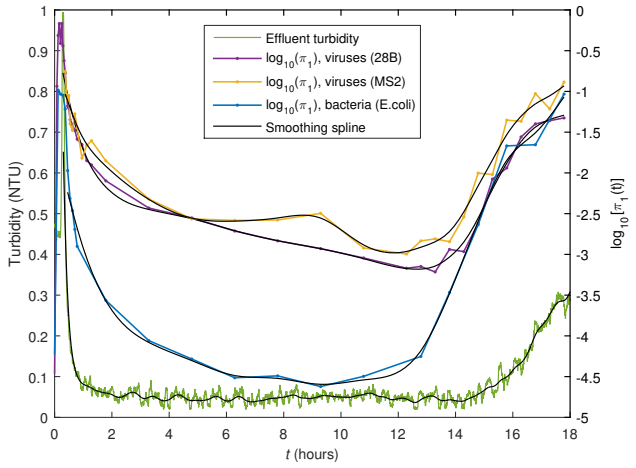

Figure 1: Data from the filtration experiment described in Section 2. After backwash, the filter was run briefly with raw water to displace the backwash water and $t = 0$ corresponds to the first arrival of coagulated water at the filter surface. The theoretical clean bed retention time in the filter was approx. 7 minutes.

MATLAB (MathWorks, 2014). Unless otherwise noted, computations reported in this paper were performed directly on the experimental data, interpolating linearly between data points to construct a continuous function $\pi_1(t)$.

3. Conceptual framework

In the following sections, the necessary mathematics of pathogen dose distributions and dose-response models will be formulated, and we will develop a simplified conceptual model for a water supply system. The concepts of probability generating and moment generating functions (abbreviated pgf and mgf, respectively) will be used; for a short review of these concepts in a QMRA-setting, the reader may consult Nilsen and Wyller (2016a) and Nilsen and Wyller (2016b) with online supporting information.

3.1. Pathogen dose distributions

Let the pathogen count (dose) in a single sample of unboiled tap water at a given location in a water distribution system be a non-negative discrete random variable X.[2] In the simplest case of a water supply with completely dispersed pathogens with a constant mean pathogen concentration c, X is by default assumed to be Poisson-distributed with a single parameter $\mathrm{E}(X) = \lambda = cv_s$, where v_s is the sample volume for ingestion. Its probability mass function (pmf) is

$$p_X(x) = \frac{e^{-\lambda}\lambda^x}{x!} \tag{2}$$

[2]We will adhere to the convention of denoting random variables with uppercase letters and corresponding instances of the variables with lowercase letters. We will however abuse notation somewhat and let some lower case symbols (e.g. c) denote both an instance of a random variable C and a function c evaluated at t (which could be thought of as a realization of a stochastic process $C(t)$).

Temporal variations in c at the point of consumption, i.e. the concentration may be thought of as a random variable C, will give rise to mixed Poisson distributions for the dose X,

$$p_X(x) = \int_0^\infty \frac{e^{-\lambda}\lambda^x}{x!} f_\Lambda(\lambda)\,\mathrm{d}\lambda \tag{3}$$

where $f_\Lambda(\lambda)$ is the probability density function (pdf) of $\Lambda = v_s C$. Such a mixed Poisson distribution has the following properties:

$$\begin{aligned} \mathrm{E}(X) &= \mathrm{E}(\Lambda) \\ \mathrm{Var}(X) &= \mathrm{E}(\Lambda) + \mathrm{Var}(\Lambda) \\ \theta_X &= 1 + \frac{\ln\left[p_X(0)\right]}{\mathrm{E}(X)} = 1 + \frac{\ln\left[M_\Lambda(-1)\right]}{\mathrm{E}(\Lambda)} \end{aligned} \tag{4}$$

Here, M_Λ is the mgf of Λ, and θ_X is known as the zero-inflation index. The latter is useful in formulating some dose-response models in the next section. As explained further in Section 3.3, we will assume in this paper that $\Lambda = k\Pi$, where k is a constant and Π is a random filtration passage probability.

Our interest in this paper is the *systematic* temporal variations in $\lambda(t) = v_s c(t)$ that arise from the filtration process and, as a working assumption, might persist until a point of consumption. These variations must however be treated as random from the point of view of the consumer since the consumer samples essentially randomly from the water supply. We need some precision in describing this sampling process. Assume that the consumer samples from a treatment plant effluent with mass flux of pathogens $\dot{m}$, given by:

$$\dot{m}(t) = q(t)c(t) \tag{5}$$

It is natural to assume that every volume of water produced has the same chance of being ingested by a consumer; i.e. the consumer samples uniformly from the total volume produced (flow proportional sampling) which, when $q(t)$ is non-constant, is *not equivalent* to sampling uniformly in time. The total volume of water $v(t)$ produced in the time interval $[0, t]$ is given by

$$v(t) = \int_0^t q(\tau)\,\mathrm{d}\tau \quad \Longleftrightarrow \quad \frac{\mathrm{d}v}{\mathrm{d}t} = q(t) \tag{6}$$

Since $q(t)$ is positive, $v(t)$ is one-to-one and may be inverted to give a function $t(v)$. When $c(t)$ is given, we may therefore express it as a function of v, $c[t(v)]$, and use the approach outlined in Appendix A to obtain the probability distribution for $\Lambda = v_s C[t(V)]$ when V is uniformly distributed on $[0, v]$. It is assumed here that v_s is so small that we may treat $\lambda(t) = v_s c(t)$ as constant during the time interval needed to sample a volume v_s.

3.2. Dose-response models

Dose-response models relate the pathogen dose distribution to the probability of the consumer suffering negative health consequences, most often identified with the establishment of an infection. For drinking water studies, the *single-hit* dose-response framework (Haas, 1983; Nilsen and Wyller, 2016a),

of which the exponential and beta-Poisson models are examples, has served as the de facto standard modeling approach. It postulates that pathogens act independently of each other in overcoming host defenses and that infection results if at least one pathogen overcomes these defenses. A generic formulation is given by

$$P_{\mathrm{I}} = 1 - \int_0^1 G_X(1-r) f_R(r)\,\mathrm{d}r \tag{7}$$

where P_{I} is the probability of infection, G_X is the pgf of X and f_R is the pdf of the so-called single-hit probability R, which may vary between hosts, but variation between individual pathogens is integrated out (Fazekas de St Groth and Moran, 1955; Haas, 2002; Schmidt et al., 2013; Nilsen and Wyller, 2016b)).

The pgf of the mixed Poisson distribution in (3) can be shown to be $M_\Lambda(-r)$, in which case equation (7) becomes

$$P_{\mathrm{I}} = 1 - \int_0^1 M_\Lambda(-r) f_R(r)\,\mathrm{d}r = 1 - \int_0^1 M_\Pi(-kr) f_R(r)\,\mathrm{d}r \tag{8}$$

where the latter equality holds for $\Lambda = k\Pi$. Since single-hit models are non-linear (concave) in the dose variable, the risk computed with a mixed Poisson dose distribution is always less than the risk computed with a Poisson distribution with the same mean (Nilsen and Wyller, 2016b, Proposition 2). There is also a clear tendency that the risk estimate from (7) decreases with increasing dispersion in X, although we are unaware of a formal result to make this stronger assertion precise in this context.[3] Nevertheless, P_{I} in (7) can be shown to be bounded from above by the following quantity (Nilsen and Wyller, 2016b, Proposition 3):

$$\begin{aligned} P_{\mathrm{I,b}} &= [1 - p_X(0)] \cdot P_{\mathrm{I}}^0\left(\frac{\mathrm{E}(X)}{1 - p_X(0)}\right) \\ &= \left(1 - e^{(\theta_X - 1)\cdot \mathrm{E}(X)}\right) \cdot P_{\mathrm{I}}^0\left(\frac{\mathrm{E}(X)}{1 - e^{(\theta_X - 1)\cdot \mathrm{E}(X)}}\right) \end{aligned} \tag{9}$$

Here $P_{\mathrm{I}}^0(x)$ represents any *concave* conditional dose-response model (Haas, 2002); in the single-hit case, it becomes

$$P_{\mathrm{I}}^0(x) = 1 - \int_0^1 (1-r)^x f_R\,\mathrm{d}r \tag{10}$$

The bound (9) can be shown to be *decreasing* with θ_X. Thus, if filter operations can be used to increase θ_X for given $\mathrm{E}(X)$, there may be some opportunities for optimization. Put another way, for a given number of pathogens delivered with a water supply, the single-hit framework suggests that it is better to concentrate them in a small volume rather than spreading them out.

The treatment above assumed that X is the dose resulting from a single-exposure. The risk resulting from n doses, independent and identically distributed (iid) as X, is given by (Nilsen and Wyller, 2016a):

$$P_{\mathrm{I}} = 1 - \int_0^1 [M_\Lambda(-r)]^n f_R(r)\,\mathrm{d}r \tag{11}$$

[3]The concept of *stochastic dominance*, widely used in expected utility theory in economics, may provide the tools needed to make progress. See Nilsen and Wyller (2016b).

3.3. Water supply system

In general, the distribution of the dose X depends on (1) the pathogen concentration in the raw water, (2) the treatment efficiency and (3) any effects of transport through the distribution system. Each of these three components may be characterized by their own variation, possibly on multiple time-scales; hence the actual distribution of X may be very complex. Therefore, in developing our conceptual model in this section, we will have to make some simplifying assumptions. To aid in the model develoment, Figure 2 shows a general conceptual layout of a water supply system with a water treatment plant that includes n filters operating in hydraulic parallel. The mass fluxes of pathogens at various locations in the system are denoted as shown in the figure.

First, we will assume that all filters have identical designs, receive identically composed influent water and are operated identically except that their filtration cycles are displaced in time to accommodate backwashing. Thus, the pathogen passage probability of a filter indexed by i is given by $\pi_i(t) = \pi_1(t - \delta_i)$, where δ_i is a time-shift, or phase-shift, relative to the reference filter $\pi_1(t)$. Furthermore, we will assume that the effluent from all filters is instantaneously mixed at the point where the parallel filter lines merge. The time evolution of pathogen concentrations in the water at this point, and therefore the distribution of X when sampling from it, then becomes a function of the $\delta_i's$. With reference to Figure 2, the net probability of passage of n filters as a function of time is given by

$$\pi(t) = \frac{\sum_{i=1}^n q_i(t) c_i(t)}{c_{\mathrm{in}}(t) \sum_{i=1}^n q_i(t)} = \frac{\sum_{i=1}^n q_i(t) \pi_i(t)}{\sum_{i=1}^n q_i(t)} = \frac{\sum_{i=1}^n q_i(t) \pi_1(t - \delta_i)}{\sum_{i=1}^n q_i(t)} \tag{12}$$

where we used the assumption that $c_{\mathrm{in}}(t)$ does not vary between filters.

In order to construct complete yet simple models, we also need to consider and make simplifying assumptions on the processes preceding and following filtration. First, it is convenient to think of the raw water pathogen concentration as a continuous time *stochastic process* $C_{\mathrm{r}}(t)$. If $C_{\mathrm{r}}(t)$ displays *non-stationarity* solely as the result of catchment processes that vary on larger time-scales (e.g. seasonal changes), there is likely to be a high degree of auto-correlation in $C_{\mathrm{r}}(t)$ for small time intervals such as the length of a filtration cycle. However, $C_{\mathrm{r}}(t)$ may also be influenced by short-term events, such as e.g. a sudden sewage leak or overflow. The question for us in this context is whether $C_{\mathrm{r}}(t)$ displays significant variation on the time scale of a single filter cycle, i.e. 0.5 - 1.5 days, or whether it can reasonably be taken as constant during such a time interval. For simplicity, we will mostly assume constant raw water concentrations.

Treatment processes upstream of filtration typically include simple straining and coagulation-sedimentation/flotation and maybe pre-chlorination. Although upsets may occur, these are processes that are expected to have a stable performance when loaded with a constant influent water quality and flow rate, and we will assume as much by modeling pre-filtration processes using a constant passage probability ϕ_1. Downstream of filtration, one typically finds disinfection processes such as chlorina-

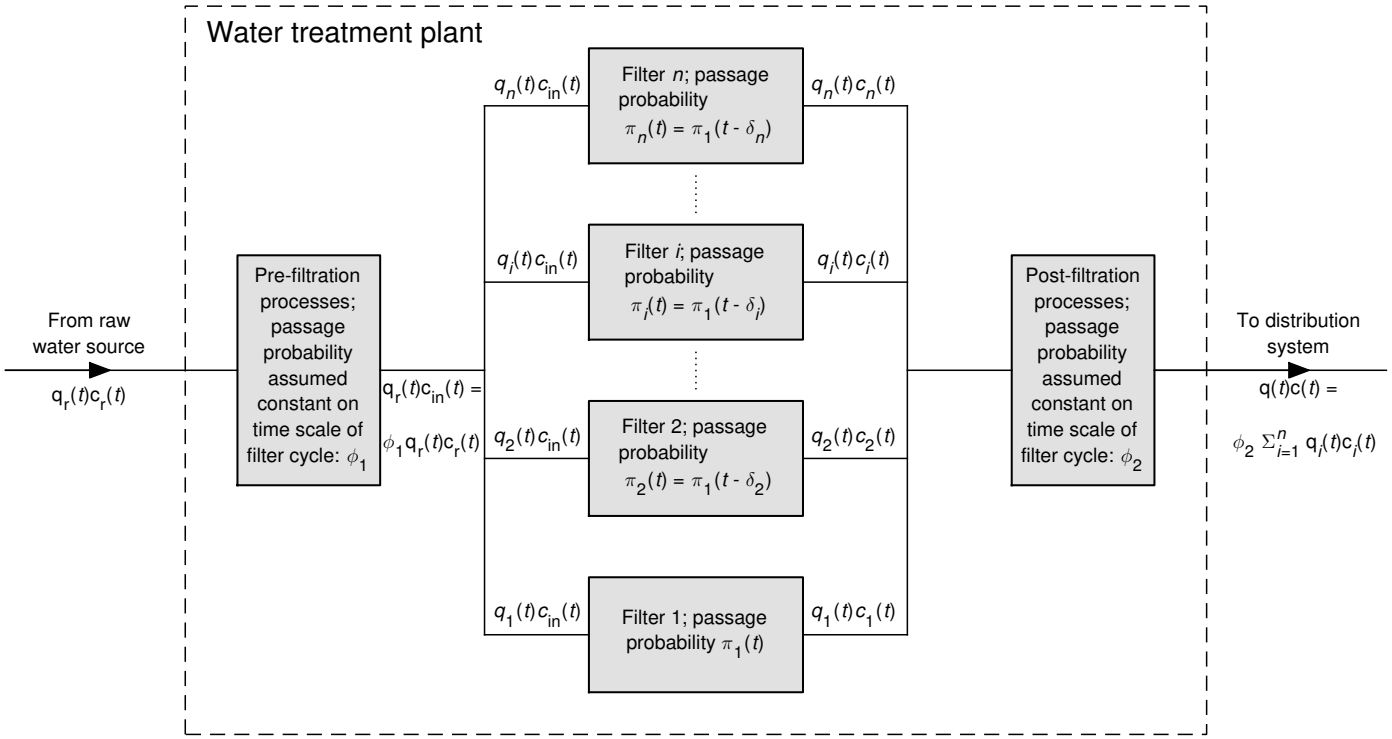

Figure 2: Conceptual layout of a water treatment plant with n filters operating in parallel. The labels represent mass fluxes of pathogens at the locations shown.

tion, UV-radiation or ozonation. These are also processes that are expected to perform in stable manner (at least on the time scale of a filter cycle) when supplied with a stable influent water quality and quantity. Furthermore, they are typically modeled using first-order decay models (e.g. the Chick-Watson model for chlorination) so that the passage probability does not depend on the influent pathogen concentration. There are however some indications that the performance of UV-radiation may depend on the current stage in the filter cycle of a preceding filtration step, through its effect on particle content (Templeton et al., 2007, 2008). For the purposes of this paper, we will describe the effect of post-filtration processes, including inactivation in the distribution system, by a constant passage probability ϕ_2. The combined effect of pre- and post-filtration processes is then $\phi = \phi_1\phi_2$.

Once treatment is completed, we particularly have to consider the extent to which temporal concentration variations persist throughout the distribution system and affect the distribution of the dose X at the tap. We will consider two extreme cases in our model building:

1. *Completely dispersive distribution system.* For this case, we will assume that all filtration-induced short-term variations in pathogen concentrations are smoothed out during distribution and that, at the time-scale of a single filtration cycle, tap water has a stable pathogen concentration equal to the mean concentration in the treatment plant effluent (adjusted for inactivation in the distribution system). Such a situation would be more likely in large systems with large flow-through reservoirs, long retention times and at locations far from the treatment plant.

2. *Completely non-dispersive distribution system.* For this case, we will assume plug-flow like behavior so that short-term filtration-induced variations in pathogen concentrations directly affect the distribution of X at the tap; the consumer might as well sample the water immediately after treatment (adjusted for inactivation in the distribution system). Such a situation would be more likely in small systems with small clear-water wells and reservoirs, short retention times and at locations close to the treatment plant.

In reality, the situation will likely be somewhere between these extremes and depend on the time-scale of filtration dynamics compared to the time-scale of dispersion in downstream processes and transport systems. Claims in the literature (Mann et al., 2007) of short-term temporal correlations between effluent turbidity at the treatment plant during normal operation and cases of reported acute gastrointestinal illness at hospital emergency units indicate that persistence of short-term variations throughout distribution networks cannot be ruled out a priori.

Table 1 summarizes the four alternatives for the concentration distribution experienced by a consumer when considering stable vs. random raw water concentrations, dispersive vs. non-dispersive distribution systems and constant passage probability ϕ in non-filtration processes. Here, Π denotes the random net probability of passage through n parallel filters when sampling uniformly in produced volume from $\pi[t(v)]$ (equation (12)). We will not consider explicitly the case of random raw water concentrations in combination with a non-dispersive distribution system. However, if C_r and Π can be taken as independent ran-

Table 1: Concentration distributions experienced by the consumer for different scenarios. The distinctions stable/random and dispersive/non-dispersive apply at the time scale of a single filter cycle.

		Post-filtration processes and distribution system	
		Dispersive	*Non-dispersive*
Raw water concentration	*Stable;* c_r	$c = \phi c_r \mathrm{E}(\Pi)$	$C = \phi c_r \Pi$
	Random; C_r	$c = \phi \mathrm{E}(C_r \Pi)$	$C = \phi C_r \Pi$

dom variables, we have

$$\mathrm{Var}(\phi C_r \Pi) = \phi^2 \mathrm{Var}(C_r \Pi) > (\phi c_r)^2 \mathrm{Var}(\Pi) \qquad (13)$$

which shows that the variance of C increases in this case as compared to the case of a constant c_r equal to $\mathrm{E}(C_r)$. The variance increases similarly if ϕ must be treated as random (at least if it can be considered independent of C_r and Π).

Finally, parallel filters are typically hydraulically connected, so that taking one filter out of service for backwashing may increase the filtration rate in the other filters, which in turn may adversely affect the filtrate quality (Kim and Lawler, 2006) and possibly lead to detachment of previously captured pathogens (Emelko, 2001). It seems plausible that the effect may depend on what stage in the filter cycle a filter is currently in. Further experimental work is needed to characterize such effects better. For our modeling, it will be assumed that the flow rate through each filter is constant and does not increase when backwashing other filters. This implies that either the flow rate through the entire treatment plant follows that of the filtration step or there are some detention volumes.

4. Analysis and results

4.1. Probability distribution implied by $\pi_1(t)$

First, we will consider the empirical pdf implied by $\pi_1(t)$ from our example data (Figure 1) when sampling uniformly from the produced volume or equivalently, in this case, sampling uniformly in time since the flow rate q was constant. For given start and end times of the production period (end of filter-to-waste and initiation of backwashing, respectively), the probability distribution of Π_1 may be derived from $\pi_1(t)$ using the relationships outlined in Appendix A. This has been done with our example data to produce Figure 3, which shows pdfs for three different production periods, for viruses and bacteria. For viruses, we have also included a comparison with a pdf derived by Teunis et al. (2009). They used data on F-specific coliphages from two plants in the Netherlands to estimate a beta-distribution for the removal during coagulation-filtration, assuming paired influent and effluent samples and gamma-distributed influent concentrations.

As seen in Figure 3, the derived pdfs for viruses and bacteria are both right (positively) skewed. The distribution for bacteria has a lower mean and more concentrated probability

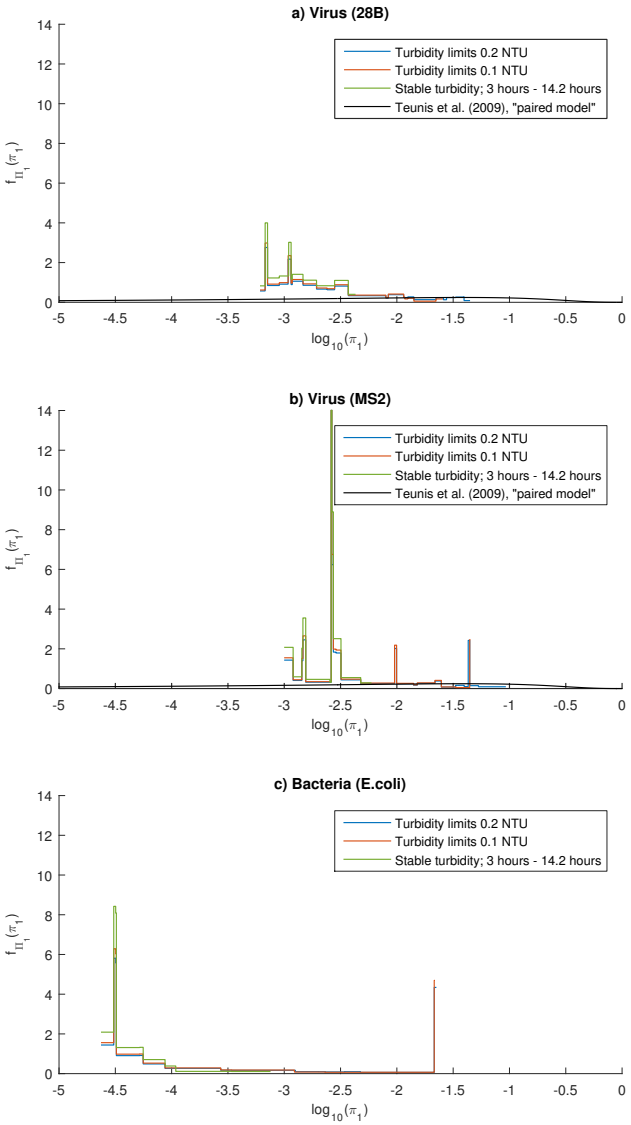

Figure 3: Probability density functions derived from $\pi_1(t)$ in the example data of Figure 1, using the method outlined in Appendix A.

mass as compared to viruses, reflecting its better and more stable removal, also seen in Figure 1. Restricting the length of the production period displaces probability mass to smaller values. It is clear that the estimated beta pdf of Teunis et al. (2009) is vastly more spread out than our empirical pdf from a single filter run, has a higher mean and a quite different shape (it is left-skewed). The data that went into estimating the beta pdf is of a very different nature (high volume sampling with a subsequent concentration step, only 17 samples in total) than our experimental data, and there was no detailed information on process characteristics or consideration of the time-scales of variation. The difference is nevertheless consistent with the observation that highly variable virus removal efficiencies for filtration are reported in the literature (Nilsen et al., 2016). The pdfs generated here, or perhaps some smoother versions of them, may be used as input for Monte-Carlo simulations in risk assessment.

4.2. Dispersive distribution system

In a completely dispersive distribution system, during a time period on the order of the length of a filter cycle, the consumer is assumed to sample from a water with a constant concentration of pathogens, c, equivalent to the mean pathogen concentration leaving the treatment plant, adjusted for inactivation in the distribution system. From Table 1, this concentration is assumed to be given by $c = \phi \mathrm{E}(C_\mathrm{r}\Pi) = \phi \mathrm{E}(C_\mathrm{r})\mathrm{E}(\Pi)$, where the latter equality holds when C_r and Π are statistically independent. Thus, in this simplified scenario, only the expected passage probability $\mathrm{E}(\Pi)$ enters the problem. At low doses, typical for normal drinking water, the risk from a single-hit dose-response model based on the Poisson distribution is approximately proportional to the mean dose $\lambda = cv_\mathrm{s}$, and hence to $\mathrm{E}(\Pi)$.

As shown in Appendix A, $\mathrm{E}(\Pi)$ is given by the volume average of $\pi[t(v)]$ (passage probability through all filters), which in turn is equal to the volume average of $\pi_1[t(v)]$ (passage probability through reference filter 1). We will consider two situations, one in which the start time of water production (end of filter-to-waste) is given and only the end time of production is free to choose, and one in which both the start time and end time are subject to choice.

4.2.1. End of filter-to-waste period given

Assume that t_1 is the time when the filter is put into operation after a backwash event (end of filter-to-waste). Then the mean probability of passage, π_1^m, between t_1 and t is given by

$$\begin{aligned} \mathrm{E}(\Pi_1)_t = \pi_1^\mathrm{m}(t) &= \frac{1}{v - v_1} \int_{v_1}^{v} \pi_1[t(v)]\,\mathrm{d}v \\ &= \frac{1}{v - v_1} \int_{t_1}^{t} \pi_1(\tau) q_1(\tau)\,\mathrm{d}\tau = \frac{1}{t - t_1} \int_{t_1}^{t} \pi_1(\tau)\,\mathrm{d}\tau \end{aligned} \tag{14}$$

where the latter equality applies when $q_1(t)$ is constant, as in the experiment that generated our example data. Assuming that $\pi_1(t)$ is differentiable, it is readily verified that potential minima of $\pi_1^\mathrm{m}(t)$ for $t > t_1$ occur when

$$\pi_1^\mathrm{m}(t) = \pi_1(t) \tag{15}$$

which, for a typical U-shaped time evolution of $\pi_1(t)$ has a unique solution. Thus, if t_1 is given, optimization of the filter operation with respect to minimizing the risk from a pathogen that passes the filter according to $\pi_1(t)$ consists of ending the filter run at a time t that solves (15).

This is illustrated in Figure 4, which shows $\pi_1^\mathrm{m}(t)$ for viruses and bacteria for three values of t_1, corresponding to the events of turbidity falling below 0.2 and 0.1 NTU, and turbidity becoming stable (after approximately 3 hours). Also shown is $\pi_1(t)$ and the normalized cumulative passage from our experimental data, defined as

$$\omega_1(t) = \frac{\int_0^t \dot{m}_1(\tau)\,\mathrm{d}\tau}{\int_0^{t_\mathrm{stop}} \dot{m}_1(t)\,\mathrm{d}t} \overset{q_1\ \mathrm{const.}}{=} \frac{\int_0^t c_1(\tau)\,\mathrm{d}\tau}{\int_0^{t_\mathrm{stop}} c_1(t)\,\mathrm{d}t} \overset{c_\mathrm{in}\ \mathrm{const.}}{=} \frac{\int_0^t \pi_1(\tau)\,\mathrm{d}\tau}{\int_0^{t_\mathrm{stop}} \pi_1(t)\,\mathrm{d}t} \tag{16}$$

where t_stop is the end time of the experimental run. Thus, $\omega_1(t)$ gives the ratio of the number of microorganisms that has passed at time t to the total number of organisms that passed during the entire experimental run.

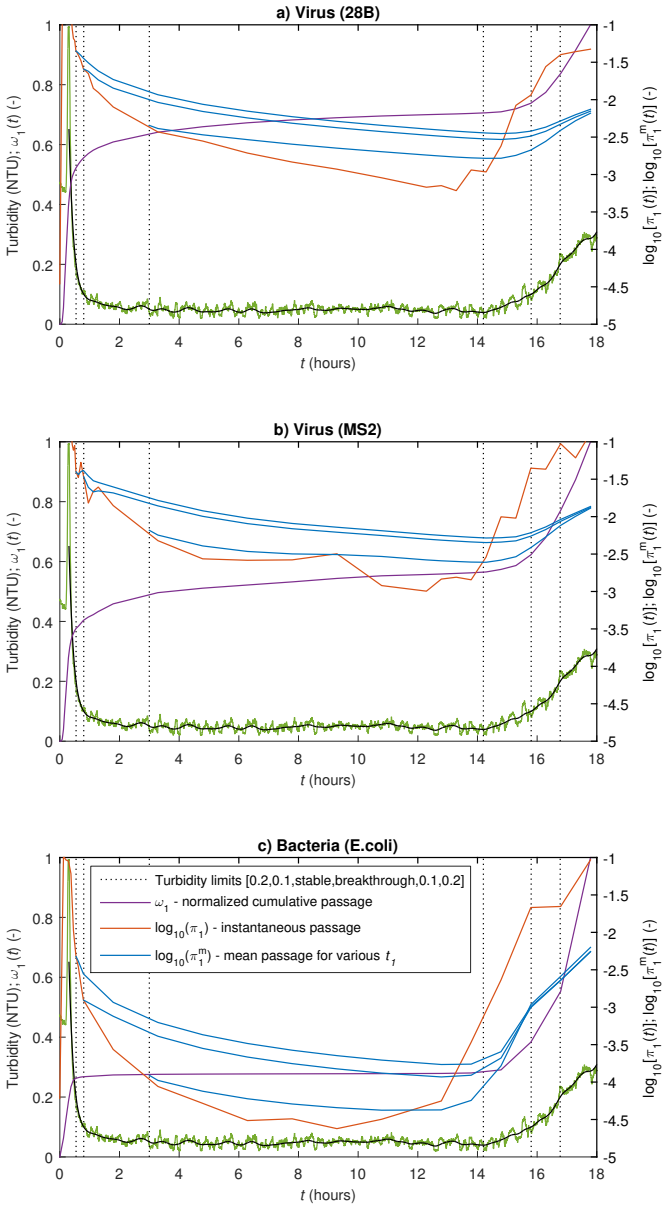

Figure 4: Normalized cumulative passage and instantaneous and mean probability of passage for viruses and bacteria.

There are several points to note in Figure 4. First, the normalized cumulative passage curves $\omega_1(t)$ are quite different for viruses and bacteria. Approximately 40-50 % of the virus passage happened in the early stages of the cycle before ripening brought effluent turbidity down to 0.2 NTU; the equivalent figure for bacteria is only about 25 %. After turbidity dropped below 0.2 NTU, $\omega_1(t)$ is quite flat for bacteria while it continues to flatten for viruses, reflecting different ripening behaviors. Consequently, most of the bacterial passage happened towards the end of the cycle.

Second, the marked difference between $\pi_1(t)$ and $\pi_1^\mathrm{m}(t)$ is ap-

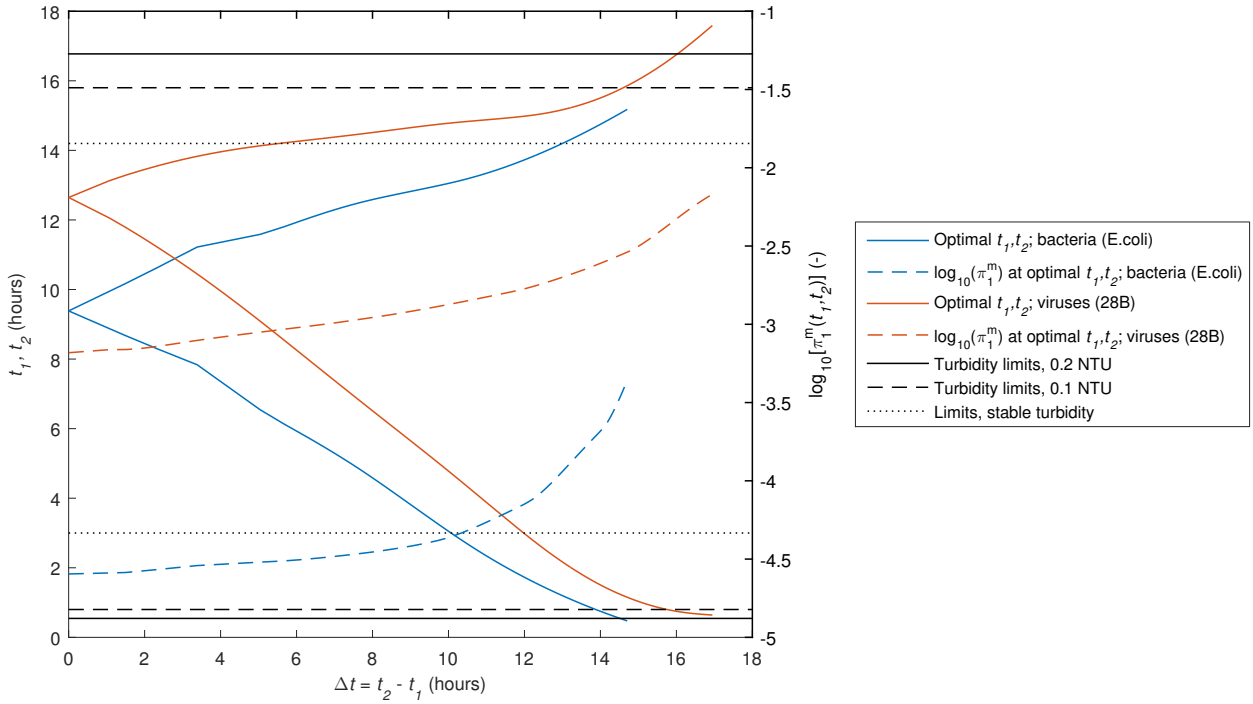

Figure 6: Optimal time limits t_1 and t_2 of the production period as a function of production period duration, Δt.

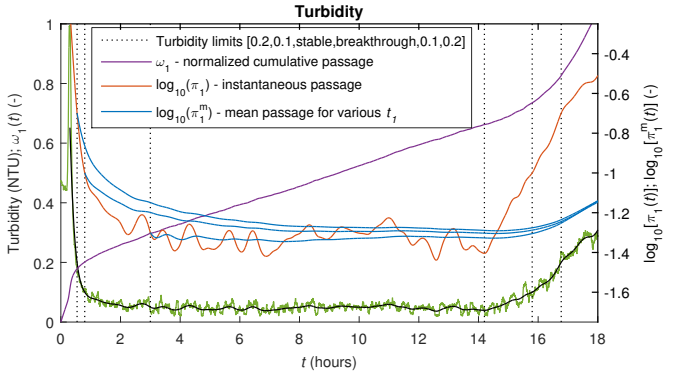

Figure 5: Normalized cumulative passage, instantaneous and mean passage for turbidity.

parent. When starting water production at turbidity 0.2 NTU, the difference is about 1 log-unit at the time of microorganism breakthrough. It is also clear that $\pi_1^m(t)$ varies somewhat depending on when the filter-to-waste period is terminated, and the effect is particularly noticeable if one postpones the production start until turbidity is completely stable, at 3 hours (usually not feasible). Once breakthrough has occurred, the different $\pi_1^m(t)$ curves start to converge.

Third, it is interesting to compare the location of minima in $\pi_1(t)$, i.e. conventional breakthrough, and minima in $\pi_1^m(t)$, i.e. the optimal end time of the filter cycle. For viruses, breakthrough occurred slightly before turbidity breakthrough, but the minimum of $\pi_1^m(t)$ for viruses occurred at (MS2) or slightly *after* (28B) turbidity breakthrough, and 1-2 hours after virus breakthrough. The location of the minimum of $\pi_1^m(t)$ for viruses does not depend strongly on t_1, the start of the production period, since the passage probability rises so quickly for viruses after breakthrough. For bacteria, the situation is different; the minima of both $\pi_1(t)$ and $\pi_1^m(t)$ occurred several hours *before* turbidity breakthrough. The exact location of the minimum of $\pi_1^m(t)$ is more sensitive to t_1 since the passage probability of bacteria rises more slowly in the time right after breakthrough. Continuing water production until turbidity reaches 0.2 NTU is clearly more detrimental to mean bacteria passage than mean virus passage, since the overall increase in $\pi_1(t)$ for bacteria is greater than for viruses. It is clear that one cannot strictly optimize for mean bacteria and mean virus passage simultaneously, but ending the filter cycle at 13-14 hours is close to optimal for all microorganisms investigated.

Figure 5 shows identical computations performed for the turbidity data, with the caveat that concepts such as "proportion of turbidity passed" may not be entirely well-defined for turbidity, which is not a strictly conserved quantity. Nevertheless, the panel indicates that a greater proportion of the effluent turbidity passage occurred during the period of stable operation, i.e. less of the turbidity passage happened during ripening and breakthrough periods, as compared to the microorganisms. Furthermore, the minimum of $\pi_1^m(t)$ for turbidity occurred almost immediately after turbidity breakthrough, and practically at the same location as for viruses.

4.2.2. Length of production period given

Filter run optimization as discussed above assumed that the starting point of water production, t_1, was given. In order to get one step closer to a truly optimized filter run, this could be relaxed so that both t_1 and the end point t_2 are free to be chosen. On the other hand, we must impose the condition that each filter

run must produce a certain volume of water in order to satisfy demand, which consists of consumer demand and the volume needed for backwashing. For constant-rate filtration, this condition corresponds to fixing the length of the production period $\Delta t = t_2 - t_1$. Thus the problem, assuming constant filtration rate, is to minimize

$$\pi_1^{\mathrm{m}}(t_1, t_2) = \frac{\int_{t_1}^{t_2} \pi_1(t)\,\mathrm{d}t}{t_2 - t_1} \tag{17}$$

subject to the constraint $t_2 - t_1 = \Delta t$. It is readily verified by standard methods (e.g. substitution or Lagrange multipliers) that this occurs only when $\pi_1(t_1) = \pi_1(t_2)$, which for a U-shaped time evolution of π_1 results in a unique solution (t_1, t_2) for each choice of Δt. Figure 6 shows the result of a numerical solution of this problem with 28B and *E.coli* data, using the spline approximations shown in Figure 1.

From the figure, we can see that the optimal production period for viruses is displaced 1.5-3 hours in time compared to the optimal period for bacteria. The longer the production period Δt, the smaller is the difference between viruses and bacteria in terms of the optimal time limits of production. Running the production from the time when turbidity falls below 0.1 NTU until turbidity breakthrough, is actually very close to the optimal production time limits for bacteria for $\Delta t \approx 14$ hours, and is not so far from the optimal production time limits for viruses for the same Δt.

4.3. Non-dispersive distribution system

Limiting the mean *concentration* of pathogens, as discussed in the previous section, will limit the risk associated with water consumption. However, with a non-dispersive distribution system, the mean *risk* on the time scale of a filter cycle depends theoretically not only on the mean concentration, but also on the higher moments of the concentration distribution. In our model (upper right corner of Table 1), where the filtration passage probability is the only varying quantity on the time scale of a filter cycle, the concentration distribution is determined by the time variation of $\pi(t)$, the net passage probability across n parallel filters. With reference to Figure 2, this is given by

$$\pi(t) = \frac{\sum_{i=1}^{n} q_i(t) c_i(t)}{c_{\mathrm{in}} \sum_{i=1}^{n} q_i(t)} = \frac{\sum_{i=1}^{n} q_i(t) \pi_i(t)}{\sum_{i=1}^{n} q_i(t)} \tag{18}$$

where $q_i(t)$ takes only two values, q (during operation) or 0 (during backwashing and filter-to-waste periods). We will further be assuming that $\pi_i(t) = \pi_i(t + t_p)$ for all i, i.e. the treatment performance of each filter is periodic with shared period t_p. The parameters of filter operation that determine $\pi(t)$ in this simple situation are the time of production start t_1, the time of production stop t_2 and the filter cycle phase shifts δ_i between filter i and reference filter 1 (Figure 2). For simplicity, we will assume the phase shifts are regularly spaced so that $\delta_i = (i-1)\delta_2$.

Figure 7 shows an example with three filters operating in parallel, with filter cycles of the second and third filter displaced 3 and 6 hours, respectively, compared to the reference filter. In the lower panel, $\pi[t(v)]$ is shown as a function of produced volume v per. unit filter area. Sampling uniformly in v from this function induces the random variable Π, and by assumption, we have the dose $\Lambda = v_{\mathrm{s}} c_{\mathrm{r}} \phi_1 \phi_2 \Pi \equiv k\Pi$ to be used in equation (8). As can be seen from Figure 7, under our assumption that $\pi_i(t)$ and $q_i(t)$ are unaffected by backwashing a filter $j \neq i$, the net passage probability improves when a poor-performing filter is taken off-line for backwash.

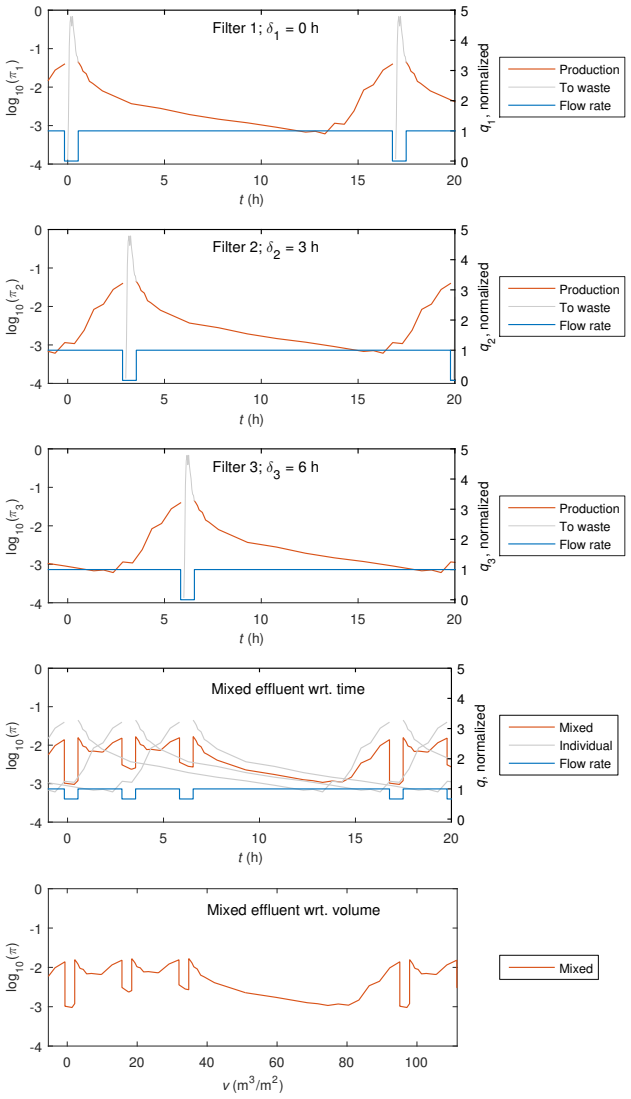

Figure 7: Reference filter performance (upper panel), time-shifted filters (2nd and 3rd panels), net passage probability $\pi(t)$ as a function of time (4th panel) and net passage probability $\pi(t)$ as a function of produced volume (lower panel).

As equation (8) shows, when $\Lambda = k\Pi$ the single-hit dose-response model is constructed with the mgf of Π evaluated at $-rk$. Furthermore, Appendix A establishes that the mgf of Π, where Π emerges from sampling uniformly in v from $\pi[t(v)]$, may be computed as

$$M_\Pi(z) = \mathrm{E}(e^{z\Pi}) = \frac{1}{v_2 - v_1} \int_{v_1}^{v_2} e^{z\pi[t(v)]}\,\mathrm{d}v \tag{19}$$

Here, $v_1 = v(t_1)$ and $v_2 = v(t_2)$.[4] This quantity can be straight-

[4] Strictly, since $\pi[t(v)]$ is periodic in both t and v, we can integrate over any interval with length $v_2 - v_1$.

forwardly evaluated numerically from the example experimental data in Figure 1.

In order to gain an understanding of the effect of filtration dynamics on risk in our model, the following risk ratio has been evaluated, where, for simplicity, we have assumed a constant single-hit probability r:

$$\frac{P_{\mathrm{I,nd}}}{P_{\mathrm{I,d}}} = \frac{1 - M_{\Pi}(-rk)}{1 - e^{-rk\mathrm{E}(\Pi)}} \tag{20}$$

The numerator is the single-exposure risk computed with the full distribution of $\Lambda = k\Pi$, where $k = c_{\mathrm{r}}\phi v_{\mathrm{s}}$, i.e. the risk we would compute in a non-dispersed distribution system. The denominator is the single-exposure risk computed with the exponential model with mean dose $\mathrm{E}(\Lambda) = k\mathrm{E}(\Pi)$, i.e. the risk we would compute in a dispersed distribution system. Contour plots of the ratio in equation (20) are shown in Figures 8 and 9 for viruses (28B) and bacteria, respectively. They show the influence of a) the number of filters in parallel, n, b) the production time limits t_1 and t_2 through their effect on effluent turbidity, c) the time-shifts δ_i of the filtration cycles with respect to the reference cycle and, d) the parameter rk through its effect on the exponential model (horizontal axes). We employed the restriction that only one filter can be in backwash at any given time, which excludes the possibility of operating 6 filters with completely stable turbidity (the missing panel).

As dictated by theory, Figures 8 and 9 show that the ratio in equation (20) is less than 1. Starting with Figure 8 for viruses, we see that the effect of variation in π on risk estimates tends to be more pronounced when there are fewer filters in parallel and when lesser restrictions are placed on turbidity. It should be noted that under normal operational conditions, when the single-exposure risk is typically less than 10^{-6}, variation in π appears to have negligible influence on risk estimates. It only becomes important under severe outbreak conditions, when the single-exposure risk is higher than 0.1 and somewhat away from 1. Under such conditions, the time-shifts of filter cycles is predicted to have a non-negligible influence on risk estimates. For example, for 4 filters operating under a turbidity limit of 0.2 NTU, choosing the smallest instead of the largest possible δ is predicted to reduce the single-exposure risk by up to $(0.9 - 0.7)/0.9 = 22\%$.

For Figure 9 for bacteria, we find the same tendencies as for viruses, but slightly more pronounced due to the characteristics of the π-variation. For the case of 4 filters operating under a turbidity limit of 0.2 NTU, choosing the smallest instead of the largest possible δ is here predicted to reduce the single-exposure risk by up to $(0.7 - 0.4)/0.7 = 42\%$.

These figures apply to the single-exposure case. For the multiple exposure case (n iid exposures), we have the corresponding ratio

$$\frac{P_{\mathrm{I,nd}}}{P_{\mathrm{I,d}}} = \frac{1 - [M_{\Pi}(-rk)]^n}{1 - e^{-nrk\mathrm{E}(\Pi)}} \tag{21}$$

It is readily shown that this ratio *increases* towards 1 as n increases since $M_{\Pi}(-rk) > e^{-rk\mathrm{E}(\Pi)}$. Thus, the effect of variations in π only tend to become less important as the number of exposures increases.

5. Discussion

In this paper, we have attempted to make some incremental progress in the quantitative understanding of the role of deep-bed filtration dynamics in microbial risk assessment, using the only dataset known to us that permits such an analysis. We have studied the effect of filtration dynamics on the probability distribution of passage probabilities (Section 4.1) and the mean passage probability (Section 4.2), as well as the effect of filtration dynamics on risk estimates when the full distribution of the passage probability is taken into account (Section 4.3). In light of the results, we will first discuss the relevance of filtration dynamics for risk assessment and optimal filter operation before addressing the interpretive limitations associated with the limited example dataset and many idealizations that were made in the model development.

5.1. Filtration dynamics and risk estimates

The existence of filtration dynamics poses two main challenges to microbial risk assessment: Correctly estimating the mean passage probability and hence mean pathogen concentrations, and the possibility that variations around the mean concentration may significantly affect risk estimates. The contour plots in Figures 8 and 9 indicate that concentration variations around the mean exert all but negligible influence in our risk model, except possibly in a situation where pathogen concentrations approach levels associated with extreme risk and attack rates. It should be noted that these risk levels are within the directly observable range of risk in dose-response feeding trials and therefore the results do not suffer from the usual uncertainty that comes from extrapolating dose-response curves to unobservable levels of risk.

Correctly estimating the mean passage probability of deep-bed filters therefore seem to be the more important aspect of filtration dynamics. As mentioned in the introduction, high-resolution sampling regimes seem to be the exception rather than the rule in studies aimed at estimating passage probabilities. In particular, Figure 4 demonstrates that filter performance in the early and final stages of the filtration cycle may have a profound impact on the mean passage probability, even when restricting effluent turbidity to less than 0.2 or 0.1 NTU. If samples had been taken only mid-cycle in our experiment when turbidity was stable, the overall mean passage probability might have been overestimated by roughly 0.75 log-units for viruses and 1.5 log-units for bacteria.

Efforts to experimentally characterize passage probabilities of deep-bed filters should therefore be designed with high-resolution sampling regimes, in particular in the early and late stages of the filter cycle. This will permit reliable integration of instantaneous passage probabilities to obtain mean passage probabilities as a function of elapsed time. To facilitate comparison between different filtration rates, it is suggested that results are reported as mean passage as a function of volume produced per unit filter area (Figure 7, lower panel). An alternative approach which is potentially cheaper and less labor-intensive is to use flow-proportional composite sampling. By taking subsamples for analysis from the composite sample at strategic

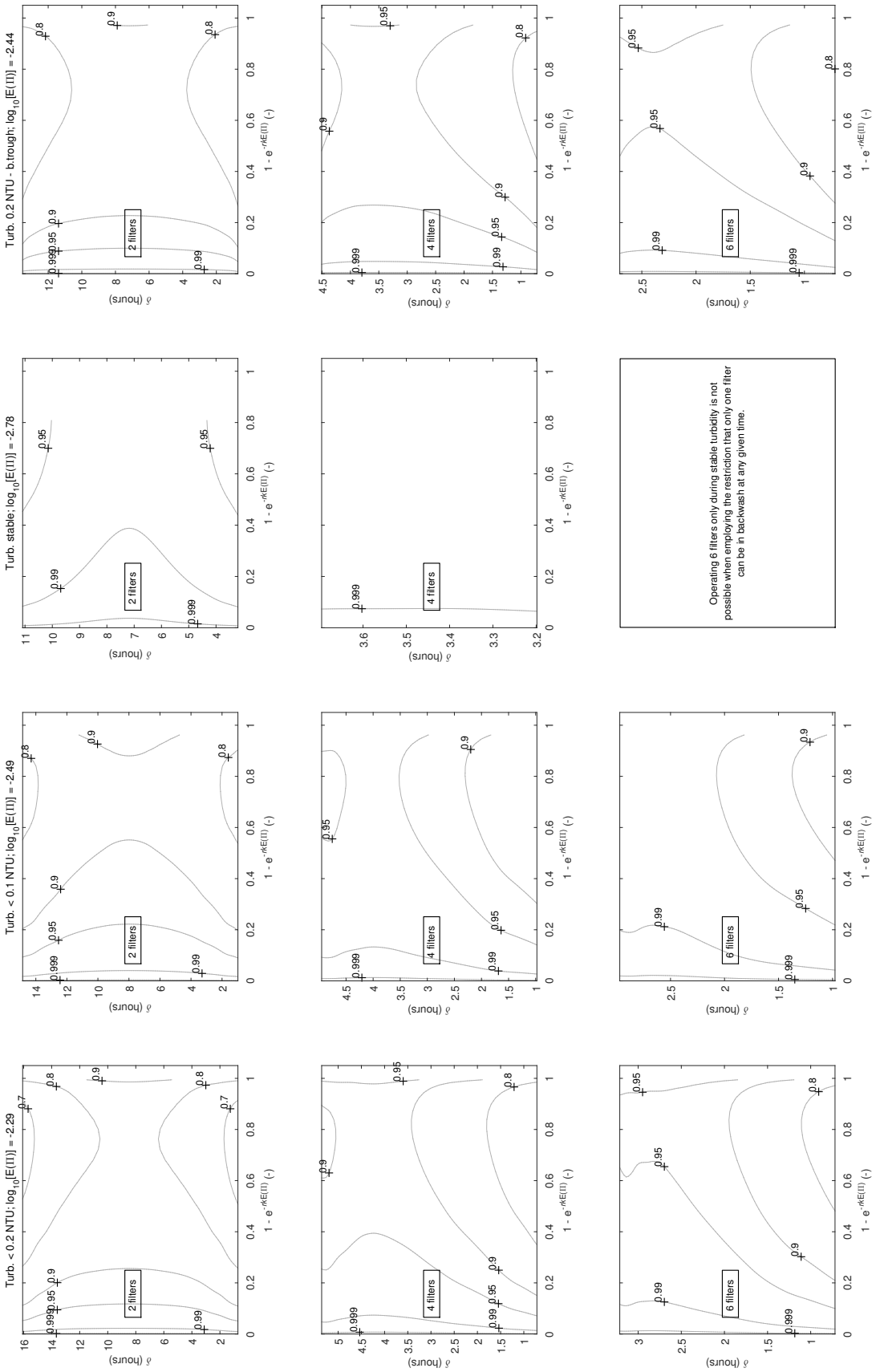

Figure 8: Contour plot of the risk ratio in equation (20) for viruses (28B). Each column corresponds to a pair of t_1, t_2-values through restrictions on effluent turbidity and each row to a certain number of filters in parallel. E(Π) differs only between columns. The vertical axis of each panel gives the cycle time-shift (Figure 2; $\delta_i = (i-1)\delta$) and the horizontal axis shows the influence of the parameter rk through its effect on the exponential model.

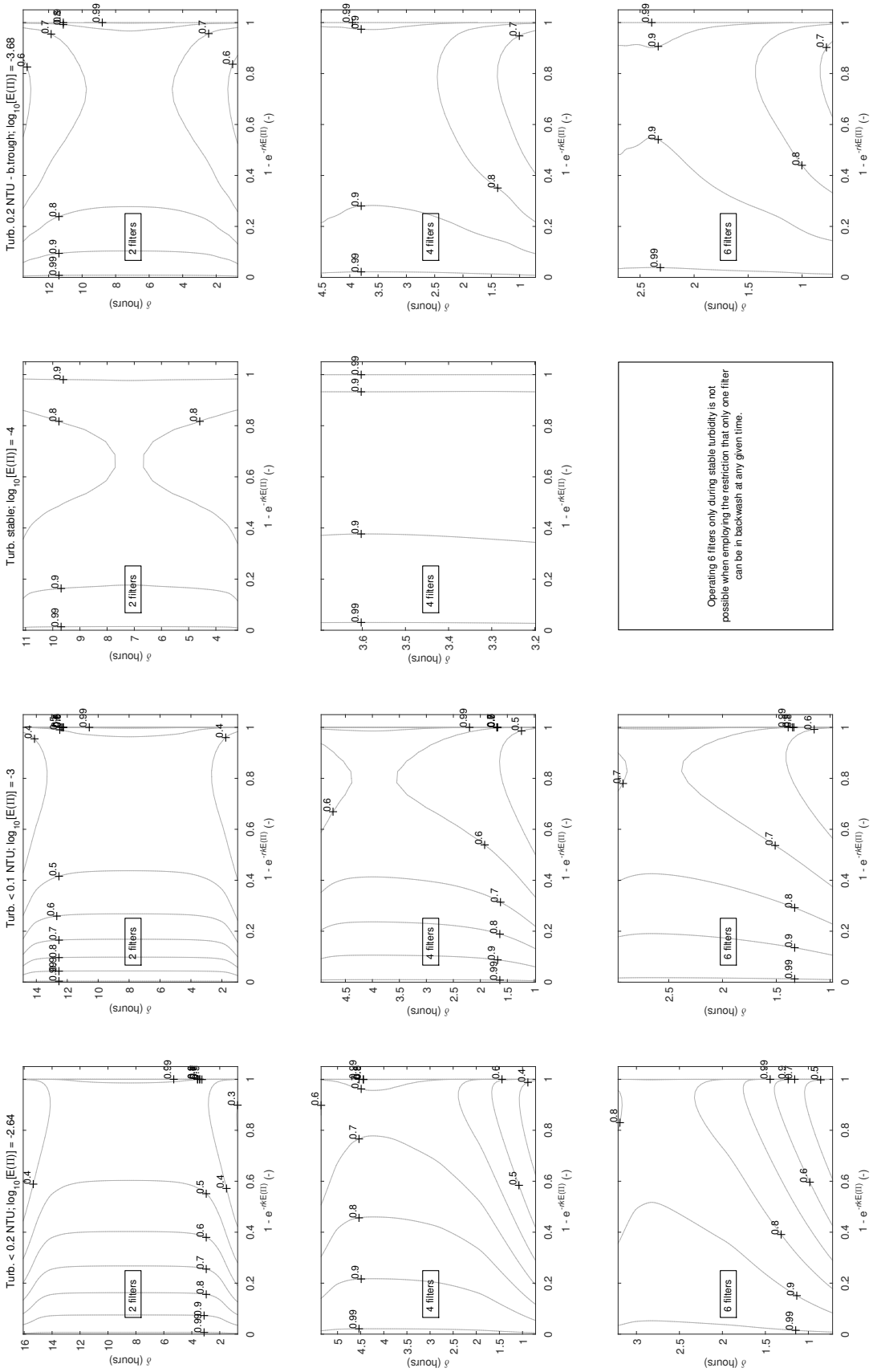

Figure 9: Contour plot of the risk ratio in equation (20) for bacteria. Each column corresponds to a pair of t_1, t_2-values through restrictions on effluent turbidity and each row to a certain number of filters in parallel. E(Π) differs only between columns. The vertical axis of each panel gives the cycle time-shift (Figure 2; $\delta_i = (i-1)\delta$) and the horizontal axis shows the influence of the parameter rk through its effect on the exponential model.

time points (e.g. when effluent turbidity crosses set limits), correct mean passage probabilities may be obtained. If such tailored sampling regimes are widely adopted, one can hopefully generate data that may reduce some of the (extreme) variation in results between different studies (Nilsen et al., 2016).

5.2. Filtration dynamics and optimal filter operation

Again, the challenge is twofold. Primarily one wishes to choose filter operational regimes that minimize the *mean* passage probability. Secondly, due to the non-linearity of dose-response models, the full distribution of passage probabilities does theoretically influence the risk estimate. Since single-hit dose-response models are concave in the dose-variable, the rule-of-thumb is that, for a given mean dose, it is better to have as much of that dose concentrated in a small volume of the produced water rather than having it evenly distributed in the total produced volume. As mentioned in Section 3.2, we don't know of a fully precise mathematical expression of this principle except for the bound in equation (9).

Figures 8 and 9, however, indicate that in our model, where the distribution of doses were controlled by choosing the time-shifts δ_i between filter cycles while keeping the mean dose constant, the full dose distribution did not significantly affect risk estimates except in the case of extremely high doses and associated high risks. This, of course, is related to the property of single-hit models that they become approximately linear as the mean dose becomes small. Thus, the results indicate that there may be some potential to reduce the impact of a extremely severe waterborne outbreak by choosing an operational regime in which filters are backwashed successively, i.e. filter i is backwashed immediately after filter $i-1$ has finished its backwash. Further work is needed to examine the realism of the model before this operational regime can be recommended, though.

Optimizing filter operation with respect to mean passage probability, and hence the mean pathogen dose, is easier to recommend. From Figures 4 and 6, it is clear that the mean passage probability is dependent on the choice of start and end times t_1 and t_2 for the water production period. Postponing the production start time will reduce the mean passage probability, but is likely infeasible in existing treatment plants since a large volume of water will have to be filtered to waste. Realistically, therefore, the more influential parameter appears to be t_2, the end time of water production, in particular for bacteria.

Continuing water production beyond turbidity breakthrough at about 14.2 hours resulted in a rapid decline in mean passage probability, completely negating the good performance up until that point. Norwegian regulations specify (among other criteria) a maximum effluent turbidity of 0.2 NTU for a filtration process to be recognized as a hygienic barrier. While it may be acceptable to choose the production start t_1 based on a predetermined turbidity limit such as 0.2 or 0.1 NTU, it would be unwise to let the end of the filtration cycle, t_2, be determined by similar criteria. Rather, the water production should stop at the very latest when turbidity starts to increase towards the end of the cycle, which signals the arrival of the so-called clogging front (Herzig et al., 1970; Adin and Rebhun, 1974) at the filter outlet. Pressure monitoring of the lower part of the filter may aid in predicting turbidity breakthrough before it actually occurs (Nilsen et al., 2016). Huck et al. (2001) developed a turbidity robustness index that may also inform decisions on filter operation and health-based performance assessments (Zhang et al., 2012).

Figure 6 clearly demonstrates that it is not possible, in general, to simultaneously minimize the mean passage probability for both viruses and bacteria. In fact, a rigorous approach to optimization of filter operation with respect to risk would have to describe the joint risk from all pathogens of relevance, accounting for their individual raw water concentrations and removal throughout treatment and distribution. Data availability for QMRA is currently not good enough to perform such rigorous analysis.

5.3. Limitations of the example data and model framework

In our modeling efforts, we relied on an idealized conceptual model of a water supply system and a single example data set. Here, we go through some of the limitations associated with our approach.

5.3.1. Example data

The example dataset represents the most highly resolved characterization of microbial removal in a single deep-bed filter cycle that we are aware of, at least for viruses. The observed variation in performance throughout the filter cycle was substantial, qualitatively as expected based on virus and bacteria relative sizes; (Clark et al., 1992; Moran et al., 1993), and is believed to represent real-world phenomena occurring in water treatment plants. Still, the data has been obtained under a single set of experimental conditions, corresponding to common filtration practice in the Nordic countries, and is not necessarily representative of filtration processes that operate under different conditions. Specifically, one may wish to conduct high-resolution characterizations using pre-sedimentation, dedicated flocculation steps, different filter rates, declining-rate filtration, different filter materials, different coagulants, filter aids/polymers and more particle-rich raw water. Furthermore, other surrogate organisms for pathogens should be tested in future high-resolution characterizations.

5.3.2. Model framework

Some of the model assumptions that should be investigated and relaxed in future research efforts, include:

- *Unaccounted-for variation.* In our model, the only varying quantity on the time scale of a filter cycle was the filtration passage probability. While filtration processes are distinguished from most other unit processes by their inherent systematic variability, even when supplied with stable influent water quality, there may be random variations in raw water concentrations and the performance of other unit processes (e.g. because of operational failure) that are relevant. If such variations are present and can be considered independent of the variation in filtration performance, it will lead to *increased* variation in the dose distributions, as shown in equation (13). We also assumed that all filters

in parallel perform identically with respect to microbial removal, which needs to be verified experimentally.

- *Hydraulic control of filters and effect on π.* We assumed that the flow rate, and therefore also the passage probability, through each individual filter were unaffected by one of the parallel filters being backwashed. This ensured that the mean passage probability was conserved when varying the time-shifts δ_i. If, instead, the performance of the operative filters deteriorate in response to hydraulic disturbances when one of the filters is being backwashed, this has to be accounted for in a model as it affects the mean passage probability. The recommendation that filters should be backwashed back-to-back may survive, though, as this will ensure that most/all filters are relatively clean when other filters are being backwashed and the potential for scouring/detachment of pathogens is minimized. Finally, it may be relevant to obtain data and build a model for declining-rate filtration, although this seems to be less common.

- *The effect of distribution systems.* We considered two extreme conceptual models of distribution systems; completely dispersive systems which smooth out concentration variations or completely non-dispersive systems which conserve concentration variations, both considered on the time-scale of a filter-cycle. It was shown that the difference between these two seem to be unimportant except under extreme outbreak conditions. This conclusion may potentially change if there is concurrent variation in other processes besides filtration, but it would likely require orders-of magnitude increases in variation to have an effect on risk estimates.

- *Dose response models.* Single-hit dose-response models are routinely used for drinking water risk assessment and have been shown to fit data well for medium-to-high doses. It is, however, a remaining scientific challenge to verify their applicability for low doses, so that extrapolations beyond the range of observations is typically necessary for drinking water studies. If the true dose-response model is non-linear even for low doses, this will affect the results of modeling efforts where variation in doses is accounted for. Furthermore, we did not consider the case of a variable single-hit probability R in our examples. Such models are "flatter" than their constant-r counterparts (Nilsen and Wyller, 2016a, Proposition 1), but qualitatively similar; we do not expect the main conclusions to change with such models.

6. Conclusions

In this paper, we have studied the effect of short-term deep-bed filtration dynamics on microbial risk estimates, using high-resolution data on filtration performance that is believed to be representative under the given conditions, together with a simplified conceptual model. Under the assumption that filtration performance is the only variable quantity on the time-scale of a single filter cycle, it was shown that concentration variations induced by filtration is unlikely to affect risk estimates when compared with a model that uses an equivalent mean concentration, except possibly in an outbreak situation with extremely high pathogen concentrations. Future studies should probe this result further by studying the effect of concurrent variation in filtration performance and other unit processes, as well as raw water concentrations. In this regard, it is suggested that variations are experimentally obtained and studied as *time series* and *stochastic processes*, in order to properly account for the time-scales of variation. This is in contrast to conventional approaches of QMRA that use simple probability distributions with no account of variation time-scales. The example data used in this study will be made available at the publisher's website, and may be used for Monte Carlo simulations for risk characterization.

Until further studies along the suggestions made above can be carried out, the main consequence for QMRA of systematic, short-term dynamic effects in microbial filtration performance, is related to the conduction of filtration experiments to correctly estimate *mean* passage probabilities. When characterizing microbial removal rates, sampling regimes must be designed so that varying performance throughout the filtration cycle may be quantified. This may be performed by frequent sampling, as in the experiment that generated the example data, or by using flow-proportional sampling with strategic sub-sampling, as discussed in Section 5.1.

Regarding optimal filter operation to minimize mean pathogen passage, it was shown that the minimum mean passage for an organism occurs *after* breakthrough of that organism. This is a result which holds as long as the curve of instantaneous organism passage vs. time is *U-shaped*. Starting water production at 0.2 NTU vs. 0.1 NTU had only a moderate influence on the mean passage of viruses and *E.coli*. The end-point of the production period was more influential in determining mean passage and it is a clear recommendation that filtration should not continue after turbidity starts increasing towards the end of a cycle, even if turbidity is still low.

7. Acknowledgements

Discussions with Arve Heistad and John Wyller were very helpful in the preparation of this manuscript.

Appendix A. The transformation-rule for functions of random variables

Assume that we have a random variable V with associated probability density function $f_V(v)$ and a differentiable function $g : \mathbb{R} \to \mathbb{R}$ that induces a new random variable $W = g(V)$. Assume that the domain of the function g may be partitioned into n intervals such that the function g is monotonic on each interval. Denote the restriction of g to interval i by g_i. Then the probability density of W is given by

$$f_W(w) = \sum_{i=1}^{n} f_V[g_i^{-1}(w)] \left| \frac{\mathrm{d}g_i^{-1}(w)}{\mathrm{d}w} \right| \tag{A.1}$$

It is assumed here that $\Pr[g'(V) = 0] = 0$. If that is not the case, the above rule can be generalized and the density $f_W(w)$ becomes a mixed discrete-continuous probability distribution, i.e. it has some point masses of probability.

When V is uniformly distributed on $[v_2, v_1]$, the rule simplifies to

$$f_W(w) = \frac{1}{v_2 - v_1} \sum_{i=1}^{n} \left| \frac{\mathrm{d}g_i^{-1}(w)}{\mathrm{d}w} \right| \tag{A.2}$$

Introduce another function $h : \mathbb{R} \to [0, 1]$ that maps w to $h(w)$. For the expected value $\mathrm{E}[h(W)]$, we have according to (A.2) and a change of variables

$$\mathrm{E}[h(W)] = \int_W h(w) f_W(w)\,\mathrm{d}w = \frac{1}{v_2 - v_1} \int_{v_1}^{v_2} h[g(v)]\,\mathrm{d}v \tag{A.3}$$

Thus, expectations over W are equivalent to simple averages over V when V is uniformly distributed, which is, of course, in agreement with intuition.

References

Adin, A., Rebhun, M., 1974. High-rate contact flocculation—filtration with cationic polyelectrolytes. Journal (American Water Works Association) 66, 109–117.

Åström, J., Pettersson, T.J.R., Reischer, G.H., Hermansson, M., 2013. Short-term microbial release during rain events from on-site sewers and cattle in a surface water source. Journal of Water and Health 11, 430–442. doi:10.2166/wh.2013.226.

Clark, S.C., Lawler, D.F., Cushing, R.S., 1992. Contact Filtration: Particle Size and Ripening. Journal (American Water Works Association) 84, 61–71.

Emelko, M.B., 2001. Removal of Cryptosporidium parvum by granular media filtration. Phd. University of Waterloo.

Emelko, M.B., Huck, P.M., Douglas, I.P., 2003. Cryptosporidium and microsphere removal during late in-cycle filtration. Journal American Water Works Association 95, 173–182.

Fazekas de St Groth, S., Moran, P.A.P., 1955. Appendix: A Mathematical Model of Virus-Cell Interaction. Journal of Hygiene 53, 291–296. doi:10.1017/S0022172400000760.

Haas, C.N., 1983. Estimation of risk due to low doses of microorganisms: a comparison of alternative methodologies. American journal of epidemiology 118, 573–582.

Haas, C.N., 2002. Conditional Dose-Response Relationships for Microorganisms: Development and Application. Risk Analysis 22, 455–463. doi:10.1111/0272-4332.00035.

Haas, C.N., Rose, J.B., Gerba, C.P., 2014. Quantitative Microbial Risk Assessment. 2 ed., John Wiley & Sons, Inc, Hoboken, New Jersey. doi:10.1002/9781118910030.

Harrington, G.W., Xagoraraki, I., Assavasilavasukul, P., Standridge, J.H., 2003. Effect of Filtration Conditions on Removal of Emerging Pathogens. Journal (American Water Works Association) 95, 95–104.

Herzig, J.P., Leclerc, D.M., Goff, P.L., 1970. Flow of suspensions through porous media—application to deep filtration. Industrial & Engineering Chemistry 62, 8–35. doi:10.1021/ie50725a003.

Hijnen, W.A., Medema, G., 2010. Elimination of Microorganisms by Water Treatment Processes. IWA Publishing.

Huck, P.M., Coffey, B.M., Emelko, M.B., Maurizio, D.D., Slawson, R.M., Anderson, W.B., van den Oever, J., Douglas, I.P., O'Melia, C.R., 2002. Effects of filter operation on Cryptosporidium removal. Journal (American Water Works Association) 94, 97–111.

Huck, P.M., Emelko, M.B., Coffee, B., Maurizio, D., O'Melia, C.R., 2001. Filter operation effects on pathogen passage. AWWA Research Foundation.

Kim, J., Lawler, D.F., 2008. Influence of particle characteristics on filter ripening. Separation Science and Technology 43, 1583–1594. doi:10.1080/01496390801974688.

Kim, J.K., Lawler, D.F., 2006. Particle detachment during hydraulic shock loads in granular media filtration. Water Science & Technology 53, 177–184. doi:10.2166/wst.2006.222.

Lilleengen, K., 1948. Typing of Salmonella typhimurium by means of bacteriophage: an experimental bacteriologic study for the purpose of devising a phago-typing method to be used an an aid in epidemiologic and epizootologic investigations in outbreaks of typhimurium infection. Phd. Royal Veterinary College, Stockholm.

Mann, A.G., Tam, C.C., Higgins, C.D., Rodrigues, L.C., 2007. The association between drinking water turbidity and gastrointestinal illness: a systematic review. BMC Public Health 7. doi:10.1186/1471-2458-7-256.

MathWorks, 2014. MATLAB, Release 2014a.

Moran, D.C., Moran, M.C., Cushing, R.S., Luwler, D.F., 1993. Particle Behavior in Deep-Bed Filtration: Part 1—Ripening and Breakthrough. Journal (American Water Works Association) 85, 69–81.

Nilsen, V., Christensen, E., Molstad, L., Myrmel, M., Heistad, A., 2016. Spatio-temporal dynamics of virus removal in dual-media contact-filtration for drinking water: Experimental results and inverse modeling Manuscript in preparation.

Nilsen, V., Wyller, J., 2016a. Qmra for drinking water: 1. revisiting the mathematical structure of single-hit dose-response models. Risk Analysis 36, 145–162.

Nilsen, V., Wyller, J., 2016b. Qmra for drinking water: 2. the effect of pathogen clustering in single-hit dose-response models. Risk Analysis 36, 163–181.

Ødegaard, H., Østerhus, S., Melin, E., Eikebrokk, B., 2010. NOM removal technologies – Norwegian experiences. Drinking Water Engineering and Science 3, 1–9. doi:10.5194/dwes-3-1-2010.

Robeck, G., Clark, N., Dostal, K., 1962. Effectiveness of water treatment processes in virus removal. Journal (American Water Works Association) 54, 1275–1292.

Schmidt, P.J., Pintar, K.D.M., Fazil, A.M., Topp, E., 2013. Harnessing the theoretical foundations of the exponential and beta-poisson dose-response models to quantify parameter uncertainty using markov chain monte carlo. Risk Analysis 33, 1677–1693. doi:10.1111/risa.12006.

Signor, R.S., Roser, D.J., Ashbolt, N.J., Ball, J.E., 2005. Quantifying the impact of runoff events on microbiological contaminant concentrations entering surface drinking source waters. Journal of Water and Health 3, 453–468. doi:10.2166/wh.2005.052.

Smeets, P.W.M.H., Dullemont, Y.J., Van Gelder, P.H.a.J.M., Van Dijk, J.C., Medema, G.J., 2008. Improved methods for modelling drinking water treatment in quantitative microbial risk assessment; a case study of Campylobacter reduction by filtration and ozonation. Journal of Water and Health 6, 301–314. doi:10.2166/wh.2008.066.

Svenson, S.B., Lönngren, J., Carlin, N., Lindberg, a.a., 1979. Salmonella bacteriophage glycanases: endorhamnosidases of Salmonella typhimurium bacteriophages. Journal of virology 32, 583–592.

Templeton, M.R., Andrews, R.C., Hofmann, R., 2007. Removal of particle-associated bacteriophages by dual-media filtration at different filter cycle stages and impacts on subsequent UV disinfection. Water Research 41, 2393–2406. doi:10.1016/j.watres.2007.02.047.

Templeton, M.R., Andrews, R.C., Hofmann, R., 2008. Particle-Associated Viruses in Water: Impacts on Disinfection Processes. Critical Reviews in Environmental Science and Technology 38, 137–164. doi:10.1080/10643380601174764.

Teunis, P., Evers, E., Slob, W., 1999. Analysis of variable fractions resulting from microbial counts. Quantitative Microbiology 1, 63–88. doi:10.1023/A:1010028411716.

Teunis, P.F.M., Rutjes, S.a., Westrell, T., de Roda Husman, A.M., 2009. Characterization of drinking water treatment for virus risk assessment. Water Research 43, 395–404. doi:10.1016/j.watres.2008.10.049.

Westrell, T., Teunis, P., van den Berg, H., Lodder, W., Ketelaars, H., Stenstr??m, T.A., de Roda Husman, A.M., 2006. Short- and long-term variations of norovirus concentrations in the Meuse river during a 2-year study period. Water Research 40, 2613–2620. doi:10.1016/j.watres.2006.05.019.

Zhang, K., Achari, G., Sadiq, R., Langford, C.H., Dore, M.H.I., 2012. An integrated performance assessment framework for water treatment plants. Water Research 46, 1673–1683. doi:10.1016/j.watres.2011.12.006.

Paper V

Nilsen, V., J. A. Wyller, and A. Heistad (2012). "Efficient incorporation of microbial metabolic lag in subsurface transport modeling." *Water Resources Research* **48** (9), W09519.

Efficient incorporation of microbial metabolic lag in subsurface transport modeling

V. Nilsen,[1] J. A. Wyller,[1] and A. Heistad[1]

Received 5 November 2011; revised 23 May 2012; accepted 21 July 2012; published 13 September 2012.

[1] Upon introduction of a degradable substrate into the environment of a microbial community, an appreciable lag may occur before a corresponding increase in microbial activity is observed. Accounting for this metabolic lag may be of importance when modeling subsurface transport of contaminants that undergo reactions mediated by microbes. We present a general technique from mathematical biology that can facilitate incorporation of metabolic lags in subsurface solute transport models involving immobile biomass. By making the metabolic activity of bacteria dependent on the local history of substrate concentrations through a convolution integral, the proposed lag formulation is conceptually related to a previously suggested approach. Computer implementation of transport models with the new lag formulation becomes particularly simple when the numerical scheme (at least partly) reduces the original problem to that of solving systems of ordinary differential equations. Example simulation results show that transport models with this lag formulation can be made to fit real experimental data reasonably well by adjusting the lag parameters. The questions of whether parameter estimates can be generalized across individual model applications and/or whether parameters can be determined by independent experiments could be addressed in future research.

Citation: Nilsen, V., J. A. Wyller, and A. Heistad (2012), Efficient incorporation of microbial metabolic lag in subsurface transport modeling, *Water Resour. Res.*, *48*, W09519, doi:10.1029/2011WR011588.

1. Introduction

[2] For survival and growth, bacteria depend on having available the right type and amount of substrate ("food"). While bacteria are able to adapt, to some extent, to local environmental changes in substrate availability, this adaptation is usually not instantaneous. A significant time lag is often observed between changes in the availability of a substrate and the bacteria's ability to utilize that substrate [*Wood et al.*, 1995]. This microbial metabolic lag may be associated with the need to synthesize intracellular or extracellular compounds that aid in substrate utilization or, especially after prolonged starvation, with the need to perform cell repair before growth can begin. The lag effect can influence the subsurface transport of biodegradable contaminants if there are interruptions in the local substrate availability and the inherent timescale of the metabolic lag is comparable to other timescales of the problem [*Sandrin et al.*, 2001; *Park et al.*, 2001].

[3] Microbial growth and lag effects have been studied both theoretically and experimentally in the context of chemostats, which provide a well-defined and controllable growth environment [*Ellermeyer et al.*, 2003]. However, metabolic lags are usually not considered in subsurface transport models involving microbially mediated reactions. The reason may be that a fundamental, mechanistic approach is very difficult and empirical models tend to complicate the model equations and introduce even more parameters to be determined experimentally or by inverse modeling. The authors have found only two studies that focus primarily on developing methods for incorporating metabolic lags in transport modeling: *Wood et al.* [1995] employed a temporal convolution integral to make the metabolic state of an immobile (not transported in the aqueous phase) biomass dependent on the history of spatially local substrate concentrations, while *Ginn* [1999] developed a more general "exposure time" approach that is applicable even to mobile biomass, e.g., in those cases where growth or metabolic change may induce detachment of bacteria from the solid material. *Şengör et al.* [2009] extended the model by *Wood et al.* [1995] slightly to account for the effect of toxic compounds. *Park et al.* [2001] also developed a simple lag model, detailed below, to improve the fit to experimental data.

[4] The purpose of the work reported in this paper was to assess the utility of a general mathematical lag model, encountered in several areas of mathematical biology [e.g., *Nordbø et al.*, 2007], when integrated into subsurface contaminant transport models and tested against earlier models and experimental data. This was motivated by the fact that this lag formulation is fairly flexible, easy to implement numerically, and that it is consistent with some observed lag phenomena [*Park et al.*, 2001], as argued below. The model

[1]Department of Mathematical Sciences and Technology, Norwegian University of Life Sciences, Ås, Norway.

Corresponding author: V. Nilsen, Department of Mathematical Sciences and Technology, Norwegian University of Life Sciences, PO Box 5003, NO-1432 Ås, Norway. (vegard.nilsen@umb.no)

0043-1397/12/2011WR011588

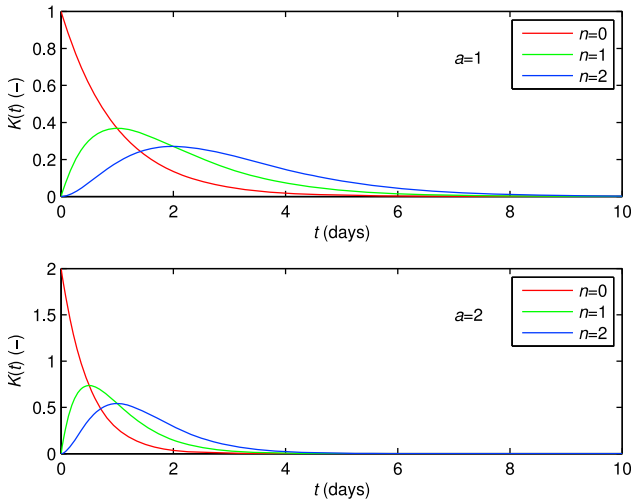

Figure 1. Plot of the temporal kernel $K^n_{a,d}(t)$ for $d = 0$ and various values of the parameters a and n. When used in the convolution integral, $t = 0$ corresponds to present time, and $t > 0$ corresponds to t time units into the past. A positive d would simply displace these curves to the right. We see that the recent past is given more weight as n decreases and a increases.

is based on the same integral convolution approach as *Wood et al.* [1995], but uses a quite different integral kernel.

2. Model Development

[5] For our purposes, the temporal change in biomass of an immobile subsurface microbial community that can be adequately represented by a single concentration variable $X(\mathbf{x}, t)$ is expressed in general terms as

$$\frac{\partial X}{\partial t} = \Psi_{\max}(X, \mathbf{c})\lambda(\mathbf{c}_l) \tag{1}$$

where $\Psi_{\max}$ is some function describing the nondelayed kinetics of biomass growth, $\mathbf{c}(\mathbf{x}, t)$ is a vector of substrate concentrations inside the biofilm and $\mathbf{c}_l(\mathbf{x}, t)$ is a set of limiting substrate concentrations that control the rate of growth (a subset of $\mathbf{c}$, possibly only one substrate). The factor λ characterizes the physiological state of the microbial community and is called the metabolic potential function, originally suggested by *Powell* [1967]. It is defined as the ratio $\Psi/\Psi_{\max}$, where Ψ is the actual (delayed) kinetics of biomass growth; it is therefore a scalar between 0 and 1.

[6] Building on chemostat studies by *Powell* [1967] and *Caperon* [1969], *Wood et al.* [1995] assumed that the metabolic potential is determined by the past history of the limiting substrate concentrations through a convolution integral. We adopt the same approach and postulate the following formulation for λ:

$$\lambda[\mathbf{c}_l(\mathbf{x}, t)] = \int_{-\infty}^{t} H[\mathbf{c}_l(\mathbf{x}, \tau)]K(t - \tau)\,d\tau \tag{2}$$

This expression should be interpreted as a weighted, smooth time average of the function H, where the integral kernel K plays the role as a weight function. H is some function that maps the limiting substrate concentrations onto the interval [0, 1]. It was suggested [e.g., *Edwards*, 1970] and later assumed [*Wood et al.*, 1995] that when c_l crosses some critical level $c_{l,c}$ (assuming from now, for simplicity, that we have only a single limiting substrate), a change in the metabolic state of the bacteria is induced. A candidate for H that captures this behavior is the Hill function:

$$H(c_l) = \frac{c_l^p}{c_{l,c}^p + c_l^p} \tag{3}$$

H is point symmetric around $(c_{l,c}, 1/2)$ and as $p \to \infty$, $H \to u(c - c_{l,c})$, where $u(c)$ is the unit step (Heaviside) function (this was used by *Wood et al.* [1995]). *Ginn* [1999] suggested a slightly different expression for H.

[7] While *Wood et al.* [1995] deduced the functional form of K by postulating a piecewise linear function for λ, we begin in the other end of the problem and suggest for K a family of functions $K^n_{a,d}$ that look complicated at first sight, but enables us to simplify the final lag formulation:

$$K^n_{a,d}(v) = \begin{cases} 0 & 0 \le v < d \\ K^n_a(v - d) & d \le v \end{cases} \tag{4}$$

where K^n_a is the gamma distribution,

$$K^n_a(v) = \frac{a^{n+1}v^n e^{-av}}{n!} \tag{5}$$

and d, $n \ge 0$ and $a > 0$ are constant parameters. It can be checked that this kernel is a normalized weight function (as is required to have $0 \le \lambda \le 1$): $\int_0^\infty K^n_{a,d}(v)dv = 1$. Figure 1 shows how the graphs of these temporal kernels look. Equation (4) simply shifts $K^n_a(v)$ d time units to the right, thereby introducing a time interval adjacent to present time, during which the weight function is 0, which may be of relevance in modeling bacterial growth.

[8] In the terminology of delay differential equations (DDEs) [*Driver*, 1977], this lag model could be described as a combination of distributed (due to the convolution integral formulation) and absolute (due to the time shifting of the kernel) delay. The distributed part could possibly be thought of as representing a (weighted) distribution of different lag times in a diverse microbial population. For $n = 0$ we have so-called weak delay, where the weight given to a point in time in the past increases monotonically as one approaches present time, while $n \ge 1$ corresponds to strong delay, where there exists some point in time in the past that is more influential than all other times (the kernel has a global maximum there). In both cases, naturally, the influence of the past goes to zero as we move far away from present time. For a recent discussion on the appropriateness of DDEs in modeling microbial population growth, see the paper by *Vadasz and Vadasz* [2010].

[9] The main result of Appendix A is that the integral expression (2) for λ, when combined with kernel (4)–(5), can be transformed into a system of ordinary differential equations in the time variable, by what is known as the *linear chain trick*. We obtain the following, where the z are auxiliary variables (the dependence on the spatial coordinates $\mathbf{x}$ is suppressed in (6)):

$$\begin{aligned} \lambda &= z_{n+1}(t) \\ z_1'(t) &= a\{H[\mathbf{c}_l(t - d)] - z_1(t)\} \\ z_2'(t) &= a[z_1(t) - z_2(t)] \\ &\vdots \\ z_{n+1}'(t) &= a[z_n(t) - z_{n+1}(t)] \end{aligned} \tag{6}$$

Table 1. Parameter Values and Boundary/Initial Conditions[a]

Parameter	Value	
	Wood et al. [1995]	*Park et al.* [2001]
Domain and Boundary Condition Parameters		
L (m)	0.56	0.141
T (days)	10	19
C_b (mg L^{-1})	20.0	See Figure 3
O_b (mg L^{-1})	132.7	
Initial Condition Parameters		
C_{in} (mg L^{-1})	0	0
O_{in} (mg L^{-1})	8.0	
X_{in} (mg (L soil)$^{-1}$)	1.64	3.72
Model Equations Parameters		
θ	0.38	0.35
D_C (m^2 $days^{-1}$)	7.47×10^{-3}	5.23×10^{-4}
D_O (m^2 $days^{-1}$)	7.58×10^{-3}	
V (m $days^{-1}$)	0.33	0.29
R	1.40	1.12
κ_C (m $days^{-1}$)	0.689	
κ_O (m $days^{-1}$)	0.119	
η (m^2 g^{-1})	1.19	
f	2.15	
μ ($days^{-1}$)	4.15	1.13
Y	0.5	0.5
K_C (mg L^{-1})	12.2	1.20
K_O (mg L^{-1})	0.1	
k_d ($days^{-1}$)	0.1	0.06
γ (L mg^{-1})	6.10×10^{-5}	

[a]All values are either cited directly or straightforwardly calculated from data reported by *Wood et al.* [1995] (originally from *Chen et al.* [1992] and *Alvarez* [1992]) and *Park et al.* [2001] (with permission from Elsevier). Parameter values associated with the lag formulation are given in Figures 2 and 3.

The expression for the initial conditions for this system is given by (A11) in the appendix. We now see the other main advantage of using this integral kernel: it eliminates the integro-differential formulation in (1) and (2) and replaces it with a system of equations involving no integrals. In (6) we still have an absolute delay d, though, but this can be handled numerically, for example by the method of steps [*Driver*, 1977; *Bocharov and Rihan*, 2000]. As we will see below, letting $d = 0$ may not always be a serious restriction.

[10] In applications, the lag formulation above would be part of a system of partial differential equations for contaminant transport with biodegradation, i.e., a system of advection-dispersion-reaction equations (examples below). In many common numerical solution strategies, the problem of solving such systems is (partly) reduced to that of solving systems of ordinary differential equations. For example, this is the case for so-called operator splitting schemes [*Carrayrou et al.*, 2004; *Morshed and Kaluarachchi*, 1995] in which (1) a system of pure transport partial differential equations (no reaction terms) and (2) a system of pure reaction ordinary differential equations (no transport terms) are solved for each time step. It is also the case for the method-of-lines approach in which spatial discretization leaves the original equations as a system of ordinary differential equations in time. In each of these cases, the above lag formulation can be implemented simply by including one or more equations in the system of ordinary differential equations, allowing for straightforward inclusion in existing numerical codes and the use of efficient packages for the numerical solution of ordinary and delay differential equations.

3. Simulation Results and Discussion

[11] The proposed lag formulation was tested with models and experimental data from two previously published laboratory column studies on the transport of organic contaminants. The first model, originally constructed without an explicit lag formulation, was used by *Chen et al.* [1992] to interpret their results from sand column experiments where benzene was degraded by microbes in the presence of hydrogen peroxide as the final electron acceptor. This model was expanded by *Wood et al.* [1995] with their lag formulation. The model equations, with the lag formulation of this paper on integral form, are the following:

$$R\frac{\partial C}{\partial t} = D_C\frac{\partial^2 C}{\partial x^2} - V\frac{\partial C}{\partial x} - \kappa_C\eta\theta^{-1}X(C-c) \tag{7}$$

$$\frac{\partial O}{\partial t} = D_O\frac{\partial^2 O}{\partial x^2} - V\frac{\partial O}{\partial x} - \kappa_O\eta\theta^{-1}X(O-o) \tag{8}$$

$$\frac{\partial(\omega c)}{\partial t} = \kappa_C\eta X(C-c) - \frac{\mu X}{Y}\left(\frac{c}{c+K_C}\right)\left(\frac{o}{o+K_O}\right)\lambda \tag{9}$$

$$\frac{\partial(\omega o)}{\partial t} = \kappa_O\eta X(O-o) - \frac{\mu X f}{Y}\left(\frac{c}{c+K_C}\right)\left(\frac{o}{o+K_O}\right)\lambda \tag{10}$$

$$\frac{\partial X}{\partial t} = \mu X\left(\frac{c}{c+K_C}\right)\left(\frac{o}{o+K_O}\right)\lambda - k_d X \tag{11}$$

$$\omega = \gamma X \tag{12}$$

$$\lambda[c(x,t)] = \int_{-\infty}^{t} H[c(x,\tau)]K(t-\tau)d\tau \tag{13}$$

[12] All variables and parameters are defined in the Notation section and the parameter values used by *Wood et al.* [1995] are stated in Table 1. Equations (7) and (8) are mass conservation equations for benzene (C) and hydrogen peroxide (O) in a mobile aqueous phase where the solutes undergo equilibrium adsorption (only benzene), advection and dispersion. Equations (9) and (10) express mass conservation for benzene (c) and hydrogen peroxide (o) in an immobile biomass phase where solutes are biodegraded by Monod kinetics (scaled by the metabolic potential λ). A first-order mass transfer relation governs the mass exchange between the phases. Equation (11) describes lag-adjusted growth and cell maintenance kinetics for the biomass (X). The water content of the aqueous phase, θ, is assumed to be practically unaffected by the fluctuations in biomass so that θ is constant, while the water content of the immobile phase, ω, is assumed to be proportional to the concentration of biomass (equation (12)). Equation (13) gives the lag formulation, with c as the limiting substrate concentration; for numerical implementation, this is replaced by the chain of equations in (6). Note that *Chen et al.* [1992] (but not *Wood et al.* [1995]) assumed a semisteady state

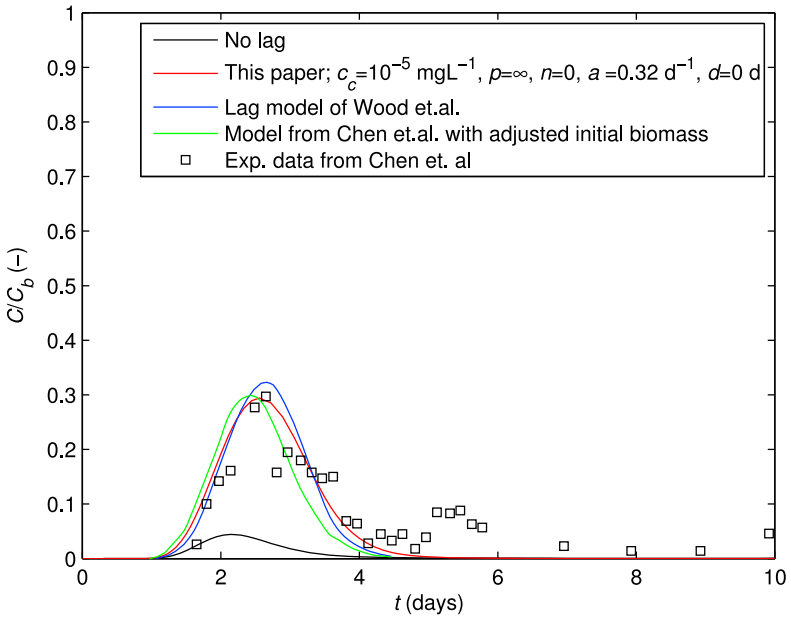

Figure 2. Comparison of models with experimental data for the system studied by *Chen et al.* [1992] and *Wood et al.* [1995]. Experimental data and the blue and green curves have been precision-read from figures in these articles.

solution at each time step by setting the derivatives in (9) and (10) equal to zero.

[13] Constant flux and no dispersive flux boundary conditions were employed at the influent ($x = 0$) and effluent ($x = L$) sides of the column, respectively:

$$-D_C\frac{\partial C}{\partial x}+VC\Big|_{(0,t)}=VC_b,\quad -D_O\frac{\partial O}{\partial x}+VO\Big|_{(0,t)}=VO_b \tag{14}$$

$$\frac{\partial C}{\partial x}\Big|_{(L,t)}=0,\quad \frac{\partial O}{\partial x}\Big|_{(L,t)}=0 \tag{15}$$

The initial functions are spatially uniform:

$$C(x,0)=c(x,0)=C_{\text{in}} \tag{16}$$

$$O(x,0)=o(x,0)=O_{\text{in}} \tag{17}$$

$$X(x,0)=X_{\text{in}}. \tag{18}$$

[14] The system of equations consisting of (7)–(18), along with (3)–(6) (where (6) is used to replace (13)) was solved by a method-of-lines approach, in which the spatial derivatives were discretized by centered finite differences. This results in a $[5 + (n + 1)] \times J$-dimensional system of ordinary differential equations (ODEs), where J is the number of grid points in the spatial discretization. The system of ODEs was integrated with a built-in MATLAB solver for stiff (due to the small parameter γ) ODE systems.

[15] Simulated breakthrough curves are shown in Figure 2. The initial value for λ was taken to be 0 (complete substrate starvation) for these simulations. Since the influent concentration $c_b \gg c_c$ (the critical benzene concentration c_c was taken from *Wood et al.* [1995]), the simulation results were insensitive to variations in the parameter p ($p \to \infty$ is shown). Several values for n were tested and it was found that having $n > 0$ (not shown) did not result in improved results for the height and timing of the breakthrough peak as compared to the case $n = 0$. Because no solver for systems of stiff delay-differential equations was available to the authors, the case of $d > 0$ was not tested with this model.

[16] As can be seen from Figure 2, the new lag formulation gives a fit to the data that is of roughly the same quality as the lag model by *Wood et al.* [1995]. This is obtained by adjusting one lag parameter, a (we fix $c_c = 10^{-5}$ mg L^{-1} and $p \to \infty$, as in *Wood et al.* [1995], and consider the fixation of $n = 0$ and $d = 0$ as model selection rather than parameter fitting). In comparison, *Wood et al.* [1995] used one more lag parameter, but it should be clearly noted that their parameters were estimated based on data from batch experiments reported by *Alvarez* [1992], in contrast with a above, that was used as a fitting parameter. The model by *Chen et al.* [1992], also shown in Figure 2, produced the fit to the data by assuming that only a certain proportion (1/8) of the initial biomass was able to degrade benzene.

[17] In general, the formulation by *Wood et al.* [1995] allows for the use of different kernels (asymmetrical response) depending on whether c_l crosses $c_{l,c}$ from above or from below. However, to ensure $0 \le \lambda \le 1$ it requires special treatment of any such crossings that occur too close to each other in time. We note that the kernel formulation in this paper is robust, in the sense that it produces $0 \le \lambda \le 1$ for any time evolution of the limiting substrate concentrations. In its present formulation, however, it lacks the possibility of specifying different responses to decreases versus increases in c_l, which could be a limitation, as discussed further below.

[18] In the second case we study here, *Park et al.* [2001] used a simplified version of the model above [*Chen et al.*, 1992] to interpret the results of column experiments in which toluene was degraded by microbes in the presence of oxygen as the final electron acceptor. Based on a priori

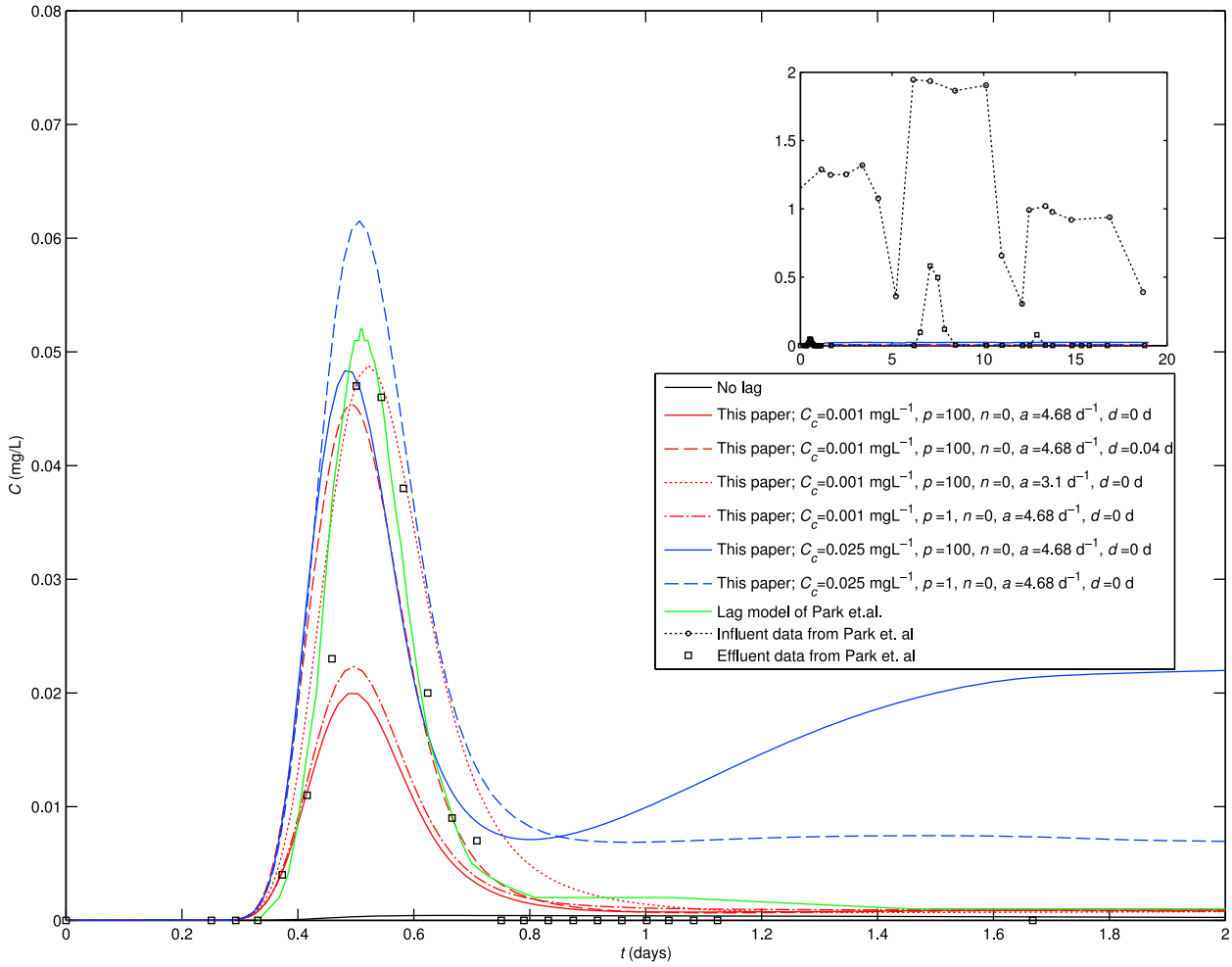

Figure 3. Comparison of experimental data from *Park et al.* [2001] with various models with and without lag. The inset shows the whole duration of the experiment, while the main view is zoomed in on the first breakthrough peak. Experimental data and the green curve have been precision-read from figures in *Park et al.* [2001] (with permission from Elsevier).

calculations, *Park et al.* [2001] assumed that (1) the biophase and aqueous phase concentrations (oxygen/toluene) would always be in equilibrium and (2) the toluene biodegradation rate would not be oxygen limited. With these assumptions, the model above simplifies to the following (with our lag formulation on integral form and C as the limiting substrate concentration; C now representing aqueous phase toluene concentrations):

$$R\frac{\partial C}{\partial t} = D_C\frac{\partial^2 C}{\partial x^2} - V\frac{\partial C}{\partial x} - \frac{\mu}{\theta Y}\left[\frac{C}{C+K_C}\right]X\lambda \tag{19}$$

$$\frac{\partial X}{\partial t} = \mu\left[\frac{C}{C+K_C}\right]X\lambda - k_d X \tag{20}$$

$$\lambda[C(x,t)] = \int_{-\infty}^{t} H[C(x,\tau)]K(t-\tau)d\tau \tag{21}$$

The boundary/initial conditions are given by (14)–(16) and (18). Parameter values used by *Park et al.* [2001] are given in Table 1. Again the initial value for λ was set to 0.

[19] *Park et al.* [2001] implemented their own simple lag model to get a (better) fit to the data. For that model, two fitting parameters were introduced: (1) a toluene concentration threshold (C_{th}; 0.06 mg/L) and (2) a lag time (T_{lag}; 1.68 h). It was assumed that only after the concentration of toluene has exceeded the threshold for the duration of the lag time, does toluene degradation begin. Also, in batch experiments, *Park et al.* [2001] determined the decline of the specific toluene degradation rate (expected to be proportional to λ) of suspended bacteria as a function of the duration of toluene starvation. They found the decline to follow a first-order form with a rate constant of 4.68 d^{-1}. The first-order form for the decline in metabolic potential is consistent with setting $n = 0$ in the lag model of this paper (see equation (6)). However, this in itself does not indicate that $n = 0$ is appropriate for modeling a *rise* in metabolic potential.

[20] The simplified system was also solved with a method-of-lines approach and since it is nonstiff, a MATLAB solver for delay differential equations with constant absolute delays was used to test the effect of having $d > 0$. Simulation results for this system for various values of the critical toluene concentration C_c (not independently estimated by *Park et al.*

[2001]), a, p and d are shown in Figure 3. As before, it was found that having $n > 0$ (not shown) did not improve the results significantly.

[21] From Figure 3, we note several points: (1) For relatively large values of C_c, the breakthrough peak is higher and C tends to level off around C_c, but in an oscillatory manner (not clearly visible in the figure). As soon as C drops below C_c, the metabolic potential starts to decrease and C will tend to increase. When C again exceeds C_c, the metabolic potential will start to increase and C will eventually decrease again. These oscillations can probably be expected whenever a model employs a single value of C_c, independent of whether C is increasing or decreasing, and C is controlled mainly through biodegradation. (2) The effect of changing p is more pronounced for larger values of C_c. In Figure 3, $p = 100$ was visually indistinguishable from $p \to \infty$. (3) Having $d = 0$ and setting a equal to the measured first-order rate constant (4.68 d^{-1}) of *Park et al.* [2001] produced only a moderately good fit. To produce a good fit with $d = 0$, it was found necessary to decrease a below the range of measurement uncertainty stated by *Park et al.* [2001]. (4) To produce a good fit with $a = 4.68$ d^{-1}, it was found necessary to introduce $d > 0$. The results seem to be very sensitive to the value of d.

[22] As seen in the inset of Figure 3, the influent concentration of toluene was time varying, with two distinct troughs and subsequent injections of toluene. Following the toluene injections, there are two distinct, surprisingly high peaks in the breakthrough curve (the hydraulic retention time was around 11 h). *Park et al.* [2001] concluded that these peaks could only have resulted from the time-varying influent toluene concentrations. We note that none of the models in Figure 3 are able to reproduce these latter peaks, even though they match the first peak reasonably well. Some mechanism may be acting, that is not understood at present.

4. Conclusions

[23] This paper has presented a temporal convolution integral approach for including microbial metabolic lags in subsurface contaminant transport modeling. It was demonstrated that the convolution formulation can be translated into a system of ordinary differential equations through the linear chain trick, allowing simple numerical implementation. Comparing simulation results with *Wood et al.* [1995], it was shown that the two formulations produced equally good fits to experimental data. The present formulation produced the fit with one less parameter, but only the formulation of *Wood et al.* [1995] had available independent parameter estimates. Comparing simulation results with *Park et al.* [2001], both models produced a good fit (by parameter fitting) to the first of the breakthrough peaks. None of the considered models could reproduce the two subsequent breakthrough peaks, and it is unclear how these could be modeled. It was noted that setting $n = 0$ in our lag model is consistent, for the declining portion of the metabolic potential function, with measurements made by *Park et al.* [2001] on substrate-starved bacteria. However, when setting a in our lag formulation equal to the corresponding measured first-order rate constant, only a moderately good fit to the data was obtained. Further research is needed to elucidate what is the proper form for a lag model, and whether independent and generalizable parameter estimates can be obtained for the lag formulation of this paper.

Appendix A: The Linear Chain Trick

[24] The transformation of the convolution integral to a system of differential equations, as in (6), is made possible by a specific choice of integral kernel (memory function). In this appendix we substantiate this technique, known as the "linear chain trick" [*Cushing*, 1977; *MacDonald*, 1978]. We begin with a general M-dimensional system of ordinary differential equations with so-called distributed delay:

$$\mathbf{y}'(t) = \mathbf{f}[\mathbf{y}(t), \lambda(t)] \tag{A1}$$

$$\mathbf{y}(t) = \phi(t),\ t \le 0 \tag{A2}$$

where $\mathbf{y}(t) = [y_1(t)\ y_2(t)\ \dots\ y_M(t)]^{\mathrm{T}}$ and $\lambda(t)$ denotes the functional

$$\lambda(t) = \int_{-\infty}^{t} H[\mathbf{y}(\tau)]K(t-\tau)d\tau \tag{A3}$$

The function $H[\mathbf{y}(t)]$ may, as far as the linear chain trick is concerned, be any mathematically admissible function. The initial history function $\phi(t)$ needs to be defined for all $t \le 0$ since the convolution integral depends on an infinite previous history.

[25] It can be shown, relatively easily, that $K^n_{a,d}(v)$ in (4)–(5) has the following properties, which we will make use of below (at $v = d$, derivatives must be interpreted as right-hand derivatives for the last two properties to hold, since the equivalent two-sided derivatives only exist for $n \ge 2$):

$$\begin{aligned}
&\lim_{v\to\infty} K^n_{a,d}(v) = 0\\
&K^n_{a,d}(d) = 0,\ n \neq 0\\
&K^0_{a,d}(d) = a\\
&\left[K^n_{a,d}(v)\right]' = a\left[K^{n-1}_{a,d}(v) - K^n_{a,d}(v)\right],\ n = 1, 2, \dots\\
&\left[K^0_{a,d}(v)\right]' = -aK^0_{a,d}(v)
\end{aligned} \tag{A4}$$

We also need the following differentiation rule, known as Leibniz's rule, which holds with mild continuity assumptions on the integrand:

$$\frac{\partial}{\partial t}\int_{q(t)}^{r(t)} h(\tau,t)d\tau = h[r(t),t]r'(t) - h[q(t),t]q'(t) + \int_{q(t)}^{r(t)} \frac{\partial}{\partial t}h(\tau,t)d\tau \tag{A5}$$

We now introduce the following auxiliary variables

$$\begin{aligned}
z_j(t) &= \int_{-\infty}^{t} H[\mathbf{y}(\tau)]K^{j-1}_{a,d}(t-\tau)d\tau\\
&= \int_{-\infty}^{t-d} H[\mathbf{y}(\tau)]K^{j-1}_{a}[t-(\tau+d)]d\tau,\\
&\quad j = 1, 2, 3, \dots, n+1
\end{aligned} \tag{A6}$$

This seemingly complicated choice of new variables will actually simplify our system. By differentiating these

equations with respect to t, making use of (A5) (with constant lower limit and $t - d$ as the upper limit) and (A4), we find for $j = 1$

$$\begin{aligned} z_1'(t) &= H[\mathbf{y}(t-d)]K_a^0(0) + \int_{-\infty}^{t-d} H[\mathbf{y}(\tau)]\{-aK_a^0[t-(\tau+d)]\}d\tau \\ &= aH[\mathbf{y}(t-d)] - a\int_{-\infty}^{t-d} H[\mathbf{y}(\tau)]K_a^0[t-(\tau+d)]d\tau \\ &= a\{H[\mathbf{y}(t-d)] - z_1(t)\} \end{aligned} \tag{A7}$$

and for $j = 2, 3, \ldots, n+1$

$$\begin{aligned} z_j'(t) &= H[\mathbf{y}(t-d)]K_a^{j-1}(0) \\ &\quad + \int_{-\infty}^{t-d} H[\mathbf{y}(\tau)]\frac{\partial}{\partial t}\{K_a^{j-1}[t-(\tau+d)]\}d\tau \\ &= a\int_{-\infty}^{t-d} H[\mathbf{y}(\tau)]\{K_a^{j-2}[t-(\tau+d)]d\tau \\ &\quad - a\int_{-\infty}^{t-d} H[\mathbf{y}(\tau)]\{K_a^{j-1}[t-(\tau+d)]\}d\tau \\ &= a[z_{j-1}(t) - z_j(t)] \end{aligned} \tag{A8}$$

We also find that

$$\begin{aligned} \lambda(t) &= \int_{-\infty}^{t} H[\mathbf{y}(\tau)]K_{a,d}^n(t-\tau)d\tau \\ &= \int_{-\infty}^{t-d} H[\mathbf{y}(\tau)]K_a^n[t-(\tau+d)]d\tau \\ &= z_{n+1} \end{aligned} \tag{A9}$$

The initial history function (A2) translates to

$$\mathbf{y}(0) = \phi(0) \tag{A10}$$

$$z_j(0) = \frac{a^j(-1)^{j-1}e^{ad}}{(j-1)!}\int_{-\infty}^{-d} H(\phi(\tau))(\tau+d)^{j-1}e^{a\tau}d\tau, \quad \text{all } j \tag{A11}$$

The final result is therefore that the M-dimensional system with combined distributed and absolute delays given by (A1)–(A2) and (4)–(5) has been transformed into the following $M + (n+1)$-dimensional system with only absolute delay

$$\mathbf{y}'(t) = \mathbf{f}(\mathbf{y}(t), z_{n+1}(t)) \tag{A12}$$

$$z_1'(t) = a\{H[\mathbf{y}(t-d)] - z_1(t)\}, \quad j = 1 \tag{A13}$$

$$z_j'(t) = a[z_{j-1}(t) - z_j(t)], \quad j = 2, 3, ..., n+1 \tag{A14}$$

with initial conditions given by (A10) and (A11). It should be noted that the linear chain trick will work as long as the kernel in the convolution integral is defined as above - its success does not depend on the particular system of differential equations of which the convolution integral is part.

[26] Finally, we note that we can generalize the integral kernel (perhaps to accommodate a very diverse microbial population) by considering a linear combination of the form

$$K_{\text{gen}}(v) = \sum_{l=0}^{L}\sum_{n=0}^{N} \alpha_{l,n}K_{a_l,d}^n(v) \tag{A15}$$

where the coefficients $\alpha_{l,n}$ are chosen so that $\alpha_{l,n} \geq 0$ and $\sum_{l=0}^{L}\sum_{n=0}^{N}\alpha_{l,n} = 1$. Here, $L + 1$ is the number of different values of a_l and $N = \max(n)$. Note that if we have only one a_l and one $n = N$, then $L = l = 0$ and all $\alpha_{l,n} = 0$ except for $\alpha_{0,N} = 1$. As before, $\int_0^\infty K_{\text{gen}}(v)dv = 1$. With this kernel, the final transformed system is $M + (L+1)(N+1)$-dimensional

$$\mathbf{y}'(t) = \mathbf{f}\left(\mathbf{y}(t), \sum_{l=0}^{L}\sum_{n=0}^{N}\alpha_{l,n}z_{l,n+1}(t)\right) \tag{A16}$$

$$z_{l,1}'(t) = a_l\{H[\mathbf{y}(t-d)] - z_{l,1}(t)\}, \quad \text{all } l;\ j = 1 \tag{A17}$$

$$z_{l,j}'(t) = a_l[z_{l,j-1}(t) - z_{l,j}(t)], \quad \text{all } l;\ j = 2, 3, \ldots, N+1 \tag{A18}$$

with initial conditions given by

$$\mathbf{y}(0) = \phi(0) \tag{A19}$$

$$z_{l,j}(0) = \frac{a_l^j(-1)^{j-1}e^{a_l d}}{(j-1)!}\int_{-\infty}^{-d} H(\phi(\tau))(\tau+d)^{j-1}e^{a_l\tau}d\tau \quad \text{all } l,j \tag{A20}$$

Since the number of parameters becomes very large in this generalized formulation, it can probably be made to fit many real systems. However, the system insight and the possibility of generalizing to other systems is likely to suffer as a result.

Notation

$X(\mathbf{x}, t)$	mass of microorganisms per unit volume of porous medium, M L^{-3}.
$\mathbf{x}(x)$, t	3-D (1-D) space (L) and time coordinates (T), respectively.
$\Psi_{\max}(X, \mathbf{c})$	microbial growth kinetic function, M L^{-3} T^{-1}.
$\lambda(\mathbf{c}_l)$	metabolic potential function, dimensionless.
$\mathbf{c}(t)$	vector of substrate concentrations in a biofilm, M L^{-3}.
$\mathbf{c}_l(t)$	vector of limiting substrate concentrations in a biofilm, a subset of $\mathbf{c}(t)$, M L^{-3}.
$H(\mathbf{c}_l)$	the Hill function (or an alternative sigmoidal function), dimensionless.
$K(v)$	general label for the temporal kernel, T^{-1}.
τ	variable of integration in the convolution integral, T.
$c_{l,c}$	parameter of the Hill function; critical limiting substrate concentrations in a biofilm, M L^{-3}.
p	steepness parameter of the Hill function, dimensionless.
$u(c)$	unit step function (Heaviside function), dimensionless.

$K_a^n(v)$ conventional linear chain trick temporal kernel, T^{-1}.
$K_{a,d}^n(v)$ time-shifted conventional linear chain trick temporal kernel, T^{-1}.
n parameter of $K_a^n(v)$, separates weak and strong delay, dimensionless.
a parameter of $K_a^n(v)$, characteristic time constant, T^{-1}.
d parameter of $K_{a,d}^n(v)$, magnitude of time shift, T.
z_j auxiliary variables of the linear chain trick, dimensionless.
C, c concentration of contaminant (benzene, toluene) in the aqueous phase and the biophase, respectively, $M\ L^{-3}$.
O, o concentration of hydrogen peroxide in the aqueous phase and the biophase, respectively, $M\ L^{-3}$.
θ water content of the aqueous phase, dimensionless.
ω water content of the biophase, dimensionless.
R retardation factor due to equilibrium adsorption of contaminant (benzene, toluene), dimensionless.
D_C, D_O dispersion coefficients of contaminant (benzene, toluene) and hydrogen peroxide, respectively, $L^2\ T^{-1}$.
V pore water velocity, $L\ T^{-1}$.
κ_C, κ_O mass transfer coefficients of benzene and hydrogen peroxide, respectively, $L\ T^{-1}$.
η effective surface area of biomass per unit biomass, $L^2\ M^{-1}$.
μ maximum specific growth rate of biomass, T^{-1}.
Y biomass created per unit mass of substrate (benzene, toluene) consumed (yield coefficient), dimensionless.
f mass of oxygen consumed per unit mass of benzene consumed, dimensionless.
K_C, K_O Monod half-saturation constants for contaminant (benzene, toluene) and hydrogen peroxide, respectively, $M\ L^{-3}$.
k_d microbial decay coefficient, T^{-1}.
γ volume of immobile phase (biophase) per unit biomass, $L^3\ M^{-1}$.
C_B, O_B boundary condition parameters for contaminant (benzene, toluene) and hydrogen peroxide, respectively, $M\ L^{-3}$.
C_{in}, O_{in}, X_{in} initial condition parameters for contaminant (benzene, toluene), hydrogen peroxide, and biomass, respectively, $M\ L^{-3}$.
c_c, C_c critical limiting substrate concentrations of benzene (in the biophase) and toluene (in the aqueous phase), respectively, $M\ L^{-3}$.
L length of column in experiments/domain of model, L.
T duration of experiments/simulation time, T.
J number of spatial grid points in numerical simulations, dimensionless.
C_{th} toluene concentration threshold in lag model of *Park et al.* [2001], $M\ L^{-3}$.
T_{lag} lag time in lag model of *Park et al.* [2001], T.
$\mathbf{y}$ dependent variable in the system of ODEs in Appendix A, dimensionless.
$\mathbf{f}$ right-hand side of the system of ODEs in Appendix A, dimensionless.
$\phi(t)$ initial history function of the system of ODEs in Appendix A, dimensionless.
r, q, h variables used for expressing the differentiation rule in Appendix A, dimensionless.
M dimension of original system of ODEs in Appendix A, dimensionless.
$K_{gen}(v)$ generalized temporal kernel in Appendix A, T^{-1}.
a_l parameters of generalized temporal kernel, T^{-1}.
$\alpha_{l,n}$ superposition parameter (weight) of generalized temporal kernel, dimensionless.
$L + 1$ number of different values of a_l in generalized temporal kernel, dimensionless.
N max(n) in generalized temporal kernel, dimensionless.

[27] **Acknowledgments.** We thank the Editor and the three reviewers for their constructive criticism during the review process. We also thank our colleague, Arkadi Ponossov, for proofreading the mathematics. Finally, for helpful comments on the numerical implementations, we thank the late Nils Svanstedt at Chalmers University of Technology/University of Gothenburg, Sweden, who sadly and unexpectedly passed away during the preparation of this paper.

References

Alvarez, P. (1992), Biodegradation of monoaromatic hydrocarbons by indigenous aquifer microorganisms under aerobic and denitrifying conditions, PhD thesis, Univ. of Mich., Ann Arbor.

Bocharov, G., and F. Rihan (2000), Numerical modelling in biosciences using delay differential equations, *J. Comput. Appl. Math.*, *125*(1–2), 183–199.

Caperon, J. (1969), Time lag in population growth response of *Isochrysis galbana* to a variable nitrate environment, *Ecology*, *50*, 188–192.

Carrayrou, J., R. Mose, and P. Behra (2004), Operator-splitting procedures for reactive transport and comparison of mass balance errors, *J. Contam. Hydrol.*, *68*(3–4), 239–268.

Chen, Y., L. Abriola, P. Alvarez, P. Anid, and T. Vogel (1992), Modeling transport and biodegradation of benzene and toluene in sandy aquifer material: Comparisons with experimental measurements, *Water Resour. Res.*, *28*(7), 1833–1847.

Cushing, J. (1977), *Integrodifferential Equations and Delay Models in Population Dynamics*, *Lect. Notes Biomath.*, vol. 20, Springer, New York.

Driver, R. (1977), *Ordinary and Delay Differential Equations*, *Appl. Math. Sci.*, vol. 20, Springer.

Edwards, V. (1970), The influence of high substrate concentrations on microbial kinetics, *Biotechnol. Bioeng.*, *12*(5), 679–712.

Ellermeyer, S., J. Hendrix, and N. Ghoochan (2003), A theoretical and empirical investigation of delayed growth response in the continuous culture of bacteria, *J. Theor. Biol.*, *222*(4), 485–494.

Ginn, T. (1999), On the distribution of multicomponent mixtures over generalized exposure time in subsurface flow and reactive transport: Foundations, and formulations for groundwater age, chemical heterogeneity, and biodegradation, *Water Resour. Res.*, *35*(5), 1395–1407.

MacDonald, N. (1978), *Time Lags in Biological Models*, *Lect. Notes Biomath.*, vol. 27, Springer, Berlin.

Morshed, J., and J. Kaluarachchi (1995), Critical assessment of the operator-splitting technique in solving the advection-dispersion-reaction equation: 2. Monod kinetics and coupled transport, *Adv. Water Resour.*, *18*(2), 101–110.

Nordbø, Ø., J. Wyller, and G. Einevoll (2007), Neural network firing-rate models on integral form, *Biol. Cybern.*, *97*(3), 195–209.

Park, J., Y. Chen, J. Kukor, and L. Abriola (2001), Influence of substrate exposure history on biodegradation in a porous medium, *J. Contam. Hydrol.*, *51*(3–4), 233–256.

Powell, E. (1967), *The Growth Rate of Microorganisms as a Function of Substrate Concentration*, vol. 34, Her Majesty's Stn. Off., London.

Sandrin, S., F. Jordan, R. Maier, and M. Brusseau (2001), Biodegradation during contaminant transport in porous media: 4. Impact of microbial lag and bacterial cell growth, *J. Contam. Hydrol.*, *50*(3–4), 225–242.

Şengör, S., S. Barua, P. Gikas, T. Ginn, B. Peyton, R. Sani, and N. Spycher (2009), Influence of heavy metals on microbial growth kinetics including lag time: Mathematical modeling and experimental verification, *Environ. Toxicol. Chem.*, *28*(10), 2020–2029.

Vadasz, P., and A. Vadasz (2010), On the distinction between lag and delay in population growth, *Microbial Ecol.*, *59*(2), 233–245.

Wood, B., T. Ginn, and C. Dawson (1995), Effects of microbial metabolic lag in contaminant transport and biodegradation modeling, *Water Resour. Res.*, *31*(3), 553–563.